

AD757870

AFFDL-TR-72-80

**ENGINEERING CRITERIA AND ANALYSIS  
METHODOLOGY FOR THE APPRAISAL OF  
POTENTIAL FRACTURE RESISTANT PRIMARY  
AIRCRAFT STRUCTURE**

*J. C. EKVALL, T. R. BRUSSAT, AND  
A. F. LIU*

*LOCKHEED-CALIFORNIA COMPANY  
BURBANK, CALIFORNIA*

*AND*

*MATTHEW CREAGER  
CONSULTANT  
CANOGA PARK, CALIFORNIA*

TECHNICAL REPORT AFFDL-TR-72-80

SEPTEMBER 1972

Approved for public release; distribution unlimited.

**AIR FORCE FLIGHT DYNAMICS LABORATORY  
AIR FORCE SYSTEMS COMMAND  
WRIGHT-PATTERSON AIR FORCE BASE, OHIO**

20080819 204



## NOTICE

When Government drawings, specifications, or other data are used for any purpose other than in connection with a definitely related Government procurement operation, the United States Government thereby incurs no responsibility nor any obligation whatsoever; and the fact that the Government may have formulated, furnished, or in any way supplied the said drawings, specifications, or other data, is not to be regarded by implication or otherwise as in any manner licensing the holder or any other person or corporation, or conveying any rights or permission to manufacture, use, or sell any patented invention that may in any way be related thereto.

Copies of this report should not be returned unless return is required by security considerations, contractual obligations, or notice on a specific document.

AD 757870

**ENGINEERING CRITERIA AND ANALYSIS  
METHODOLOGY FOR THE APPRAISAL OF  
POTENTIAL FRACTURE RESISTANT PRIMARY  
AIRCRAFT STRUCTURE**

*J. C. EKVALL, T. R. BRUSSAT, A. F. LIU  
LOCKHEED-CALIFORNIA COMPANY  
BURBANK, CALIFORNIA  
AND  
MATTHEW CREAGER  
CONSULTANT  
CANOGA PARK, CALIFORNIA*

Approved for public release; distribution unlimited.

## F O R E W O R D

The report was prepared by the Lockheed-California Company under Air Force Contract F33615-71-C-1324. The work was administrated under the direction of the Structures Division (FBR), Air Force Flight Dynamics Laboratory, with Mr. Howard A. Wood as the Air Force project engineer. The report covers the work conducted from 15 February 1971 through 15 August 1972.

This program was conducted under the supervision of Mr. W. J. Crichlow (15 February - 1 July 1971) and Mr. R. B. Ostrom (1 July 1971 - 15 August 1972), Structural Mechanics Group Engineer and Mr. J. C. Wordsworth, Structural Analysis Department Manager in the Structures Division of the Science & Engineering Branch, Lockheed-California Company.

The project leader for this program was Mr. J. C. Ekvall, with Dr. Matthew Creager acting as primary consultant. In addition to the authors, the work of the following personnel in the Structural Analysis Department is gratefully acknowledged: Mr. A. C. Jackson for the Preliminary Design, Section 5.4, Mr. R. D. Mijares for the Structural Weight Comparison, Section 5.6, and Mr. P. B. Hamlett for performing the crack growth computations.

All work under this contract was performed at the Lockheed-California Company, Burbank, California.

This technical report has been reviewed and is approved.

Francis J. Janik, Jr.  
Chief, Solid Mechanics Branch  
Structures Division  
AF Flight Dynamics Laboratory



## ABSTRACT

Design criteria and analysis procedures are presented in a manner such that a design system can be implemented to minimize the occurrence of major structural failures due to the presence of undetected damage. The design criteria define a flaw growth durability requirement and crack growth structural integrity requirements for three classes of inspectability of the structure; non-inspectable, NDI in-service inspectable, and walk-around inspectable. Currently available crack growth and residual strength methods of analysis are presented which can be used to predict the remaining life and strength of damaged structure. To illustrate the use of the criteria and methods of analysis, a design study has been conducted of the lower wing surface of a fighter/attack aircraft. The results of this study indicate that the structure could meet the design criteria with little or no weight penalty using 7075-T76 aluminum and annealed Ti-6Al-4V, and provided adequate inspection techniques and inspection frequencies are applied throughout the life of the aircraft.

## TABLE OF CONTENTS

<u>SECTION</u>	<u>Page</u>
1.0 INTRODUCTION	1-1
2.0 SUMMARY AND CONCLUSIONS	2-1
3.0 ENGINEERING CRITERIA	3-1
3.1 EXISTING CRITERIA	3-1
3.1.1 Pressure Vessels	3-1
3.1.2 Civil Aircraft	3-1
3.1.3 Air Force Aircraft	3-2
3.2 CRITERIA CONSIDERATIONS	3-10
3.2.1 Load Environment	3-10
3.2.2 Dynamic Effects	3-14
3.2.3 Damage Limits	3-20
3.2.4 Material Properties	3-31
3.3 CRITERIA DEVELOPMENT	3-36
3.3.1 Introduction	3-36
3.3.2 Initial "Ideal" Criteria	3-38
3.3.3 Final Criteria	3-46
3.4 RECOMMENDED CRITERIA	3-52
4.0 ANALYTICAL PROCEDURES	4-1
4.1 INTRODUCTION	4-1
4.2 FATIGUE ANALYSIS	4-1
4.3 STRESS INTENSITY FACTORS FOR COMMON CRACK (FLAW) GEOMETRIES	4-6
4.3.1 Introduction	4-6
4.3.2 Thru-the-Thickness Crack at the Center of a Plate	4-10
4.3.3 Part-Thru Crack (Surface Flaw) in a Plate	4-10
4.3.4 Corner Crack (Flaw)	4-16
4.3.5 Cracks (Flaws) Emanating from the Edge of a Hole	4-18
4.3.6 Cracks in the Vicinity of Reinforcements	4-22
4.4 FATIGUE CRACK GROWTH ANALYSIS	4-27
4.5 SUSTAINED LOAD CRACK GROWTH ANALYSIS	4-30

TABLE OF CONTENTS (Contd.)

<u>SECTION</u>	<u>Page</u>
4.6 RESIDUAL STRENGTH ANALYSIS	4-36
4.6.1 Redundant Structure (Single Member Broken)	4-36
4.6.2 Structure Containing Crack(s)	4-41
4.7 DYNAMIC CRACK ARREST	4-57
5.0 APPLICATION STUDY	5-1
5.1 DESIGN PROBLEM DEFINITION	5-1
5.2 DESIGN LOADS	5-7
5.3 MATERIAL PROPERTIES AND ALLOWABLES	5-10
5.4 PRELIMINARY DESIGN	5-19
5.4.1 Stress Assumptions	5-19
5.4.2 Integrally Stiffened Wing	5-19
5.4.3 Zee-Stiffened Wing	5-19
5.4.4 Multi-Spar Plate Wing	5-22
5.4.5 Resizing for Final Design Stress Allowables	5-22
5.5 DESIGN STRESS ALLOWABLES	5-26
5.5.1 Fatigue Analysis	5-26
5.5.2 Fatigue Crack Growth	5-30
5.5.3 Residual Strength Analysis	5-57
5.5.4 Environmental Effects	5-64
5.5.5 Summary of Design Stress Allowables	5-67
5.6 STRUCTURAL WEIGHT COMPARISON	5-69
5.7 EVALUATION	5-75
5.7.1 Durability Requirement	5-75
5.7.2 Structural Integrity Requirements	5-75
5.7.3 Structural Weight Evaluation	5-78
6.0 REFERENCES	6-1
APPENDICES	
A PROPOSED AIR FORCE SERVICE LIFE REQUIREMENTS	A-1
B. FRACTURE TOUGHNESS PROPERTIES OF MATERIALS	B-1



TABLE OF CONTENTS (Contd.)

<u>SECTION</u>		<u>Page</u>
APPENDICES (Contd.)		
C	SUSTAINED-LOAD SPECTRUM	C-1
D	RESULTS OF CRACK GROWTH ANALYSIS	D-1
E	STRESS INTENSITY FACTORS FOR A PART-THRU CRACK IN A PLATE	E-1
F	THE CRACK GROWTH RESISTANCE CURVE APPROACH TO RESIDUAL STRENGTH PREDICTION	F-1
G	LIST OF SYMBOLS	G-1

## LIST OF FIGURES

<u>FIGURE</u>	<u>TITLE</u>	<u>Page</u>
3-1	Typical Crack Growth Curves for Walk-Around and NDI In-Service Inspectable Structure	3-6
3-2	Crack Growth Requirements for Fail-Safe Structure with One Member Broken.	3-8
3-3	Maneuver Load-Factor Data for Several Fighter/Attack Aircraft	3-11
3-4	Dynamic Load Applied to a Tensile Bar	3-15
3-5	Schematic of Flaw-Size Distribution Before and After Inspection	3-21
3-6	Effectiveness of Inspection for Lower Wing Surface of Transport Aircraft	3-24
3-7	"Detectable" Crack Lengths	3-26
3-8	Results of the First Inspection for C-130 Aircraft Fleet	3-27
3-9	Relation Between Crack-Size Found and Flight-Hours Since Previous Inspection for C-130 Aircraft	3-28
3-10	Damage Accumulation	3-39
3-11	Variation of Probability of Failure	3-40
3-12	Failure Analysis History	3-43
4-1	Flow Diagram of Fatigue Analysis Procedure	4-2
4-2	GAG Cycle Definition for Fatigue Analysis	4-4
4-3	Method of Calculating Magnitude of GAG Cycle	4-5
4-4	Three Basic Modes of Crack Surface Displacement	4-6
4-5	Cross-Sectional Views of Common Flaw Geometries	4-8
4-6	Cracked Finite-Width Plate Loaded in Tension, $f_g$ , or Shear, $f_s$	4-11
4-7	Panel Length Effects on Crack Tip Stress Intensity for Center Cracked, Panels, Elastic Analysis	4-12
4-8	Part-Thru Crack Geometry	4-13
4-9	Combined Crack Shape and Front Surface Correction	4-15

# LIST OF FIGURES (Contd.)

<u>FIGURE</u>	<u>TITLE</u>	<u>Page</u>
4-10	Corner Crack or Cracks at the Edge of a Circular Hole	4-17
4-11	Part-Thru Crack(s) at the Edge of a Circular Hole	4-19
4-12	Geometric Coefficient for Crack or Cracks at the Edge of a Circular Hole	4-20
4-13	Geometric Coefficient for a Crack Emanating from an Elliptical Hole	4-21
4-14	The General Stress-Intensity Approach to Prediction of Crack Propagation in Structures Under Variable-Amplitude Loading	4-28
4-15	Schematic Curves Showing the Environmental Delayed-Failure of Specimens Subjected to Sustained Loads	4-32
4-16	Effect of Environment and Time at Sustained Load on Fracture Toughness for Titanium Alloys and Steel	4-33
4-17	Constant Load Subcritical Crack-Growth of AM 350 Steel in Purified Argon Environment	4-34
4-18	Stress Distribution Across a Three-Plank Fail-Safe Test Panel with the Middle Plank Broken	4-38
4-19	Effective Width in Side Planks for Flat Panels with Longitudinal Splices	4-40
4-20	Influence of the Degree of Redundancy on the Residual Static Strength of Multi-Plank Panel with One Plank Broken	4-42
4-21	Effect of Thickness on Fracture Toughness Properties	4-44
4-22	Thru-the-Thickness Cracks in a Reinforced Panel	4-46
4-23	Design Curves for Reinforced Flat Panels	4-49
4-24	Fracture Toughness Properties for 2024-T3 and T351 Aluminum	4-53
4-25	Fracture Toughness Properties for 7075-T7651 Aluminum Alloy	4-54
4-26	Correlation Between Test Failure Load and Predicted Failure Load	4-55
4-27	Percent Deviation of Test Results vs. Reinforced Variable	4-56
5-1	Flighter/Attack Aircraft - Wing Weight Distribution	5-3
5-2	Fighter/Attack Aircraft - Wing Limit Loads	5-8



# LIST OF FIGURES (Contd.)

<u>FIGURE</u>	<u>TITLE</u>	<u>Page</u>
5-3	Loading Spectra for Typical Fighter Aircraft	5-9
5-4	Constant-Life Diagram for Standardized Aluminum Alloy, $K_t = 4$ , $F_{tu} = 77$ ksi	5-12
5-5	Constant-Life Diagram for Ti-6Al-4V Annealed Sheet and Plate, $K_t = 5$ , $F_{tu} = 135-155$ ksi	5-14
5-6	Fracture Toughness of 7075-T76 Aluminum Alloy Sheet and Plate	5-15
5-7	Fracture Toughness of Ti-6Al-4V, Mill Annealed Sheet and Plate	5-16
5-8	Schematic Cross-Sections of Stiffened Skin Designs	5-20
5-9	Ultimate Design Tension Stress Allowable for 7075-T76 Aluminum Structure and Fatigue Quality Index = 4.0	5-27
5-10	Ultimate Design Tension Stress Allowable for Ti-6Al-4V Structure and a Fatigue Quality Index = 5.0	5-28
5-11	Distribution Curve for Aircraft Structural Component Test Values of Fatigue Quality Index	5-29
5-12	Sample Two-Flight-Long Sequence of Cyclic Loads	5-32
5-13	Growth-Rate, $da/dF$ , versus $\alpha_s$ for Spectrum Loading	5-35
5-14	Elementary Geometries for the Crack Propagation Analysis	5-38
5-15	Ultimate Design Tension Stress Allowables for Durability Requirement - Aluminum Structure	5-42
5-16	Ultimate Design Tension Stress Allowables for Durability Requirement - Titanium Structure	5-43
5-17	Ultimate Design Tension Stress Allowables for Aluminum Non- Inspectable Structure	5-46
5-18	Ultimate Design Tension Stress Allowables for Titanium Non- Inspectable Structure	5-47
5-19	Ultimate Design Tension Stress Allowables for a Broken Zee- Stiffener and Thru-Thickness Crack in 7075-T76 Aluminum	5-50
5-20	Ultimate Design Tension Stress Allowables for a Broken Zee- Stiffener and a Thru-Thickness Crack in Ti-6Al-4V	5-51
5-21	Ultimate Design Tension Stress Allowables for a Cracked Riser and Thru-Thickness Skin Crack in 7075-T76 Aluminum	5-52
5-22	Ultimate Design Tension Stress Allowables for a Cracked Riser and Thru-Thickness Skin Crack in Ti-6Al-4V	5-53

# LIST OF FIGURES (Contd.)

<u>FIGURE</u>	<u>TITLE</u>	<u>Page</u>
5-23	Ultimate Design Tension Stress Allowables for a Broken Spar Cap and Thru-Thickness Crack in 7075-T76 Aluminum	5-54
5-24	Ultimate Design Tension Stress Allowables for a Broken Spar and Thru-Thickness Skin Crack in Ti-6Al-4V	5-55
5-25	Lower Surface Wing Weight Variations	5-72
B-1	Notched-Bend Specimen	B-2
B-2	$K_{Ic}$ versus Tensile Yield Strength, Ti-6Al-4V Mill Annealed	B-4
B-3	Four-Point Notched-Bend $K_{Ic}$ Data for Ti-6Al-4V Mill Annealed, Log-Normal Distribution	B-5
B-4	Effect of Stress Rate on $K_{Ic}$ for Ti-6Al-4V, Beta-STA-1250	B-9
B-5	Effect of Stress State on $K_{Ic}$ for Ti-4Al-3Mo-1V, Beta-STA-1150	B-9
B-6	Four-Point Notched-Bend $K_{Ic}$ Data for 7075-T6 Aluminum Alloy, Log-Normal Distribution	B-11
B-7	MIL-HDBK-5 B-Scale $K_{Ic}$ Values for D6AC Steel as a Function of Heat Treatment	B-17
B-8	Residual Strength for Ti-6Al-4V Mill Annealed, W = 24 in.	B-18
B-9	Residual Strength for Ti-6Al-4V Mill Annealed, W = 8 in.	B-19
B-10	Effect of Loading Rate on Residual Strength of Ti-6Al-4V Mill Annealed, 0.21 in. Thickness Plate, Longitudinal Grain Direction	B-24
B-11	Effect of Loading Rate on Residual Strength of Ti-6Al-4V Mill Annealed, 0.05 in. Thickness Sheet, Longitudinal Grain Direction	B-25
B-12	Effect of Loading Rate of Residual Strength of Ti-6Al-4V Mill Annealed, 0.05 - 0.063 in. Thickness Sheet, Transverse Grain Direction	B-26
B-13	Effect of Loading Rate on Residual Strength of Ti-6Al-4V Mill Annealed, 0.025 in. Thickness Sheet, Transverse Grain Direction	B-27
B-14	Effect of Thickness on Fracture Toughness of Ti-6Al-4V Mill Annealed	B-28
B-15	Fracture Toughness Properties for 7075-T6 Aluminum, Longitudinal Grain	B-31
B-16	Fracture Toughness Properties of 7075-T6 Aluminum, Transverse Grain	B-32

# LIST OF FIGURES (Contd.)

<u>FIGURE</u>	<u>TITLE</u>	<u>Page</u>
C-1	Zero-to $N_{Z_{max}}$ Load Cycle	C-3
C-2	Cyclic Load Spectrum	C-6
C-3	Sustained Load Spectrum	C-6
D-1	Crack Growth Curves for Semi-Circular Flaws Initiating at a Surface or Internal Corner in 7075-T76 Aluminum - Severe Spectrum	D-2
D-2	Crack Growth Curves for Semi-Circular Flaws Initiating at a Surface or Internal Corner in Ti-6Al-4V - Severe Spectrum	D-3
D-3	Crack Growth Curves for Semi-Circular Flaws Initiating at a Surface or Internal Corner in 7075-T76 Aluminum - Typical Spectrum	D-4
D-4	Crack Growth Curves for Semi-Circular Flaws Initiating at a Surface or Internal Corner in Ti-6Al-4V, Typical Spectrum	D-5
D-5	Crack Growth Curves for Double Corner Flaws at a Hole in 7075-T76 Aluminum	D-6
D-6	Crack Growth Curves for Double Corner Flaws at a Hole in Ti-6Al-4V	D-7
D-7	Crack Growth Curves for a Broken Zee Stiffener and a Double Corner Flaw at a Hole in 7075-T76 Aluminum	D-8
D-8	Crack Growth Curves for a Broken Zee Stiffener and Thru-Thickness Skin Crack in Ti-6Al-4V	D-9
D-9	Crack Growth Curves for Thru-Thickness Crack in 7075-T76 Aluminum Integrally Stiffened Skin Planks	D-10
D-10	Crack Growth Curves for Thru-Thickness Crack in Ti-6Al-4V Integrally Stiffened Skin Planks	D-11
D-11	Crack Growth Curves for Cracked Riser and Thru-Thickness Skin Crack in 7075-T76 Aluminum	D-12
D-12	Crack Growth Curves for Cracked Riser and Thru-Thickness Skin Crack in Ti-6Al-4V	D-13
D-13	Crack Growth Curves for a Broken Spar Cap and Thru-Thickness Skin Crack in 7075-T76 Aluminum	D-14
D-14	Crack Growth Curves for a Broken Spar Cap and Thru-Thickness Skin Crack in Ti-6Al-4V	D-15
D-15	Crack Growth Curves for Thru-Thickness Crack in Unstiffened 7075-T76 Aluminum Skin	D-16
D-16	Crack Growth Curves for Thru-Thickness Crack in Unstiffened Ti-6Al-4V Skin	D-17



# LIST OF FIGURES (Contd.)

<u>FIGURE</u>	<u>TITLE</u>	<u>Page</u>
E-1	Front Surface Geometric Coefficient for a Semi-Circular Part-Thru Crack	E-3
E-2	Front Surface Parameter $M_1$ for a Semi-Elliptical Part-Thru Crack	E-4
E-3	Comparison of Kobayashi's and Irwin's Plasticity Factors	E-7
E-4	Estimated Back Surface Coefficient	E-9
E-5	Comparison of Back Surface Coefficients	E-10
E-6	Rice and Levy's Numerical Solution for a Part-Thru Crack	E-11
E-7	Comparison of Rice-Levy's Approximate and Numerical Solutions for a Part-Thru Crack	E-12
E-8	Back Surface Coefficient for Ti-5Al-2.5Sn (ELI) Base Metal and Weldments	E-14
E-9	Back Surface Coefficient for 2219-T87 Aluminum Plate	E-15
F-1	Resistance Curve Failure Prediction	F-2
F-2	Structural Intensity Structural Coefficient for a Center-Cracked Panel	F-4
F-3	$K_r$ Curve for 2024-T3 Clad Aluminum ( $t = 0.08$ inch)	F-5
F-4	Schematic Solution to Example 1	F-6
F-5	Stress Intensity Structural Coefficient for Example 2 Reinforced Panel	F-7
F-6	Schematic Solution for Example Problem 2	F-8

# LIST OF TABLES

<u>TABLE</u>	<u>TITLE</u>	<u>Page</u>
3-1	Summary of Proposed Air Force Service Life Requirements	3-5
3-2	Flaw-Size Detectability by Various Inspection Techniques	3-23
3-3	Summary of Flaw-Size Detectability	3-30
3-4	Recommended Damage Tolerant Design Criteria	3-53
4-1	Values of $\lambda$ for 11-Spar Structure	4-24
4-2	Values of $\lambda$ for Zee-Stiffened Structure	4-25
4-3	Values of $\lambda$ for Integrally Stiffened Structure	4-26
4-4	Test Panel Configurations	4-52
5-1	Typical Fighter/Attack Aircraft Characteristics	5-2
5-2	Damage Tolerance Requirements Applicable to Fighter/Attack Aircraft	5-4
5-3	Properties of Materials Considered for Application Study	5-11
5-4	Constant Amplitude Rate of Growth of One End of a Crack, 7075-T76	5-18
5-5	Constant Amplitude Rate of Growth of One End of a Crack, Ti-6Al-4V	5-18
5-6	D6AC Steel 220 ksi 3-Spar Integrally Stiffened Wing Sizing	5-21
5-7	Ti-6Al-4V Annealed 3-Spar Integrally Stiffened Wing Sizing	5-21
5-8	7075-T76 Aluminum 3-Spar Integrally Stiffened Wing Sizing	5-21
5-9	D6AC Steel 220 ksi 3-Spar Zee-Stiffened Wing Sizing	5-23
5-10	Ti-6Al-4V Annealed 3-Spar Zee-Stiffened Wing Sizing	5-23
5-11	7075-T76 Aluminum 3-Spar Zee-Stiffened Wing Sizing	5-23
5-12	D6AC Steel 220 ksi 11-Spar Unstiffened Skin Wing Sizing	5-24
5-13	Ti-6Al-4V Annealed 11-Spar Unstiffened Skin Wing Sizing	5-24
5-14	7075-T76 Aluminum 11-Spar Unstiffened Skin Wing Sizing	5-24
5-15	Resized 7075-T76 Aluminum Integrally Stiffened Structure	5-25
5-16	Resized 7075-T76 Aluminum Zee-Stiffened Structure	5-25

LIST OF TABLES (Contd.)

<u>TABLE</u>	<u>TITLE</u>	<u>Page</u>
5-17	Sequence of Cycles for the Sample Load History of Figure 5-12	5-33
5-18	Typical and Severe Load Spectra	5-34
5-19	Conversion Factors to Apply Analysis to Typical Spectrum	5-36
5-20	Values of $M'/\phi$ for a Shallow Part-Thru Crack, Case II	5-39
5-21	Bowie Correction for Corner Crack ( $r = 0.125$ in.)	5-40
5-22	Summary of Ultimate Design Tension Stress Allowables to Meet Durability Requirement	5-44
5-23	Summary of Stress Allowables for Non-Inspectable Structure	5-48
5-24	Ultimate Design Tension Stress Allowables for NDI In-Service Inspectable Structure	5-56
5-25	Summary of Residual Strength Calculations for Skin Cracks Between Effective Reinforcements	5-59
5-26	Summary of Residual Strength Calculations for 8-inch Skin Crack Not Influenced by Reinforcements	5-61
5-27	Ultimate Design Tension Stress Allowables for Walk-Around Inspectable Damage	5-65
5-28	Summary of Sustained Load Calculations	5-66
5-29	Summary of Ultimate Design Tension Stress Allowables to Meet Various Design Criteria	5-68
5-30	Baseline Titanium and Steel Estimated Wing Weights	5-70
5-31	Baseline Aluminum Estimated Wing Weights	5-71
5-32	Summary of Lower Surface Wing Weights to Meet Various Criteria	5-73
B-1	Four Point Notched-Bend $K_{Ic}$ Data for Ti-6Al-4V Mill Annealed	B-3
B-2	Summary of Ti-6Al-4V Mill Annealed $K_{Ic}$ Allowable Data	B-8
B-3	Four-Point Notched-Bend $K_{Ic}$ Values for 7075-T6 Aluminum Alloy	B-10
B-4	7075-T6 Aluminum $K_{Ic}$ Allowable Data	B-12
B-5	Heat Treat Methods vs. Heat Treat Operations for D6AC Steel	B-14
B-6	Summary of D6AC Steel $K_{Ic}$ Data	B-15
B-7	D6AC Steel $K_{Ic}$ Allowable Data	B-16

LIST OF TABLES (Contd.)

<u>TABLE</u>	<u>TITLE</u>	<u>Page</u>
B-8	$K_c$ Data for Ti-6Al-4V Mill Annealed	B-21
B-9	$K_c$ Data for 7075-T6 Clad Aluminum Alloy	B-29
B-10	$K_c$ Data for 7075-T6 Bare Aluminum Alloy	B-30
C-1	Calculation of $c(r)$ From Flight Test Data on Pullout Maneuvers of a Typical Fighter Aircraft	C-4
C-2	Example Calculation of High Load Portion of a Sustained Load Spectrum	C-8



## 1.0 INTRODUCTION

Design criteria for aircraft structures have evolved over a period of years based on aircraft service experience. Safe-life design criteria were initiated in the aircraft design system in the 1940's as the result of some fatal aircraft crashes due to fatigue cracking of structural components. These criteria have been updated and improved, and new aircraft must still meet fatigue life requirements to prevent early fatigue cracking problems in service. However, the service experience of high maneuver load factor aircraft which were designed on the basis of the safe-life concept has not been totally satisfactory.

As a result of the Comet crashes in the 1950's the fail-safe design approach was introduced. This approach embodies the concept that fatigued or otherwise damaged structure can continue to function satisfactorily under any loading condition within the normal operating envelope for the vehicle until discovery and remedial action can be accomplished. Commercial structures designed to meet fail-safe requirements have had an excellent safety record. For example, FAA records indicate that commercial aircraft have experienced numerous fatigue and extensive corrosion cracks and other damage without resulting loss of the aircraft.

Recent experiences of catastrophic failure on first line military aircraft have focused attention on the engineering criteria used to design and qualify aircraft structures. Generally these catastrophic failures initiated from small cracks in the structure that were not detected by production or in-service inspections. All aircraft structures contain flaws, defects, or other anomalies which are inherent in the basic material or which are introduced during the fabrication processes and in service. Under service loading conditions these defects, or damage, can grow to critical proportions if undetected. Fracture mechanics analyses have been utilized to a large extent to correct design deficiencies and to establish safe inspection intervals to prevent recurrence of catastrophic failures. The results obtained from the application of these analyses demonstrated the need for new design criteria which consider the existence and growth of small flaws and cracks in aircraft structure.

The research and development program reported herein was conducted to develop design criteria and analysis procedures such that a design system can be implemented to minimize the occurrences of major structural failures due to the presence of undetected damage. A number of damage tolerant design criteria have been developed in the past; however, these criteria are incomplete in many respects. In this program an attempt was made to develop a complete set of design criteria that would provide equal probabilities of failure for various structural and inspection classifications. However, with current technology it was not possible to determine definitive quantities that would provide equal probabilities of failure. Although this approach had to be abandoned, it did provide a useful framework for establishing the final recommended design criteria.

Section 3.4 presents the recommended set of design criteria which considers the existence of flaws or damage present in aircraft structures, and provides a sufficient crack growth period so that the damage can be detected before catastrophic failure. The recommended criteria define damage tolerance requirements as a function of the inspectability of the structure, i.e., noninspectable, NDI in-service inspectable, or walk-around inspectable. Factors which were considered as part of the criteria development included the appropriate definition of material properties to be used in design analysis, the loads that must be considered for residual strength determinations, and the degree of damage that must be considered for each inspectability classification. In addition, dynamic effects are discussed and a recommendation is made on an appropriate factor to cover the load increase in redundant members due to failure of adjacent elements.

Design of aircraft structures to meet the recommended design criteria requires the use of analytical procedures to predict the fatigue, crack growth and residual strength of damaged structure. These methods of analysis have been evolving over the past 30 years. For fatigue life prediction, the Palmgren-Miner method of analysis is most generally used. Various methods of analysis have been developed for predicting crack growth and residual strength. While there are no generally accepted crack growth or residual strength methods of analysis, most methods used are based on fracture mechanics theory.



Currently available analysis procedures applicable to the design of damage tolerant structure to meet the Section 3.4 design criteria are presented in Section 4.0. The applicability of the analysis methods and the results of the analysis must be tempered to a large extent by engineering judgement. In this respect, the methods presented reflect the approaches and procedures of the Lockheed-California Company. In many cases other analysis methods could be developed, or used, that would provide equally valid results.

A design study was performed to demonstrate the way the procedures presented in Section 4.0 can be used to develop structural designs to meet the criteria given in Section 3.0. The application selected for this design study was the lower wing surface of a fighter/attack aircraft. Some of the catastrophic failures mentioned above have occurred in lower wing surface structure, and therefore the design was expected to be affected by the damage tolerance criteria developed in this program. The effect of the criteria on the allowable design stress and structural weight was evaluated for three structural configurations made from two materials. The design study also had an important role in the many iterations that were involved in determining the final form of the design criteria.

## 2.0 SUMMARY AND CONCLUSIONS

Design criteria were developed (Table 3-4) that define a crack growth durability requirement and structural integrity requirements for three classes of inspectability; non-inspectable, NDI in-service inspectable, and walk-around inspectable structure. An acceptable design is one which meets the durability requirement and one of the structural integrity requirements. The durability requirements, and the non-inspectable and NDI in-service inspectable structural integrity requirements are in terms of a specified crack growth period from an initial damage size to failure. The structural integrity requirement for walk-around inspectable structure is in terms of a residual strength capability for a damage size that could be missed by a walk-around inspection.

The recommended criteria were developed using the information gained from reviewing existing criteria, inspection capabilities and concepts involved in a set of "ideal" criteria which were formulated early in the program. The aim of the "ideal" criteria was to equate the probabilities of failure for all structural and inspection classifications, thereby coupling fail-safe and safe life concepts in a rational manner. However, based on state-of-the-art analysis methodology, these types of criteria are presently impossible to implement.

The recommended criteria specify that the damage size that might be missed by a given type of inspection shall not grow to a critical size within a specified period of service time, i.e., some number of inspections or lifetimes. Based on an evaluation of available inspection data to determine the damage sizes that have a small probability of being missed during inspection, the following initial damage sizes were selected: a 0.25 inch crack for production inspections in areas away from design details, a 0.05 inch crack for production inspections in the vicinity of critical design details such as holes, a 3 to 4 inch crack for NDI in-service inspections and a 8 to 10 inch crack for walk-around inspections.



An application study was performed which consisted of designing the lower wing surface of a fighter/attack aircraft to meet the recommended design criteria. Design stress allowables and structural weights were established for three design concepts for each of two materials. Available analysis methodology was utilized to size the structure to meet the recommended criteria.

Because of the difficulty in calculating the crack growth period of complex non-inspectable structure starting with a small initial crack size, it is recommended that some representative testing be conducted to establish more reliable design stress allowables for this case. To perform the analysis a sequence of events has to be assumed as the crack progresses through and across various structural elements. Current state-of-the-art precludes performing this calculation. For other applications the growth sequence for cracks in a non-inspectable structure may be less complex and the level of confidence in the analysis procedure may be increased.

Structure can be designed to meet the recommended design criteria with little or no weight penalty. This conclusion is in part due to the fact that the two materials considered in this study have good crack growth and fracture toughness properties. It should be noted that none of the structural configurations considered met all the structural integrity requirements; and that when there was a weight impact due to damage tolerant design criteria, it was due to the durability requirement.

Based on the application study an initial damage size of 3 to 4 inches for NDI in-service inspectable structure appears to result in very short crack growth periods or alternatively, in very high weight penalties. Regularly scheduled depot inspections will decrease the number of occurrences of structural failures; however, unless depot inspection techniques are significantly improved, it would appear that regularly scheduled depot inspections cannot be solely relied upon to prevent catastrophic failures in aircraft structure.

Damage tolerant design requires analysis procedures for the various aspects of fatigue and fracture. Analysis procedures necessary for evaluating a design with respect to damage tolerant design criteria are presented in Section 4.0. These procedures include extensions to previously published compendiums of damage tolerant design analysis techniques. Some of these procedures may be unique to Lockheed, and it is recognized that other sets of analysis procedures could be assembled which would be equally adequate. For completeness, general procedures previously presented have also been included.

The analysis procedures described include methods for:

- (a) Predicting the initiation of crack in nominally undamaged structure due to cyclic loading (fatigue).
- (b) Predicting the growth of flaws and fatigue cracks under cyclic loading.
- (c) Predicting the combined effects of sustained loads and detrimental environments (stress corrosion cracking).
- (d) Predicting the residual strength of structure containing large cracks.
- (e) Predicting possible dynamic effects
- (f) Predicting stress intensity factors for use in (b) through (e) above.

The application study demonstrates that when applying fracture mechanics analysis techniques during the design of complex structures, many approximations and assumptions must be made (e.g., failure sequencing, part-thru crack to the thru-the-thickness crack transition, plasticity effects, overload retardation effects, etc.). Any suggested analysis procedure and design criteria must be tempered with that fact. Steps which add complexity or sophistication to the analysis at the expense of large amounts of computation may not improve the reliability of the result enough to be economically justifiable. In fact, to include such complexity may even detract from the design process by giving the resultant structure a false appearance of integrity.



### 3.0 ENGINEERING CRITERIA

#### 3.1 EXISTING CRITERIA

##### 3.1.1 Pressure Vessels

Fracture mechanics analysis was first applied to the design of rocket motor case structures. Some of the rocket motor case failures in the 1950's indicated a need for better control of flaws in high strength materials and consideration of the existence of these flaws in the design of pressure vessels. As a result, a leak-before-break criterion at stresses equal to the yield strength of the material was used as a basis for design. Proof testing was conducted at maximum operating pressures to ensure that flaws larger than the critical size did not pass non-destructive inspection. Reference 3-1 now recommends that pressure vessels should be designed to criteria which include the following:

- o "The maximum permissible initial flaw size in metallic pressure vessels shall be the largest flaw which cannot attain the critical flaw size within the required life span of the vessel."
- o "Each pressure vessel shall be subjected to a proof test. The proof-test factor shall be equal to, or greater than, one divided by the allowable initial-to-critical stress-intensity ratio."
- o "Analytical and experimental verification that the probable service failure mode is leakage rather than catastrophic failure shall be required when assurance of safe operational life cannot be provided by proof test."

##### 3.1.2 Civil Aircraft

For civil transport aircraft, the fail-safe concept was implemented into the structural design system to avoid catastrophic failures such as the Comet crashes in the early 1950's. On March 13, 1956, CAR 46 was amended to permit fail-safe strength substantiation as an alternate to fatigue substantiation. Since that time civil transport aircraft designed to this or similar criteria have had a good flight safety record.

Fail-safe design criteria given in FAR 25 (Reference 3-2) for civil transport aircraft specify load requirements in conjunction with damage criteria. The fail-safe strength requirement in Reference 3-2 states that "It must be shown by analysis,

tests, or both, that catastrophic failure or excessive structural deformation, that could adversely affect the flight characteristics of the airplane, are not probable after fatigue failure or obvious partial failure of a single principal structural element. After these types of failure of a single principal structural element, the remaining structure must be able to withstand static loads corresponding to "approximately 80 percent limit flight maneuver and gust loads. In addition the fail safe loads "must be multiplied by a factor of 1.15 unless the dynamic effects of failure under static load are otherwise considered." The intent of this requirement is to provide for sufficient damage tolerance so that fatigue cracks or other damage will be discovered at regularly scheduled inspection intervals before catastrophic failure occurs.

Fail-safe evaluation is also permitted for flight structure of rotorcraft (References 3-3 and 3-4) as an alternate to establishing limited or unlimited replacement times based on fatigue analysis and testing. In this case it must be shown that there is an extremely remote possibility a readily detectable partial failure will grow to catastrophic failure, provided structural inspections are performed as specified. Fail-safe substantiation in this case is based on demonstrating a safe crack growth period rather than demonstrating a residual strength capability.

### 3.3.3 Air Force Aircraft

Until recently Navy and Air Force aircraft were designed to MIL-A-8860 series specifications. All aircraft designed to these specifications must meet the fatigue requirements in accordance with Reference 3-5. Fail-safe requirements, as specified in Reference 3-6, are to be considered to the extent practicable for some types of military aircraft, generally transport and patrol type aircraft only. In the past fighter/attack type aircraft have not been designed to meet Reference 3-6 fail-safe requirements. Structures designed fail-safe according to MIL-A-8861 shall be capable of supporting 50 percent ultimate strength for flight loads following a fatigue failure or obvious partial failure of a single principal structural element.

Because of a number of catastrophic failures in service over the last several years, the Air Force has been developing revisions to the Air Force Structural Integrity Program (ASIP)(Reference 3-7) and to the Military Specifications which



outline damage tolerance considerations for the design of new aircraft structure. An in-depth review of fracture control procedures is given in Reference 3-8 with specific reference to the impact of inspectability, structural arrangement and material on proposed analysis requirements for safe crack growth. Reference 3-8 presents example safe crack growth requirements and illustrates how fracture mechanics analysis methodology can be utilized to select materials and establish design stress allowables to meet these requirements.

The criteria for the B-1 aircraft was the first formal attempt to apply crack growth requirements in addition to fatigue life and fail-safe strength requirements to the design of a new structure. Damage tolerance and fail-safe criteria for the B-1 bomber aircraft are specified in Reference 3-9 and discussed in Reference 3-10. The following lists some of the important aspects of these criteria.

- a. The load determining the damage size at the end of life is defined as the maximum service spectrum load or limit load, whichever is larger.
- b. The dynamic release of energy during failure of a single principal structural element due to the maximum spectrum load shall be taken into account for fail-safe structure, i.e., structure which is comprised of multiple load paths or incorporates crack stoppers which provide damage tolerant characteristics.
- c. Catastrophic loss of aircraft shall not occur within a specified inspection interval of  $1/4$  lifetime for readily inspectable damage tolerant structure. The fatigue life of the remaining structure after failure of a principal structural element shall equal or exceed  $1/4$  lifetime times a factor of 1.0 (leak-before-break) or 2.0 (otherwise).
- d. Crack growth from an initial flaw to failure of a principal structural element plus  $1/2$  fatigue life of the remaining structure after failure shall equal or exceed 1 lifetime for not-readily inspectable damage tolerant structure.
- e. It must be shown by fracture mechanics analysis that initial cracks or flaws will not propagate to critical crack length during one lifetime of the aircraft for structures that are not damage tolerant. The initial flaw size used for the analysis is a 0.15 in. x 0.45 in. surface flaw or a 0.15

in. thru-the-thickness flaw. To use a smaller initial flaw size the contractor must demonstrate NDI techniques with 95% probability and 50% confidence. The minimum flaw size must be  $> 0.05$  inches.

- f. Damage tolerance tests are required to demonstrate that the above requirements are met.
- g. Plane strain fracture toughness tests are required on all materials used where thicknesses permit.

Recently service life requirements for inclusion in MIL-STD XXX (USAF) "Aircraft Structural Integrity Program (ASIP)" have been drafted and are now in the approval cycle of the Air Force. These service life requirements, dated 15 October 1971, have been included as Appendix A and are summarized in Table 3-1. These criteria separate the structure into two basic classifications which are called monolithic "slow crack growth" structure and fail-safe structure. The criteria also separate the structure into three inspectability classes, i.e., walk-around, in-service NDI inspectable, and non-inspectable. In addition, instead of specifying a flaw size, the flaw shape parameter  $a/Q$  has been specified. Comments regarding these proposed criteria are presented below:

Monolithic "Slow Crack Growth" Criteria - The proposed ASIP criteria appear deficient in that they do not distinguish between the maximum flaw size  $(a/Q)_i$  that can escape detection at time of manufacture, and the larger maximum flaw size that can escape detection at in-service inspections. Since the criteria are based only on  $(a/Q)_i$ , flaws or cracks that exist in the structure initially may propagate to catastrophic failure between the regularly-scheduled in-service inspections.

This deficiency is illustrated in Figure 3-1 for the walk-around and NDI inspectable structure. Both curves illustrated meet the proposed ASIP requirements, i.e., that the maximum undetectable initial flaw size,  $a_i$ , shall not grow to catastrophic failure in one inspection interval for walk-around inspectable structure and two inspection intervals for NDI inspectable structure. However, the cracks are likely to go undetected until the crack sizes are  $a_v$  for NDI inspections or  $a_w$  for walk-around inspections. Therefore, catastrophic failures could occur in a matter of a few flights after reaching crack size,  $a_w$ . For the NDI inspectable case, the crack would very likely be missed at the second inspection and would grow to



TABLE 3-1 SUMMARY OF PROPOSED AIR FORCE SERVICE LIFE REQUIREMENTS

DESIGN CONCEPT	DESIGN CRITERIA	DESIGN REQUIREMENTS	
		DURABILITY (SAFE LIFE)	DAMAGE TOLERANCE
Monolithic "Slow Crack Growth"	Flaws or defects shall not attain the critical size required for unstable rapid crack propagation during the period of unrepai red service use.	The structure shall withstand four structural service lifetimes without fatigue cracking and one service lifetime without general corrosion or crack initiation due to mechanisms other than fatigue	Maximum undetectable sized flaws or defects shall not grow to a critical size within one inspection interval or two inspection intervals or one lifetime depending on degree of inspectability
Fail-Safe	Unstable crack propagation shall be locally contained through use of multiple loads paths crack stoppers and/or fail-free structural components		Subsequent to the failure of a single member or load path the maximum possible flaw size in the remaining structure shall not grow to critical size in one inspection interval, two inspections intervals, or the remaining life of the structure depending on the degree of inspectability.

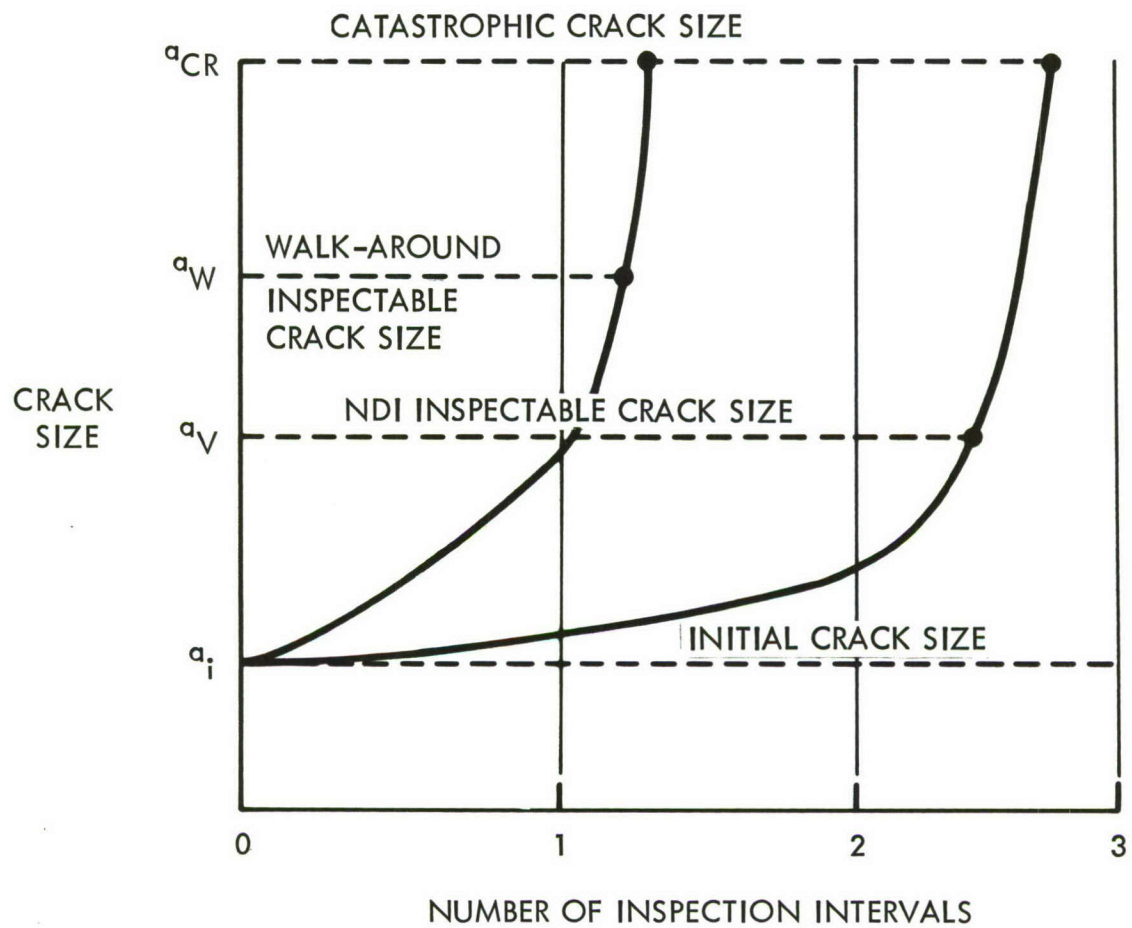


FIGURE 3-1. TYPICAL CRACK GROWTH CURVES FOR WALK-AROUND AND NDI IN-SERVICE INSPECTABLE STRUCTURE



catastrophic failure before the third inspection is performed. Therefore, the safe crack growth period for in-service inspectable structure should be related to the maximum flaw size that could exist in the structure after the in-service inspection, rather than related to initial flaw size. The NDI inspection capabilities are reviewed in Section 3.2.3 to aid in establishing in-service inspectability requirements and the size of cracks that can exist after a given type of inspection has been accomplished. These in-service inspection sizes should then be used as the starting crack size rather than the initial size established using production inspection techniques.

Fail-Safe Criteria - For fail-safe design the proposed criteria states that "subsequent to failure of a single member or load path (at the most critical time during the service life) the maximum possible flaw size in the remaining structure (i.e., the size at time of failure) will not grow to critical size (at limit or maximum spectrum load whichever is larger) in either one or two scheduled inspection intervals depending on the degree of inspectability" (i.e., walk-around - one inspection interval or 1/4 service lifetime minimum, and NDI - two inspection intervals). This means that the increase in stress due to the broken member must be accounted for as well as the growth of the initial flaw up to the time the member fails. The most critical time for a failure to occur is right after an inspection. The in-service inspectable crack growth requirements for the above criteria are illustrated in Figure 3-2.

These criteria are difficult to use in the preliminary stages of design since the amount of crack growth from the initial flaw and the increase in stress due to the failure of a single member are not known. As discussed above for the monolithic slow crack growth structure, the damage size that is likely to be missed by the in-service inspection should be used as the starting point rather than the initial flaw size plus some growth of the initial size. If a broken member is likely to be missed by an inspection then this should be included as part of the damage size.

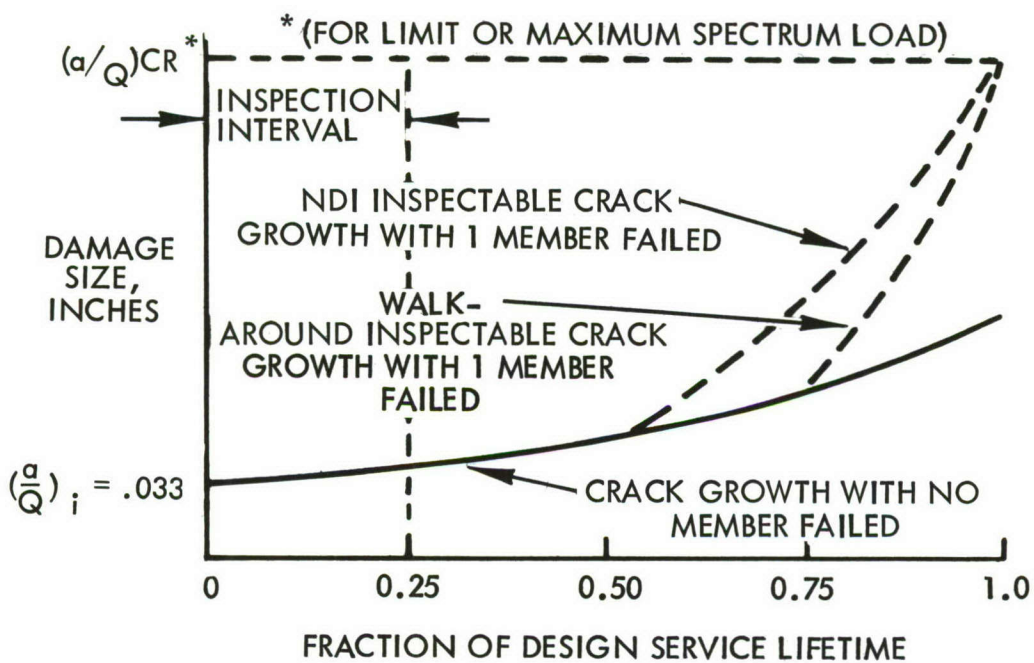


FIGURE 3-2. CRACK GROWTH REQUIREMENTS FOR FAIL-SAFE STRUCTURE WITH ONE MEMBER BROKEN. (REFERENCE APPENDIX A)

These fail-safe criteria are also very severe compared to the monolithic slow crack growth criteria. The period of unrepaired service usage for walk-around and NDI inspectable structures is the same for both design classifications, but the initial damage size that must be assumed is much larger for fail-safe structure. The damage size for fail-safe structure, as illustrated in Figure 3-2 must include the crack growth of the initial flaw  $(a/Q)_i$  plus a broken member, whereas for the monolithic structure only an initial flaw size has to be assumed. Therefore, the monolithic slow crack growth structure will in general be lighter than a fail-safe design.

Finally, the crack growth period from the assumed initial damage size (damage size that is likely to be missed by a given inspection) to catastrophic failure should be related to the inspection interval. If walk-around inspections are required every flight, then the period of unrepaired service usage should be only a few flights rather than  $1/4$  of a lifetime as specified in the Appendix A requirements. Similarly for NDI inspectable structure, the maximum size crack that is likely to be missed should not grow to a critical size in one inspection interval, which is of the order of  $1/4$  lifetime.

The Air Force criteria are still being reviewed and evaluated. The results from this and other studies as well as the experience obtained from the application to the B-1 aircraft will be used to modify and improve the criteria.



## 3.2 CRITERIA CONSIDERATIONS

### 3.2.1 Load Environment

For purposes of establishing damage tolerant criteria, four types of loadings need to be considered:

- (1) Cyclic, or fatigue loads
- (2) Sustained loads
- (3) Dynamic loads
- (4) Residual strength loads

#### Cyclic Loads

Present procedure is to require design verification for a specified loading spectrum followed by the application of some "life reduction factor". There are basically two ways to do this. One is to use a loading spectrum representative of average anticipated service usage and apply a factor to cover both scatter and the possibility of more severe usage. The other is to select a loading spectrum representing severe usage of the aircraft and use a smaller factor to cover only the possibility of statistical scatter. (The term "statistical scatter" here includes differences between analysis or test and actual service experience, second-order variations in load environment among nominally identical aircraft and missions, and inherent scatter in the fatigue or fatigue crack propagation phenomena.)

Cyclic loads data for various fighter, trainer and attack aircraft (Reference 3-11 thru 3-15) were briefly reviewed in terms of the variation in loads due to variations in usage severity and plotted in Figure 3-3. The variation in frequency of occurrence of a given load level among the published data is as much as a factor of 100. Of course, only a portion of this variation is attributable to differences in usage among nominally identical aircraft. For example, in Figure 3-3 a factor of 16 can be observed on the frequency of exceedance of a 4-G load in an F104C between an air-to-ground gunnery mission at high angle of attack and an air-to-air gunnery mission. Over a period of time, such load severity scatter tends to be averaged out and the differences in aircraft usage among the fleet would be something less than a factor of 16.



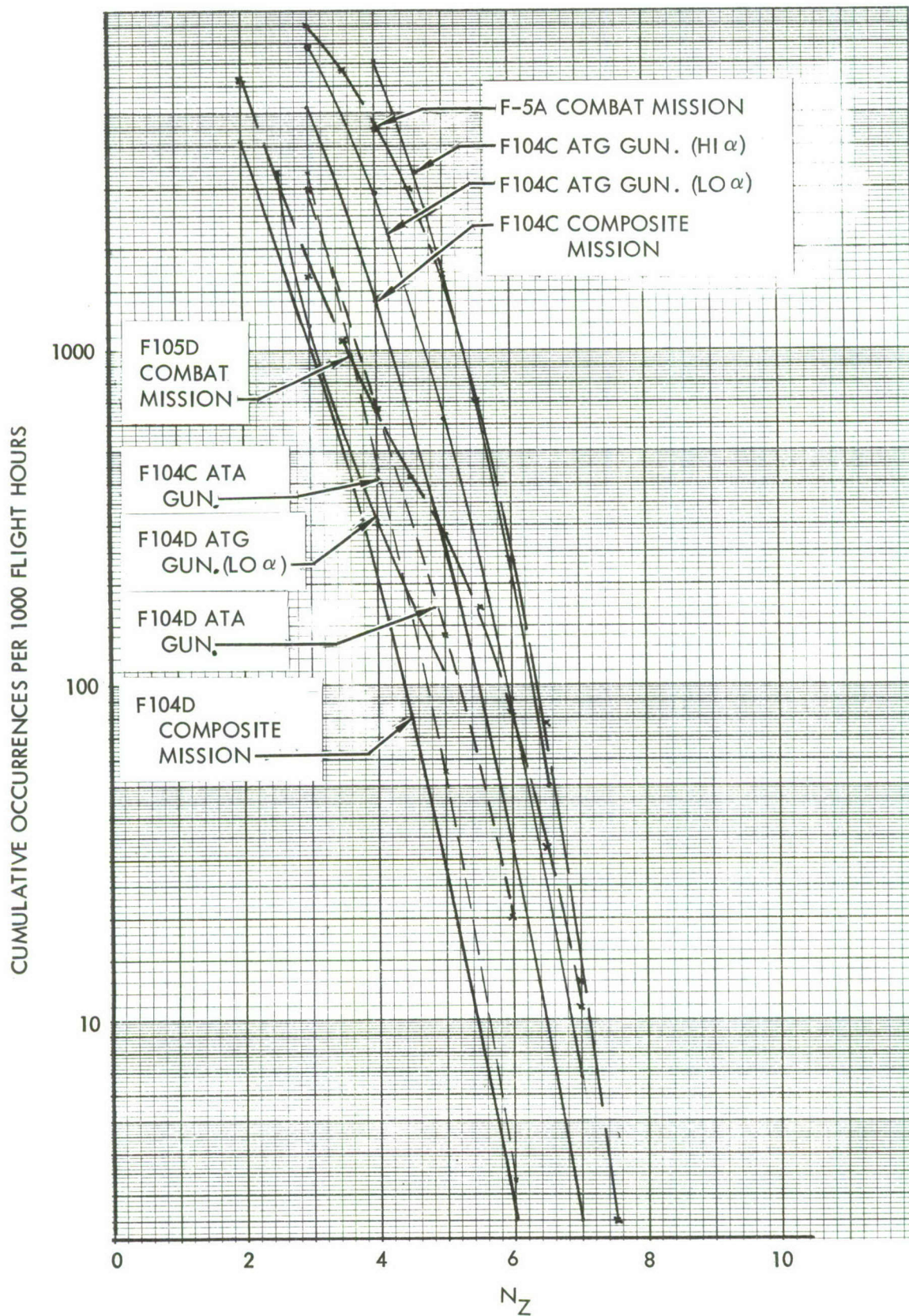


FIGURE 3-3. MANEUVER LOAD-FACTOR DATA FOR SEVERAL FIGHTER/ATTACK AIRCRAFT



## Sustained Loads

Several investigators have found evidence to indicate that time at load and slow loading rates can be significant considerations in crack growth analysis. It is well-known that crack growth in the presence of corrosive environment is time dependent, the crack growth rate per cycle being greater at lower cyclic frequencies. Wei and Landes (Reference 3-16) and Bucci (Reference 3-17) have found, as a first order approximation for a steel and a titanium alloy, that for fatigue cycling above  $K_{Isc}$  the crack growth rate  $da/dt$  due to accumulated time at load in a corrosive environment adds linearly to the crack growth rate due to simple cycling in a corrosion free condition. Below  $K_{Isc}$  Barsom (Reference 3-18) relates the extent of crack growth acceleration by corrosion to low loading rates. Possible decreased fracture toughness at low loading rates and low temperatures are discussed in Section 3.2.4 and Appendix B. Perhaps the most significant load real-time considerations have been some observations of partial or complete elimination of crack retardation effects in crack growth, as discussed briefly in Section 4.4.

Accelerated testing does not measure these real-time effects. Therefore, a study was conducted to identify loading rates, cyclic frequencies and length of time spent at various load levels typical of fighter aircraft.

Load factor vs. time records were reviewed for eighteen high load-factor pullout maneuvers. This work is summarized in Appendix C. It was concluded that real-time effects for this class of maneuvers could be characterized by specifying a cyclic loading frequency and a sinusoidal load-time curve:

$$N_Z(t) = N_{Z_{\max}} \sin [2\pi f t] \quad (3-1)$$

where  $N_{Z_{\max}}$  is the peak load factor for the maneuver and, for the data reviewed, the frequency,  $f$ , in cycles per minute is given approximately by

$$f = 1.2 N_{Z_{\max}}$$

The cumulative time in exceedance of any load factor for the life of the aircraft can then be calculated by the procedure developed in Appendix C.

### Dynamic Loads

The review of maneuver load flight test data conducted included consideration of maximum loading rates to assess possible dynamic effects. It was found that a significant increase in load required at least 0.1 second. The relationship of such loading rates to dynamic response of the structure is discussed in Section 3.2.2.

### Residual Strength Loads

The primary aim of damage tolerant design is to limit the probability of catastrophic failure of damaged structure before inspection and repair. Therefore, damage tolerant criteria should be related as directly as possible to that probability. The probability of catastrophic failure is determined by the probability of developing critical damage and the probability of exceeding the critical load for that damage. Clearly then, when establishing criteria for fail-safe load requirements, the important question is the likelihood of occurrence of that load.

Design limit load for commercial aircraft is seldom exceeded. The same is true of military transports. Fighters and trainers, however, will often exceed design limit load, even by as much as 25 percent. Therefore, while fail-safety at 80 percent of limit load may be adequate for transports, it is inadequate for maneuver-critical aircraft.

Analysis of VG and VGH data for a typical commercial transport has indicated that exceedance of 80 percent of limit load can be expected to occur once in 500 flight-hours. (For the aircraft considered, the average flight was 42 minutes, so 500 hours corresponded roughly to 700 flights). In contrast, data from 10 types of fighters and trainers (Reference 3-13) indicate that exceedance every 500 flight-hours of 112% of design limit load can be expected.

The somewhat conservative guidelines in Reference 3-19 show a similar contrast between military transport and fighters or trainers. The estimated once per 1000 hours load for transports is only about 80% of limit load, whereas for fighters and trainers it is about 125% of limit load.



The frequency of high loads depends upon the mission usage of the aircraft. Exceedance of limit load for a fighter is relatively likely during combat and combat training, and relatively unlikely for other missions (Reference 3-20).

Thus a fail-safe load criterion based strictly on percentage of design limit load for all types of aircraft or usages would not correlate in a simple manner to the probability of occurrence of that load. Therefore, the fail-safe load criterion for the design of a new aircraft should be based on a specified frequency of load occurrence for a representative mix of anticipated service missions.

### 3.2.2 Dynamic Effects

The effect of a dynamic load on a damaged structure can manifest itself in two distinct ways. One is the local amplification of structural loads at the damaged location; the other is the manner in which the material itself responds to the dynamic loading as a result of strain rate effects. It is important to separate these effects clearly since the load amplification aspects are analytical while the material response must be generated empirically. For strain rate sensitive materials, variations in pertinent material properties may exist. These are discussed in Section 3.2.4.

Load amplification aspects can be broken down into two distinct parts, the effect of dynamic loading on flawed structure and on unflawed structure.

Dynamic Factors for Structures with Flaws - At present, it appears that in a given structure the determination of dynamic factors in flawed structures must be determined from tests. In this case strain rate effects will be lumped with load amplification effects and generalization of test results will be difficult. A test is necessary since, for dynamic loads applied to cracked structure, the analysis cannot be handled simply. Ravera, Sih and Embley (References 3-21 and 3-22) have shown that for a finite crack there is an amplification factor of 1.23 simply due to reflections from the opposite crack tip. In addition, the dynamic amplification of the load due to the reflections from the local structure surrounding the crack must be considered. This is analogous to the fact that the effect of a stress concentrator (like a hole) on the stress intensity factor at the crack tip cannot be ignored. Since the failure criteria for a crack are

local criteria (as opposed to gross area ultimate stress type failure criteria), all local effects must be considered.

Dynamic Factors for Structure Not Containing Flaws - It should first be noted that the dynamic factor should be applied to the dynamic portion of the load only. Present Federal Aviation Agency requirements (Reference 3-2) include a factor of 15 percent on the overall static load. There appears to be no analytical justification (except a desire for conservatism) for having a factor applied to the overall static load. Elementary considerations indicate a maximum factor of 2.0 on the dynamic load. This factor may be derived on an energy basis, but this tends to obscure the actual source of the load amplification. Consideration of the details of a simple model, such as that shown in Figure 3-4 below, clarifies the conditions under which the factor will be 2.0 and demonstrates that for the cases which we are interested, it may be substantially lower.

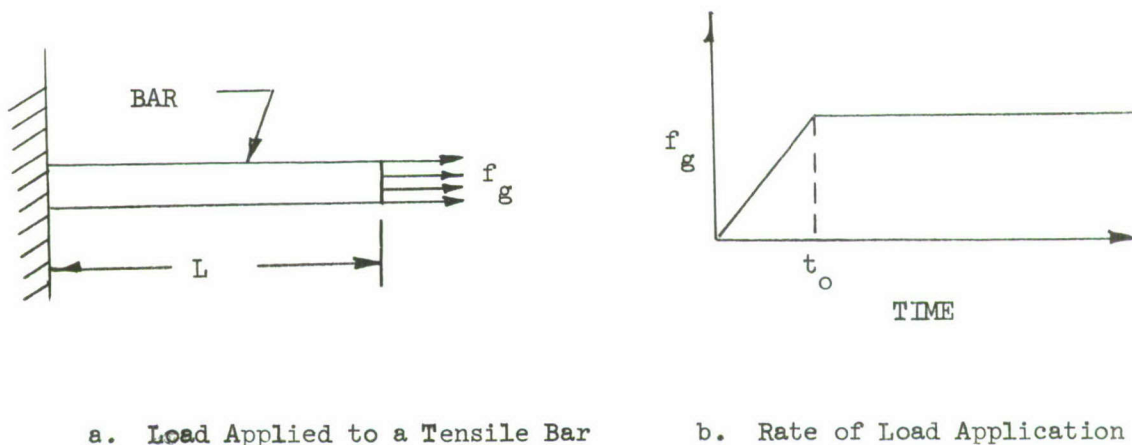


FIGURE 3-4 DYNAMIC LOAD APPLIED TO A TENSILE BAR

The model consists of a simple tensile bar which is subjected to a tensile load at one end. The stress amplification factor will be 2.0 when the following conditions are met:

1.  $t_0 < 2 \frac{L}{c}$ , where  $c$  is the stress wave velocity
2. The bar is rigidly supported.

The dynamic factor comes entirely from the reflected stress wave and to obtain a rational dynamic factor one must consider what affects the magnitude of this reflected wave.

Reflections from the fixed end are equal in magnitude to the initial stress wave and are of the same sign. Thus, reflections from the fixed end add to the initial applied stress; and if no other reflections occur, then the dynamic factor, which is applied to the nominal stress to give the peak stress, will be 2.0. This peak stress first occurs at the location of the reflection, the fixed end. On the other hand, reflections from the loaded right hand end will be of the same magnitude, but opposite in sign. Thus, reflection from the loaded end reduces the stress level. If the length of the bar is short or the loading rate slow, reflected waves from the loaded end will arrive at the fixed end even prior to the application of the maximum load to the right hand end. For sufficiently slow rates or sufficiently short bars these waves will essentially cancel out the wave from the fixed end; thus eliminating the dynamic effect. The solution of the equations governing the dynamic effects for the bar give the dynamic factor as:

$$\text{dynamic factor} = \left(1 + \frac{2 \frac{L}{c}}{t_o}\right), \text{ when } t_o \geq 2 \frac{L}{c} \text{ and one end is fixed.}$$

When  $t_o$  is less than  $2 \frac{L}{c}$ , the wave reflected from the loaded end arrives at the fixed end too late to reduce the peak stress and the dynamic factor is 2.0.

We may consider which loads should be treated as dynamic loads since condition "1" serves as a simple gage of whether a load is dynamic or quasi-static. It may be considered quasi-static if

$$t_o \gg 2 \frac{L}{c}$$

One may consider two types of dynamic loading:

- o external - due to maneuver, gust, landing, etc.
- o internal - due to failure of a nearby component.



For metals,  $c$  is on the order of 15,000 ft/sec. For significant increases in load the shortest value of rise time observed on fighters, and transports due to flight and landing conditions is on the order of 0.1 sec. Therefore, since continuous sections of the structure are considerably less than 750 ft., all significant normally encountered external loads may be considered quasi-static. Note also that a wave traveling that distance will be damped out considerably.

For failure of a component, it may be assumed that a crack propagates across a width "W" at a speed on the order of 20 percent of  $c$ . The shortest rise time then would be

$$\frac{W/2}{0.2c}$$

This would yield the following condition for assuming this to be a quasi-static process

$$W \gg .8 L$$

This condition will rarely be met. In fact, usually  $L > W$  (e.g., in a wing structure  $L$  corresponds to the span and  $W$  to the chord). Therefore a dynamic factor should be applied to the analysis when considering the failure of a component of a redundant structure.

To determine the magnitude of that factor, the condition of most concern is the fixed end condition. With any other condition, only a portion of the wave is reflected. It can be shown from elementary bar theory that when  $t_0$  is less than  $2 \frac{L}{c}$  and the support is modeled as another bar, the ratio of the reflected wave to the incident wave is

$$\frac{A_2 E_2 \sqrt{\frac{\rho_2}{E_2}} - A_1 E_1 \sqrt{\frac{\rho_1}{E_1}}}{A_2 E_2 \sqrt{\frac{\rho_2}{E_2}} + A_1 E_1 \sqrt{\frac{\rho_1}{E_1}}}$$

where the subscript 2 refers to the support and the subscript 1 refers to the bar element, and  $A$ ,  $E$  and  $\rho$  are the area, modulus and mass density, respectively.

The density-to-modulus ratio is essentially the same for all metals, and therefore the dynamic factor is primarily a function of the relative stiffness of the element and the support, and is approximately equal to

$$1 + \frac{A_2 E_2 - A_1 E_1}{A_2 E_2 + A_1 E_1}$$

For a fixed end,  $A_2 E_2$  is infinite and the dynamic factor approaches 2.0.

Good aircraft design will rarely contain locations where area changes exceed 25 percent. At those locations where substantial changes in stiffness do take place, joints will usually be bolted or riveted. Mechanically fastened joints have sufficient flexibility to make positive reflection impossible. Under these conditions a conservative estimate of the dynamic factor is

$$1 + \frac{1.25 - 1}{1.25 + 1} \approx 1.1$$

In a one dimensional dynamic problem, stress wave reflection can only occur at two surfaces. This tends to limit the maximum stresses. However, in a structure there is no limit to the theoretical value of the stress amplification. Many stress waves may interact and reinforce one another; thereby producing high values of stress magnifications. A pertinent question is whether this may make the above analysis unconservative.

First it is to be noted that we are considering the failure of an undamaged (uncracked) redundant element after the sudden failure of a nearby primary element in the redundant structure. In design considerations, the failure criteria applied to undamaged structure are simply ultimate strength criteria. The effects of stress raisers (except as they may reduce the net area) such as cutouts are ignored. This procedure has been proven by many years of experience to be reasonable and sufficiently conservative. Stress magnifications, due to the reinforcement of stress waves reflected from many surfaces, is in general a local effect as is the stress concentration at a cutout. Therefore, ignoring these local magnifications in dynamic problems should have the same degree of correctness as the similar procedure regarding cutouts. This procedure works primarily because local yielding takes place and dissipates the highly localized

effect. This yielding should be more effective in the dynamic case, since it will tend to damp out the stress wave. Therefore, it is felt that for design purposes, except where a dynamic factor may be particularly intense (in analogy with a crack as a stress concentrator), the factor of 1.1 is adequate.

This dynamic factor of 1.1 is substantially lower than the 15% FAA criteria since the 15% is applied to the overall static load. There is experimental evidence to support the lower factor. Tests were reported in Reference 3-23 on an aluminum wing box beam structure in which one of the aluminum skin panels was failed dynamically while the box beam structure was subjected to limit load. The structure did not fail due to the dynamic cut. The loads were then increased until the structure failed. The structural failure occurred after increasing the loads less than 5 percent. Similarly panel tests, where cracks were suddenly created (by "guillotining" a loaded panel) have been observed to fail after increasing the load less than 12 percent. These results, coupled with in-service failure experience of redundant structures lead one to accept this relatively low dynamic factor as realistic. Of course, if there are locations on an aircraft structure where large sudden changes in area or stiffness occur, the effects of these must be taken into account as described above.

The above discussion is an attempt to develop a rational factor for accounting for dynamic effects in fail-safe design. The conclusions drawn are consistent with experience. However, since corroborating data are limited, it must be emphasized that a definitive experimental program is required to validate the use of a single factor, such as the 1.1 value recommended, over a wide range of materials and types of structural configuration.



### 3.2.3 Damage Limits

Two types of flaw size distribution must be considered for establishing criteria; (1) the initial flaw size distribution in the structure when it is delivered to the customer and (2) the flaw size distribution in the structure after an in-service inspection has been made. Some of the considerations that will affect the flaw size distribution are illustrated in Figure 3-5. The initial flaw size distribution is unknown so NDI techniques are utilized to reduce the size distribution. The NDI method specified will have some minimum flaw size detectability depending on the technique used. However, no NDI method is 100% effective so flaws larger than the minimum detectable size will exist in the structure after the inspection has been accomplished (dashed curve in Figure 3-5). If the flaw size distribution after NDI is unsatisfactory, proof testing could be conducted which would provide an upper limit on the flaw size existing in the structure. Because of variations in material properties, proof loadings, etc., the upper limit cut-off cannot be precisely defined but is indicated as a range in Figure 3-5. The final flaw size distribution after proof testing would be indicated by the dotted line in Figure 3-5.

Flaws which make up the initial flaw size distribution of new aircraft components come from three major sources: those existing in the as-received mill product, those introduced during processing and those caused by handling or assembly. Mill products can contain defects such as inclusions or laminations, internal defects such as cracks and porosity, and surface defects such as pits, scratches and cracks. Processing operations such as machining, welding and plating are potential defect producers. Machining operations such as grinding, honing or drilling can produce cracks or cause a metallurgical transformation to a brittle phase. Welding can produce defects as a result of incomplete fusion, impurity segregation, transformed areas and residual stresses. Plating operations can lead to surface contamination, hydrogen embrittlement, and cracks in the coating layer that degrade the substrate. Handling operations during manufacturing and assembly can produce surface defects such as pits, scratches and cracks.

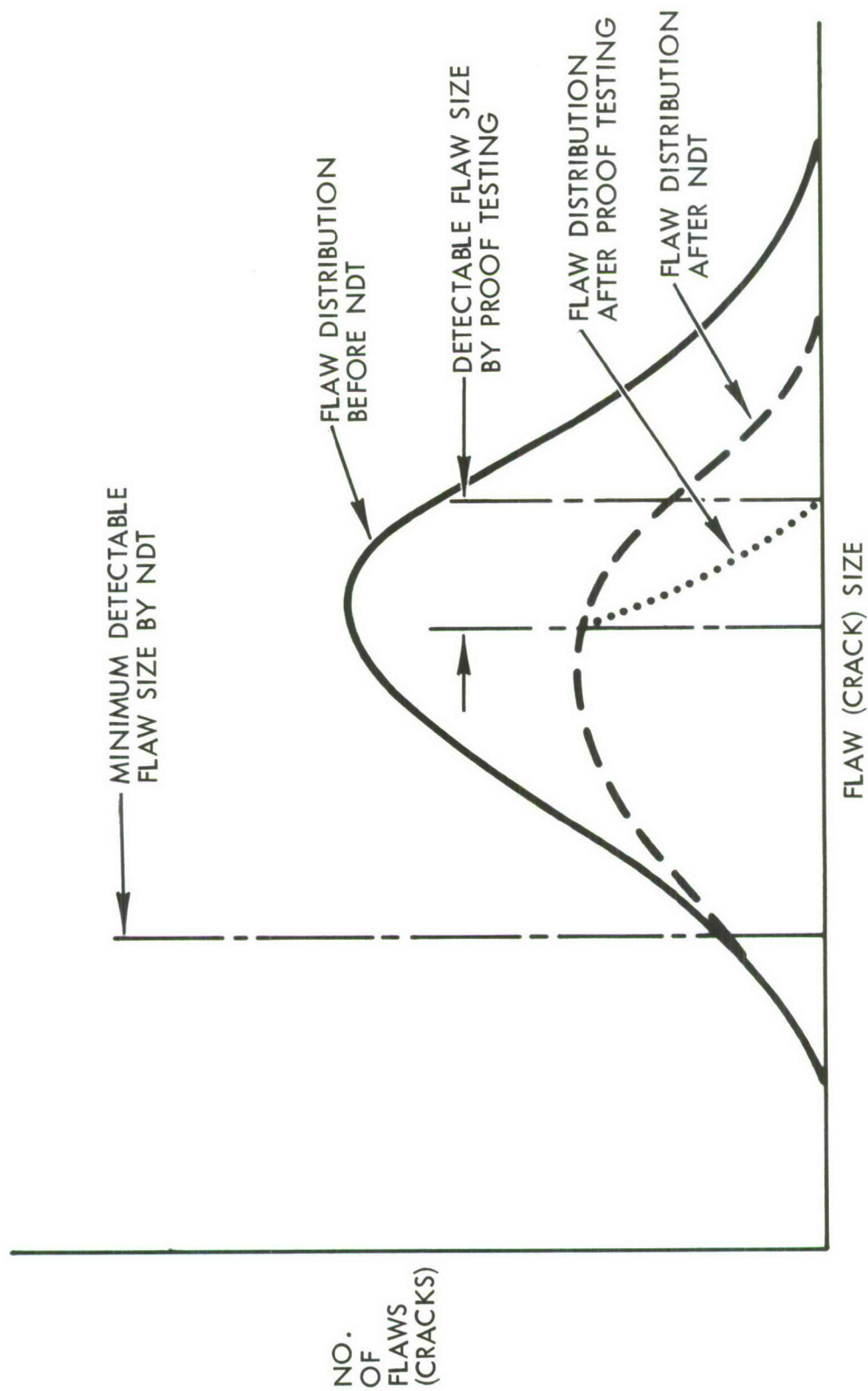


FIGURE 3-5 SCHEMATIC OF FLAW SIZE DISTRIBUTION BEFORE AND AFTER INSPECTION

Various investigators have been studying the flaw size detectability of various NDI techniques under production and laboratory conditions. The results of two studies conducted on flaw size detectability are summarized in Table 3-2 . These data show that minimum flaw sizes of the order of .03 inch can be detected by several techniques if the flaw location is known; however, flaw sizes of the order of 0.3 inch can be missed if the location is not known. One interesting result from these studies is that the visual detection method is about as good as some of the more sophisticated NDI techniques. Of course these results reflect the detectability as the result of one inspection. Parts are usually inspected several times during production and by more than one NDI method. Multiple inspections by more than one technique will probably improve the detectability limits. Other factors which will enhance inspectability are smooth or polished surfaces and the application of tensile stresses in the vicinity of the area being inspected.

Even though an aircraft structure may be relatively flaw-free when delivered to the customer, cracks can initiate and grow in-service for a number of reasons, e.g., as a result of improper use or maintenance, corrosion, fretting, and projectile impact. Therefore, in-service inspections are relied upon to detect the damage, from whatever the source, before it reaches catastrophic proportions.

The results from some in-service inspections were reviewed to determine the size of cracks that are likely to be missed after an inspection in the field or at a maintenance base. Figure 3-6 shows the results of an inspection for the lower surface of a transport wing. Crack lengths from 0.06 inch to about 3 inches in length were found. However, the data show that the number of cracks detected decreases for crack lengths less than 1 inch. This is contrary to what would be expected as shown in Figure 3-6. Therefore, it can be assumed that undiscovered cracks were present in the aircraft after the inspection was completed as indicated by the cross hatched area. This can be considered typical where unaided visual inspection techniques are utilized for the general surface structure (in these inspections the surface was viewed from one side only). These data indicate that approximately 10



TABLE 3-2      FLAW SIZE DETECTABILITY BY VARIOUS INSPECTION TECHNIQUES

<u>Damage Detection Method</u>	Minimum Inspectable Size (Inch)	
	<u>Damage Location Known</u> (Ref. 3-24)	<u>Damage Location Unknown*</u> (Ref. 3-25)
Visual	0.03 (Al., Steel)	--
Ultrasonics	0.05 (Al.) 0.03 (Ti)	0.25 (Al.) 0.2 (Steel)
Delta Ultrasonics	0.03 <sup>4</sup> (Ti)	--
Penetrant	0.03 (Al.) 0.025 (Ti)	0.25 (Al.) 0.35 (Steel)
Magnetic Particle	--	0.3 (Steel)
X-Ray	0.21 (Al.) 0.07 (Ti)	> 0.5 (Al., Steel)

\*Minimum detectability limit for 100% detection for all specimens in the program.

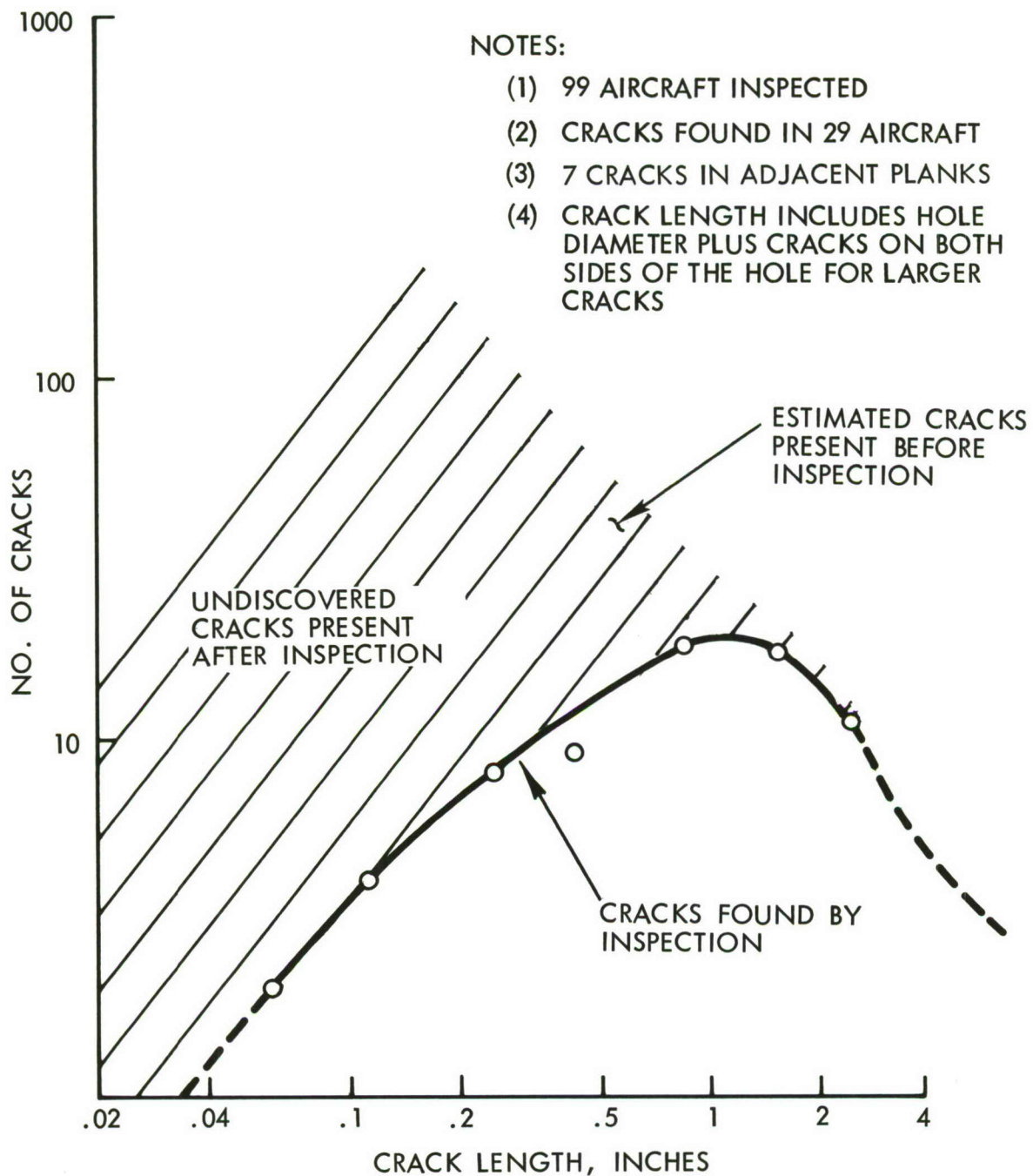


FIGURE 3-6. EFFECTIVENESS OF INSPECTION FOR LOWER WING SURFACE OF TRANSPORT AIRCRAFT.

aircraft had cracks 0.5 inches long or longer in the fleet of aircraft (99 vehicles) after the visual inspection was completed.

The occurrence of multiple cracks in the same vicinity of adjacent members is also of interest for redundant structures. The simultaneous propagation of cracks in adjacent members may nullify the added safety of redundancy. The inspection data in Figure 3-6 indicates that 7 out of 29 aircraft found with cracks also contained cracks in the adjacent planks (within 6 inches of the same spanwise wing station). Therefore, there is a high probability that if one member of a redundant structure is cracked, the adjacent member may also be cracked.

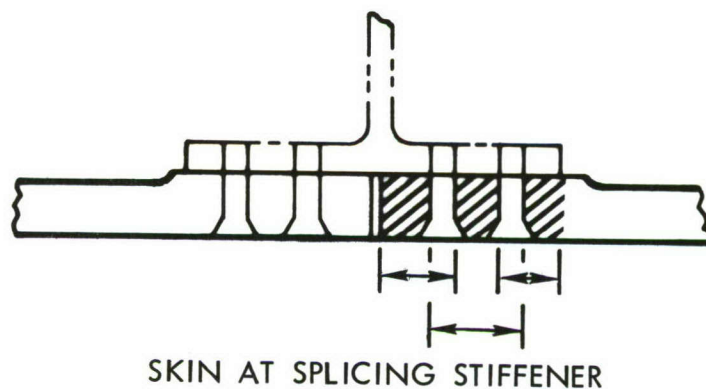
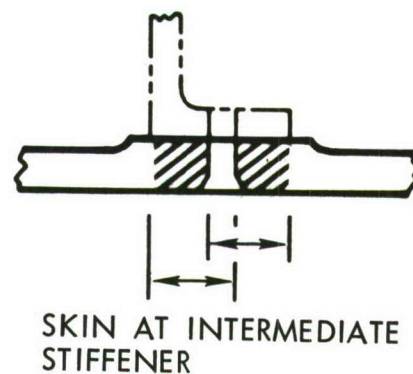
In Reference 3-26 the size of "detectable" cracks was defined in connection with the B-52G-H Wing Cyclic Test program. "Detectable" crack lengths were defined as one which would be found by close visual inspection with magnification during routine or depot level inspections. Typical examples of minimum "detectable" lengths in cracked stiffeners and skins are shown in Figure 3-7. Using the definitions in Figure 3-7, a survey was performed of the inboard wing lower surface to derive an average "detectable" crack length, which was found to be 0.625 in. The 0.625 inch average crack length is in general agreement with the data presented in Figure 3-6.

Crack data obtained from the C-130 inspection program were also studied. Figure 3-8 shows a histogram plot of the number of cracks versus crack length for all cracks discovered as a result of the first inspection on all aircraft. The crack lengths on opposite sides of the hole were combined, but the hole diameter was not included in the crack length measurements.

There were 30 cracks greater than 1-inch in length discovered on the first C-130 inspection. However, since the C-130 aircraft was fail-safe for fairly large cracks (> 6 in.) these longer cracks did not present a safety hazard during normal operation of the aircraft.

To get some idea of what size cracks might be missed on a given inspection, the repeat inspection data for cracks equal to or larger than 1-inch in length were studied. Figure 3-9 is a plot of the data obtained from the repeat inspections showing the relation between crack size and the flight hours since the previous inspection.





NOTE: DEFINITION OF DETECTABLE CRACK LENGTHS INDICATED BY ARROWS AND CROSS HATCHED AREAS

FIGURE 3-7. "DETECTABLE" CRACK LENGTHS (REFERENCE 3-25)

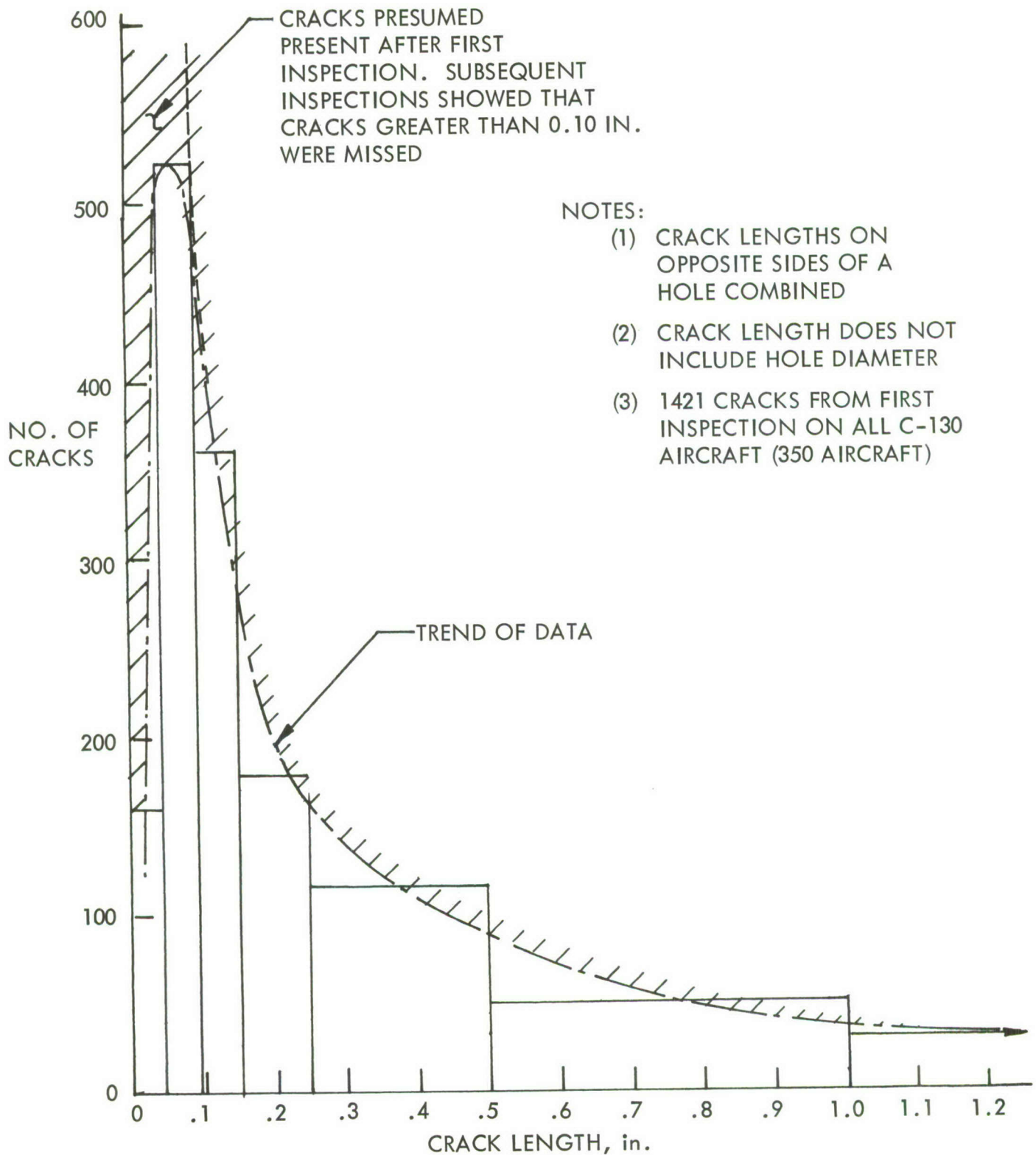


Figure 3-8 RESULTS OF THE FIRST INSPECTION FOR C-130 AIRCRAFT FLEET

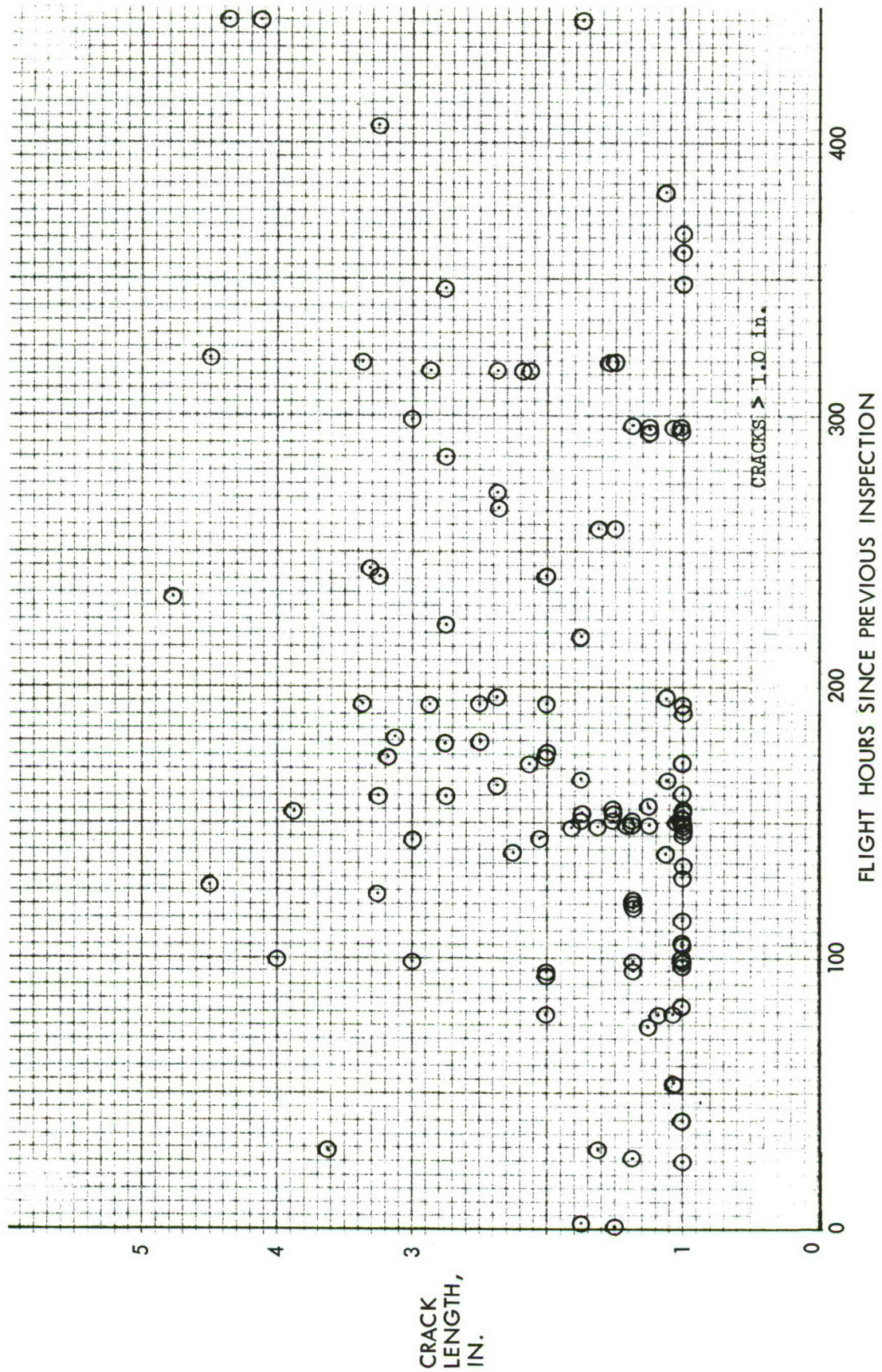


FIGURE 3-9 RELATION BETWEEN CRACK SIZE FOUND AND FLIGHT HOURS SINCE PREVIOUS INSPECTION FOR C-130 AIRCRAFT (350 AIRCRAFT)



A spot check of the crack growth rate indicated that one crack had a growth rate of approximately 1.5 inches per 100 flight hours with most of the data being below 1.0 inch per 100 hours. If 1 inch per 100 flight hours is assumed as the crack growth rate of the cracks that were missed, then the following size cracks were missed on the inspection previous to the one when the cracks were discovered.

<u>Crack Length Missed</u>	<u>No. of Cracks if Crack Growth Rate Was 1 in./100 Flight Hours</u>
3 - 3.3	3
> 2	7
> 1.5	11
> 1	21

These data indicate that cracks as large as 3.3 inches could be missed in a fleet of aircraft where rather extensive areas of the structure are inspected by visual inspection techniques.

One other source of data on cracks missed by in-service inspections are cracks that have caused catastrophic failures in service. The following tables lists two catastrophic failures that have occurred on fighter/attack type aircraft.

<u>Aircraft</u>	<u>Crack Size that Caused Loss of Aircraft, inches</u>	<u>Location</u>
F-100 (Reference 3-28)	1.5	Lower surface of wing center section *
F-104 (Reference 3-29)	0.75	Lower wing surface at the aileron servo adjustment hole at W.S. 80.7.

\* This area of the structure was not walk-around inspectable.

Since the F-104 aircraft received a walk-around inspection by the pilot before each flight and usually by the maintenance chief each day, this failure gives an indication of the crack size being missed on a walk-around inspection. Reference 3-28 also cites some cracks discovered in-service on F-100 aircraft ranging from 1/16 inch to 8 or 10 inches in length in areas that receive walk-

around inspections. Therefore, it appears that cracks of the order of 1 - 2 inches can very likely be missed on a walk-around with a possibility of missing cracks as large as 8 - 10 inches in length.

Based on the above data, the sizes of flaws or cracks that might exist in a given structure after inspection can be briefly summarized in the following table.

TABLE 3-3 SUMMARY OF FLAW-SIZE DETECTABILITY

Type of Inspection	Detectability Limit, in.	Maximum Flaw or Crack Size Missed by Inspection, in.
Visual, ultrasonics, penetrant or magnetic particle during production or in local areas of the structure during IRAN (where special attention is focused)	0.025 - 0.05	0.2 - 0.35
X-Ray	0.07 - 0.26	> 0.5
Visual during depot (IRAN) inspections	0.05 in.	3 - 4
Walk-around inspection	1 in.	8 - 10

The detectability limit is not too meaningful, since there is no relation between this limit and the size of cracks likely to be missed. For the various types of inspections to be meaningful, the initial assumed crack size should be of the order of the maximum crack size that can be missed by the inspection. Even then there is a small but finite probability that cracks greater than indicated in the above table would be missed by the various types of inspections. Therefore, if visual inspection techniques are to be the primary inspection method at IRAN, the initial crack size should be of the order of 4 inches or more. To rely on a walk-around inspection, the initial crack size would have to be approximately 8 or more inches long.

One reason why fail-safe structure for commercial aircraft have been so reliable may be because the fail-safe damage size is generally greater than 10 inches, and hence the structure will sustain cracks which can be detected by walk-around inspections or by maintenance personnel when they are working on the aircraft for various reasons.

The first and second row in the above table reflect limits in discoverability of cracks on plain structure having no design detail. No data exists for limits on the discoverability of cracks in the vicinity of holes. At hole locations the material can be viewed thru-the-thickness as well as at the surfaces. More importantly, holes receive special inspections as to surface finish, and dimensional tolerance. Therefore, one may assume that cracks significantly smaller than those in plain plate structure could be readily discovered in hole locations. Furthermore, the total probability is obviously remote that a crack significantly larger than the minimum detectable size but less than the maximum size that can be missed will be (1) introduced in fabrication at a hole, (2) located where the stresses will be highest, (3) oriented perpendicular to what will be the loading direction, and (4) not be discovered.

#### 3.2.4 Material Properties

Analysis and tests conducted to meet engineering criteria must account for variations in material properties due to the scatter of data and also account for factors that might significantly affect the material properties. The discussion in this section will deal mainly with fracture toughness and crack growth properties since static and fatigue properties are currently covered by MIL-HDBK-5B and military specifications.

##### Static Allowables

"A" and "B" values in MIL-HDBK-5B are used for final sizing of aircraft structure. The "A" and "B" values are defined as the mechanical property value above which 99% ("A") or 90% ("B") of the population values is expected to fall, with a confidence of 95%. Graphical or chi-squared tests for normality of distribution are usually made. Sufficient tensile tests (300 samples minimum) are conducted to establish "A" and "B" values for each heat treat and material thickness used. Procedures for relating other properties, such as shear or bearing allowables, from smaller sample sizes are given in Chapter 9 of MIL-HDBK-5B.



## Fatigue Allowables

Constant-life diagrams given in MIL-HDBK-5B are based on typical (50 percent probability) values because generally there is an insufficient amount of data available to develop higher probability diagrams. Fatigue analyses are usually conducted using best fit S-N data, and life reduction factors are applied to the analyses to achieve the desired degree of reliability. A life reduction factor of four is currently required for Air Force Aircraft. This is considered adequate provided that the constant-life diagrams used are applicable for the materials and processes actually used on the aircraft. Full-scale fatigue tests are also required to substantiate the design. Localized areas that develop fatigue crack problems in the fatigue test can usually be resolved by improvements in design detail rather than by adding additional weight to the structure.

## Residual Strength Allowables

### (1) $K_{Ic}$ Values

Tentative test methods for obtaining valid  $K_{Ic}$  data are given in Reference 3-29. The data obtained from these tests will provide  $K_{Ic}$  values that can be used for the design of fracture critical parts. The data presented in Appendix B for Ti-6Al-4V and 7075-T6 aluminum were not obtained using the type of specimen recommended in Reference 3-29; however, the data obtained on the four-point notch bend specimen should be approximately the same as that obtained from the three-point notch bend specimens recommended in Reference 3-29.

Plane strain failures usually originate at small flaws with little slow stable growth and no prior warning. Fracture control for the presence of small flaws relies almost entirely on the material fracture toughness properties. Therefore, the  $K_{Ic}$  values used for residual strength design should be established using guaranteed minimum values until sufficient data are available to establish Air Force approved A or B values.

Statistical analysis of  $K_{Ic}$  data for titanium and aluminum alloys in Appendix B exhibit a log-normal distribution. In all the data examined, the MIL-HDBK-5B B-basis values are in close agreement with the so called guaranteed minimum values based on log-normal distribution and sample standard deviation. It is desirable

to derive statistically reliable  $K_{Ic}$  values based on known probability distributions and known population standard deviations for the material. However, sufficient data are not available to determine the distribution and population standard deviation, and it would be very expensive to develop the data.

As shown in Appendix B, the  $K_{Ic}$  values can be affected by both temperature and loading rate. The values used for design should be applicable for the temperatures and loading rates likely to be encountered in service. Other factors that could affect the fracture toughness properties should be investigated.

In establishing  $K_{Ic}$  values for design, the effect of material processing on the fracture toughness properties should be fully explored. For example, the  $K_{Ic}$  values for D6AC material discussed in Appendix B were quite sensitive to the quench rate. Therefore, sufficient tests should be conducted over the full range of processing variables to be sure that some step in the process does not have a detrimental effect on the  $K_{Ic}$  value. The trends and relationships investigated should include the effects of heat-to-heat variations, and a reasonable range of heat treat and process practices ( $\pm$  °F,  $\pm$  hours, etc.). Since there is no known relationship between fracture toughness properties and tensile properties, the effects of material processing will have to be investigated using fracture toughness tests. In fact, fracture toughness tests cut from prolongations of fabricated parts may be required to provide adequate assurance that the  $K_{Ic}$  values used for design are equaled or exceeded in fracture critical areas of the aircraft structure.

## (2) $K_c$ values

Currently  $K_c$  data are obtained on rather large (24 inch x 72 inch or larger) center-cracked panels. The expense of conducting these tests prohibits obtaining sufficient data to establish A or B-basis allowables for the  $K_c$  values. Smaller, less expensive tests can be used to obtain R-curves; however, the use of R-curves for sizing damage tolerant structure is not generally accepted at this time.



Fifty percent probability values were used for the design of damage tolerant structure where reinforcements or redundant members act as crack stoppers. As shown in Section 4.6.2, design curves were obtained which provide conservative predictions when compared with residual strength tests conducted on aircraft structure.

For monolithic structure, reliance is placed on finding the crack by periodic inspections before the crack reaches catastrophic proportions. In the case of monolithic structure, the inspectable or critical crack size is directly related to the  $K_{Ic}$  fracture toughness properties of the material. Since it does not seem practical to obtain A or B-basis  $K_{Ic}$  values, some factor should be applied to the fail-safe design load or to the  $K_{Ic}$  allowable to achieve the desired degree of reliability. In the current study the 50% probability  $K_{Ic}$  values were reduced approximately 30% to give the equivalent of B-basis  $K_{Ic}$  values as discussed in Section 5.3.

#### Fatigue Crack Propagation Allowables

Current testing for fatigue crack propagation uses primarily center-cracked panels or compact tension specimens. Both specimen types are relatively inexpensive to test and replicate data can be obtained. Like fatigue, typical, or best-fit values of crack growth rate vs. cyclic stress intensity are utilized in analysis, and some reduction factor may be applied to the analysis to attempt to account for uncertainties in service environment and usage. Unlike fatigue there is no commonly agreed-upon reduction factor for fatigue crack propagation analysis. It is fairly clear that the crack propagation process has relatively low scatter ( $\pm 20$  percent on crack growth rate within a controlled set of tests) compared to factors of  $\pm 200$  percent for fatigue. Therefore, the life reduction factor for crack propagation should be substantially lower than that for fatigue and may be as low as 1.0 if a conservative fatigue spectrum is used.

As in fatigue, some full-scale spectrum crack propagation testing should be required if long crack growth periods are considered important to the safety and durability of the aircraft.



For structures subjected to large numbers of cycles, the life of an initially damaged structure may be primarily determined by the initial crack length and the basic fatigue crack propagation material properties. The size of the crack at catastrophic failure, and consequently the critical fracture toughness often play relatively minor roles. This is due to the fact that much of the life for high cycle life structures is spent at crack sizes very near the initial crack size. Therefore, for structural configuration - load spectrum combinations where normal material property scatter in the  $K_{IC}$  and  $K_{IC}$  will not affect the life significantly, the extra expense of developing A or B-basis values of fracture toughness is not warranted. In these cases typical values are adequate for design purposes. However this does not mean that the actual material used in the structure need not have controlled toughness values. It simply means that for the verification of an acceptable design, the use of A or B-values is not always necessary.

### 3.3 CRITERIA DEVELOPMENT

#### 3.3.1 INTRODUCTION

Although a number of damage tolerant design criteria have been developed in the past, no rationale has been given for their form and no basis has been given for values of various factors. This has no doubt often been due to the constraints of the document in which the design criteria have been presented. This report does not suffer from that type of constraint. It is recognized that any criteria proposed will include to some extent the prejudices and opinions of the writers and that before being adopted by others, modifications may be necessary. In addition, with the passage of time, information will become available which will enable rational decisions to be made, where initially the criteria may have been based on engineering judgments. For these reasons it is felt that the most valuable contribution which could be made would be the development and exposition of a rational framework for such criteria with an emphasis on explaining the reasons for the engineering judgments that must be made.

With this goal in mind, logical, reasonably consistent damage tolerant design criteria, based upon the aim of having criteria which contained equal probabilities of failure for all acceptable structural and inspection classifications, were developed early in the course of this study. It was anticipated that during the application phase of the program, necessary modifications to the initial criteria would become apparent. This was not the case. It was discovered that to develop and use non-arbitrary, rational criteria, quantities that are presently impossible to determine would need to be known. However, the development of these initial "ideal" criteria did enable the determination of the elements that make up criteria and an examination of their inter-relationships to be made. Conceptually the initial "ideal" criteria have merit and can serve as a goal in the development of criteria that can be utilized with the technology levels presently available. For this reason the initial "ideal" criteria which were developed are presented.

First, consider what must be done to develop approximately equivalent criteria for all types of structures. The criteria in References 3-7 thru 3-10 classify the structure according to both configuration and inspectability. The configuration classifications are identical or similar to the following:

- I Redundant Structure
- II Primary Structure with Crack Stoppers
- III Monolithic Structure

The inspectability classifications are identical or similar to the following:

- A. Walk-around inspectable, i.e., damage that is obvious within a small number of flights. An example of this type of structure includes locations where fuel leakage is probable.
- B. NDI in-service inspectable, i.e., by visual or NDI techniques.
- C. Non-inspectable.

While the inspectability classifications are a necessary part of damage tolerant criteria (since inspectability determines the damage sizes to be considered), configuration classifications are not. In fact it is desirable to have criteria which do not distinguish between configuration classes. This is not only because the criteria will be more general, but because it will then be easier to develop criteria which treat structures equally. As a result, when a particular structure is evaluated in comparison to another, the criteria themselves will not prejudice one structural class over another. Therefore, an attempt is made to develop criteria without specific reference to a particular structural class. However it is convenient, when developing the criteria, to consider particular structural configurations as examples. In addition, it will be shown that due to practical considerations it is necessary to distinguish between structural classifications when applying the criteria.

The basis for the initial criteria was the fact that the probability of catastrophic failure actually occurring will be equal to the product of the probability of a damage of a given size existing and the probability of a sufficiently large load occurring to cause a catastrophic failure with that damage present. This implies that for each damage tolerant component one must be concerned with load level and with the length of time significant damage may be present. While this concept is significant, particularly since it ties together "fail-safe" loads and life, the application of this concept appear to be impossible at this point in time as discussed below.



In an attempt to apply the above probabilistic concepts some inconsistencies were found in the approach. They have been included in the following discussion for two reasons. It was found that other investigators (e.g., References 3-30 and 3-31) dealing with similar problems encountered similar inconsistencies, and it is felt that this is the simplest way of demonstrating the difficulties in utilizing the above concepts as well as demonstrating what must be done when that approach can no longer be strictly adhered to.

### 3.3.2 Initial "Ideal" Criteria

#### (1) Development

To provide a reference for discussion, consider structure of inspectability Class B (NDI in-service inspectable). Additionally assume that a damage ( $a_0$ ) is initially present which is the size of the largest flaw that could be missed during a regularly scheduled inspection. (Some probability and confidence level must actually be defined here.) This last assumption is appropriate for all inspection intervals after the first. It may be practical to assume a smaller damage size after the initial fabrication inspection.

Schematic plots of damage size versus time (or flights) are given in Figure 3-10. The curves in Figure 3-10 represent a deterministic process and may be assumed to be developed from an analysis, a single test, or an average of several tests. In each case the appropriate criteria will contain a relationship between  $\Delta t$  (time to grow a crack from  $a_0$  to the critical size) and the inspection interval,  $I$ . This relationship will depend on the statistical variability of the material properties, actual service spectrum, etc., as well as the probability of error or deviation in any of the input information ( $a_0$ , loads, etc.). If all these probabilities are equal and since it is assumed that the discovery of a crack of size  $a_0$  or larger is almost a certainty; then the probability of a flaw greater than  $a_0$  existing in each class of the structure will be equal if  $\Delta t$  for each structural class is the same. This does not mean that each of these structures are equally safe. The probability of failure for each of these structures as a function of time, is schematically indicated in Figure 3-11. In each case the probability of failure corresponds to the probability that load exceeding the critical load for that damage level will occur.

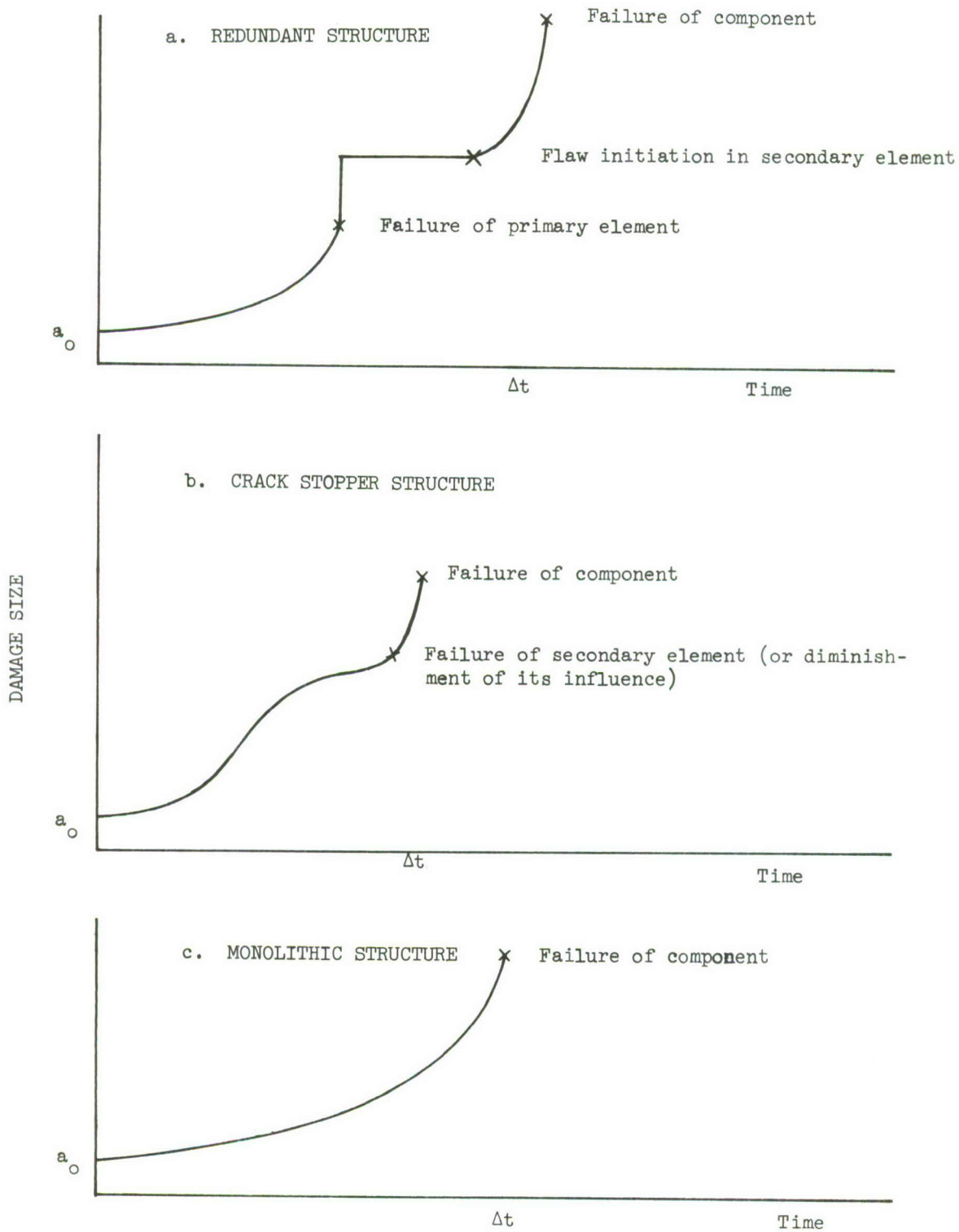


FIGURE 3-10 DAMAGE ACCUMULATION

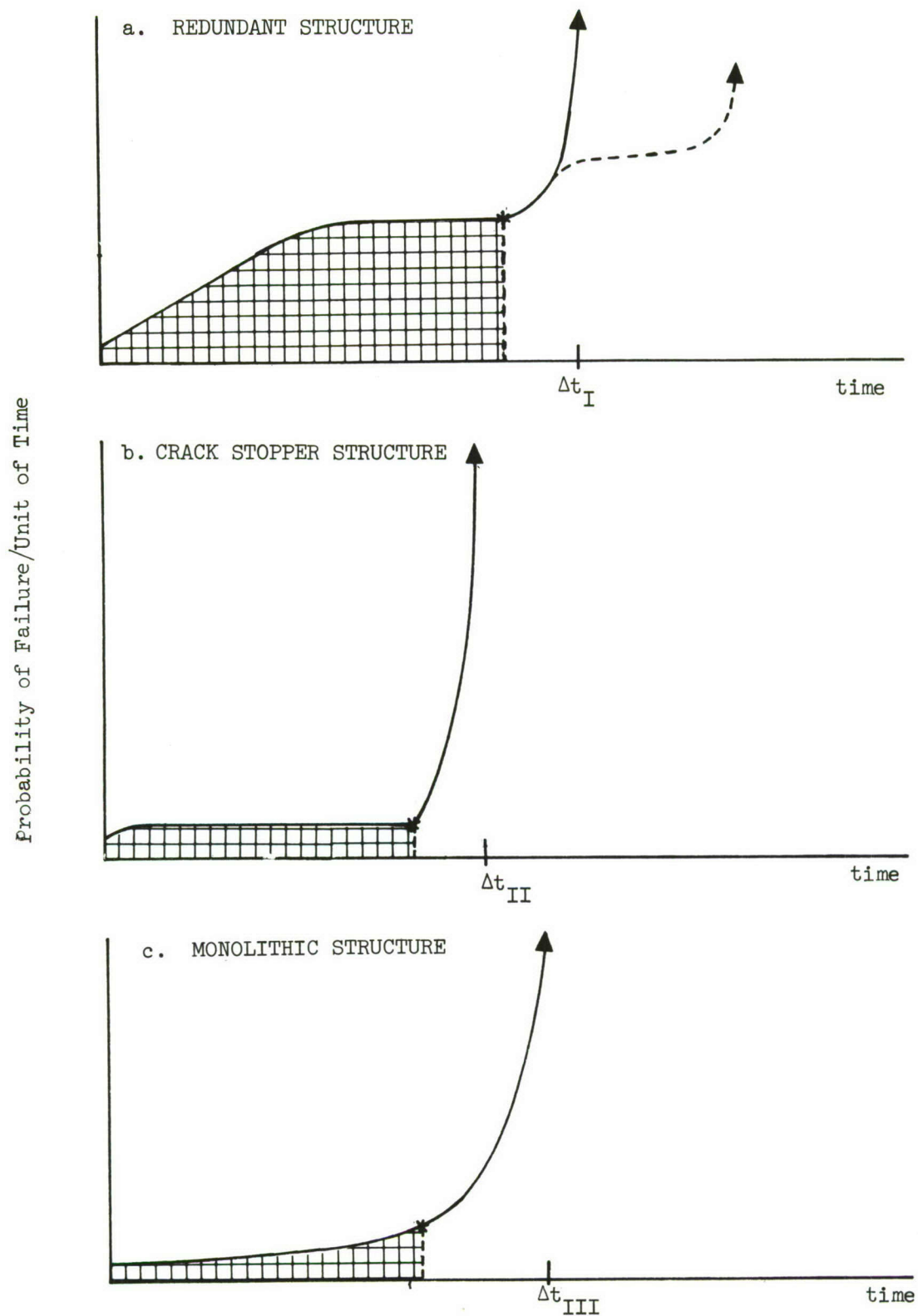


FIGURE 3-11 VARIATION OF PROBABILITY OF FAILURE



For redundant structure, this probability of failure increases as the crack grows across the initially damaged element, remains constant during the incubation period for forming a crack in the adjacent element, then increases rapidly as the crack grows across the second element. Multiple redundant structure will exhibit a series of plateaus, as indicated by the dotted line in Figure 3-11a. In Figure 3-11b, a constant probability of failure over much of the life is indicated. This corresponds to the load level required to cause failure when the damage is slightly beyond the crack stopper. In monolithic structure (Figure 3-11c), the probability of failure increases slowly at first and then accelerates rapidly toward the end of the life. This latter characteristic is present in all three classes of structure.

The aim of an inspection procedure is to insure discovery of the damage prior to the time of rapid rise in the crack growth curve, i.e., prior to the starred (\*) positions in Figure 3-11. The probability of failure during this period of time is indicated by the cross-hatched areas in Figure 3-11. Since the rise of the curve is very rapid after  $t^*$ , there is little difference between  $t^*$  and the final failure point, therefore no distinction will be made between these two points. It is desired that the criteria ensure that the value of the cross-hatched area is in each case less than some appropriate value (although the actual meaning of this value in terms of probability of failure will never be known). For reasonably uniform criteria, the areas in Figure 3-11 for Structures I, II and III should be the same order of magnitude. Note that since the reliability for this process is anticipated to be high in terms of confidence levels (i.e., .999...), variations in failure probability within the same order of magnitude will only affect the last significant figure of the overall structural reliability. Actually it is not the area under these particular curves that is of interest. As mentioned previously, these curves were constructed by assuming that the phenomena affecting these curves were known. An estimate of the maximum errors in this curve should be made, and the criteria should be based on a shifted curve incorporating the estimate of error. Consistent criteria would fix the areas under the shifted curve. It is impossible to develop a simple rule for insuring that these areas are all within an order of magnitude. A reasonable approximation to the area will be the product of the smallest estimate of  $\Delta t$  and the probability of occurrence of the load that will cause

catastrophic failure when the damage is at an appropriate fail-safe damage size. (initially it was thought that the mid-life damage size was appropriate. See Figure 3-12).

Thus the fail-safe load, designated as the load that the structure must support while the fail-safe damage is present, should be chosen such that the product of its anticipated frequency of occurrence and the smallest estimate of  $\Delta t$  is a constant, for all structural and all inspectability classifications.

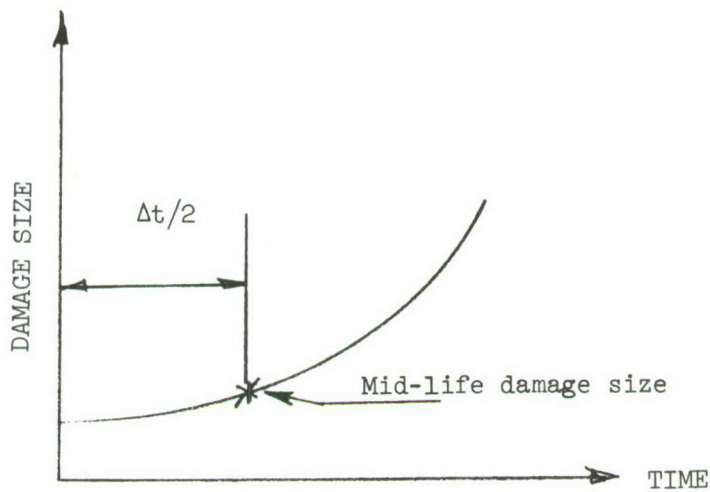
## (2) Discussion

The above criteria appeared to be a good approach up until it was applied during the application study portion of this program. Preliminary checks (mainly on the residual strength aspects of the criteria) failed to show the inconsistencies that were present.

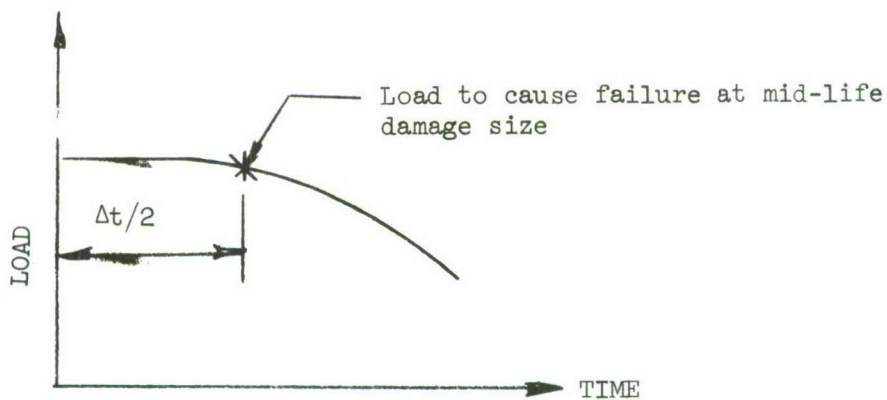
The fundamental inconsistency in the above approach involves the emphasis on the cross-hatched areas of Figure 3-11. In attempting to apply the initial "ideal" criteria it soon becomes apparent that, since the maximum spectrum load determines the damage size at the end of life (i.e., catastrophic failure due to the application of the maximum spectrum load would occur at  $\Delta t$ ); no load in the applied spectrum is large enough to cause catastrophic failure prior to the crack reaching the critical damage size (up to the starred point in Figure 3-12). Thus even an estimate of the probability of failure in this region requires an extrapolation of the spectrum to the less than once-per-lifetime loads. Therefore, based on our current knowledge of frequency of load occurrence data, the probability of failure cannot be calculated during the period of time indicated by the cross-hatched areas in Figure 3-11.

The inability to utilize probabilistic concepts for crack propagation and failure analysis to produce rational damage tolerant aircraft design criteria arises for a number of reasons. Consideration of descriptive equations for constant amplitude crack growth will aid in examining the basic problems associated with the above approach for the more complex loadings which occur in aircraft usage.

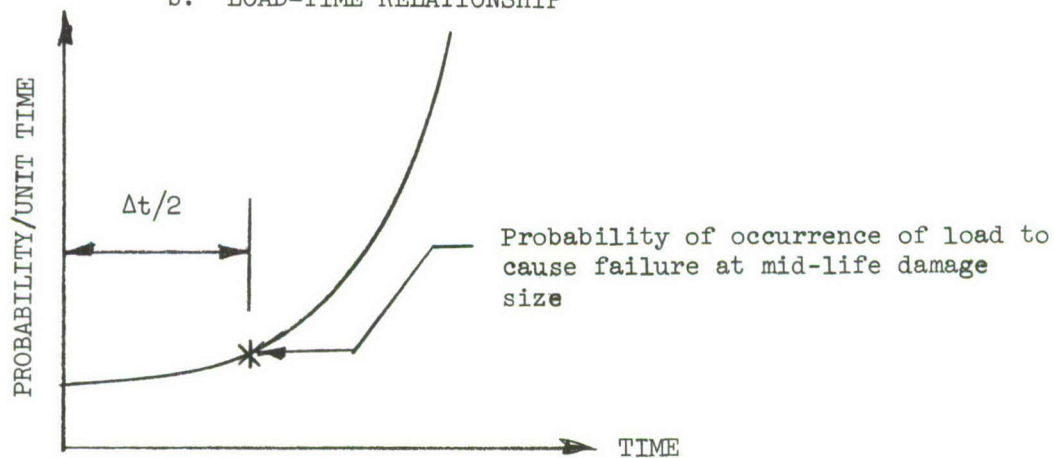
For constant amplitude loading (zero range ratio) crack growth behavior where a power crack growth law



a. DAMAGE-TIME RELATIONSHIP



b. LOAD-TIME RELATIONSHIP



c. PROBABILITY-TIME RELATIONSHIP

FIGURE 3-12. FAILURE ANALYSIS HISTORY



$$\left(\frac{da}{dN} = CK^m, K = \lambda f_g \sqrt{\pi a}\right)$$

is applicable, the relation between life, (N), initial crack size ( $a_o$ ) and final crack size ( $a_f$ ) is:

$$N = \left(\frac{2}{m-2}\right) \left(\frac{\pi^{m/2}}{C f_g^m \lambda^m}\right) \left[ \frac{1}{a_o^{(m-2)/2}} - \frac{1}{a_f^{(m-2)/2}} \right] \quad (3-2)$$

for the simple structural case of  $\lambda = \text{constant}$ .

Note that, since  $m$  is invariably greater than two and if  $a_o$  is sufficiently small, the final crack size will not affect the life significantly. This equation can be rewritten in terms of  $K_c$ , the critical value of  $K$  as

$$N = \left(\frac{2}{m-2}\right) \frac{\pi^{m/2}}{C f_g^m \lambda^m} \left[ \frac{1}{a_o^{(m-2)/2}} - \left(\frac{\lambda f_g \sqrt{\pi}}{K_c}\right)^{m-2} \right] \quad (3-3)$$

For a given initial crack length, the probability of attaining a given life will be a function of the statistical variations in  $C$ ,  $m$ ,  $K_c$  and  $f_g$ . For variable amplitude loadings, the basic equations used to represent fatigue crack growth behavior may be somewhat different, however the trends produced by the variables will be the same. Thus it may be seen that in general the statistical variation in  $K_c$  is not significant for cases where  $a_o$  is small. Also one may observe that for larger values of  $m$ , variations (or errors) in  $\lambda$ ,  $f_g$ ,  $a_o$  and  $K_c$  are much more significant than they are at lower values of  $m$ .

A power law is at best only an approximation of fatigue crack growth behavior over a limited range of stress intensity factors and crack growth rates. The general behavior may be thought of as a series of power laws each valid over a particular range of stress intensity factor, with a particular  $m$  and  $C$  for each range. For large values of the stress intensity factor (approaching  $K_c$ ), the value of  $m$  increases substantially above the value which characterizes crack growth behavior over the ranges which are appropriate for the major portion of the crack growth period for cracks in aircraft components. Therefore variations in the variables  $\lambda$ ,  $f_g$ ,  $a_o$ , and  $K_c$  have a more significant effect on life predictions when only higher values of the stress intensity factor are used for the prediction.

In the prediction of lives for aircraft structure, the quantity that is known least reliably and which is subject to the widest variability from aircraft to aircraft within the same fleet is the set of applied loads. This is not true in many other applications where crack propagation at high stress intensities is considered. Pressure vessels used in space and missile applications are examples where the stresses are known fairly well. Therefore, even though life predictions are often made using high stress intensity factors in other aerospace applications, the reliability of a similar calculation for an aircraft component is sufficiently low to prevent the result of that type of calculation from having any real meaning.

The above arguments are intended to show that at large damage sizes, when the stress intensity factors which control the crack propagation rates are large, the crack growth calculation is too highly dependent on input variables to be meaningful and therefore minor variations in the statistical description of damage present would require test data that specifically reflect variations in growth rates at these large damage sizes.

Although data exist on the statistical distribution of fatigue lives, this reflects primarily the variation in the early portions of crack life, and does not reflect the wider variations of the latter portion of life. This latter variation may be enormous. Variations in the latter portion of life of a factor of ten might only vary the overall life by 10%. On the other hand the probability of failure (for a given initial crack size) during the early portion of life (represented by the cross-hatched areas in Figure 3-11) is so remote as to require a severe extrapolation of the load spectrum to calculate it.

Thus although it is possible to calculate the probability of failure for a given damage size toward the end of life, the accuracy in determining the probability of that damage size occurring is unknown; and although it is possible to determine the probability of a damage size (given an initial damage) occurring early in life, it is impossible, due to the need to extrapolate the spectrum, to determine the corresponding probability of failure load occurrence. To compute the probability of failure it is necessary to know both the probability of a given damage occurring (and the length of time



that damage remains) and the probability of catastrophic failure occurring for that damage size. And since both these probabilities presently are not known, a probabilistic approach must be abandoned.

It is somewhat surprising that other investigators have not noted this inability to obtain reliable values for both required probabilities simultaneously. For example, in References 3-30 and 3-31 a probability of failure for an initially damaged structure is calculated; however in those publications it is assumed that the statistical distribution of remaining lives is the same for long cracks (with short remaining lives) as it is for short cracks (including cracks of length zero). The validity of this assumption, particularly towards the end of life where the probability of failure is high; is uncertain and subsequently the calculated probability of failure is unreliable.

### 3.3.3 Final Criteria

As will be seen subsequently, the primary outcome of abandoning the probabilistic approach will be an inability to directly tie the magnitude of the load requirement for residual strength capability to the life requirement for a structure.

The above probability based criteria did have a coupled residual strength and life requirement. Each component had to last a specific length of time (flights) from an initially damaged state. The attempt was made to consider the total probability of residual strength failure during this time period by selecting the damage size at mid-life to represent all sizes for use in the residual strength analysis. (The use of the mid-life damage size would have been proper if failure probability varied linearly with time). By this means the stringency of the strength requirement was directly related to the stringency of the life requirement in a manner that was intended to insure the attainment of a high degree of reliability for each structural component.

It is interesting to note (see Section 3.1) that most other criteria dealing with "damage tolerant" or "fail-safe" or "safe-life" structure not only do not couple residual strength requirements and life requirements directly, but do not specify both types of requirements for the same structure. Usually the criteria are separated: one class of structure must only meet a life requirement (often called safe-life) and another class of structure must only meet a residual strength requirement (often called fail-safe). Since many of these



criteria have been at least partially successful, it is pertinent to inquire with the above probabilistic criteria in mind as to the validity of the separated criteria approach.

Consider a structure that must meet a life requirement only. The discussion of the initial ideal criteria showed that the probability of failure for most of the life is vanishingly small for an initially damaged structure that has to meet a life requirement. In fact the probability of failure during any given flight is so small for most of the life (except at the very end) that it is impossible to calculate. (Although the sum of probabilities for all these flights is non-zero). It is easy to see that if the life requirement is sufficiently stringent, the probability of failure during service will be low since the residual strength of the structure will be high at all times during the life of the structure, even though the residual strength is not specified directly. Thus a sufficiently demanding life requirement indirectly results in maintaining high residual strength requirements during the life of the structure.

Now consider a structure subject to a fail-safe type of requirement. Here, a structure is required to maintain a minimum residual strength while containing a specified damage size. The damage size specified in a fail-safe requirement is usually quite large, sufficiently large in fact to be discovered on a walk-around inspection (see Section 3.2.3). Thus it could only remain undetected for a few flights. The discussion of the initial "ideal" criteria has indicated that crack propagation rates at these large damage sizes are subject to wide variations. However if the residual strength criterion is sufficiently stringent, the propagation rates of large cracks will be slow enough to ensure their safe discovery. Since the length of time the crack will be undiscovered at this crack length is short, a small but finite probability of failure in a given flight is acceptable.

Thus the total probability of failure for a safe-life type of criterion and a fail-safe type of criterion may both be made as small as is desired if the individual criterion is made sufficiently stringent.

It should be noted that the existing criteria discussed in Section 3.1 seem to have the proper balance from a failure probability viewpoint. For example; the end of life for the life requirements are all determined by a load which has a very low probability of occurrence (e.g., maximum spectrum load or limit load); the residual strength requirements however specify a load magnitude with a higher probability of occurrence, this goes along with the shorter duration of time the damage is assumed to be present. Note also that the load designation in a life requirement is used to determine the end of the life of a damaged component and the load designation in a residual strength requirement reflects the probability of failure during the life of a damaged component.

Thus we may conclude that the separation of residual strength requirements and life requirements produce a satisfactory result, providing the criteria are sufficiently stringent. In addition we may note that since the probability of failure as a crack grows from a small size to a large size cannot be determined (as discussed above) and since the crack growth rates for large damage sizes cannot be predicted accurately (as discussed above) the separation of life and residual strength requirements according to damage sizes and inspections is absolutely necessary. The separation is not necessarily determined by structural classification (e.g., monolithic, redundant, etc.). In fact, the separation of criteria by structural classification should be avoided since it inhibits criteria generality and would probably introduce undesirable and unnecessary complications.

The central question in damage tolerant design criteria involves the determination of appropriate damage levels. In the consideration of damage levels in Section 3.2.3, three distinct damage levels seem to have meaning for all classes of structure:

- o An initial damage size (maximum size missed during inspection at time of fabrication).
- o NDI in-service inspectable damage size (maximum size missed during visual depot inspection).
- o Walk-around inspectable damage size (maximum size missed during walk-around inspection).



While assigning a residual strength requirement to the third damage size has meaning, residual strength requirements for the first two would not. This is due to the fact that only very high magnitude, very low rate of occurrence loads can cause catastrophic failure over most of the life. The rate of occurrence of these loads is in fact too low to be determined. Of course it is still meaningful to use a specified load to determine the end of life for these two cases.

Similarly, a life requirement has meaning for the first two damage sizes but not for the third damage size. This is primarily due to the fact that at large damage sizes and anticipated stress levels, subsequent life predictions will only be in the range of a few flights and accuracy in such predictions is very poor. Thus a residual strength concept must be used. The only difficulty is in choosing an appropriate fail-safe load to furnish reasonable assurance that failure will not occur when the damage corresponds to a walk-around inspectable size. It is at this point that we suffer from not being able to maintain the probabilistic approach prescribed earlier. Each of the damage levels called out would have had both a residual strength and a life criterion associated with it. While the residual strength requirement might not have had impact on the first two cases and life might not have had impact on the last case, each of the life requirements and residual strength requirements would have been coupled, so as to make the separate determination of a fail-safe load unnecessary. In lieu of an appropriate coupling procedure to establish the fail-safe load, one must depend on past experience. In Section 3.2.1 it is indicated that commercial fail-safe requirements have been successful using as the fail-safe load (for similar damage sizes) 80% of limit load, which roughly corresponds to the once-per-500-hour, or once-per-700-flight, load for a particular commercial vehicle. Although for many other commercial vehicles the 80% limit load condition would correspond to fewer flights it seems reasonable to use the once-per-700-flight load as an assurance of remaining conservative. Note that this results in a fail-safe load frequency of occurrence based on flights, not hours; this is appropriate since the residual strength criteria are tied to walk-around inspections, the number of which correspond to the number of flights. Note that, the dynamic factor discussed in Section 3.2.2 should be applied to the fail-safe load when the walk-around inspectable damage corresponds to having an entire structural element broken.



The life requirements to furnish reasonable assurance that failure will not occur are reasonably obvious. For non-inspectable structure an initial crack must not grow during one lifetime to a size where failure is probable. For inspectable structure a visually inspectable crack must not grow during one inspection interval to a size where failure is probable. A life reduction factor which would insure conservatism may be necessary for the above life requirements. The magnitude of this factor depends to a large degree on the method of analysis used to make the life prediction (see Section 3.2.4). If design verification tests are used to determine design acceptability, smaller factors would be required than the factors used when only analysis is conducted.

In Section 3.2.3 two sizes of flaws which may be present and missed by inspection at the time of initial fabrication were discussed. The smaller size corresponded to a flaw emanating from a hole, the larger size corresponded to a flaw which may be present in areas away from structural details. This would suggest two separate life calculations, one using the smaller flaw size and considering design details, and one using the larger size and not considering design details. Additional motivation for two separate calculations is that since the probability of the largest crack that could be missed occurring at a high stress concentration is low, the probability of the occurrence of the larger crack in areas away from structural details is comparable to the probability that a smaller crack will be present near a hole. Also note that the calculation of the life of a crack emanating from a hole where the fastener and local yielding (due to the stress concentration at the hole) can affect the growth rate in a complex manner, is an approximate procedure. It therefore may be desirable at some future time to replace this calculation with the simpler one (as is done in fatigue) which involves a larger damage size but ignores structural details. This may be particularly advantageous in the early stages of design.

The use of the small flaw size and the consideration of design details (primarily holes) is the approach that has been used in many of the recent applications for crack life analysis. The use of the larger crack sizes and ignoring design details may at first seem to be a new unorthodox approach. It is as far as fracture mechanics type approaches are concerned. However, it follows very closely the approach taken in the design of aircraft structures for fatigue.

All the design details for purposes of fatigue analysis is usually lumped in an empirical fatigue quality factor. In our case a similar result would be obtained if the larger initial flaw size was varied for different structural details. This is probably not necessary since the presence of a crack in the vicinity of the structural detail is the single most important factor.

For a structure to be safe it does not need to meet all three structural integrity requirements; i.e., the life requirement for an initial fabrication flaw, the life requirement for an NDI in-service inspectable flaw, and the residual strength requirements for a walk-around inspectable damage size. The structure need only meet one of these three requirements. However, replacement of parts or repairs of cracked structure is expensive and should be avoided even when the structure may be shown to be safe for large damage sizes. Thus some overall durability requirement should be imposed. This follows the broad manner in which fatigue criteria are applied to aircraft structure. It seems logical and consistent to use the damage size and analysis discussed above which corresponded to the maximum flaw size which could be missed in areas of the structure away from design details. An appropriate life reduction factor, which will be a function of the spectrum and analysis procedures must be used to satisfy this requirement in the same manner that life reduction factors are used in the previously discussed life requirements.

Although most of the discussion of crack growth in this section referred principally to crack growth due to cyclic loadings, all that has been said is applicable to sustained load crack growth due to environmental effects as well. Therefore, the life requirements are to be used with reference to stress corrosion cracking in the exact manner as they would be for fatigue crack propagation. The life reduction factors will not necessarily be the same for stress corrosion cracking since the methods of analysis and material property variations are different from those for fatigue crack propagation.

### 3.4 RECOMMENDED CRITERIA

A summary of the recommended criteria is presented in Table 3 4. An acceptable structure will meet one of the structural integrity requirements and the durability requirement. In addition to performing an analysis, analysis verification tests and limited design verification tests are required to demonstrate that the requirements are met.

The actual damage sizes and factors will vary from application to application and will depend on inspection techniques and structural detail. For a typical fighter/attack aircraft, representative damage levels and factors are given in the applications analysis section.



TABLE 3-4 RECOMMENDED DAMAGE TOLERANT DESIGN CRITERIA (1)

Inspectability Classification	Structural Integrity Requirements	Durability Requirements
Non-inspectable	The initial damage size, $a_i$ , shall not attain the critical size (4) during $S_i$ service lifetimes. (2) <sup>i</sup>	An initial crack size (surface flaw or thru-thickness crack which corresponds to the maximum flaw size that may be missed in the structure) shall not attain the critical size in $S_d$ service lifetimes. The effect of design details on crack growth behavior is ignored.
NDI In-service inspectable	The NDI in-service inspectable damage size, $a_v$ , shall not attain the critical size (4) during $S_v$ inspection intervals. (2) <sup>v</sup>	
Walk-around inspectable	The structure shall be capable of supporting the once per 700 flight load (3) with walk-around inspectable damage, $a_w$ .	

- (1) An acceptable structure will meet one structural integrity requirement and the durability requirement
- (2) The influence of design detail on crack growth behavior considered.
- (3) 10% of the cut load should be added to this when  $a_w$  corresponds to having an entire structural element broken.
- (4) Damage size that will grow catastrophically to failure for the maximum spectrum load (generally equal to or greater than the load that stresses the structure to design limit stress).

## 4.0 ANALYTICAL PROCEDURES

### 4.1 INTRODUCTION

This section discusses various methods of analysis which are available for preliminary sizing of aircraft structure to meet requirements such as those specified in Section 3.0. These include methods for predicting time to fatigue crack initiation, the growth of cracks due to fatigue and sustained loadings, and the residual strength of damaged (cracked structure). Some stress intensity formulas for flaw geometries which are useful for fatigue crack propagation and fracture analysis are presented and discussed. Also the energy criteria required to arrest a running crack are reviewed as well as methods of analysis for predicting this phenomenon.

### 4.2 FATIGUE ANALYSIS

The analysis procedure for predicting the fatigue life for a given design stress or the design stress for a given fatigue life is illustrated in the flow diagram of Figure 4-1. The fatigue loading spectra together with the relation between load and stress are used to define the fatigue stress spectra. For preliminary design, various load/stress relationships are assumed so that the relation between design stress and fatigue life can be obtained. The fatigue stress spectra and the fatigue allowables, in the form of constant-life diagrams, are the input data required for the fatigue analysis. The fatigue calculations are performed using some damage rule which defines the relation between the applied stresses and number of cycles, and the allowable stresses and number of cycles required to initiate a fatigue crack.

The method of fatigue analysis generally used is based on the Palmgren-Miner method of analysis. The basic equation is expressed as follows:

$$D = \sum_{i=1}^k \frac{n_i}{N_i} \quad (4-1)$$

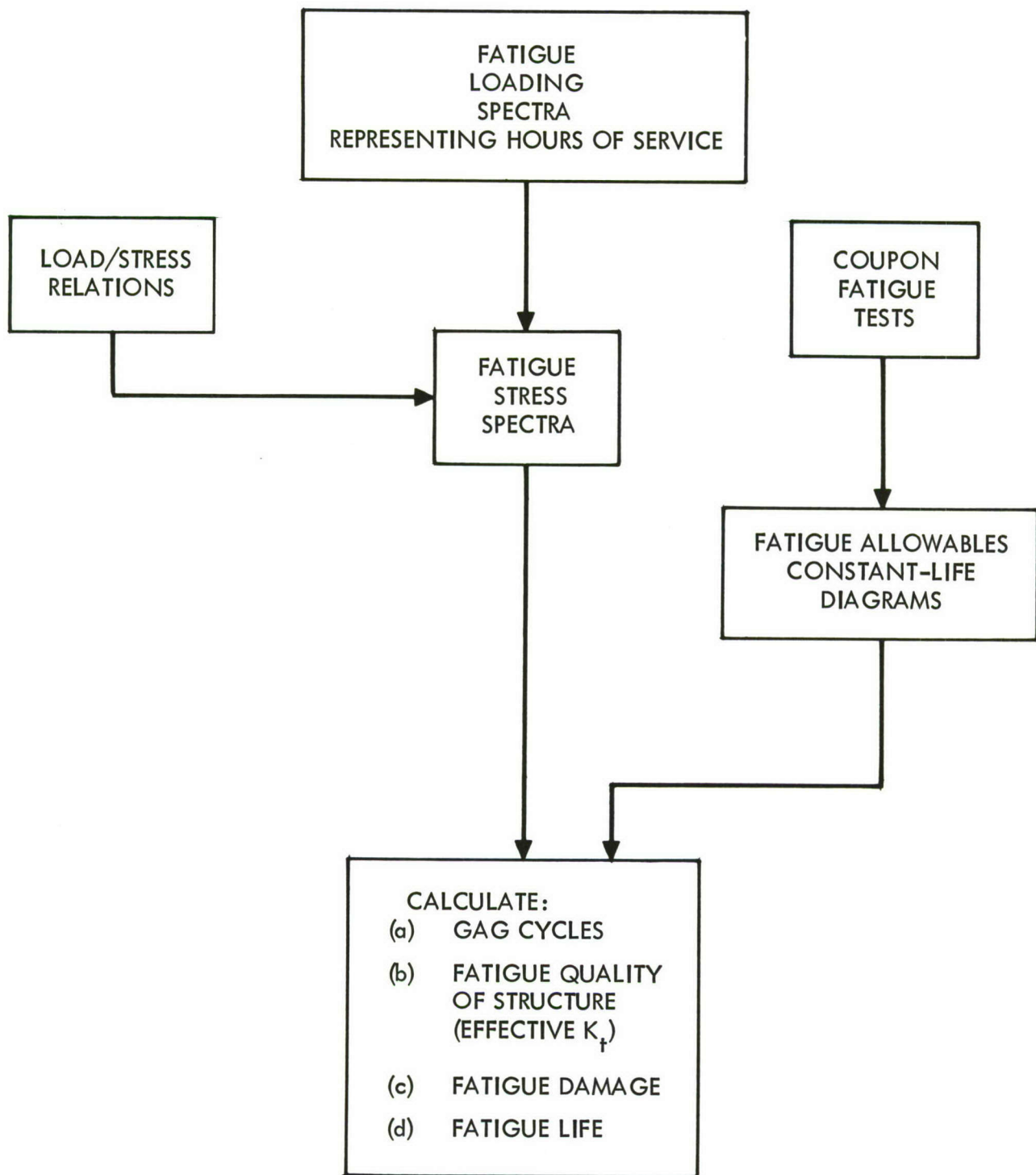


FIGURE 4-1 FLOW DIAGRAM OF FATIGUE ANALYSIS PROCEDURE



where

$n_i$  = number of loading cycles at the  $i^{\text{th}}$  stress level

$N_i$  = number of loading cycles to failure for the  $i^{\text{th}}$  stress level based on constant amplitude S-N data for the applicable material and  $K_t$  value.

$k$  = number of stress levels considered in the analysis.

The magnitude and number of ground-air-ground (GAG) cycles must be accounted for in the analysis as well as the cyclic variations of stress for individual loading spectra.

Figure 4-2 illustrates the definition of the GAG cycle used in this program, i.e., the once-per-flight peak-to-peak cycle. The once-per-flight peak-to-peak cycle is recommended for use because it provides a good correlation between spectrum fatigue tests conducted on notched coupons and fatigue analyses (for example see References 4-1 and 4-2). The magnitude of the GAG cycle to be used in the analysis can be determined from the cumulative summation of stress spectra as shown in Figure 4-3. The fatigue calculations using Equation 4-1 are rather simple although quite time consuming if done by hand for a large number of loading cycles, which is usually the case. Computer programs, such as the one given in Reference 4-3, can be used to improve the speed and accuracy of the calculations. A computer program similar to the one given in Reference 4-3 was used to perform the calculations in this analysis.

The fatigue quality of the structure is generally determined from the results of fatigue tests of components or the complete airframe structure. The fatigue quality index can be calculated at each crack location developed during fatigue testing using Equation 4-1. Fatigue analyses are conducted using a set of constant amplitude S-N curves for various values of  $K_t$  obtained from simple notched coupons. The stress spectra that was sustained at each critical point to fatigue crack initiation in the test is determined from the spectra of applied loads. The results of the analyses are interpolated to determine the specific S-N curve which makes the D value in Equation 4-1 equal to one for the test life. The value of  $K_t$  associated with the S-N curve is a measure of the fatigue quality index. The results of some analyses conducted from various component tests are presented and discussed in Section 5.5.1.

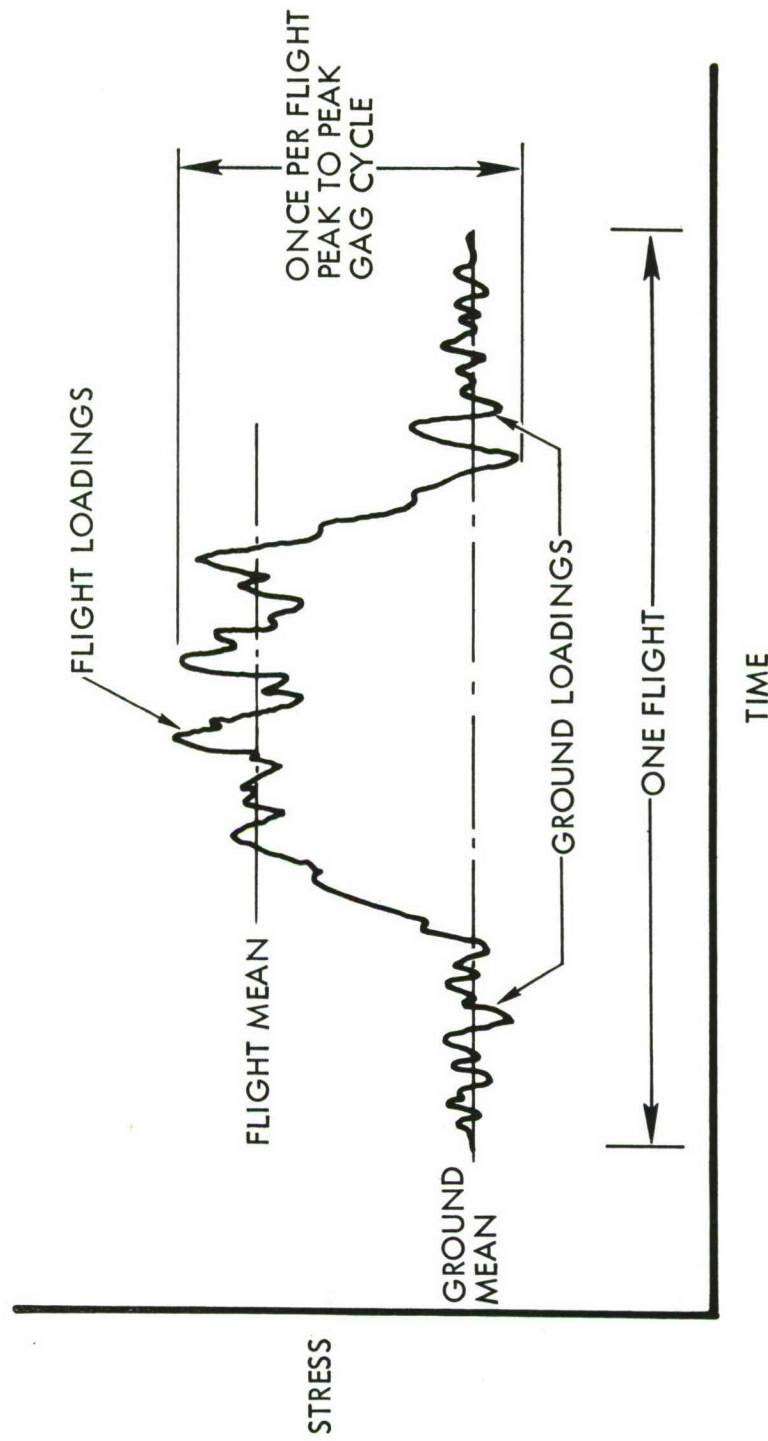


FIGURE 4-2 GAG CYCLE DEFINITION FOR FATIGUE ANALYSIS

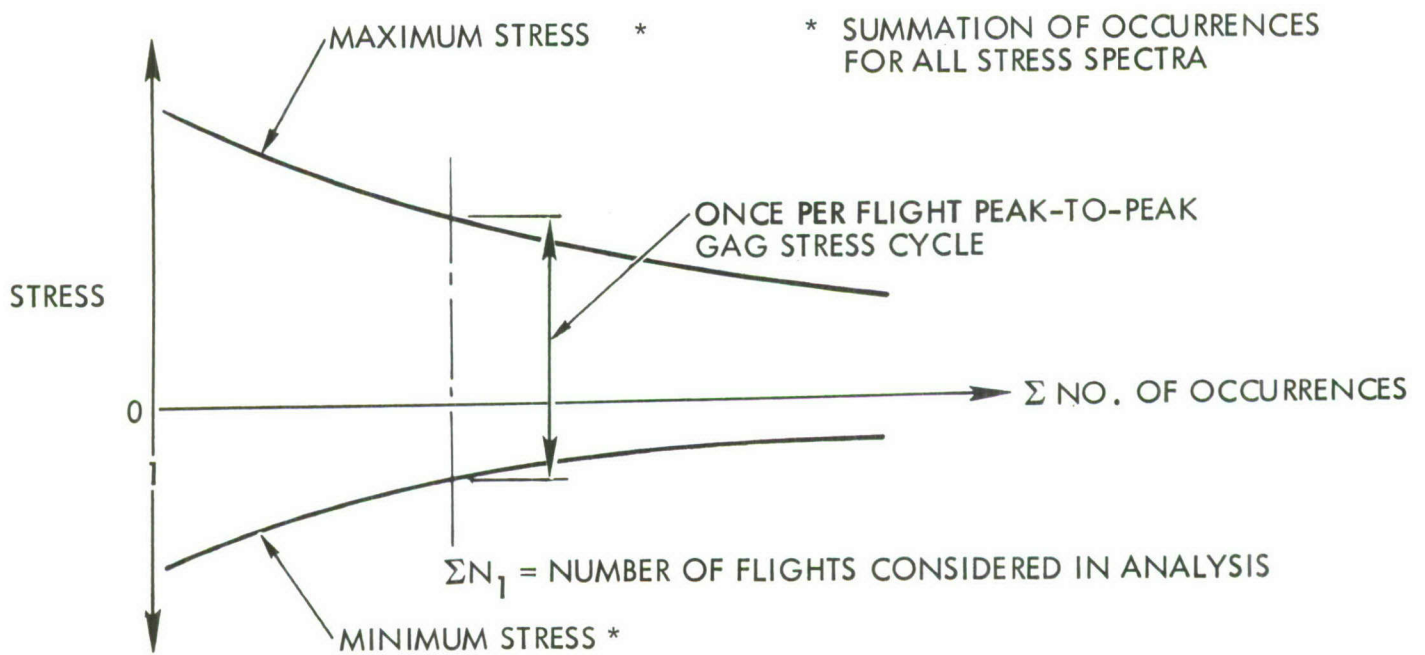


FIGURE 4-3 METHOD OF CALCULATING MAGNITUDE OF GAG CYCLE



## 4.3 STRESS INTENSITY FACTORS FOR COMMON CRACK (FLAW) GEOMETRIES

### 4.3.1 Introduction

In general, when a structure, e.g., a plate, containing a crack or flaw is subjected to arbitrary loading, the stress field near the crack tip can be divided into three basic types, each associated with a local mode of deformation as illustrated in Figure 4-4. The tensile mode, (Mode 1) is associated with local displacement in which the crack surfaces move directly apart. The shear mode, (Mode 2) is characterized by displacements in which the crack surfaces slide over one another in the direction perpendicular to the leading edge of the crack. The torsion mode, (Mode 3), results in the crack surfaces sliding with respect to one another in the direction parallel to the leading edge of the crack. For each of these modes, the stresses near the crack tip are proportional to a constant divided by  $\sqrt{r}$ , where  $r$  is the distance from the crack tip to the point of interest. This constant is called the stress intensity factor and is termed  $K_1$ ,  $K_2$ , or  $K_3$  for the three displacement modes, 1, 2, 3, respectively. The magnitudes of these parameters depend upon the configuration of the structure, the crack size, as well as the loads. The linear superposition of these three modes is sufficient to describe the most general case of crack tip stress fields. In this report Mode 3 will not be considered.

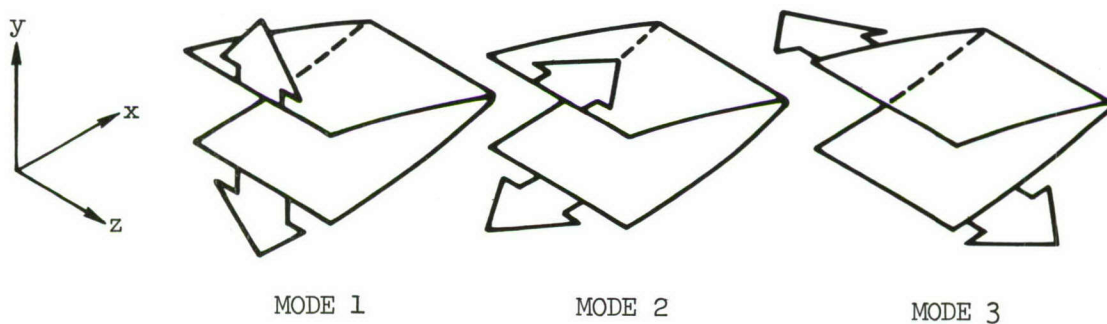


FIGURE 4-4 THREE BASIC MODES OF CRACK SURFACE DISPLACEMENT

It will be assumed that the damage sizes are such that fracture mechanics principles are applicable. That is, it will be assumed that for all structures and damages to be considered, some region exists where the crack tip stress intensity factor,  $K$ , describes the stresses. This condition will exist only for the case of small-scale yielding, i.e., when the plastic zone radius,

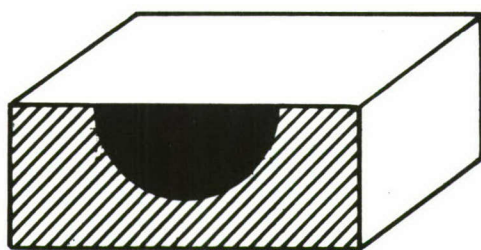
$$r_p = \theta \left( \frac{K}{F_{ty}} \right)^2 \quad (4-2)$$

(where  $\theta$  is a constant, most often approximated for plane stress by  $1/2\pi$  or  $\pi/16$ , and  $F_{ty}$  is tensile yield strength) is small compared to any dimension of the structure, including crack length but excluding, for thru-the-thickness cracks, the sheet thickness. The  $K$ -governed region must also be large compared to material microstructural dimensions such as grain size. Thus there exist upper and lower bounds to the damage size that will be analyzable. Fortunately, the most important range of engineering interest is within these bounds.

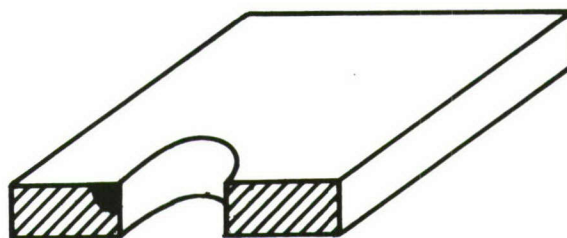
Two excellent compendiums (References 4-4 and 4-5) of stress intensity factor expressions for a variety of structural configurations already exist, making the inclusion of this type of general data unnecessary. The only stress intensity relations presented here will be those which may now be covered in greater depth than they were in the two references or those which may be needed for conducting analyses of service failures.

Stress intensity expressions are presented for the configurations listed below and illustrated in Figure 4-5:

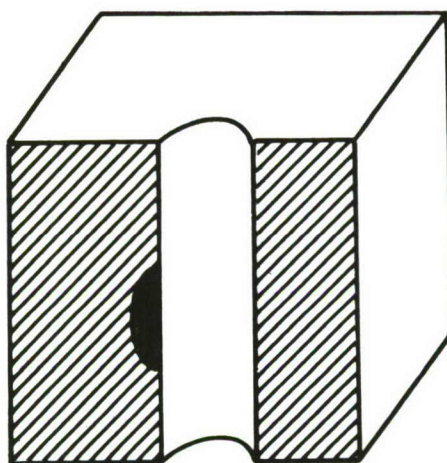
- (1) Thru-the-thickness crack at the center of a plate (Figure 4-5d)
- (2) Part-thru crack (Figure 4-5a)
- (3) Corner crack (similar to Figure 4-5b except crack is not at the edge of a hole).
- (4) Cracks (1) through (3) emanating from the edge of a hole (Figure 4-5b,c,e).
- (5) Crack in the vicinity of reinforcements (see Figure 4-22 page 4-46).



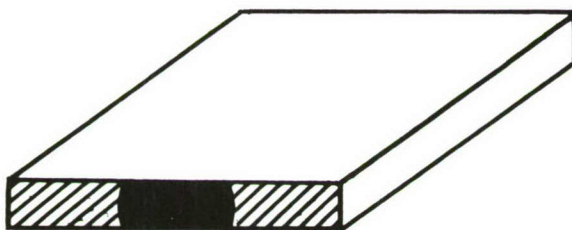
a. Part-Thru Crack



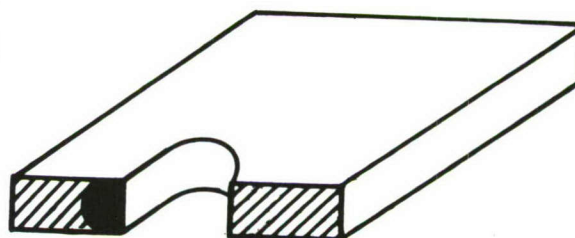
b. Corner Crack at the Edge of a Hole



c. Part-Thru Crack at the Edge of a Hole



d. Thru-the-Thickness Crack



e. Thru-the-Thickness Crack at the Edge of a Hole

FIGURE 4-5 CROSS-SECTIONAL VIEWS OF COMMON FLAW GEOMETRIES



In general, the stress intensity factor can be expressed as

$$K = f_g \cdot \alpha \cdot M_p \quad (4-3)$$

where  $f_g$  is the applied uniform stress remote from the crack,  $\alpha$  is a lumped geometric factor and  $M_p$  is a plasticity correction factor. For most configurations encountered in design, the stress intensity is proportional to the square root of crack length and it is convenient to write it in the form

$$K = f_g \lambda \sqrt{\pi a} M_p \quad (4-4)$$

where  $a$  is the length dimension associated with one tip of the crack and  $\lambda$  is the dimensionless geometric coefficient.

The geometric coefficient is a function of the structural geometry, crack geometry and type of loading (i.e., uniform tension, uniform shear, point tension forces, etc.).

The plasticity term is discussed in References 4-6 and 4-7. In this section, the  $M_p$  term is deleted from all the recommended stress intensity factor expressions. The reasons for doing this are:

1. For computing values of  $K_c$  (plane stress or mixed mode fracture toughness) from test results of laboratory coupons, the  $M_p$  factor is not included in the MIL-HDBK-5 proposed procedures.
2. If the  $M_p$  factor was included in the calculation of  $K_c$ , then, accordingly, the fracture stress, in any failure predictions, would be

$$F_g = K_c (\alpha \cdot M_p)^{-1} \quad (4-5)$$

In other words, the  $M_p$  factor included in the value of  $K_c$  would tend to be canceled by the  $M_p$  term in the calculated  $K$  during the process of residual strength prediction. Of course the magnitude of these two  $M_p$  terms would not be identical, but for many cases the difference is negligible.

3. Stress intensity factors for  $K_{Ic}$  type specimens are usually developed by compliance methods. The effects of plasticity are reflected in the compliance measurements. However, the crack tip plastic zone in plane strain failures is usually small therefore its effect can be neglected.

When  $M_p$  is neglected, and when loads (rather than displacements) are imposed on the boundary, the stress intensity formula for any two-dimensional configuration is the same for plane stress and plane strain.

#### 4.3.2 Thru-the-Thickness Crack at the Center of a Plate

Here we consider the stress intensity factor for a flat plate, of finite width  $W$ , containing a straight line crack of length  $2a$ , oriented normal to a uniformly applied tensile load (see Figure 4-6). When the plate is subjected to tension,  $f_g$ , or shear,  $f_s$ , the crack tip stress intensity factors are respectively

$$K_1 = f_g \sqrt{\pi a} \cdot \phi_1 \quad (4-6a, b)$$

$$K_2 = f_s \sqrt{\pi a} \cdot \phi_2$$

where the geometric coefficient  $\phi_1$  is (Reference 4-8)

$$\phi_1 = \left[ \sec \left( \frac{\pi a}{W} \right) \right]^{\frac{1}{2}} \quad (4-7)$$

and  $\phi_2$  is not known but the expression for  $\phi_1$  is probably a reasonable approximation. Note that the value of  $\phi_1$  reduces to unity for  $W = \infty$  or  $2a/W = 0$ .

If the length of the plate is too short, an additional adjustment in the equation for the stress intensity factor is required. The effect of panel length has been worked out by Fichter (Reference 4-9) and is graphically presented in Figure 4-7. As shown in the figure, for Equation (4-6) to be valid without adjustment, the panel length has to be six times longer than the crack length. In most residual strength tests of panels, the crack length is equal or less than one-half of the panel width. Therefore, Equation (4-6) is valid with  $L \geq 3W$ .

#### 4.3.3 Part-Thru Crack (Surface Flaw) in a Plate

A typical part-thru crack in a plate is shown in Figure 4-8. As opposed to the thru-the-thickness crack, the stress intensity of this crack varies along the crack periphery. It is usually assumed that the crack is semi-elliptical in shape, having its major axis  $2c$  (the visible crack length on the surface) and

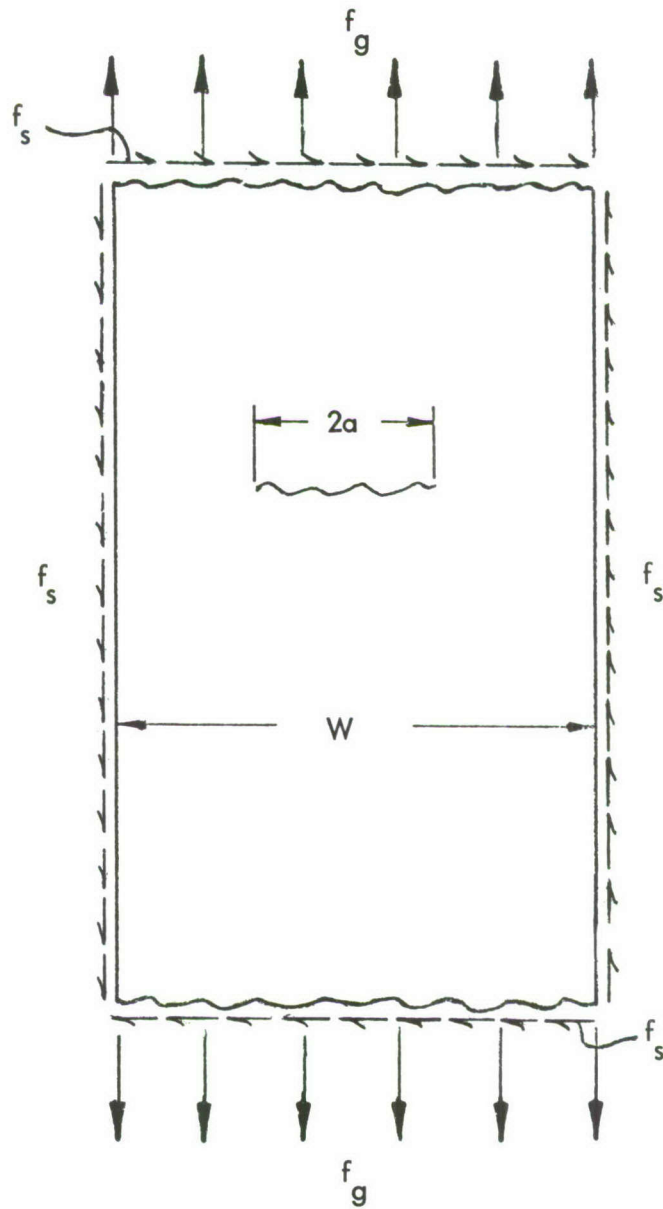


FIGURE 4-6 CRACKED FINITE-WIDTH PLATE LOADED  
IN TENSION,  $f_g$ , OR SHEAR,  $f_s$



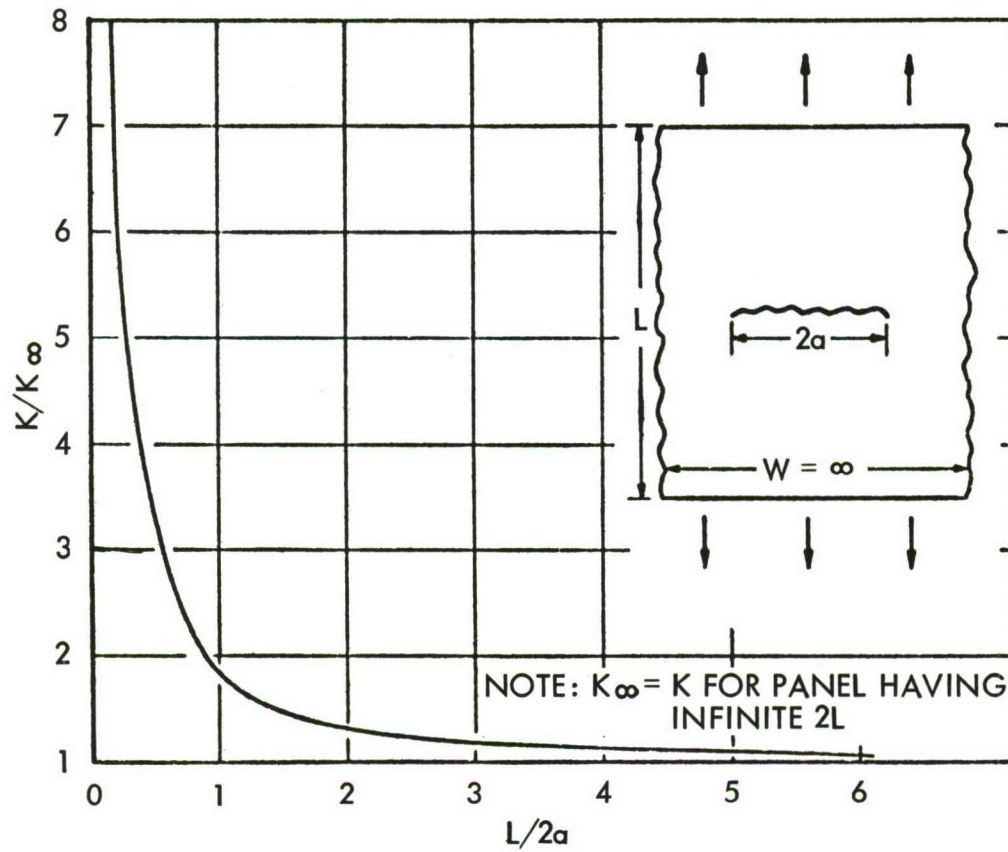


FIGURE 4-7 PANEL LENGTH EFFECTS ON CRACK TIP STRESS INTENSITY FOR CENTER CRACKED PANELS, ELASTIC ANALYSIS (REFERENCE 4-9)

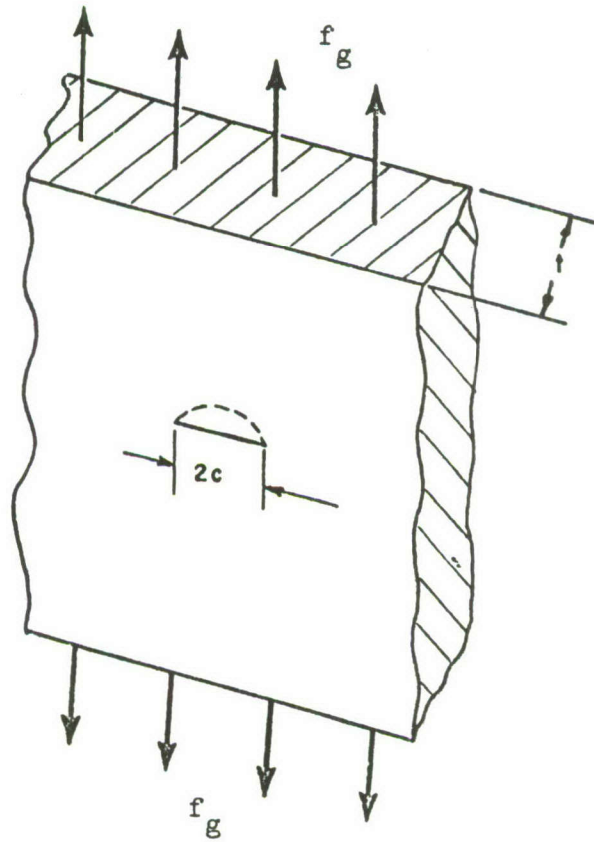
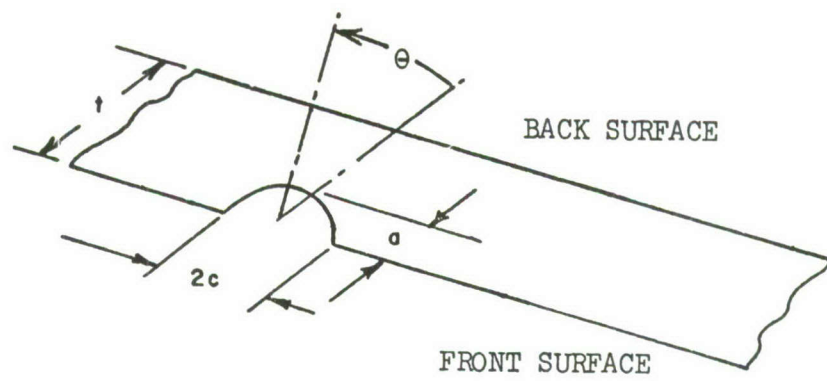


FIGURE 4-8 PART-THRU CRACK GEOMETRY

semi-minor axis  $a$  (the depth of the crack). The crack shape usually ranges from  $a/2c = 0.5$  (a semi-circle) to  $a/2c = 0$  (a scratch).

The stress intensity expression for the deepest ( $\theta = 0$ ) point on the periphery of a part-thru-crack is

$$K = f_g \sqrt{\pi a} \left[ \frac{M_1'}{\phi} \cdot \alpha_b \right] \cdot M_p \quad (4-8)$$

where

$M_1'$  = Geometric coefficient to account for the influence of the front free surface on the stress intensity factor, a function of  $(a/2c)$ .

$\phi$  = Geometric coefficient to account for the influence of crack shape, a function of  $(a/2c)$

$\alpha_b$  = Geometric coefficient to account for the influence of the back free surface, a function of  $a/2c$  and  $a/t$ .

A detailed review of the development of the geometric coefficients and the plasticity factor is presented in Appendix E. Extracted from that discussion and summarized below are the recommended approaches for design analysis.

The combined crack shape and front surface factor,  $M_1'/\phi$  is plotted in Figure 4-9. The plasticity factor  $M_p$ , as discussed above, is assumed equal to unity. The use of the back surface coefficient  $\alpha_b$  and the fracture mechanics analysis of deep part-thru cracks deserves at least brief discussion here.

A part-thru crack in a plate, if it grows in a stable manner, eventually becomes a thru-the-thickness crack. Just prior to this transition, in the range of larger values of  $a/t$ , the crack shape changes and neither an ideal semi-elliptic crack nor an ideal rectangular thru-the-thickness crack approximate the true shape. Furthermore, in this same transition range the crack tip plastic zone is large compared to the dimension  $(t-a)$ , violating one condition for the applicability of fracture mechanics theory.

Nevertheless, in the absence of a better available approach fracture mechanics theory is used for part-thru flaws even when  $a/t$  is large. Appendix E presents various approaches for estimating the back-surface geometric coefficient  $\alpha_b$  as a function of  $a/t$  and the shape of the semi-elliptic crack. One possible 'transition criterion' (for deciding when the crack should begin to be modeled as a thru-the-



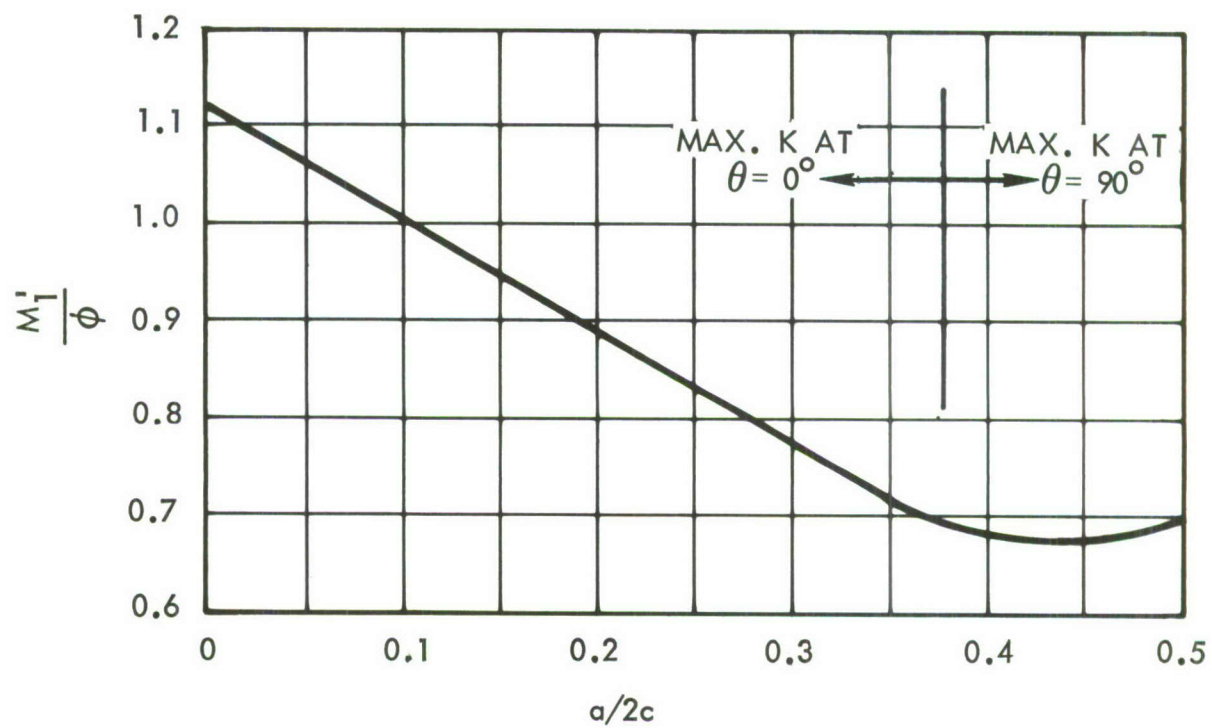


FIGURE 4-9 COMBINED CRACK SHAPE AND FRONT SURFACE CORRECTION

thickness crack) is also discussed in Appendix E (see Equation (E-4)). These Appendix E approaches are among the most accurate available procedures for stress intensity analysis of part-thru cracks in the large  $a/t$  range. It must be recognized, however, that they add computational complexity while the questions raised above concerning the flaw shape and large plastic zone size remain essentially unanswered.

Fracture mechanics calculations carried out for the design of large-scale structure require simplifications for the sake of expediency. In the case of a part-thru crack, the back surface coefficient (function of  $a/t$ ) would be different at each location of the structure having a different thickness. The value of  $\alpha_b$  is nearly unity at small  $a/t$  values. The simplified approach used in the application study (Section 5.0) is (1) to let  $\alpha_b = 1$  for all  $a/t$  values and (2) as a transition criterion, to treat the crack as a part-thru crack for  $a/t < 1$  and as a thru-the-thickness crack for  $a/t > 1$ . These two assumptions tend to compensate each other since the introduced inaccuracies are in opposing directions.

#### 4.3.4 Corner Crack (Flaw)

As an extension of the part-thru crack problem, a small crack or flaw at the corner of a plate, especially at the edge of a bolt hole as shown in Figure 4-10, has received increasing attention in the design of fail-safe aircraft structure. In analyzing in-service failures of structural or machine components, it is frequently found that this type of crack is approximately a quarter circle. Applying Smith's solution for a semi-circular crack, Liu has derived an approximate expression for a corner crack emanating from an edge of a quarter infinite solid (Reference 4-10 and 4-11). The maximum stress intensity factor on the periphery of the crack was found to be

$$K = f_g \sqrt{2a} \quad (4-9)$$

Liu also showed that the same expression could be obtained if an alternative approach, based on Sneddon's solution for a penny shaped crack (Reference 4-12), was used.

To obtain a solution for the configuration shown in Figure 4-10, simply superimpose a back surface geometry coefficient  $\alpha_b$  and a hole geometry coefficient in Equation (4-9) to account for the effects of the finite thickness and the edge of the hole. The hole geometry coefficient will be discussed next, in Section 4.3.5.

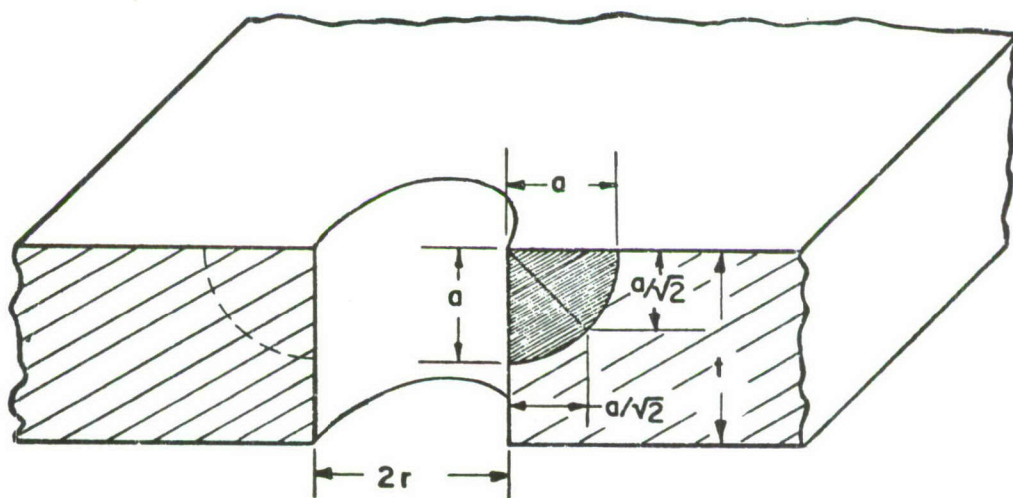


FIGURE 4-10 CORNER CRACK OR CRACKS AT THE EDGE OF A CIRCULAR HOLE



#### 4.3.5 Cracks (Flaws) Emanating from the Edge of a Hole

There are three types of cracks or flaws which might emanate from the edge of a hole. The crack could be a part-thru crack or a pair of part-thru cracks at the edge of a hole in a big piece of material as shown in Figure 4-11. Or, it could be a corner crack or a pair of corner cracks at the edge of a hole in a plate as shown in Figure 4-10. Finally, the corner crack might propagate and become a thru-the-thickness crack. A geometric coefficient is required to account for the influence of the hole in all these cases. Furthermore, the shape of the hole can generally be classified in three different categories; a circular hole, an elliptical hole and a rectangular hole.

The geometric coefficients for the circular and the elliptical hole configurations are given in Figures 4-12 and 4-13. In Figure 4-12,  $r$  is the radius of the hole and  $L$  is the appropriate crack length as shown in the sketch. For Figure 4-13,  $\rho$  is the radius of the ellipse where the crack started, and  $2C$  can be either the major or the minor axis of the ellipse. In other words, a horizontal ellipse would be those having  $\rho/C < 1.0$  and a vertical ellipse would be those having  $\rho/C > 1.0$ . The line for  $\rho/C = 1.0$  would apply to a circle; i.e., this line is the same line just shown in Figure 4-12 for the two-crack case.

Using the curves in Figures 4-12 and 4-13, the stress intensity factor for symmetric thru-the-thickness cracks at a hole in the center of a long finite-width plate loaded in tension is

$$K = f_g \sqrt{\pi a} \phi_1 F\left(\frac{a}{r}\right) \quad (4-10)$$

if the hole is circular, and is

$$K = f_g \sqrt{\pi a} \phi_1 F\left(\frac{a}{C}\right) \quad (4-11)$$

if the hole is elliptical.

Note that the curves given in Figures 4-12 and 4-13 were derived by two dimensional analysis and that the 1.12 free edge correction factor was already included in the solution. Therefore, except for the thru-the-thickness crack case,

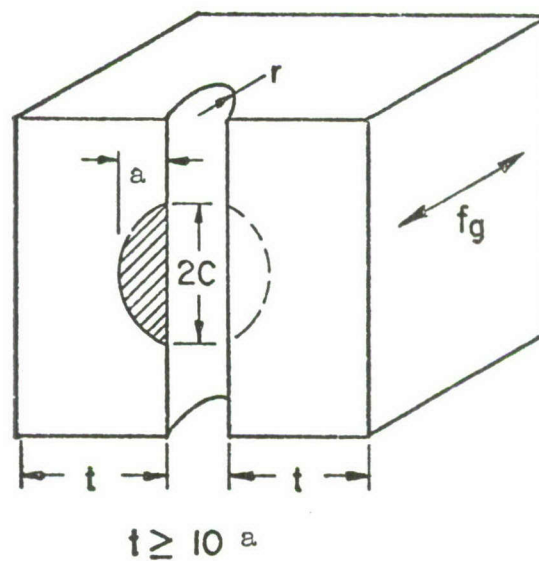


FIGURE 4-11 PART-THRU CRACK(S) AT THE  
EDGE OF A CIRCULAR HOLE

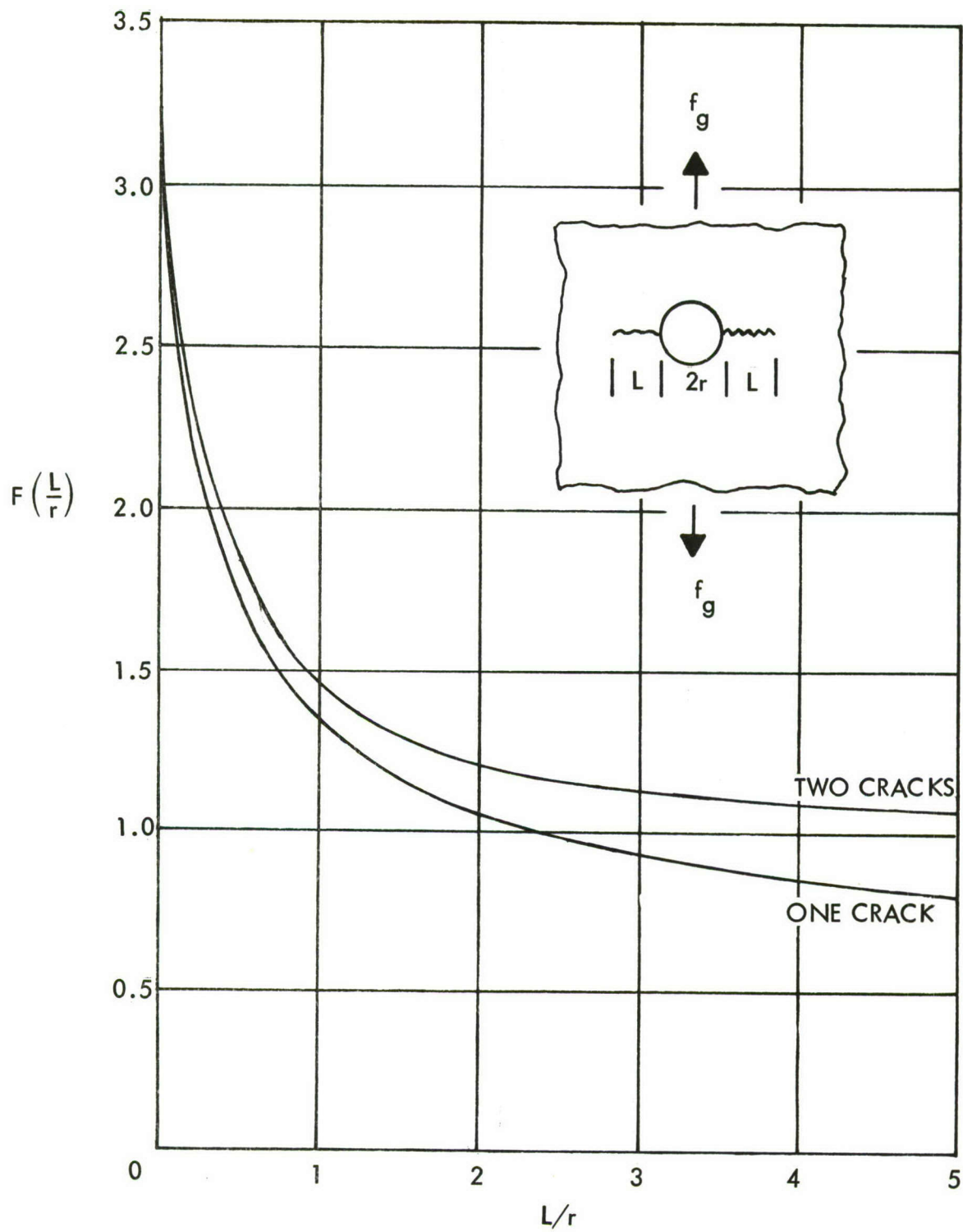


FIGURE 4-12 GEOMETRIC COEFFICIENT FOR CRACK OR CRACKS AT THE EDGE OF A CIRCULAR HOLE (REFERENCE 4-13)



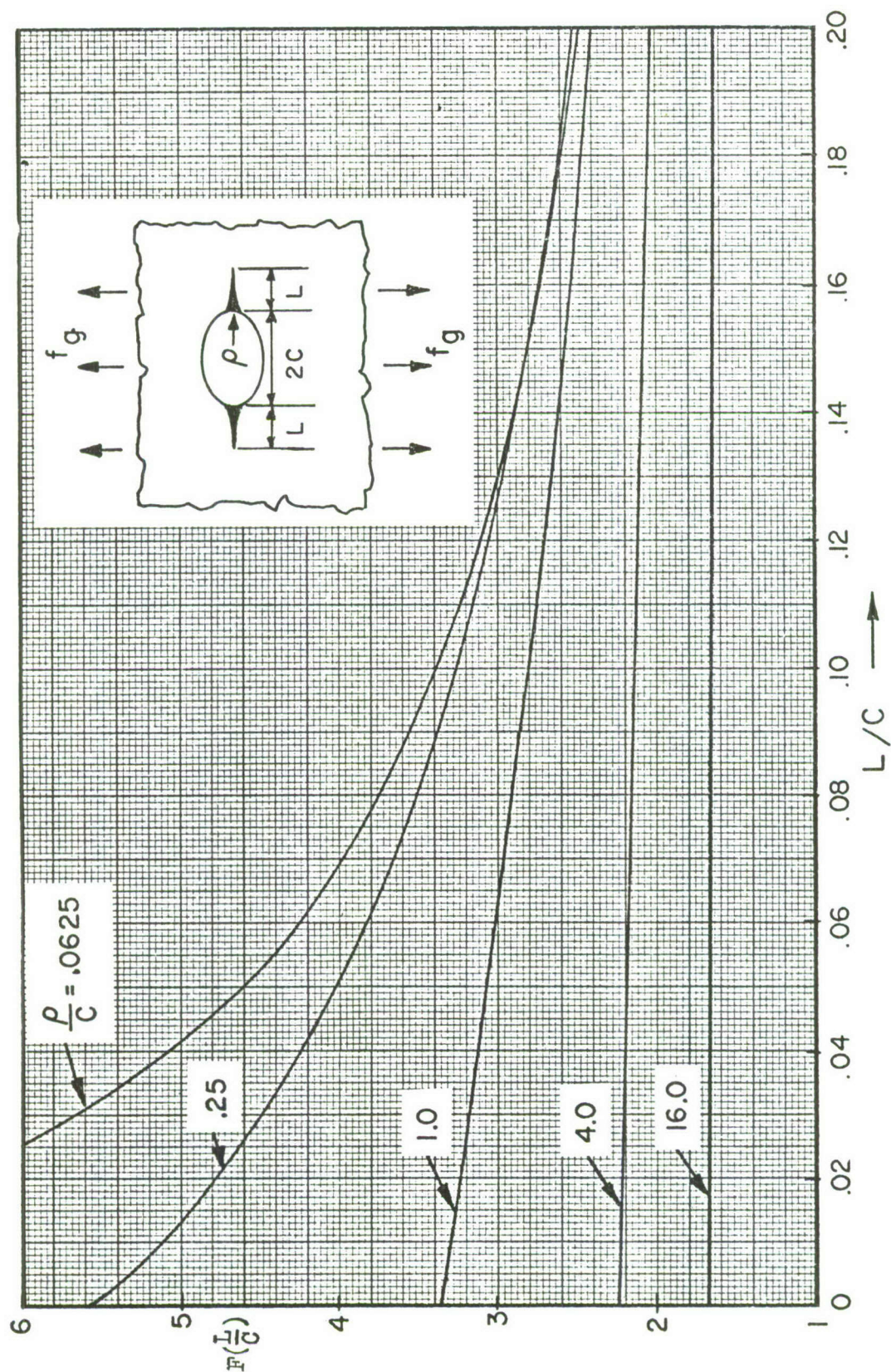


FIGURE 4-13 GEOMETRIC COEFFICIENT FOR A CRACK EMANATING FROM AN ELLIPTICAL HOLE  
(REFERENCE 4-14)



the computed stress intensity factor must be divided by 1.12. For example, the K-expressions for the part-thru crack at a circular hole and at an elliptical hole is

$$K = f_g \sqrt{\pi a} \cdot \frac{M_1'}{\phi} \cdot F\left(\frac{a}{r}\right)/1.12 \quad (4-12)$$

and

$$K = f_g \sqrt{\pi a} \cdot \frac{M_1'}{\phi} \cdot F\left(\frac{a}{c}\right)/1.12 \quad (4-13)$$

For a corner crack at a hole, one further consideration is necessary. Because distances from the edge of the hole to points on the crack front vary from zero (at the edge of the hole) to a maximum of  $a$  (on the surface of the plate), the "proper" value of  $L$  is not obvious. (For the part-thru crack the same variation occurs but the choice of  $L = a$  is in line with both tradition and intuition). The value of  $L$  chosen for a corner crack at a hole (Reference 4-11) is the value at the middle point ( $\theta = 45^\circ$ ),  $L = a/\sqrt{2}$ . Then the stress intensity expression for corner cracks at circular and elliptical holes becomes

$$K = f_g \sqrt{2a} \cdot \alpha_b \cdot F\left(\frac{L}{r}\right)/1.12 \quad (4-14)$$

and

$$K = f_g \sqrt{2a} \cdot \alpha_b \cdot F\left(\frac{L}{c}\right)/1.12 \quad (4-15)$$

where the back surface coefficient  $\alpha_b$  is unity, but would otherwise be based upon a circular shape ( $a = c$ ) and the crack-"depth"-to-thickness ratio ( $a/\sqrt{2} t$ ).

#### 4.3.6 Cracks in the Vicinity of Reinforcements

The effect of reinforcements on the stress intensity factor has been accounted for by using a technique based on a combination of References 4-15, 4-16, and 4-17. Reference 4-16 presents stress intensity factors for cracked sheets with regularly spaced intact stiffeners. Reference 4-17 contains the stress intensity factors for a sheet with a single broken stiffener. Each of these references present their results in the form of coefficient  $\lambda$ , defined in Appendix G.

In those cases where both intact and broken stiffeners will produce an effect on the stress intensity factor, it is assumed that the actual  $\lambda$  is the product of the  $\lambda$  calculated by considering the broken stiffener alone and the  $\lambda$  calculated by considering the intact stiffeners only.

In the case of integral stiffeners it is assumed (based on Reference 4-18) that the propagating crack grows up the stiffener at the same rate as it grows in the skin. Therefore the crack length when the integral stiffener is completely broken can be determined. The stress intensity solutions for the completely severed stiffener case and for the totally intact stiffener cases are known. The  $\lambda$  for the partially broken configurations are determined by linear interpolation of  $\lambda$  between the two known (intact and broken) cases.

A flat strap attached to the skin carries an approximately uniform load when a crack grows under it. This is not true for a stiffener of more complex cross sections. When compared to the areas of a flat strap, the area of a zee-stiffener or integral riser is not as effective in picking up the load from the cracked skin. The analysis in Reference 4-16 and 4-17 assume a fully effective uniform tensile load-carrying stiffener, which implies that the centroid of the stiffener aligns with the skin middle surface. Therefore estimates for the effective area  $\bar{A}_e$  of eccentric stiffeners have to be made before References 4-16 and 4-17 can be used properly. Section 4.6.2 introduces the effective area and gives equations for calculating  $\bar{A}_e$  for various types of reinforcements.

Since the load carried by a stiffener is proportional to its area, the full stiffener area is used when analyzing the effects of transferring the load back into the skin for the broken stiffener cases.

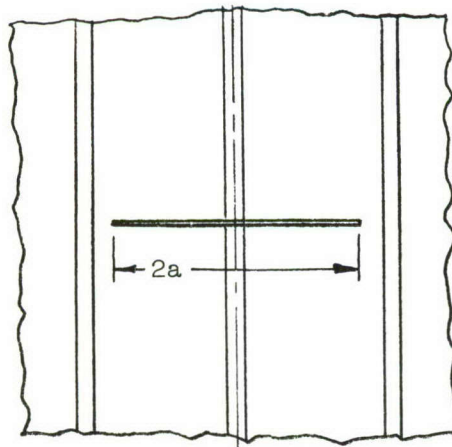
Values of  $\lambda$  for the configurations used in the analysis described in Section 5 are summarized in Tables 4-1 through 4-3. It should be emphasized that these tables are presented here as examples. They are not applicable to any general case, but rather apply to the specific design and crack configurations analyzed in the application study.



TABLE 4-1 VALUES OF  $\lambda$  FOR 11-SPAR STRUCTURE

$$K = \lambda f_g \sqrt{\pi a}$$

a	<u>Titanium</u>	<u>Aluminum</u>
	$\lambda$	$\lambda$
.5	2.4	2.25
1.0	2.05	1.9
1.5	1.85	1.72
2.0	1.75	1.68
2.5	1.62	1.42
3.0	1.52	1.37
3.5	1.45	1.3
4.0	1.4	1.25
4.5	1.38	1.22
5.0	1.32	1.2

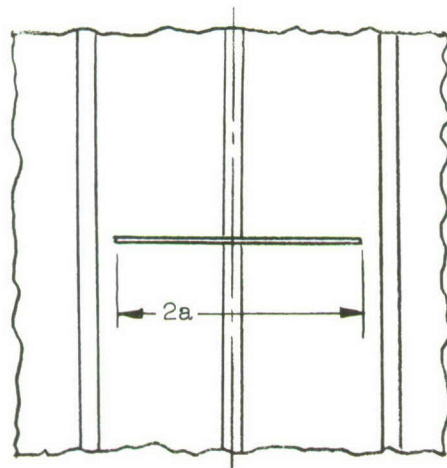


broken center spar,  
others intact

TABLE 4-2 VALUES OF  $\lambda$  FOR ZEE-STIFFENED STRUCTURE

$$K = \lambda f_g \sqrt{\pi a}$$

a	<u>Titanium</u>	<u>Aluminum</u>
	$\lambda$	$\lambda$
.5	2.0	2.1
1.0	1.65	1.85
1.5	1.42	1.55
2.0	1.32	1.4
2.5	1.28	1.55
3	1.2	1.24
3.2	1.14	1.16
4.0	.94	.97
4.8	.75	.75
5.6	.82	.75
6.4	.74	.725

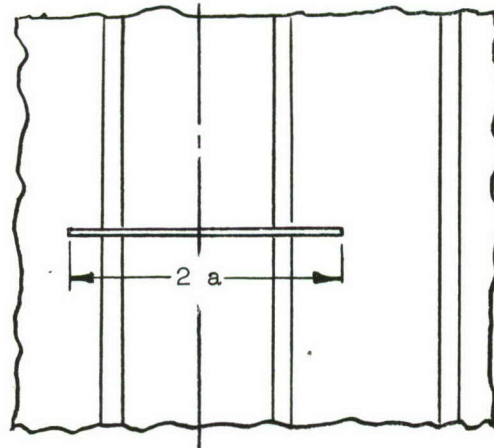
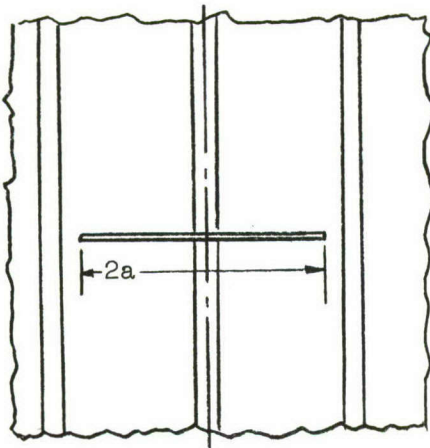


center stiffener broken,  
others intact

TABLE 4-3 VALUES OF  $\lambda$  FOR INTEGRALLY STIFFENED STRUCTURE

$$K = \lambda f_g \sqrt{\pi a}$$

ONE STIFFENER BROKEN **		TWO STIFFENERS BROKEN **	
a	$\lambda$ *	a	$\lambda$ *
1	1.72	.2	.98
1.5	1.34	.4	.97
2.0	.66	.6	.92
4	1.80	.8	.83
		1.0	.46
		2.2	1.66
		3.0	1.35



\*  $\lambda$ 's are same for both titanium and aluminum

\*\* Cracks grow through stiffener at same rate as through skin.



#### 4.4 FATIGUE CRACK GROWTH ANALYSIS

If conditions are such that fracture mechanics is applicable, the crack propagation rate for a given material is a unique function of stress intensity, and the constant-amplitude K-rate curve,  $\frac{da}{dN} = \frac{da}{dN} (\Delta K, K_{\max})$ , is a material property.

Various investigators have found means for defining a single K-rate relationship accurate for all range ratios, R. Written in functional form, the most popular are

$$\frac{da}{dN} = \frac{da}{dN} (\Delta K) \quad (\text{Paris})$$

$$\frac{da}{dN} = \frac{da}{dN} \left( \frac{\Delta K^m}{K_c - K_{\max}} \right) \quad (\text{Forman}) \quad (4-16 \text{ a, b, c})$$

$$\frac{da}{dN} = \frac{da}{dN} (K_{\max}^{1-m} \Delta K^m) \quad (\text{Erdogan, Walker})$$

As Figure 4-14 indicates, the first step in the general prediction procedure is to utilize one of the Equations (4-16 a, b, c) along with existing constant amplitude crack growth rate data to generate a K-rate curve for the material.

Step II in the prediction process is to generate the variable amplitude rate curve for a particular sequence of loading events. This step may be bypassed; however the computational effort saved by this step is enormous. The only assumption involved in using this step is that the geometry factor  $\alpha$  does not change significantly during any one flight. This is certainly true for any calculation involving hundreds of flights.

Let us suppose that the loading spectrum is given in terms of  $Z_i$  the  $i^{\text{th}}$  load level in the spectrum, and  $n_i$ , the number of occurrences per unit time. Load level  $Z_i$  may be expressed in whatever load-related units are convenient for presenting the spectrum, e.g., stress, total load, or (as in Section 5.3) vertical load factor. Let S be defined as the conversion factor from load to stress, i.e.,

$$f_{gi} = Z_i \cdot S \quad (4-17)$$

Using Equation (4-3), the  $i^{\text{th}}$  level of stress intensity factor corresponding to a particular value of the geometry factor  $\alpha$  is

$$K_i = Z_i \cdot \alpha_s \quad (4-18a)$$

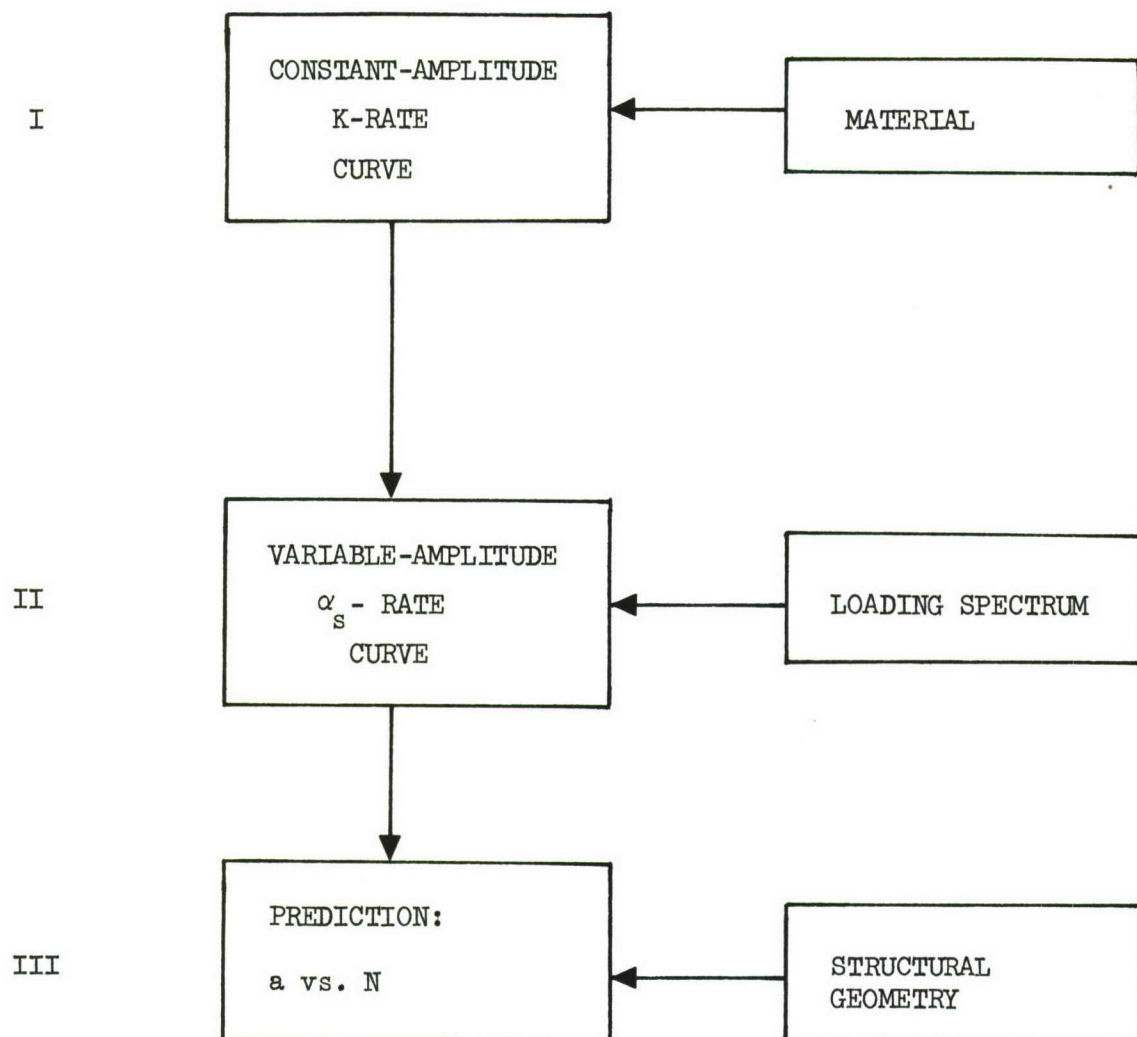


FIGURE 4-14 THE GENERAL STRESS-INTENSITY APPROACH TO PREDICTION OF CRACK PROPAGATION IN STRUCTURE UNDER VARIABLE-AMPLITUDE LOADING

where the stress-adjusted geometry factor  $\alpha_s$  is defined by the relationship

$$\alpha_s = S \cdot \alpha \quad (4-18b)$$

To calculate crack growth due to any load cycle in a loading spectrum, the simplest procedure is to assume that the crack growth rate is the same as for constant amplitude loading, so that

$$\frac{da}{dN_i} = \frac{da}{dN_i} (\Delta K_i, K_{max_i}) \quad (4-19)$$

using Equation (4-16 a, b, c) directly. Then for a particular value of  $\alpha_s$  (Equation (4-18a)), the average crack growth rate per flight-hour is

$$\frac{da}{dF} = \sum_{i=1}^k (n_i \cdot \frac{da}{dN_i}) \quad (4-20)$$

where  $n_i$  is the number of occurrences per hour of the  $i^{th}$  cyclic load level and  $k$  is the number of different cyclic load levels in the loading spectrum. This procedure is often conservative because it ignores any growth-retardation effects of occasional large cyclic stresses.

Recently, attempts have been made to develop crack growth modeling to define how the stress-strain field in the plastic zone around the tip of a crack responds to variable amplitude loads and thereby influences further crack growth. Current interest is focused on the observation that occasional high loads cause permanent plastic deformation at the crack tip which alters the influence of the subsequent loading cycles on crack growth.

So far, the approach has been to introduce and try simple empirical models of crack growth retardation following occasional high loadings. The first such models were apparently those of Wheeler, Reference 4-19 and Willenborg, et al, (Reference 4-20). These approaches assume that the crack growth is slower than the normal constant-amplitude rate for a given sequence of load cycles if they are preceded by a higher amplitude loading. The constant-amplitude rate curve, Equation (4-17) is used as a baseline in these retardation models.

The question of whether or not to rely on crack retardation effects in design analysis remains open. However, working with titanium, Jonas and Wei (Reference 4-21) have observed that retardation effects can be partially or fully washed out by a large



compression cycle, or by simple relaxation at zero load, following an overload. Working with aluminum, Raju (Reference 4-22) has similarly observed that relaxation at elevated temperature after application of a high stress cycle can reduce or eliminate retardation.

Unfortunately these same conditions readily occur on aircraft structure in service. For example, the lower-wing surface of a typical fighter wing will experience compression loads due to negative load factors, and elevated temperatures during high-speed flight. Furthermore, any structural member will experience prolonged periods between flights during which the load is essentially zero. Therefore beneficial crack-retardation effects may be greatly reduced, and the prudent approach at present is to neglect these effects in design analysis.

Equations (4-18a), (4-19) and (4-20) are used at selected values of  $\alpha_s$  to generate points on a spectrum crack growth rate curve,  $da/dF$  vs.  $\alpha_s$ . Simple curve fitting is used to complete the curve.

The last step in crack growth prediction depicted in Figure 4-14 is the numerical integration of this rate curve between an initial and final crack length. This step, which is rapid computationally, is repeated for each required combination of crack geometry and value of  $S$ . The initial configuration of the cracked structure and a known crack growth path provides a relationship between the geometry factor  $\alpha$  and the crack dimension  $a$ . Thus for any value of  $S$ ,  $\alpha_s$  is a known function of  $a$ , permitting integration of the  $\alpha'_s$ -rate curve.

A series of  $S$ -values are selected to study the effect of design changes that would proportionally increase or reduce all the stresses in the spectrum. The result of the calculations is a 3-dimensional plot of number of hours versus crack length versus  $S$  (representing design stress level) for each damage configuration of interest. Appendix D for example presents several such plots.

#### 4.5 SUSTAINED LOAD CRACK GROWTH ANALYSIS

Certain environments can have a very pronounced effect on crack propagation. The effect can be thought of as the promotion of time dependent crack extension at levels of stress intensity,  $K$ , less than the critical values ( $K_c$  or  $K_{Ic}$ ). Processes commonly referred to as stress corrosion cracking or hydrogen-embrittlement cracking are sustained load examples of this. When the crack grows to a

critical length in a corrosive environment rapid fracture will occur; however it has been shown (Reference 4-23) that the final absolute values of fracture toughness ( $K_c$  or  $K_{Ic}$ ) obtained in this manner will be the same as the fracture toughness obtained by monotonically increasing load tests conducted in non-corrosive environments normally encountered by aircraft (e.g., water, NaCl solution, fuel, etc.)

Figure 4-15 illustrates sustained load environmental crack growth behavior. Curves such as that shown in Figure 4-15 may be obtained by loading a series of specimens to various percentages of the static failure stress (i.e., various percentages of the baseline critical stress intensity factor value for the same crack size) and maintaining these loads until fracture, or for a very long period of time. The initial stress intensities are calculated based upon the corresponding initial crack size or flaw size ( $2a_i$  or  $a_i$  and  $2c_i$ ) and the sustained load applied to the specimens in the environment. These stress intensity factors are usually termed  $K_i$ . The time required to fracture depends upon the applied stress level and properties of the material. The times to failure of these specimens are recorded and are plotted against their  $K_i$  values. No failures will occur for stress intensities below the threshold level called  $K_{scc}$  or  $K_{Isc}$  (plane strain). The sensitivity for aluminum and titanium alloys usually can be determined within a period of six hours of sustained load testing. However, considerable hours of testing are required for establishing a real threshold level for steels. Example test data for Ti-6Al-4V, and D6AC steel are given in Figure 4-16. Aluminum alloys are usually less sensitive to static environmental effects.

During an environmental sustained load test, the increments of the crack extension may be recorded so that a crack length versus time curve is obtained. A typical crack extension versus time curve is shown in Figure 4-17. From the crack length versus time curve obtained from the same tests, a crack growth rate curve,  $da/dt$  versus  $K$  (or  $\Delta K$ ), can be obtained. This curve has been shown to be a basic material property.

Wei and Landes (Reference 4-27) have shown that the mechanism for environment-enhanced crack growth under sustained load and in fatigue are inter-related for certain materials. However, more studies and development work are required in order to develop a method for analyzing accumulated crack extensions under repeated fatigue and sustained load cycles.

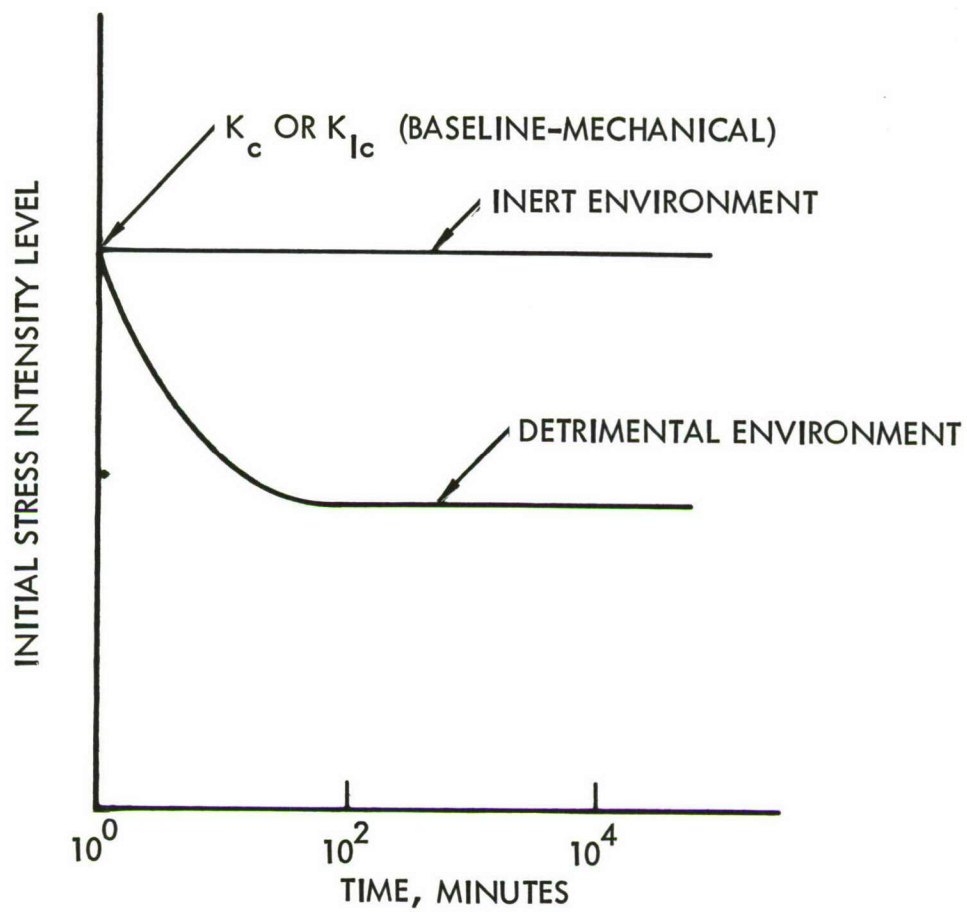


FIGURE 4-15 SCHEMATIC CURVES SHOWING THE ENVIRONMENTAL DELAYED FAILURE BEHAVIOR OF SPECIMENS SUBJECTED TO SUSTAINED LOADS.



Environment: 3.5% Salt Solution

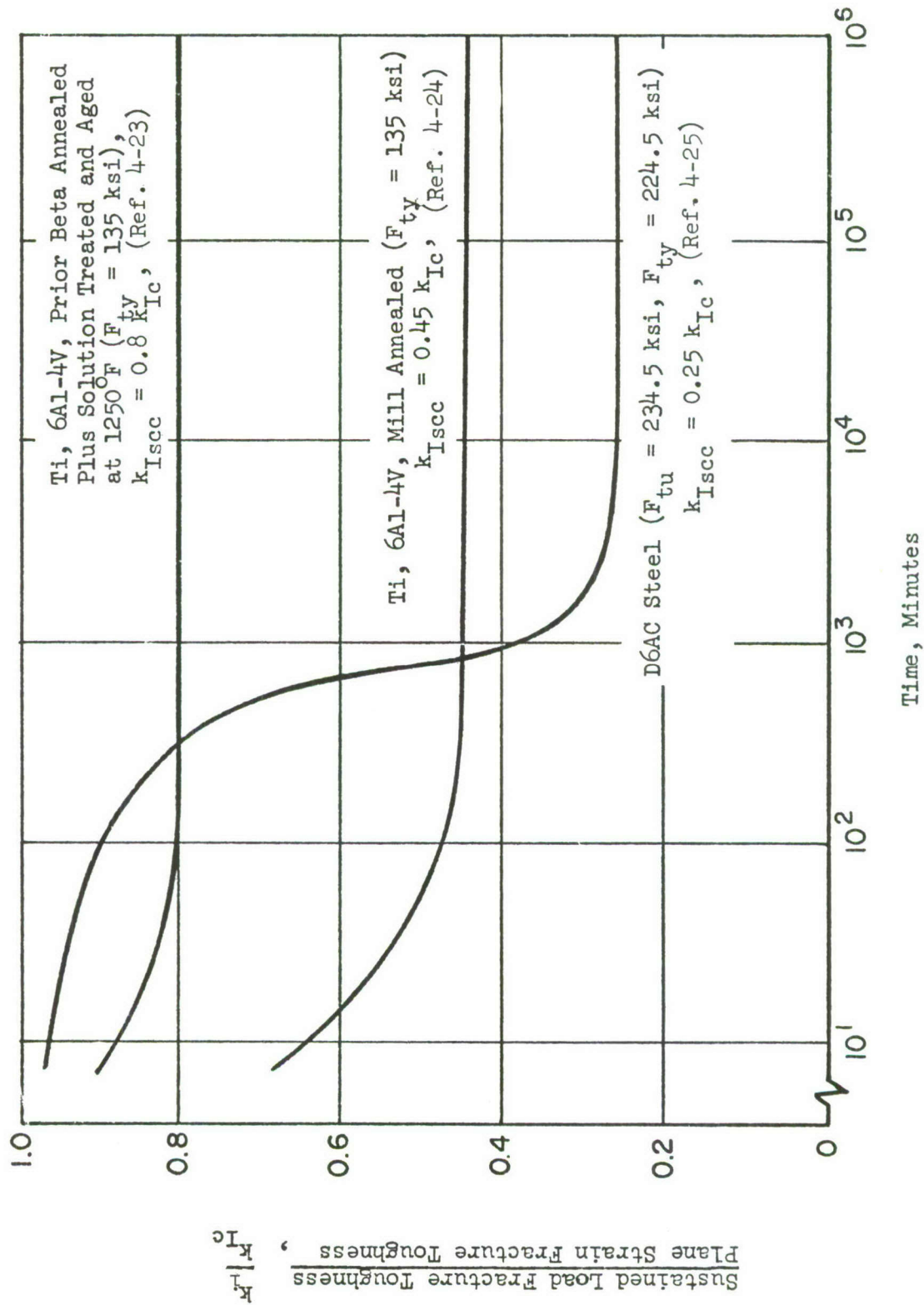


FIGURE 4-16 EFFECT OF ENVIRONMENT AND TIME AT SUSTAINED LOAD ON FRACTURE TOUGHNESS FOR TITANIUM ALLOYS AND STEEL

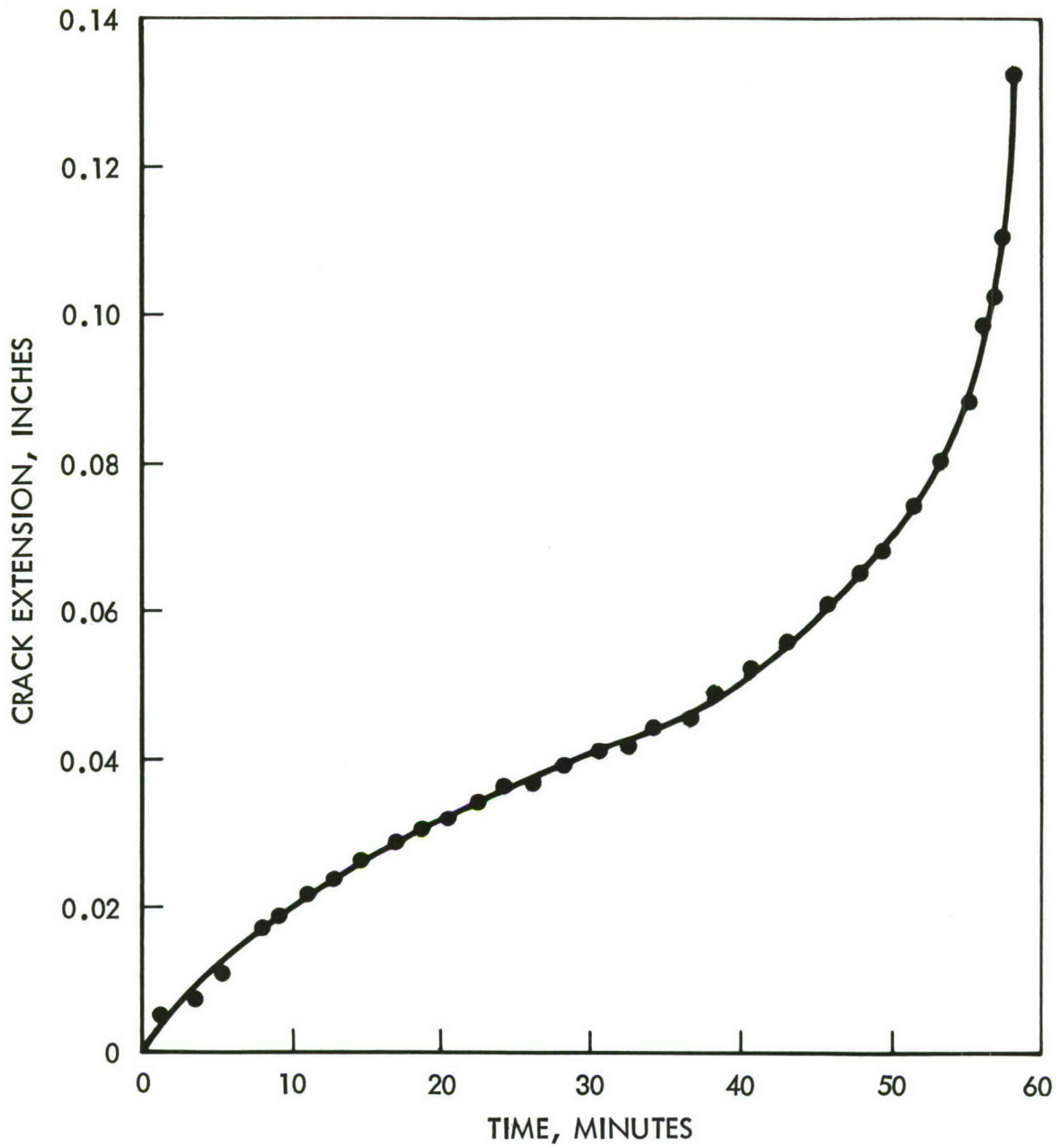


FIGURE 4-17 CONSTANT LOAD SUBCRITICAL CRACK GROWTH OF AM 350 STEEL  
IN PURIFIED ARGON ENVIRONMENT (REFERENCE 4-26)

For aircraft design purposes, the effect of environmental crack growth behavior can be considered in the following two ways. The first accounts for the sustained loads expected to be applied the predominant period of time the aircraft is in the presence of a detrimental environment. The second accounts for the effect of environment on fatigue crack propagation rates.

- o The ground and steady-state (1-g) flight stress levels may be compared to the stress required to produce stress intensities above  $K_{Isc}$  for the damage sizes of interest. If the ground or 1-g flight stresses are lower, then it may be assumed that significant crack growth due to the major sustained loads will not take place.
- o For fatigue crack propagation a growth rate curve obtained in a realistic environment should be used for the analysis. Considering the accuracy of current methods of crack growth analysis, the use of cyclic applied loads and a reasonable crack growth rate should account for any small amount of crack growth that might be contributed by sustained loads.



#### 4.6 RESIDUAL STRENGTH ANALYSIS

Residual strength analysis is conducted to determine the capability of a structure containing significant pre-damage to withstand a single, monotonically increasing load for a short time without catastrophic failure. To perform the residual strength analysis, the three following elements are required:

- (1) A structural analysis (stresses, stress intensity factors, etc.)
- (2) A failure criteria (critical stress, critical K, tangency to a resistance (R) curve, etc.)
- (3) Material properties (ultimate strength,  $K_c$ , R-curve, etc.)

For redundant structure, it is assumed that one entire member is totally broken. Thus no crack is present and the residual strength is determined by relating the stress redistribution due to the broken member to the ultimate strength of the material as discussed in Section 4.6.1. For other types of structure the assumed damage is a crack, and classical fracture mechanics can be used as an analytical tool. Presently a critical stress intensity approach is used, as discussed in Section 4.6.2. Recent research has developed the application of the crack growth resistance curve to predict residual strength of cracked plate or shell structure. (See Appendix F). Although not used in the analyses conducted in the application study, the R-curve approach is potentially a powerful tool which corrects some of the weaknesses of the critical K method.

##### 4.6.1 Redundant Structure (Single Member Broken)

Many designs lend themselves to partitioning in the interest of fail-safe damage tolerance with little or no increase in cost, weight or complications. Examples include longerons made of back-to-back channels in place of I-beams, back-to-back angles in place of T-sections, and panelization of wing surfaces. These multi-member redundant structures, any single member of which may be completely fractured, require only static strength principles to predict allowable strengths. Fatigue analysis or fatigue tests may be required to determine the safe inspection intervals after one member is broken.

Test of damaged structure (Reference 4-28) have shown that the use of splices as crack stoppers is an effective device for providing "fail-safe" structure. The relatively flexible plank splices protect the adjacent planks from the

severity of the stress concentration existing at the tip of a fatigue crack. While there is a shear diffusion problem in routing the cut load through the splice attachments into the adjacent structure, this is usually less severe than the stress condition surrounding the tip of the crack. A balance of many factors is involved in optimizing the degree of panelization, including the reserve strength in the adjacent planks, and the compromise in the rivet design for high strength yet flexible deformation characteristics for maximum relief of the load concentration.

The following procedures describes an analysis method for designing longitudinally-spliced panels, based on the experimental results reported in Reference 4-28.

Suppose a spliced panel is made up of three planks as shown in Figure 4-18, and assume that a crack has propagated completely across the middle plank. The fail-safe criterion for this configuration is:

$$\begin{aligned} (f_g + f_{we}) &< F_{tu} \quad \dots \text{fail-safe} \\ &\geq F_{tu} \quad \dots \text{not fail-safe} \end{aligned} \tag{4-21}$$

where  $f_g$  is the applied stress, ksi

$f_{we}$  is the additional stress picked up by the side-planks due to failure of the middle plank, i.e.,

$$f_{we} = \frac{P_{cut}}{2A_1}$$

and

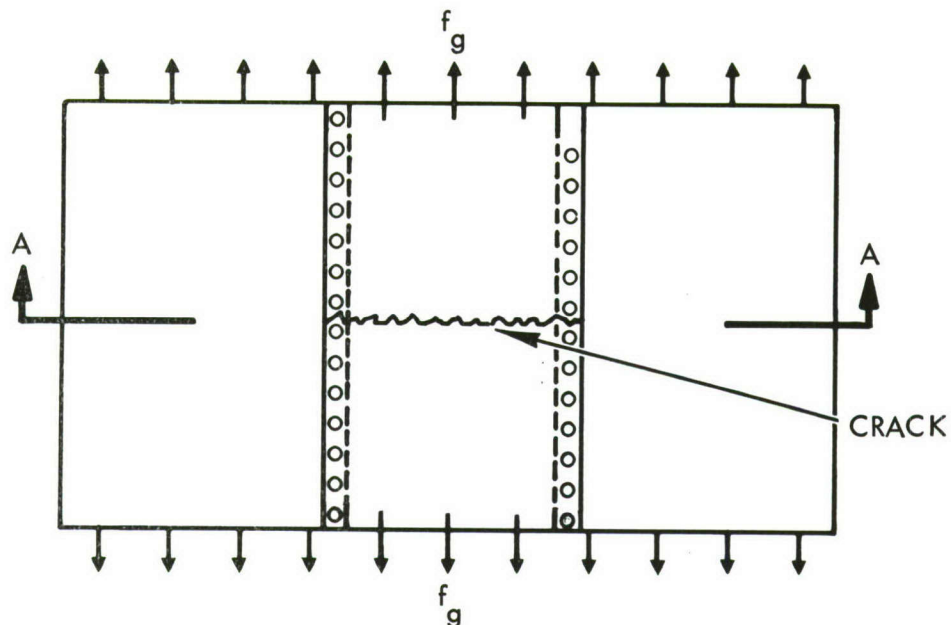
$$P_{cut} = f_g w_m t_m$$

$$A_1 = w_e \cdot t_s$$

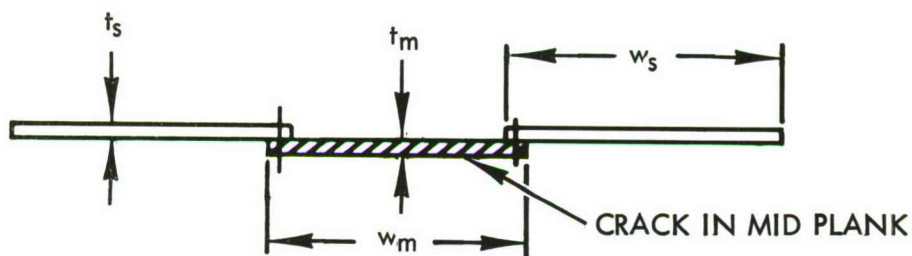
$F_{tu}$  = tensile ultimate strength of the side planks, ksi

$w_m$  = width of the middle plank, inch

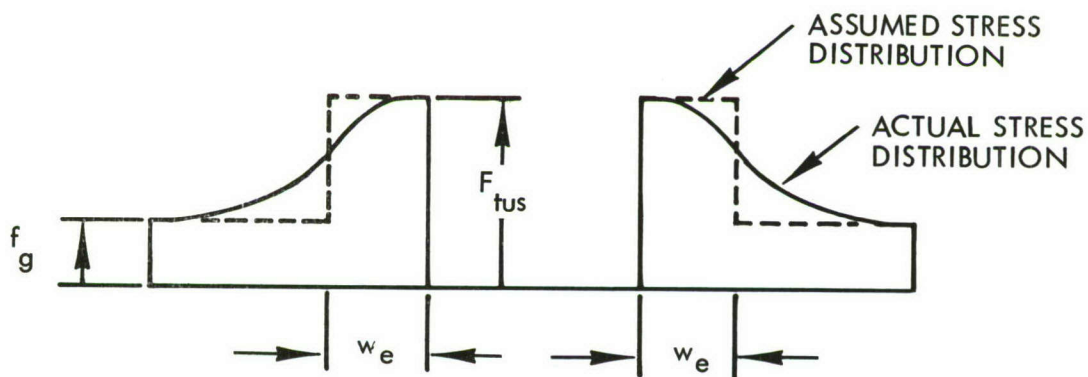
$t_m$  = thickness of the middle plank, inch



a. TEST PANEL CONFIGURATION



b. SECTION A-A



c. STRESS DISTRIBUTION ACROSS SECTION A-A

FIGURE 4-18 STRESS DISTRIBUTION ACROSS A THREE-PLANK FAIL-SAFE TEST PANEL WITH THE MIDDLE PLANK BROKEN



$t_s$  = thickness of the side planks, inch

$w_e$  = experimentally determined parameter, called the "effective width",  
i.e., one half of the cut load, after failure of the middle plank,  
is sustained by the "effective width" in each of the side planks.

Figure 4-19 shows that the effective width,  $w_e$ , is a function of the sheet materials, the attachment strength, the attachment spacing and the attachment load-deflection characteristics. Substituting into Equation (4-21) and solving for the marginal case:

$$f_g + \frac{f_g w_m t_m}{2w_e t_s} = F_{tu}$$

or

(4-22)

$$\frac{f_g}{F_{tu}} = \frac{1}{1 + \frac{w_m t_m}{2w_e t_s}}$$

Now consider a wide panel  $W$ , bounded by beam caps, and divided into  $n$  equal-sized, smaller panels of width  $w_m$ , such that  $W = n \cdot w_m$ . For  $t_s = t_m$  and  $f_g = F_g$ , the allowable stress, Equation (4-22), becomes:

$$\frac{F_g}{F_{tu}} = \frac{1}{1 + \frac{W}{2nw_e}} = \frac{n\beta}{n\beta + 1} \quad (4-23)$$

where  $\beta = 2w_e/W$

Equation (4-23) is plotted in Figure 4-20 showing the critical residual strength ratio for any number of small panels, from  $n = 1$  through 15, as a function of the effective width parameter  $2w_e/W$ . For a required stress level, knowing " $w_e$ ", the degree of panelization may be determined, or for a given degree of panelization " $n$ ", and  $w_e$ , the allowable gross area residual strength level may be determined.

The curves in Figures 4-19 and 4-20 can be used as a basis for designing wing surface structure which is panelized to achieve a fail-safe design. It should be



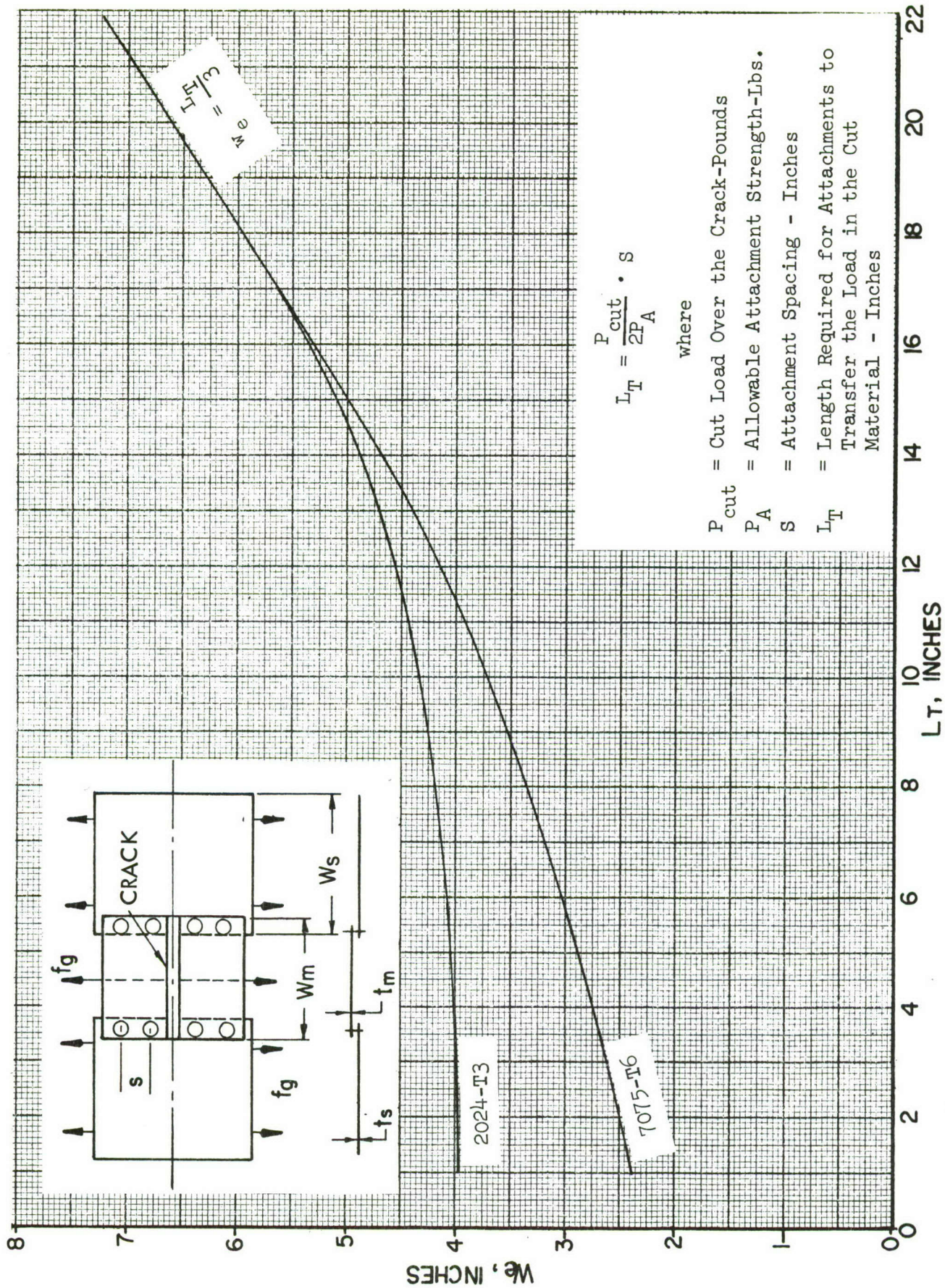


FIGURE 4-19 EFFECTIVE WIDTH IN SIDE PLANKS FOR FLAT PANELS WITH LONGITUDINAL SPLICES  
(REFERENCE 4-28)



noted that the curves in Figure 4-19 were empirically generated and extrapolations to other materials (particularly for  $L/T < 16$ ), should be done with care. For back-to-back members, the structure must be able to support fail-safe loading conditions with one member broken. Therefore, for back-to-back members static strength analysis methods can be used by considering the redistribution of loads due to the broken member.

#### 4.6.2 Structure Containing Crack(s)

##### (1) Unreinforced Plane Structure

The critical K criterion is used for the residual strength analysis of unreinforced plane structure. Failure is assumed to occur when the stress intensity factor reaches critical values for single mode loading termed  $K_{1c}$ ,  $K_{2c}$ , or  $K_{3c}$ , respectively. (Subscripts 1c, 2c and 3c are used to denote both plane stress and plane strain, critical stress intensities for Modes 1, 2, or 3 as distinguished from  $K_{Ic}$  for plane strain stress intensities). For analysis purposes these parameters are considered material constants. The criteria for fracture under combined tension and in-plane shear loading conditions states that failure will occur when

$$\left(\frac{K_1}{K_{1c}}\right)^u + \left(\frac{K_2}{K_{2c}}\right)^v \geq 1 \quad (4-24)$$

where u and v are empirical constants. A reasonable choice of u and v is 2 based on the limited amount of available data for aluminum alloys.

For design purposes this is a straight-forward approach providing that the crack length used is the initial crack length and that  $f_g$  corresponds to the maximum load. Since there is often a significant amount of slow stable growth prior to catastrophic failure, the maximum load and the initial crack length do not occur at the same point in time. A stress intensity factor calculated using these quantities in a sense is meaningless. However, if the final crack length, corresponding to the maximum load, is proportional or approximately proportional to the initial crack length, the procedure remains rational. This is because the  $K_c$  values are simply scaled by this proportionality factor.



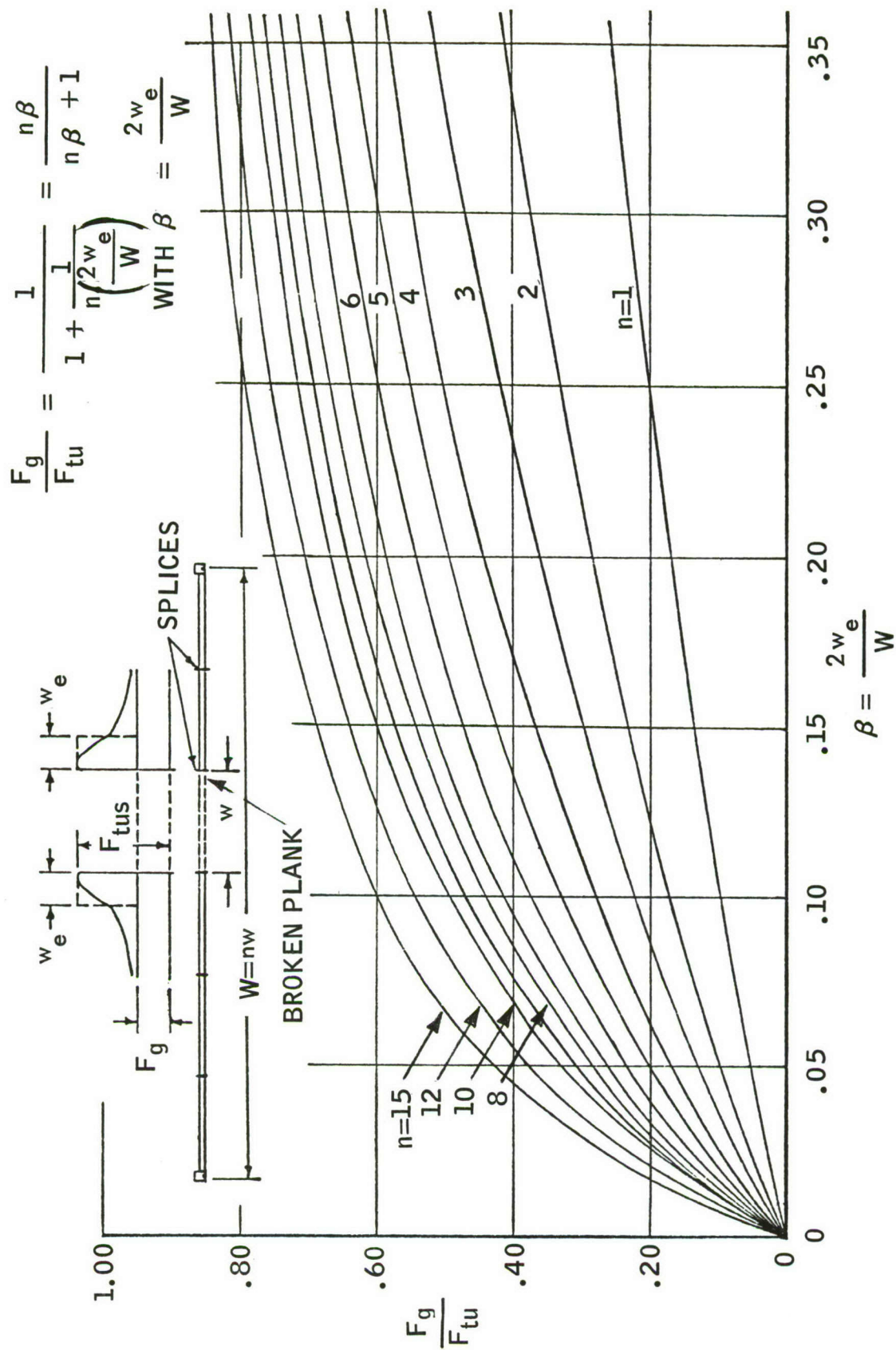


FIGURE 4-20. INFLUENCE OF THE DEGREE OF REDUNDANCY ON THE RESIDUAL STATIC STRENGTH OF MULTI-PLANK PANEL WITH ONE PLANK BROKEN

If  $f_s = 0$ , Equation (4-24) reduces to

$$K_1 = K_{1c} \quad (4-25)$$

or, if  $f_g = 0$ , then Equation (4-24) becomes

$$K_2 = K_{2c} \quad (4-26)$$

The critical stress intensity factors  $K_{1c}$  and  $K_{2c}$  may be determined by conducting fracture tests of precracked specimens under pure tension or pure shear, respectively. The critical stress intensity factors are then determined from the test results by substituting the gross area stress at panel failure and the initial crack length into Equation (4-6) to give  $K_{1c}$  and  $K_{2c}$ .

In addition to the crack displacement modes, the state of stress at the crack front must also be considered. For loads in the plane of the plate, the state of stress can vary between plane stress and plane strain. In the case of a fully embedded crack (flaw), the constraint at the crack front (or along the crack periphery) is very high, thus it is in plane strain. For a thru-the-thickness crack in a thick plate, the state of stress at the crack tip in the mid-thickness of the plate is triaxial; this case is also plane strain. The triaxial stress condition (plane strain) at the crack tip changes gradually with decreasing plate thickness to a biaxial state of stress (plane stress) in a thin sheet.

Although there is no difference in K-formulae for the conditions of plane stress or plane strain, the critical stress intensity factor, i.e., the fracture index for a material, does vary with the structural configuration and crack morphology and is thickness dependent. For the tensile mode failure, the critical stress intensity factor is designated  $K_{Ic}$  for plane strain and  $K_c$  for plane stress (or any other material thicknesses which do not produce plane strain failure). The plane strain stress intensity factor  $K_{Ic}$  can be regarded as the minimum threshold of  $K_c$  value for large thicknesses. See Figure 4-21.

$K_c$  will not be a function of the configuration if the test panel is sufficiently long and wide and if  $a/W$  is an appropriate range. For all configurations  $K_c$  is thickness dependent;  $K_c$  data generated on appropriately sized panels can be

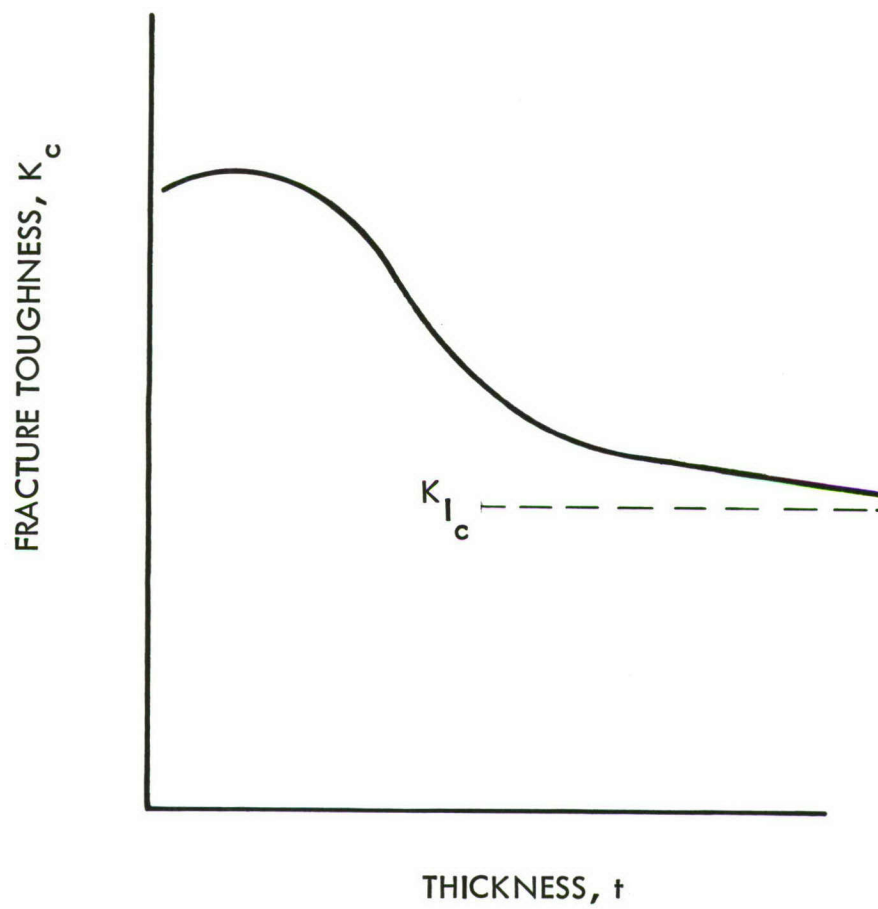


FIGURE 4-21 EFFECT OF THICKNESS ON FRACTURE TOUGHNESS PROPERTIES



used to make predictions on panels which are also of the proper size. For ranges outside of this,  $K_c$  is an inappropriate predictive tool.  $K_c$  values for many materials are presently available.

## (2) Reinforced Plane Structure

Several design techniques may be used to increase the fail-safe efficiency of reinforced plane structure. These techniques can best be classified as crack interrupters, such as splices or holes and as crack growth inhibitors, primarily fail-safe straps and reinforcements. In this section, attention will be focused on a configuration in which a relatively large flat panel is reinforced with a series of parallel stringers or straps. The loading condition considered will be one in which the applied loads are parallel to the stringers. Any damage present will be assumed to be perpendicular to this load and the stringers. (See Figure 4-22).

In general, a variety of failure modes are possible for this configuration. Either the panel, the reinforcement, or the attachment may fail first and each may fail in a number of different ways.

There have been a number of investigations (References 4-28 thru 4-44), both analytical and experimental, involving the damage tolerance of reinforced flat panels of this type. Only a few of these have attempted to systematically study the effect of configuration and material variables.

Three analytical investigations (References 4-36, 4-37 and 4-40), modeling an infinite linearly elastic cracked plate with linearly elastic reinforcements and rigid attachments, have established the effect of elastic material properties and geometric variables. For example Poe (Reference 4-40) has pointed out that as  $a$  increases the maximum load carried by the reinforcement asymptotically approaches a limiting value

$$P_{\max} = \left( A \frac{E_f}{E_s} + Bt \right) f_g \quad (4-27)$$

where

$A$  is the stringer area,  
 $E_f, E_s$  are the moduli of the stringer and skin, respectively

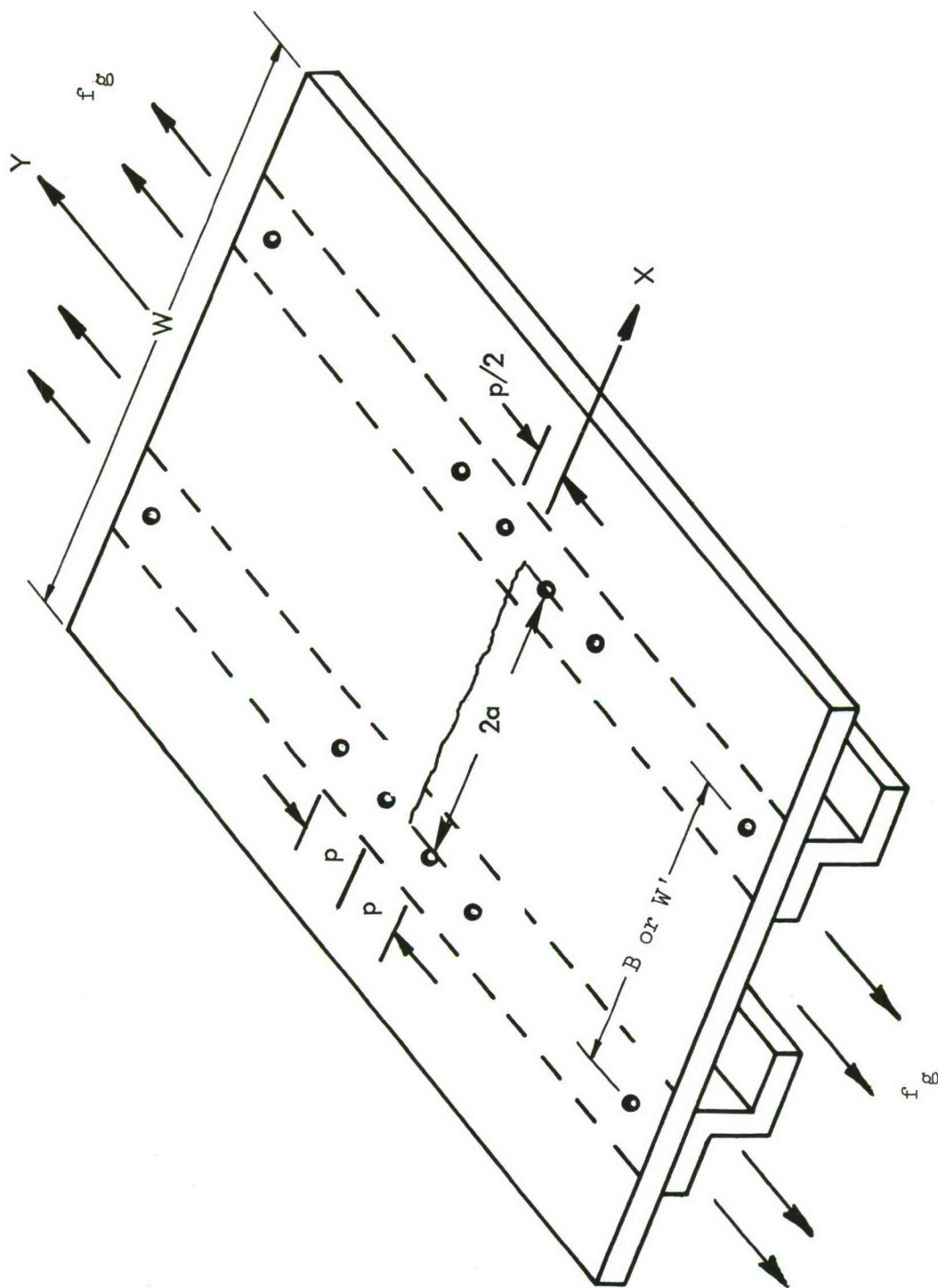


FIGURE 4-22 THRU-THE-THICKNESS CRACKS IN A REINFORCED PANEL

B is the stringer spacing,  
 t is the skin thickness,  
 $f_g$  is the applied stress in the panel.

The maximum stress in the stringer is simply

$$f = \left( \frac{E_f}{E_s} + \frac{Bt}{A} \right) f_g \quad (4-28)$$

Thus minimizing the stringer to skin modulus ratio and the skin to stringer area ratio decreases the propensity of the configuration to be reinforcement critical, i.e., it makes failure of the skin first more likely.

These analytic investigations also indicate that increased stringer to skin stiffness (area times modulus) ratio and decreased attachment spacing tend to lower the skin stresses in the crack tip vicinity and thereby make a skin critical situation less likely. On the other hand, a recent experimental investigation by Liu and Ekvall (Reference 4-42) indicates that for a wide class of stiffener configurations (having small cross-sectional area) the stiffener modulus is a secondary variable affecting the residual strength. They found that a pertinent stiffener property was the product of the stiffener yield strength and area. It must be emphasized that the above tests were all skin critical (as evidenced by film and strain gage records) since reinforcement critical tests could be expected to correlate with the reinforcement ultimate strength and consequently the reinforcement yield strength in the same manner. Liu and Ekvall also indicated that the low cycle fatigue property of the stiffener material should also be considered to insure that the reinforcement will be effective for a reasonable length of time.

With this background, the analysis procedure for reinforced plane structure will now be described. Consider the case of reinforcements attached to a plate as shown in Figure 4-22. The panel is subjected to uniform extension stress  $f_g$ . The stress intensity for the skin crack is reduced by the presence of a stiffener. A portion of the load acting on the skin is transmitted through the fastener and will be carried by the stiffener. Consequently, the general stress intensity factor K for this case will consist of two terms, the term involved with the



overall stress acting on the skin,  $K'$  (based on uniform stress and crack length only), for the reinforced panel and the term involved with the transmitted load in the reinforcement,  $k_r$ , i.e., when  $K$  reaches  $K_c$ ,

$$K_c = K' - k_r \quad (4-29)$$

where the minus sign for the  $k_r$  term refers to the reduced crack tip stress intensity due to the effect of the stiffener. In other words, the term  $k_r$  quantitatively reflects the efficiency of the reinforcement, and may be a function of stiffener material and fastener material, size and spacing.

It is convenient to express the efficiency term in a dimensionless form, e.g., K-ratio, stress ratio, or load ratio.

Dividing Equation (4-29) by the constant  $K_c$  and rearranging terms gives

$$\frac{K'}{K_c} = \frac{k_r}{K_c} + 1 \quad (4-30)$$

If  $F'$  is the gross area stress at fracture for a reinforced panel, then

$$\frac{K'}{K_c} = \frac{F'}{F_g}$$

for a given crack length and we obtain

$$\frac{F'}{F_g} = \frac{k_r}{K_c} + 1 \quad (4-31)$$

Since  $K_c$  is a constant,  $F'/F_g$  is still a function of  $k_r$ , and  $k_r$  is a function of many stiffening variables. This ratio  $F'/F_g$  is the efficiency of the structure and will be represented by  $\gamma$ , where

$$\gamma = f(A, F_{tyf}, E_f, p, \text{etc.})$$

Based on available data for reinforced flat panels, a set of design curves has been constructed (References 4-28 and 4-41). This set of design curves, presented in Figure 4-23, correlates the reinforcement efficiency parameter,  $\gamma$ ,

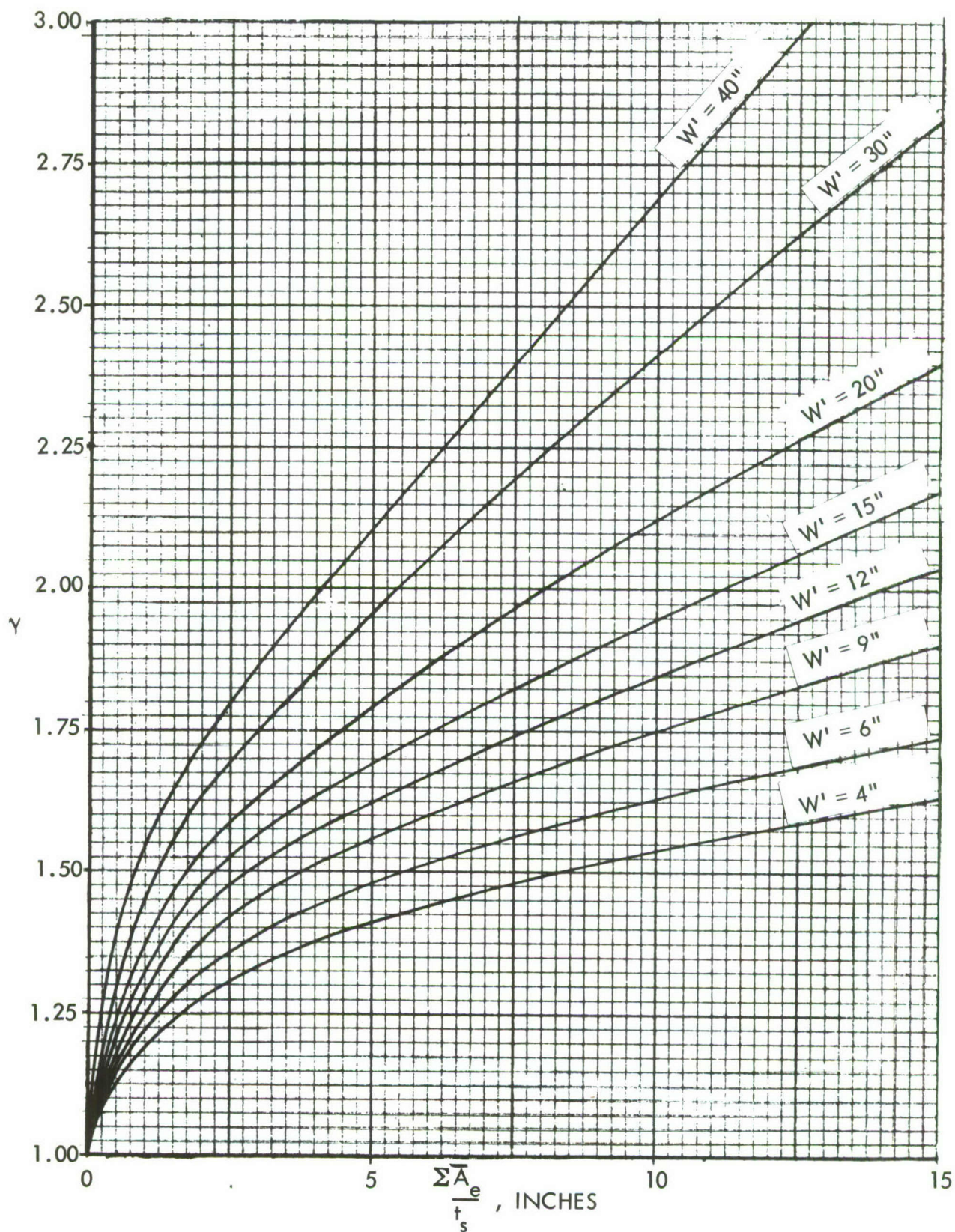


FIGURE 4-23 DESIGN CURVES FOR REINFORCED FLAT PANELS



and a lumped stiffening parameter

$$\Sigma \bar{A}_e / t$$

where

$t$  is the skin thickness.

According to References 4-28, 4-40 and 4-41, if the reinforcement area is small, as in the case of a flat strap, the fracture process will take place in the plastic range of the strap material. If, however, the reinforcement is relatively large, e.g., a heavy stringer, the reinforcement material remains in the elastic stress-strain range throughout the fracture process. Therefore, the reinforcement effective area can be approximated by

$$\bar{A}_e = A \cdot (F_{tyf} / F_{tys}) \quad (4-32)$$

for a flat strap. For the case of a stringer

$$\bar{A}_e = A_e \cdot (E_f / E_s) \quad (4-33)$$

with

$$A_e = A \left[ 1 + \left( \frac{y}{\rho} \right)^2 \right]^{-1} \quad (4-34)$$

accounting for eccentric loading from the cracked sheet.

The  $(\Sigma)$  sign in  $\Sigma \bar{A}_e / t$  stands for the sum of the intact stiffeners which contribute the stiffening effect to the cracked area. For example, the  $(\Sigma)$  will be 2 for the case shown in Figure 4-22.

Next consider the case of a reinforced panel subjected to combined tension and shear, i.e., where shear stresses parallel to the crack are combined with tension stresses perpendicular to the crack. Assuming that the stiffener does not carry any shear load, Equation (4-24) becomes

$$\left( \frac{K_1}{K_c} \right)^2 + \left( \frac{K_2}{K_{2c}} \right)^2 = 1 \quad (4-35)$$



The analysis method presented above has been checked with fail-safe panel tests summarized in Table 4-4. To perform the residual strength analysis, the  $K_c$  value for the sheet or plate material and the structural efficiency curve are needed. The structural efficiency curves are the family of  $\gamma$ -curves given in Figure 4-23. Figures 4-24 and 4-25 give the  $K_c$  allowables for 2024-T3 and 7075-T7651 aluminum sheet and plate, the skin materials for the 24 test panels given in Table 4-4. Although the majority of the data points are applicable to thin sheet structures, a wide range of reinforcement effective area to sheet thickness ratios are included. The correlation between prediction and test results are shown in Figure 4-26. In Figure 4-27, the deviation of the predictions are presented as a function of the reinforcement variable; the deviations range between  $\pm 20$  percent. Furthermore, comparison between the actual  $K_c$  values for the test panels and the allowable  $K_c$  values (see Table 4-4) show that the allowable curves given in Figures 4-24 and 4-25 are reliable.

TABLE 4-4 TEST PANEL CONFIGURATIONS

PANEL NO.	STIFFENER							SKIN		
	TYPE	F <sub>typ</sub> , ksi (ACTUAL)	F <sub>tyf</sub> , ksi (TYPICAL)	A <sub>2</sub> , INCH	A <sub>p</sub> , INCH	SPACING B, INCH	REMARKS	TYPE	K <sub>c</sub> , ksi √in. (ACTUAL)	K <sub>c</sub> , ksi √in. (ALLOWABLE)
101A	.063 x .85 BARE 2024-T3 STRAP	49.7	50	.0535	.0535	6.0	7 STRAPS (CENTER ONE BROKEN)	.063 x 48 BARE 2024-T3(L)	117.5	100
101B	.063 x .85 BARE 2024-T3 STRAP	49.7	50	.0535	.0535	6.0	7 STRAPS (CENTER ONE BROKEN)	.063 x 48 BARE 2024-T3(L)	117.5	100
103A	.063 x .85 AISI 430 STEEL ANNEALED STRAP	46.7	45	.0535	.0535	6.0	7 STRAPS (CENTER ONE BROKEN)	.063 x 48 BARE 2024-T3(L)	117.5	100
103B	.063 x .85 AISI 430 STEEL ANNEALED STRAP	46.7	45	.0535	.0535	6.0	7 STRAPS (CENTER ONE BROKEN)	.063 x 48 BARE 2024-T3(L)	117.5	100
105A	.063 x .85 STAINLESS STEEL (301 FH) STRAP	165.0	140	.0535	.0535	6.0	7 STRAPS (CENTER ONE BROKEN)	.063 x 48 BARE 2024-T3(L)	117.5	100
107A	.063 x .85 Ti-6Al-4V DUPLEX ANNEALED STRAP	147.0	128	.0535	.0535	6.0	7 STRAPS (CENTER ONE BROKEN)	.063 x 48 BARE 2024-T3(L)	117.5	100
115A	.063 x .875 2024-T3 STRAP + 2024-T3 STRINGER	50.9 STG 49.7 STRAP	50	.19	.085	7.5	7 STIFFENERS (CENTER ONE BROKEN)	.063 x 48 BARE 2024-T3(L)	117.5	100
117A	BARE 2024-T3 STRINGER	48.6	50	.066	.027	5.0	9 STRINGERS (CENTER ONE BROKEN)	.063 x 48 BARE 2024-T3(L)	117.5	100
111A	BARE 2024-T3 STRINGER	50.9	50	.135	.052	6.0	7 STRINGERS (CENTER ONE BROKEN)	.063 x 48 BARE 2024-T3(L)	117.5	100
103	.08 x 1.25 CLAD 7075-T6 STRAP	69.3	73	.10	.10	7.5	7 STRAPS (CENTER ONE BROKEN)	.0756 x 48 CLAD 2024-T3(L)	104.3	100
105	.125 x .8 CLAD 7075-T6 STRAP	72.9	73	.10	.10	7.5	7 STRAPS (CENTER ONE BROKEN)	.0756 x 48 CLAD 2024-T3(L)	104.3	100
107	.10 x 1.0 CLAD 7075-T6 STRAP	69.7	73	.10	.10	7.5	7 STRAPS (CENTER ONE BROKEN)	.0756 x 48 CLAD 2024-T3(L)	104.3	100
109	.08 x 1.25 CLAD 7075-T6 STRAP	69.3	73	.10	.10	7.5	7 STRAPS (CENTER ONE BROKEN)	.0756 x 48 CLAD 2024-T3(L)	104.3	100
115	.08 x 1.25 CLAD 7075-T6 STRAP	69.3	73	.10	.10	7.5	7 STRAPS (CENTER ONE BROKEN)	.0756 x 48 CLAD 2024-T3(L)	104.3	100
117	.125 x .8 CLAD 7075-T3 STRAP	72.9	73	.10	.10	7.5	7 STRAPS (CENTER ONE BROKEN)	.0756 x 48 CLAD 2024-T3(L)	104.3	100
113	.10 x 1.0 CLAD 7075-T6 STRAP	69.7	73	.10	.10	7.5	7 STRAPS (CENTER ONE BROKEN)	.0756 x 48 CLAD 2024-T3(L)	104.3	100
SCT-54	7075-T6 I-BEAM	80.9	73	1.649	1.2	7.76	5 STIFFENERS (CENTER ONE BROKEN)	.22 x 39 BARE 7075-T7651		62
42-101	7075-T6 CLAD STRINGER	63.1	73	.168	.067	8.55	3 STRINGERS (CENTER ONE BROKEN)	.071 x 38 CLAD 2024-T3(L)		100
42-103	7075-T6 CLAD STRINGER	68.1	73	.22	.076	8.55	3 STRINGERS (CENTER ONE BROKEN)	.071 x 38 CLAD 2024-T3(L)		100
52-125	.0203 x 4.57 7075-T6 STRAP, BONDED	64.1	73	.0928	.0928	20.0	2 STRAPS, STRAIGHT EDGE	.071 x 42 CLAD 2024-T3(T)	108.3	91
52-133	.0211 x 4.57 Ti-6Al-4V STRAP, BONDED	132.8	128	.0964	.0964	20.0	2 STRAPS, STRAIGHT EDGE	.071 x 42 CLAD 2024-T3(T)	108.3	91
52-155	.0164 x 3.75 Ti-6Al-4V STRAP, BONDED	141.1	128	.0615	.0615	20.0	2 STRAPS, SCALLOPED EDGE	.071 x 42 CLAD 2024-T3(T)	108.3	91
52-167	.0233 x 3.75 Ti-6Al-4V STRAP, BONDED	138.8	128	.0874	.0874	20.0	2 STRAPS SCALLOPED EDGE	.071 x 42 CLAD 2024-T3(T)	108.3	91
52-149	.012 x 3.75 Ti-6Al-6V-2Sn STRAP, BONDED	154.4	150	.045	.045	20.0	2 STRAPS SCALLOPED EDGE	.071 x 42 CLAD 2024-T3(T)	108.3	91



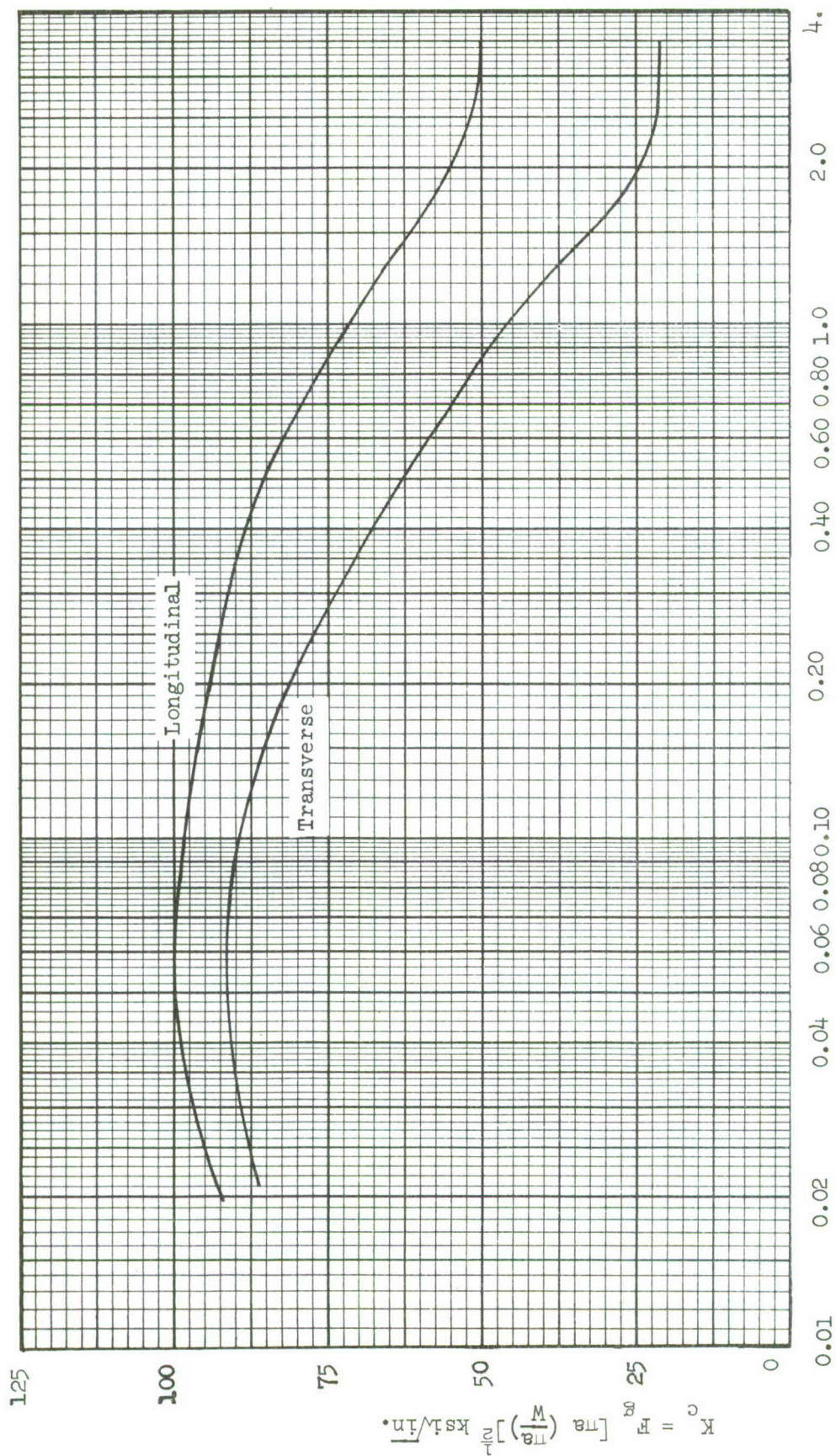
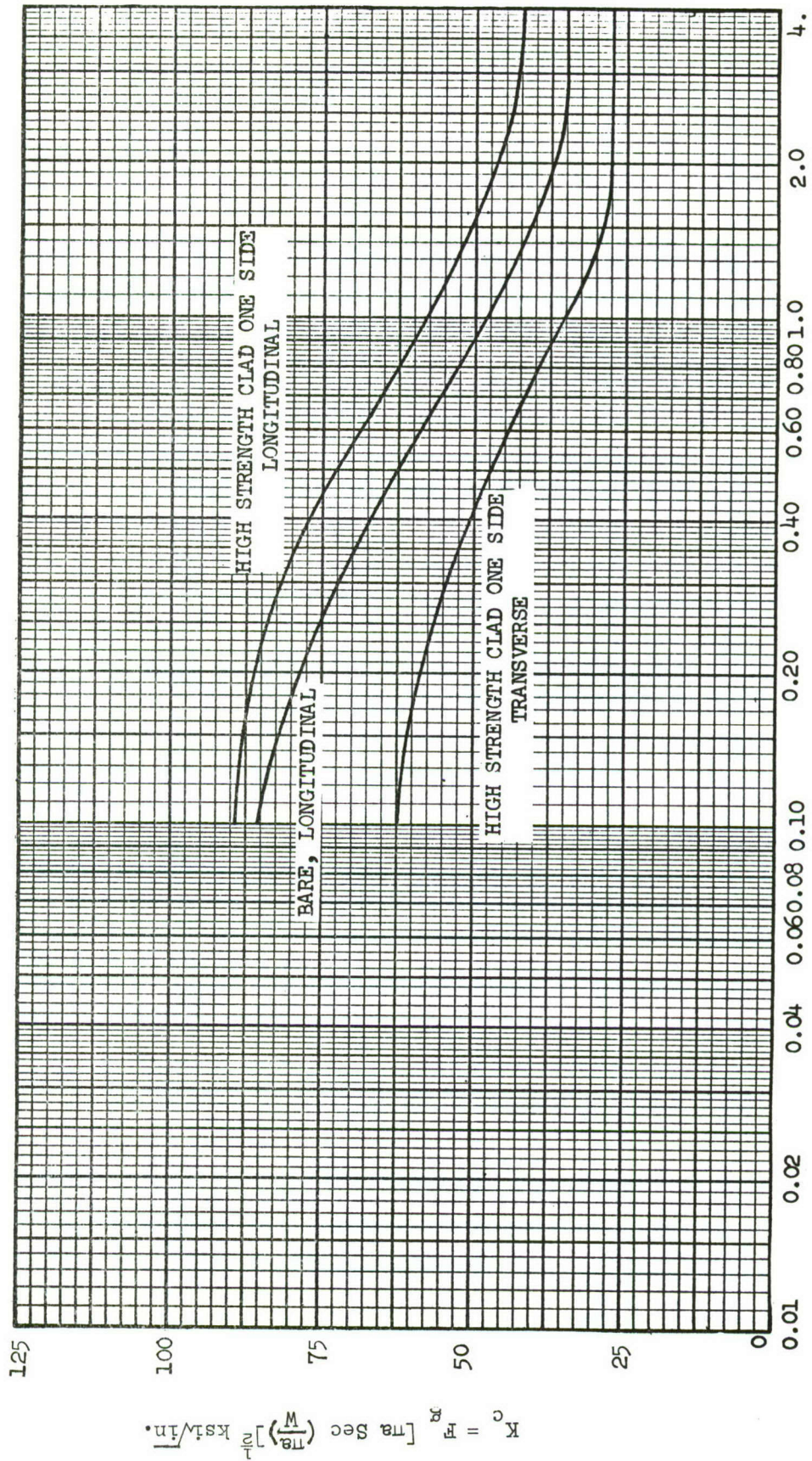


FIGURE 4-24 FRACTURE TOUGHNESS PROPERTIES FOR 2024-T3 and T351 ALUMINUM  
FINISHED THICKNESS (AFTER MACHINING)  $t$ , INCH





FINISHED THICKNESS (AFTER MACHINING)  $t$ , INCH

FIGURE 4-25 FRACTURE TOUGHNESS PROPERTIES FOR 7075-T7651 ALUMINUM ALLOY



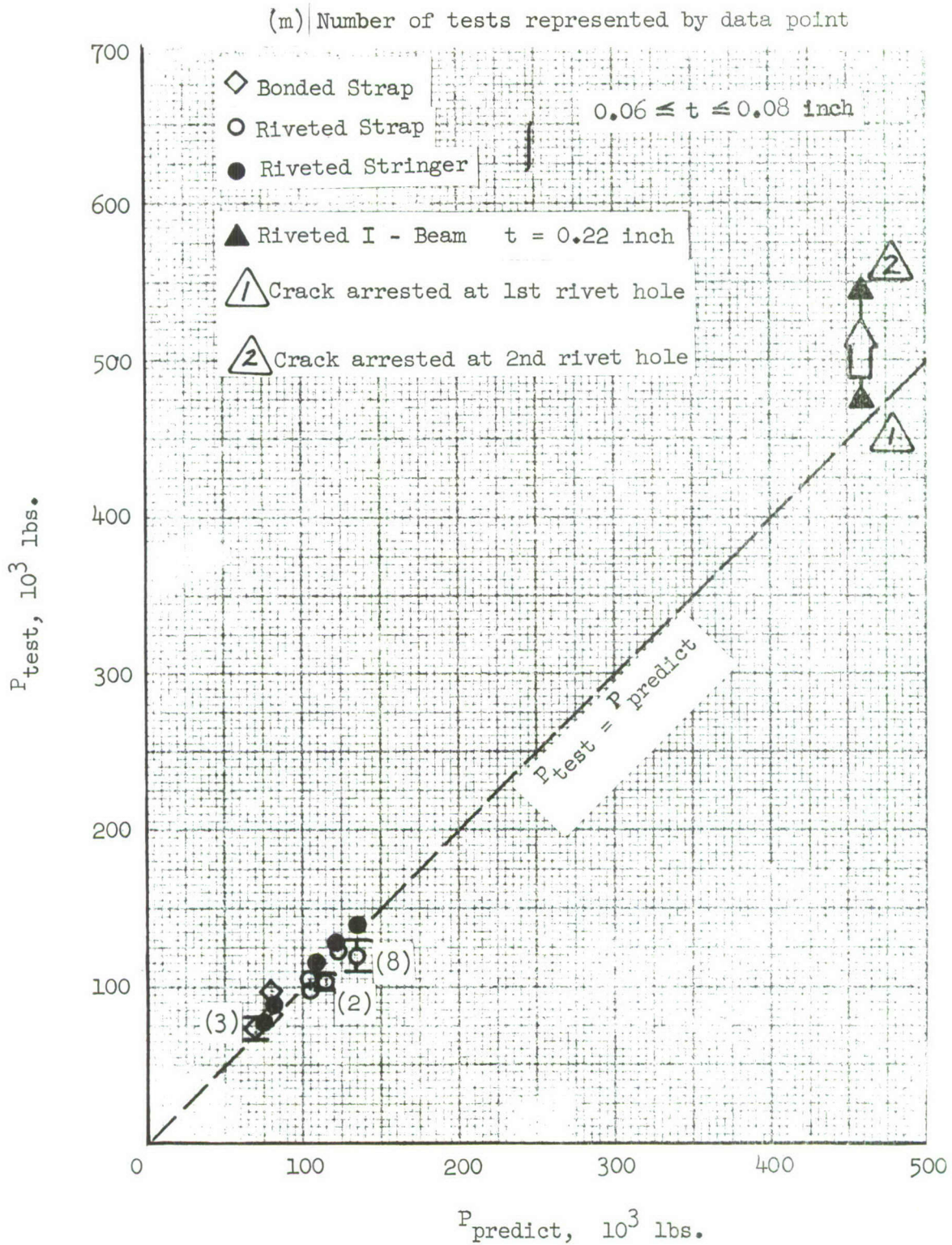


FIGURE 4-26 CORRELATION BETWEEN TEST FAILURE LOAD AND PREDICTED FAILURE LOAD

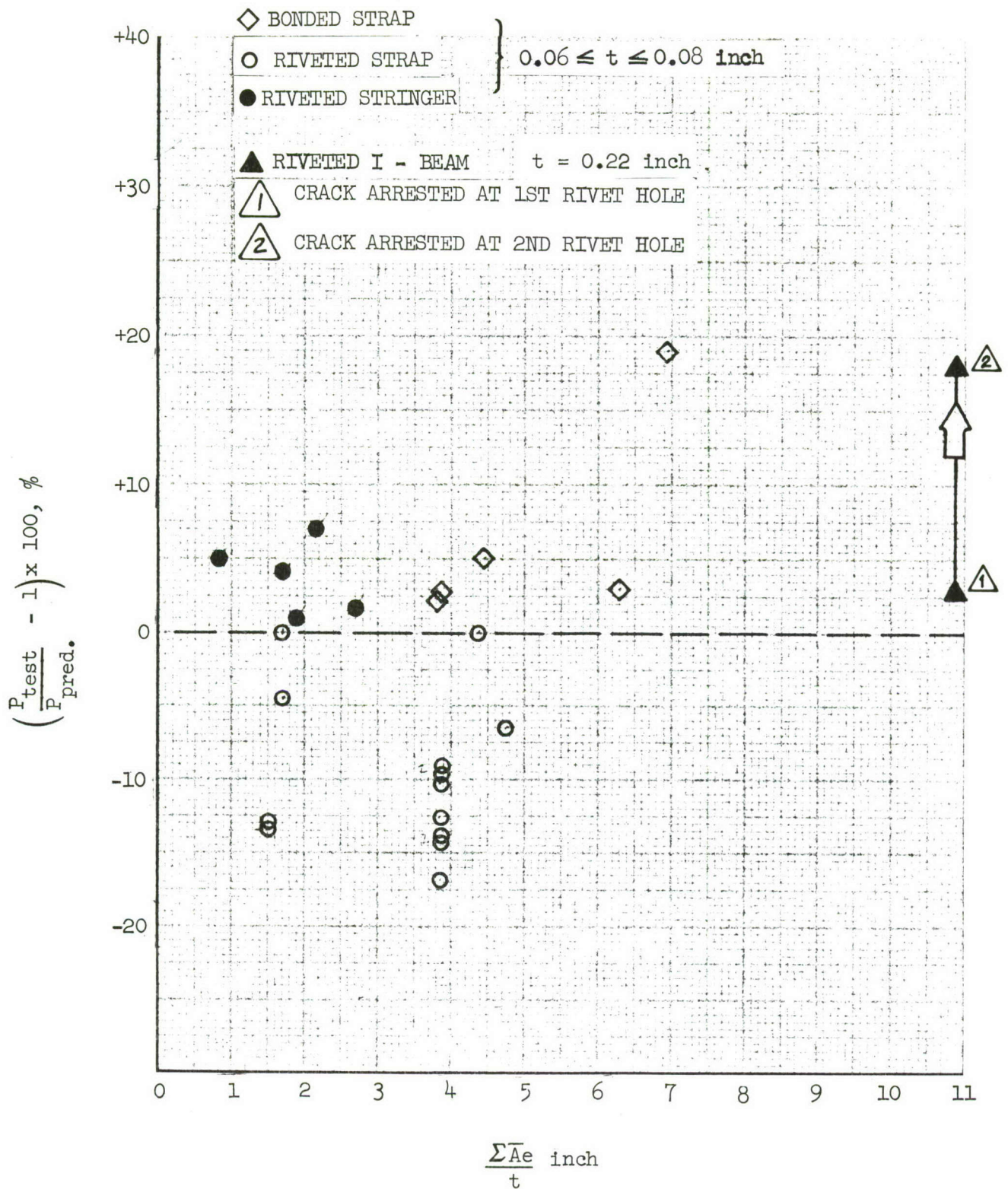


FIGURE 4-27 PERCENT DEVIATION OF TEST RESULTS VS. REINFORCEMENT VARIABLE



#### 4.7 DYNAMIC CRACK ARREST

This section considers the present analysis capability available for the prediction of dynamic crack arrest. The minimal information available is discussed and a simple technique for determining a bound on behavior is presented. Unfortunately, the information available at this time precludes the accurate prediction of dynamic crack arrest for structures of general interest.

Some investigators (e.g., Swift and Wang - Reference 4-45) dealing with the prediction of crack arrest successfully perform analysis by purely static considerations only. This is primarily because the materials that have been tested are sufficiently ductile to grow in a quasi-static fashion only (2024-T3 and 7075-T6 aluminum fall into this category). Most investigators of dynamic crack propagation phenomenon have been concerned with the starting crack or the steady-state, constant-velocity situation; few have considered the arrest phenomenon. However, a reasonably comprehensive article by Bluhm (Reference 4-46) does exist and offers a great deal of insight into the qualitative aspects of the problem. In addition, articles are appearing which consider specialized cases of crack arrest (see Reference 4-47 for example).

A number of exact analytical representations (References 4-48 thru 4-51) for the crack tip stress field for a crack propagating at constant velocity are available. There is however some confusion regarding conclusions drawn concerning available strain energy release rates. This confusion is clarified considerably by Erdogan (Reference 4-52). Additional worthwhile discussions are given by Rice (Reference 4-53), Sih (Reference 4-54), and Embley and Sih (Reference 4-55). During the time of the present investigation a few papers (Reference 4-56 and 4-57) on the acceleration of cracks have appeared. However, they appear to be too specific to be of general use for complex structures.

From a careful reading of all of the information available to date, it is concluded that until it becomes possible to analyze an accelerating or decelerating crack in the type of structures under consideration, only a lower bound can be determined for the available strain energy release rates of a running crack. The primary reason for reaching this conclusion is indicated by the following which is paraphrased from Rice (Reference 4-53).

Two general types of dynamic problems have been considered. Yoffe (Reference 4-48) and Craggs (Reference 4-49) dealt with similar problems, the former with a crack of constant length being opened at one end and closed at the other with constant speed, and the latter with a semi-infinite crack subjected to surface loads with points of application moving at the same speed as the crack. Broberg (Reference 4-50) and Baker (Reference 4-51) treat the crack as suddenly opening from zero length and symmetrically growing with constant velocity.... The Yoffe-Craggs solutions result in dynamic stress-intensity factors independent of velocity and thus identical to the corresponding static problems. Employing a Griffith-type theory to predict the load required to maintain a given velocity, their solutions indicate a steady decrease of load to zero at the Rayleigh surface wave velocity. As we shall discuss subsequently, this unacceptable result is related to the neglect of an analysis of how their steady-state condition is achieved. The more realistic Broberg-Baker analysis leads to a dynamic stress-intensity factor whose ratio to the static value for the same crack length decreases to zero at the Rayleigh surface speed .... Returning to the Craggs-Yoffe analysis and their predicted drop in required load with increasing velocity, it is clear that any finite region near the crack tip would have an infinite strain energy (and kinetic energy). Essentially, then, their result simply says that if a cracked body has an enormous amount of energy near the tip, very little load is required to maintain the crack speed. Thus, the important point in interpreting such steady-state solutions is the question as to how the energy content was achieved.

Therefore until solutions which incorporate the manner in which steady state conditions were achieved (i.e., the effects of various acceleration histories) are available, only rough estimates on behavior can hope to be determined. It would be useful to establish upper and lower load bounds on crack arrest phenomena. However, even this cannot be completely done.

It is desirable to be able to determine upper and lower bounds on the crack arrest load. The bounds may be designated  $P_U$  and  $P_L$  where if

$$P \geq P_U, \text{ the crack will not arrest}$$

$$P \leq P_L, \text{ the crack will definitely arrest.}$$

and  $P$  is the applied load.

It is presently possible to get values for  $P_U$  but not  $P_L$ . The reason for this is essentially given above where it states " . . . if a cracked body has an



enormous amount of energy near the tip very little load is required to maintain the crack speed". Therefore no lower bound can be determined without knowledge of the crack tip energy content.

A value for  $P_U$  can be obtained from a straightforward static analysis. Since if a static analysis indicates that the crack will not arrest, it may be assumed that an appropriate dynamic analysis would yield the same result. By a static analysis we mean to compare the total strain energy release rate that has been available and the total dissipated energy. That is, if

$$\int_{a_i}^a \mathcal{G} da \geq \int_{a_i}^a \mathcal{G}_c da \quad (4-36)$$

where

- $\mathcal{G}$  is the strain energy release rate from a static analysis,
- $\mathcal{G}_c$  is the critical value of  $\mathcal{G}$
- $a$  is the crack length,
- $a_i$  is the crack length when  $\mathcal{G}$  first equals  $\mathcal{G}_c$  ;

then the crack will not arrest.

A lower estimate for  $P_U$  may be obtained by including some dynamic considerations in the analysis. As an example, consider a reinforced panel. It may be noted that information from (or to) a reinforcement or structural boundary must travel at a finite speed. Therefore the force that a crack tip experiences due to a reinforcement corresponds to the force produced when the crack was at a previous position. Since this crack closing force is lower at shorter crack lengths, the available strain energy release rate will be greater. If it is assumed that the load information passes through the panel at the dilational wave velocity and an appropriate value for the crack speed is used, an approximate  $\mathcal{G}$  versus  $a$  curve can be developed which incorporates these dynamic effects. This can then be used in the above inequality to establish a value for  $P_U$ .

The above discussion has presented what is essentially a minimum criterion for a structure to be capable of arresting a running crack. That is; the lowest value



of  $P_U$  arrived at as described above must be greater than the required load carrying capability of the damaged structure. This, of course, neglects the effects of material property variations with strain rates, since the above was a discussion of the variation of available strain energy release rate with velocity and not the variation of dissipated strain energy release rate ( $\mathcal{G}_c$ ) with velocity. That is a subject that can only be approached empirically.

In addition, and more importantly a technique for determining a value for  $P_L$  has not been presented. It appears that at this point in time any dependence on dynamic crack arrest capability in a structure must be supported for the most part by sound engineering judgment and experience in lieu of a complete analytical approach to the problem.

## 5.0 APPLICATION STUDY

### 5.1 DESIGN PROBLEM DEFINITION

A design study was performed to illustrate the effect the recommended criteria (Section 3.4) would have on the design of aircraft structure. The application selected for this study is the lower wing surface structure of a fighter/attack type aircraft. This type of structure was selected for the following reasons:

- o The lower surfaces of fighter wings have been having problems with regard to small flaws causing catastrophic failures.
- o This part of the aircraft structure is likely to be affected by the criteria and procedures developed in this program.
- o The results of a study of this application will be indicative of the results that can be expected in other areas of the aircraft structure.

The wing structure considered is applicable for an approximately 60,000-pound gross weight, high performance fighter/attack type aircraft similar to some current aircraft and to anticipated future fighter/attack aircraft. However, the effect of elevated or reduced temperature was not considered. For particular aircraft projects, temperature effects would have to be considered if the structure is subjected to an elevated or reduced temperature environment.

Typical characteristics for the aircraft selected for this study are given in Table 5-1. The design gross weight was taken to be the takeoff weight less the fuel weight (about 1/3) in the wings. It was assumed that the wing fuel would be used up to reach target areas where high maneuver loads would occur. The assumed weight distribution for the attack aircraft wing is given in Figure 5-1. The wing-fuselage intersection occurs at W.S. 48. Missiles are attached at W.S. 328. The airfoil section is assumed to be convex. The front spar is at 15% chord and the rear spar at 65% chord. The thickness and chord both taper linearly between the root and the tip.

The basic structure considered in this study was a multi-spar wing box with various types of lower skin surfaces. The number of spars was selected to provide a near optimum structural arrangement using three types of skin surfaces; unstiffened skin, integrally-stiffened skin, and zee-stiffened skin. Also, the use of both single and multiple planked skin surfaces was evaluated for the unstiffened skin configuration.

TABLE 5-1 TYPICAL FIGHTER/ATTACK AIRCRAFT CHARACTERISTICS

Characteristic	Measurement
Aircraft and Wing Characteristics	
Takeoff gross weight (lb)	58,000
Design gross weight (lb)	52,800
Gross area of wing (ft <sup>2</sup> )	725
Ultimate design load factor	11.00
Aspect ratio	4.0
Thickness to chord ratio at the root of wing (%)	6
Thickness to chord ratio at the tip of wing (%)	6
Sweep angle at 25% of the chord (degrees)	35
Taper ratio (tip chord divided by root chord)	0.25
Wing Weight (lb)	
Upper surfaces, including joints and fasteners	2,000
Lower surfaces, including joints and fasteners	1,480
Beam webs, including joints and fasteners	800
Ribs	750
Leading and trailing edges	450
Fairings and access doors	300
Ailerons	170
Leading and trailing edge flaps	800
Spoilers	100
	<hr/>
TOTAL	6,850



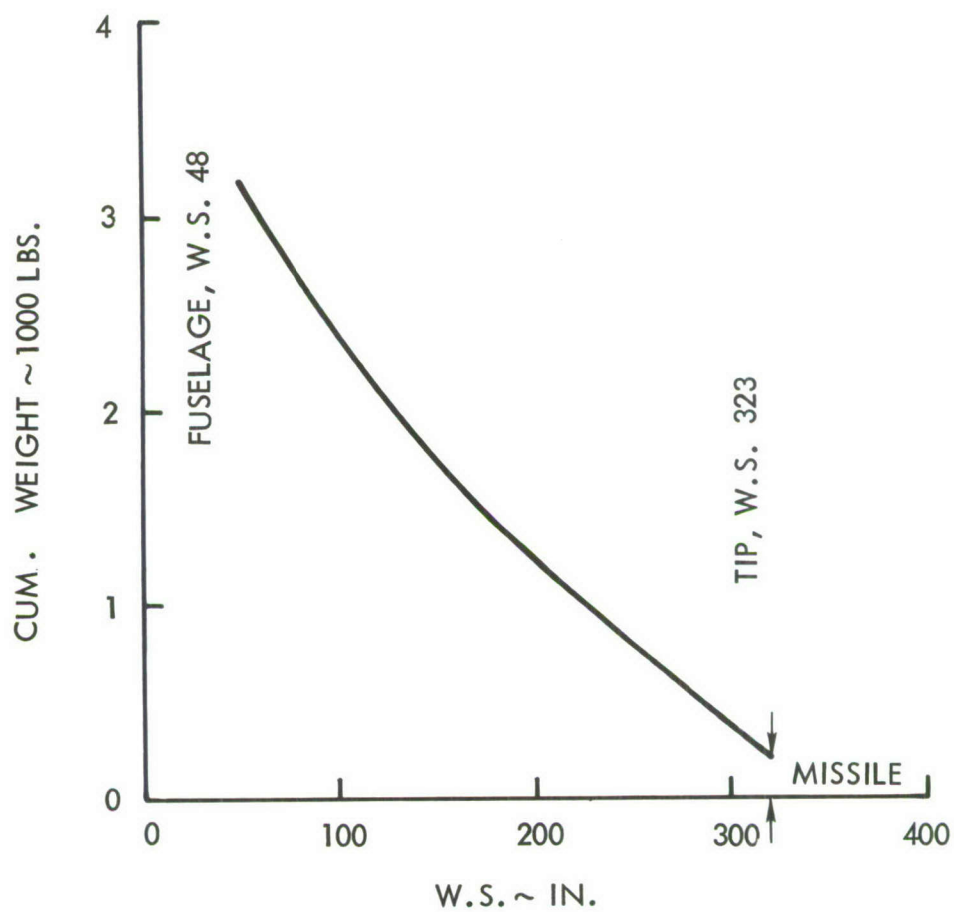


FIGURE 5-1 FIGHTER/ATTACK AIRCRAFT - WING WEIGHT DISTRIBUTION

The lower wing surface structure has been designed to meet the criteria given in Section 3.4. In this study damage sizes  $a_i$ ,  $a_v$  and  $a_w$  are selected which are considered to be representative for each inspectability classification. The factors  $S_i$ ,  $S_v$  and  $S_d$  are specified which will provide approximately equal levels of reliability. As discussed in Section 3.3, these factors must be selected on the basis of experience and an understanding of the reliability of the analysis methods or tests which are used. The damage sizes and factors selected for this study are summarized in Table 5-2 and discussed below.

TABLE 5-2 DAMAGE TOLERANCE REQUIREMENTS APPLICABLE TO FIGHTER/ATTACK AIRCRAFT

<u>Requirement</u>	<u>Damage Size</u>	<u>Life Requirement</u>
<u>Structural Integrity</u>		
Non-inspectable	$a_i = 0.05$ in.	$S_i = 2.0$ (Average Spectrum)
NDI In-service Inspectable	$a_v = 3-4$ in.	$S_v = 1.0$ (Severe Spectrum)
Walk-around Inspectable	$a_w = 8-10$ in.	None
<u>Durability</u>	$a_i = 0.125$ in.	$S_d = 2.0$ (Average Spectrum)

An initial damage size for non-inspectable structure of  $a_i = 0.05$  in., i.e., a crack length of 0.10 inch, was selected as being the maximum size that is likely to be missed during production and fabrication inspections at the most critical locations in the structure. The initial damage size,  $a_i$ , is based on data presented in Section 3.2.3 and is consistent with the goals of current Air Force programs to demonstrate flaw detection capabilities in production. The durability requirement assumes  $a_i = 0.125$  inch and covers the largest damage size that might be missed by inspection and considers that it could occur anywhere in the structure (except at points of high stress concentration, i.e., ignoring effects of design details).

The analysis of inspection data given in Section 3.2.3 indicates that skin cracks 3 - 4 inches long could be missed by an NDI in-service inspection at IRAN. The most critical damage of this size for the lower wing surface structure would be a broken reinforcement member. Members on the inside of the wing box are difficult to inspect, and a detection of damage in a member such as a stiffener or riser that is almost broken is not certain. Also if such extensive damage were present, it would be likely to cause a small crack, also undetectable to be introduced in the inside surface of the adjacent skin. Therefore, the damage size,  $a_v$ , was taken to be a broken stiffener, riser, or spar cap plus a thru-thickness skin crack equal to the hole diameter plus two thicknesses of skin.

The walk-around inspectable damage size was taken to be approximately 8 - 10 inches, i.e., the largest size the crack is likely to grow to before being detected. The eight-inch crack size was selected for the zee-stiffened and integrally-stiffened structure as this corresponds to an even multiple of the reinforcement spacing. For the unstiffened skin structure a broken plank 11.7 inches wide was taken as the walk-around inspectable damage size. Since the reinforcing members cannot be seen by the walk-around inspection, it was assumed that any members attached to the skin across the crack were broken. This damage size corresponds approximately to the damage that has been assumed for fail-safe designs in the past, i.e., a single member broken and a skin crack to the adjacent intact stringers.

The selection of the  $S_i$ ,  $S_v$  and  $S_d$  values depends on the scatter and accuracy of the method of crack growth analysis and the severity of the fatigue loading spectrum used in the analysis. Since retardation effects were not considered in the crack growth analysis, it is felt that the results should be conservative. Between NDI in-service inspections, of the order of  $1/4$  lifetime, an aircraft could very likely experience the most severe usage, and therefore the severe spectrum with  $S_v = 1.0$  was used. Non-inspectable structure must be good for at least one lifetime, so the average spectrum is applicable since it is not likely that an aircraft would experience the most severe usage for one lifetime. However, due to the uncertainty of the crack growth sequence, as explained in Section 5.5.2, a  $S_i$  factor of 2.0 was considered appropriate. Also, the average spectrum with  $S_d = 2.0$  is used for the durability requirement.

To evolve a structural design using the above design criteria for the lower wing surface structure, the following tasks were performed:

- o Developed design load conditions (including fatigue loading spectra applicable for the anticipated service usage).
- o Selected two materials from three candidates showing potential for meeting these criteria with a minimum impact on structural weight.
- o Established material properties for the two selected materials.
- o Sized the structure for static design loads for three design concepts, zee-stiffened skin, integrally-stiffened skin, and multi-spar unstiffened skin.
- o Resized the three structural design concepts as required to meet the fatigue requirements.



- o Investigated the effect on structural weight of the various alternative design criteria when applied to the three design concepts, using each of the two materials.

The work conducted in each of these steps is discussed in the following sections.

## 5.2 DESIGN LOADS

Design limit loads for the fighter/attack wing for shear, bending, and torsion are given in Figure 5-2. These loads were developed using the wing weight distribution given in Figure 5-1 and a limit maneuver load factor of 7.33 at a design gross weight of 52,800 pounds.

Fatigue loading spectra applicable to the lower surface of the wing of a typical fighter/attack aircraft are shown in Figure 5-3. Two spectra, one representing typical usage and one representing relatively severe usage, are shown.

Generally in the design process such loading spectra would be developed by the following procedure: Each of the two spectra would be developed on the basis of a number of assumed missions, say four. Each assumed mission would be described in terms of the amount of time spent in each of several flight conditions (e.g., climb, cruise, air-to-air combat, air-to-ground combat). Fatigue spectra for each condition, from, for example, Reference 5-1 would be combined to provide a fatigue spectrum for each mission. The missions would be weighted according to how often they would be expected to be flown. The weighted average of the fatigue spectra for the four severe missions would give a fatigue spectrum representative of severe usage. Likewise, the weighted average of the spectra for the four typical missions would provide a spectrum representing typical usage.

For this example, however, the typical and severe spectra were not developed by this general method. Rather, load-factor data from representative maneuver critical aircraft were reviewed; the typical spectrum corresponds to the mean of these data and the severe spectrum corresponds to the mean of the most severe 1/3 of the data. This was done so that this design exercise will provide results representative of all maneuver-critical fighter/attack aircraft.

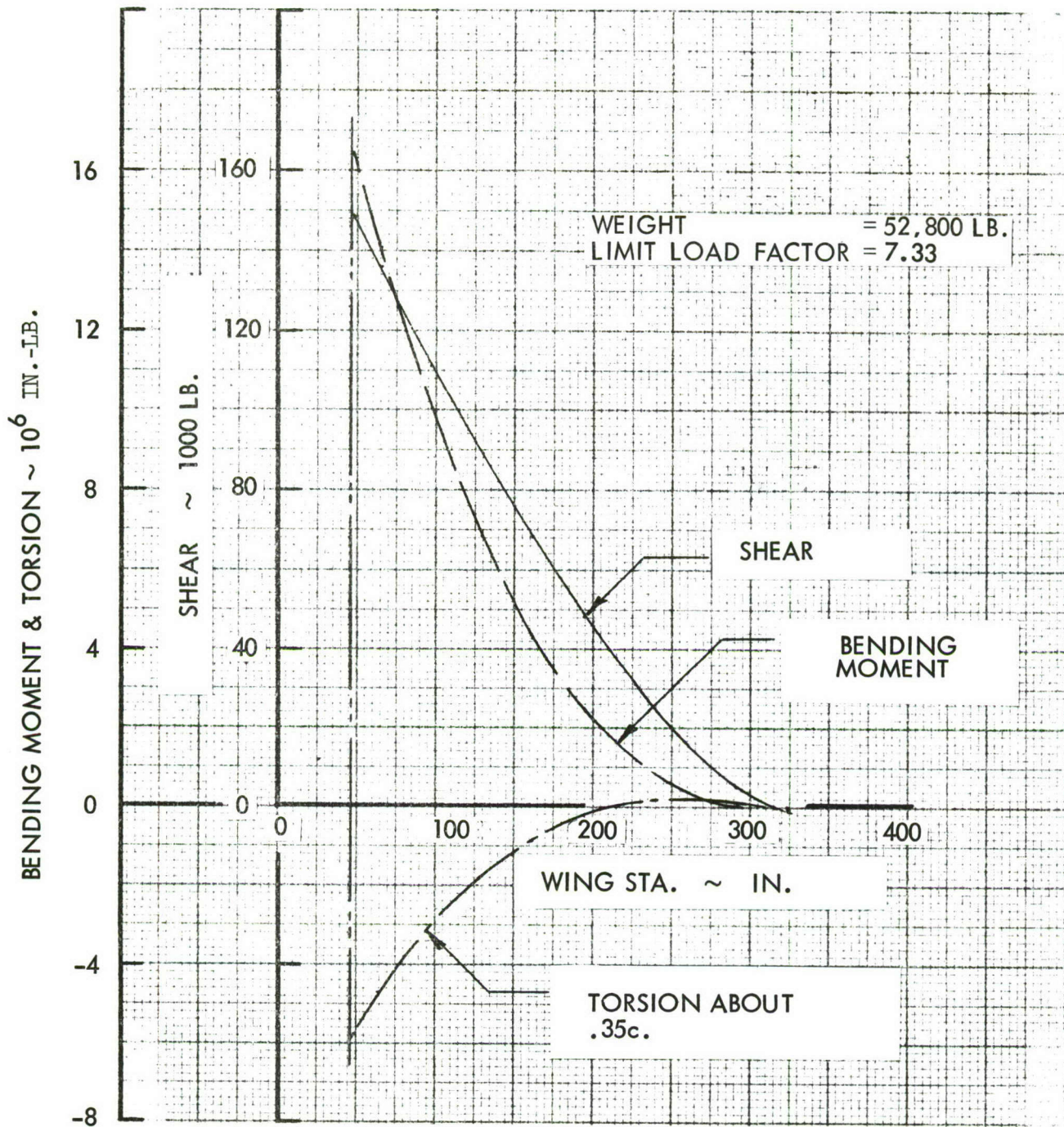


FIGURE 5-2 FIGHTER/ATTACK AIRCRAFT-WING LIMIT LOADS



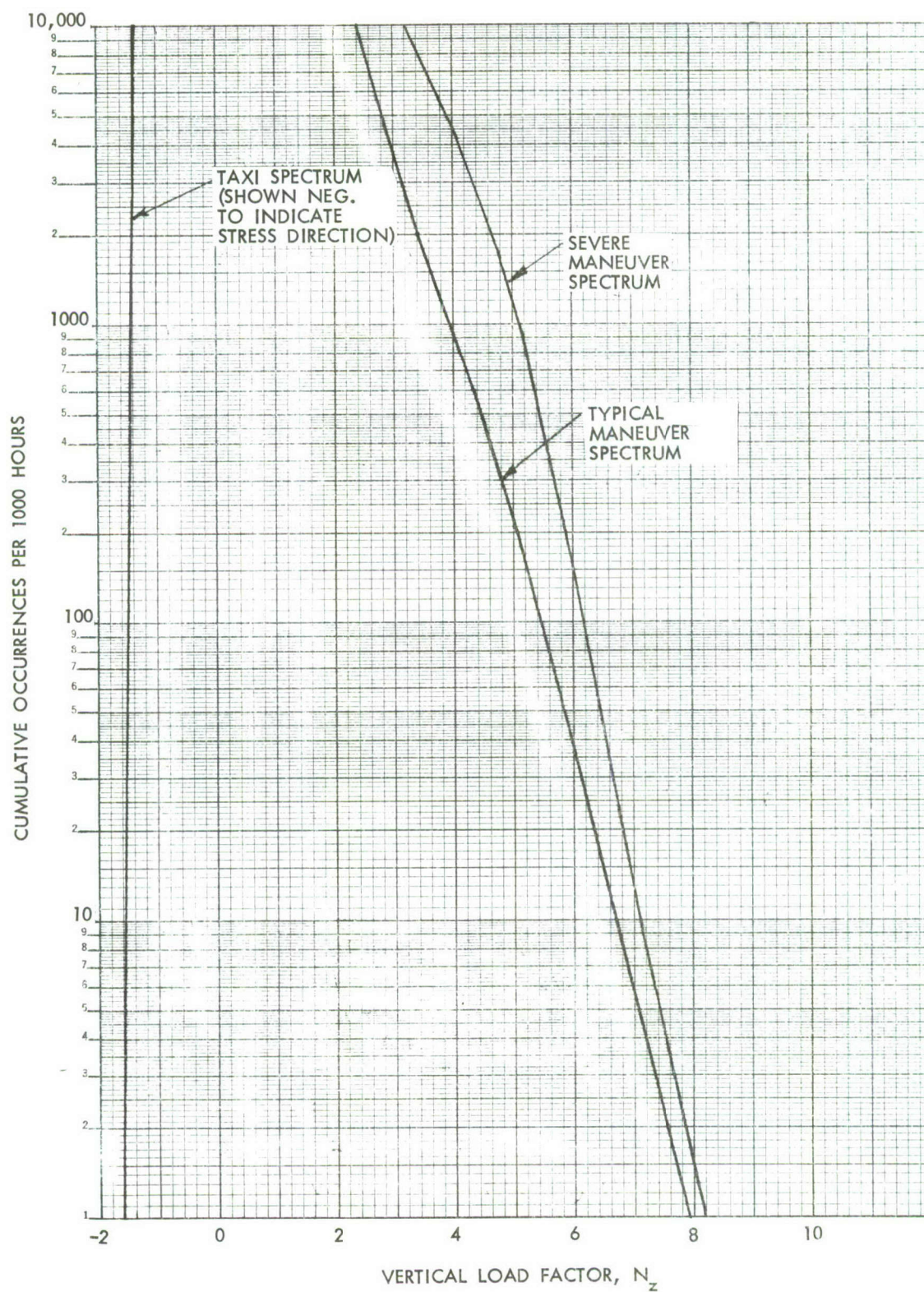


FIGURE 5-3 LOADING SPECTRA TYPICAL FIGHTER AIRCRAFT

### 5.3 MATERIAL PROPERTIES AND ALLOWABLES

A comparison of the properties for three materials which are considered for the design study is given in Table 5-3. Additional properties, not indicated in the table but having impact on the final design include, properties affecting compression stability, i.e., modulus of elasticity and minimum gage requirements for each material.

In addition to those quantities discussed in Section 4.8, a fatigue parameter  $F_{\text{fatigue}}$  has been included for comparative purposes. This quantity is the constant amplitude stress level (for  $R = 0$ ) which will result in a life of 30,000 cycles for aluminum at a  $K_t$  of 4 and for titanium at a  $K_t$  of 5. The yield and ultimate strengths are minimum guaranteed values, the plane strain fracture toughness properties are B-basis values; all other values are typical. A comparison of these tabulated values and the results of the preliminary designs indicated that the steel design would be quite heavy; therefore, it was decided to limit the application study to Ti-6Al-4V and 7075-T76 aluminum. It was felt that these two materials would be more than sufficient for evaluating the damage tolerant design criteria.

#### Static Properties

The mechanical properties used for the preliminary design of the structure (Section 5.4) are S-values (minimum guaranteed values) obtained from MIL-HDBK-5B (Reference 5-2) and are given in Table 5-3.

#### Fatigue Properties

The standardized aluminum alloy constant-life diagram for  $K_t = 4.0$  shown in Figure 5-4 (Reference 5-3) is used to represent the fatigue design properties of structure made from 7075-T76 sheet and plate. Tests results reported in Reference 5-4 show that this standardized aluminum alloy constant-life diagram conservatively represents the fatigue properties of 7075-T76 machined plate and extrusions. The basis for selecting a  $K_t$  value of 4.0 is discussed in Section 5.5.1.



TABLE 5-3 PROPERTIES OF MATERIALS CONSIDERED FOR APPLICATION STUDY

Material Properties	Property Values			Property Values/Density		
	D6AC Steel	Ti-6Al-4V	7075-T76 Aluminum	D6AC Steel	Ti-6Al-4V	7075-T76 Aluminum
$F_{tu}$ , ksi	220	130	69	786	813	690
$F_{ty}$ , ksi	198	126	58	707	788	580
$E$ , $10^3$ ksi	29	16	10.3	104	100	103
$G$ , $10^3$ ksi	11	6.2	3.9	39	39	39
$F_{fatigue}^*$ , ksi	-	47	20	-	294	200
$K_{Ic}$ , ksi $\sqrt{in.}$	88	63.5	35	314	397	350
$K_c^{**}$ , ksi $\sqrt{in.}$	-	220	85	-	1375	850
$K_{Iscc}^{**}$ , ksi $\sqrt{in.}$	22	31	35	79	194	350
$K_{10^{-5}}$ , ksi $\sqrt{in.}$	22	21.2	16.1	79	133	161
$K_{10^{-6}}$ , ksi $\sqrt{in.}$	13.5	11	7.8	48	69	78
$w$ , lb/in. <sup>3</sup>	.28	.16	.10	1	1	1

\*  $R = 0$ ,  $N = 30,000$  cycles,  $K_t = 4.0$  for Aluminum and  $K_t = 5.0$  for Titanium.

\*\* Maximum value with respect to thickness



# TEST DATA

Type of Specimen:  $K_t = 4$   
 Specimen Geometry: Edge Notched Sheet  
 Samples  
 Thickness = N. A. (Not Applicable)  
 Surface Finish: N. A.  
 Type of Loading: Axial  
 Loading Frequency = N. A.  
 Atmosphere: Air  
 Temperature: Room Temperature  
 Basis: 50% Probability

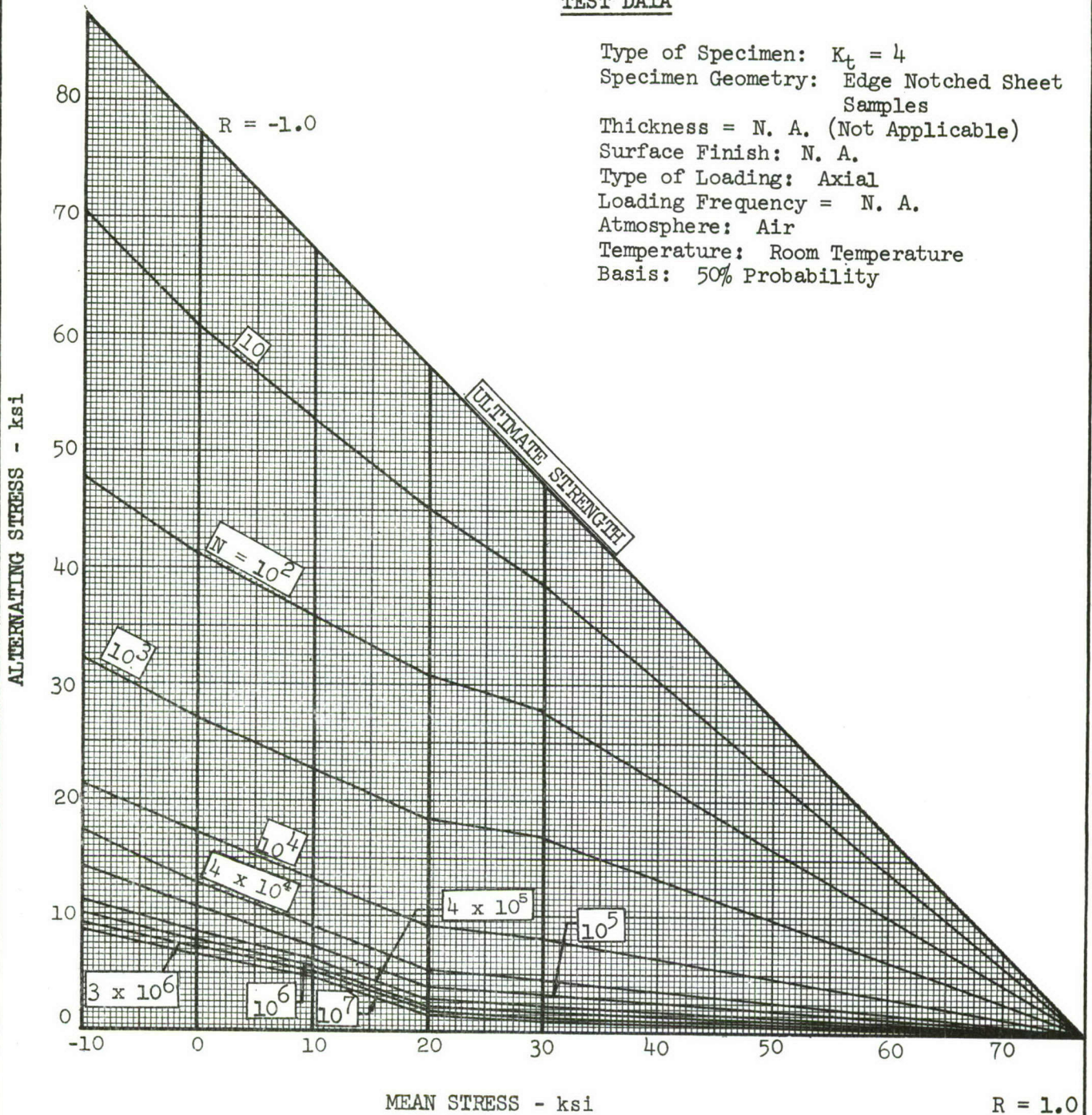


FIGURE 5-4 CONSTANT-LIFE DIAGRAM FOR STANDARDIZED ALUMINUM ALLOY  
 $K_t = 4$ ,  $F_{tu} = 77$  ksi

The data given in References 5-2 and 5-3 were used to establish a constant-life diagram to represent the fatigue properties of Ti-6Al-4V annealed sheet and plate material with an ultimate tensile strength of 135-155 ksi. The constant-life diagram for  $K_t = 5.0$  developed from these data is given in Figure 5-5. The basis for selecting a  $K_t$  value of 5.0 for titanium is also discussed in Section 5.5.1.

#### Fracture Toughness Properties

The fracture toughness properties for 7075-T76 aluminum alloy used for the application analysis are given in Figure 5-6. For the design of damage tolerant structure the average  $K_{Ic}$  values of the material are used. In Section 4.6.5 it is shown that the use of the average material properties in conjunction with the applied method of analysis provided conservative predictions of the residual strength for the reinforced structure tested. For the design of monolithic structure the equivalent of B-value properties are used. The equivalent B-value properties given in Figure 5-6 were obtained by evaluating the scatter in the data given in Reference 5-5 and Appendix B. The analysis of the data given in Appendix B indicates that the B-values are approximately equivalent to the minimum values obtained for each test group. A comparison between the minimum values and the average values given in Appendix B and Reference 5-5 indicated that a 30% reduction of the average values would give the equivalent of the B-values.

The fracture toughness properties for Ti-6Al-4V annealed sheet and plate are presented and discussed in Appendix B. The average and the equivalent B-values obtained from these data are given in Figure 5-7. The equivalent B-values were obtained as described above for aluminum alloys.

#### Sustained Load Crack Growth Properties

The sustained load crack growth properties for Ti-6Al-4V annealed material are discussed in Section 4.4 and shown in Figure 4-9. No probability basis is given for these allowables since insufficient data are available to establish a basis.



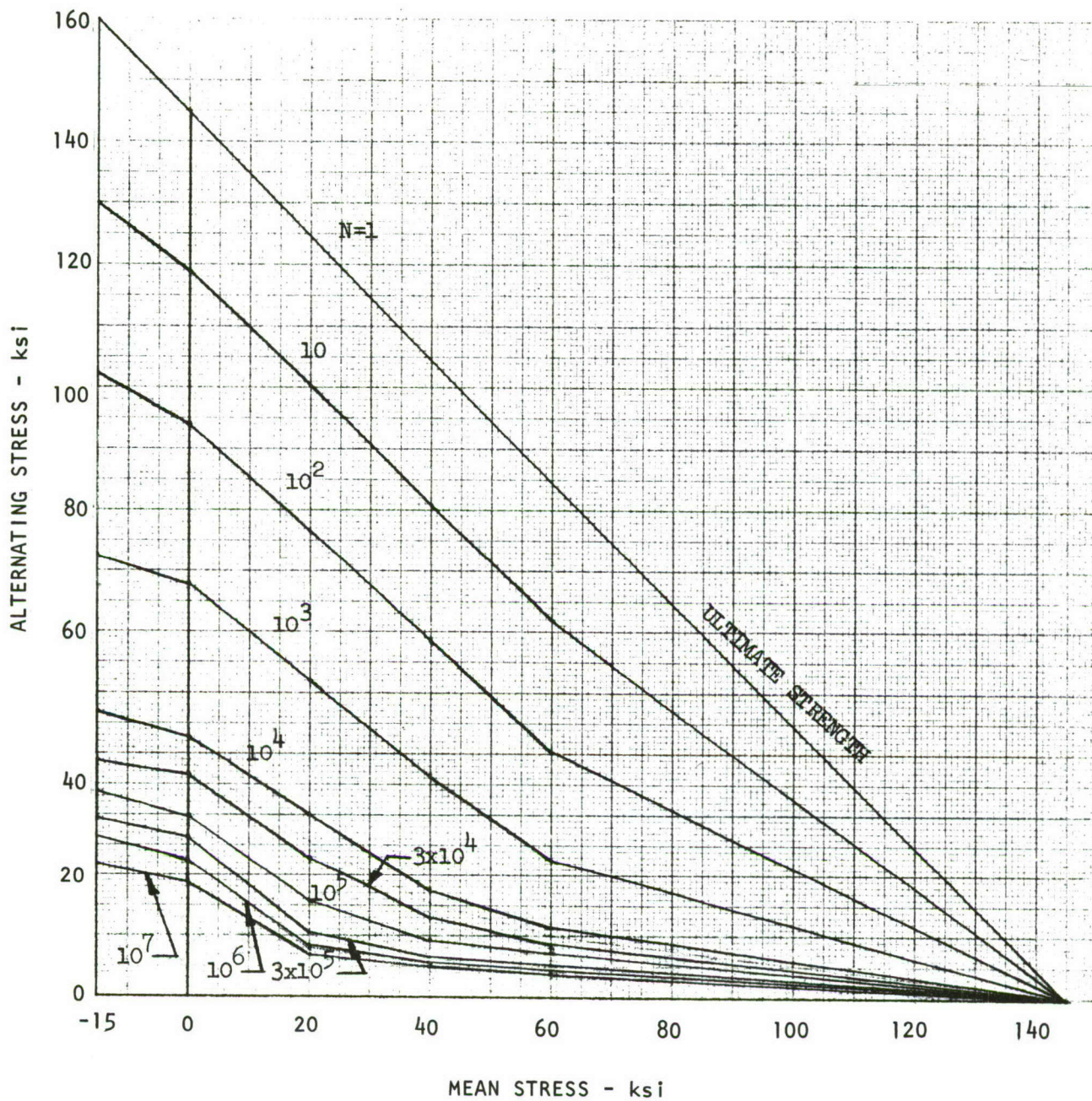


FIGURE 5-5 CONSTANT-LIFE DIAGRAM FOR Ti-6Al-4V ANNEALED SHEET AND PLATE,  $K_t = 5.0$ ,  $F_{tu} = 135 - 155$  ksi



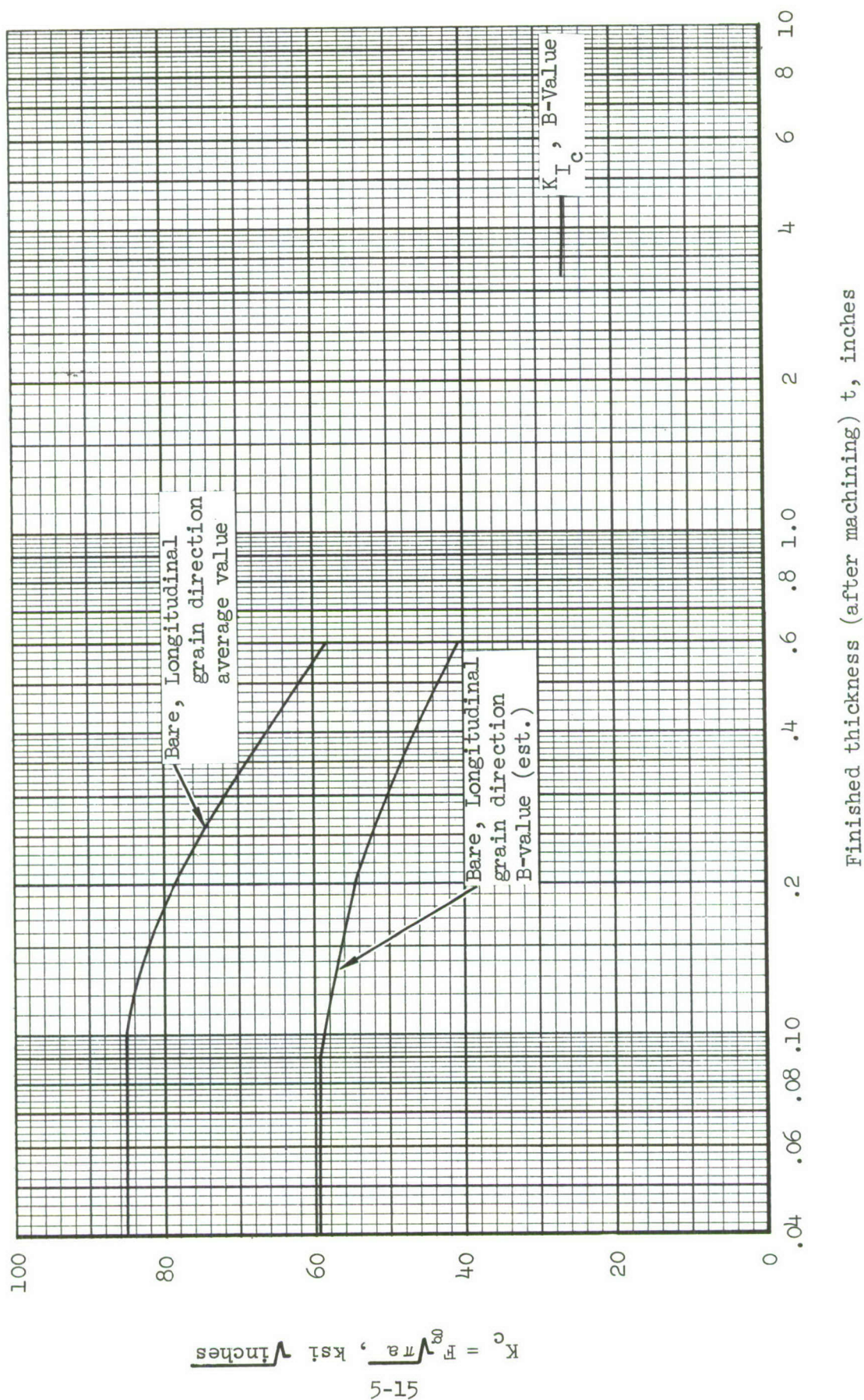


FIGURE 5-6 FRACTURE TOUGHNESS OF 7075-T76 ALUMINUM ALLOY SHEET AND PLATE



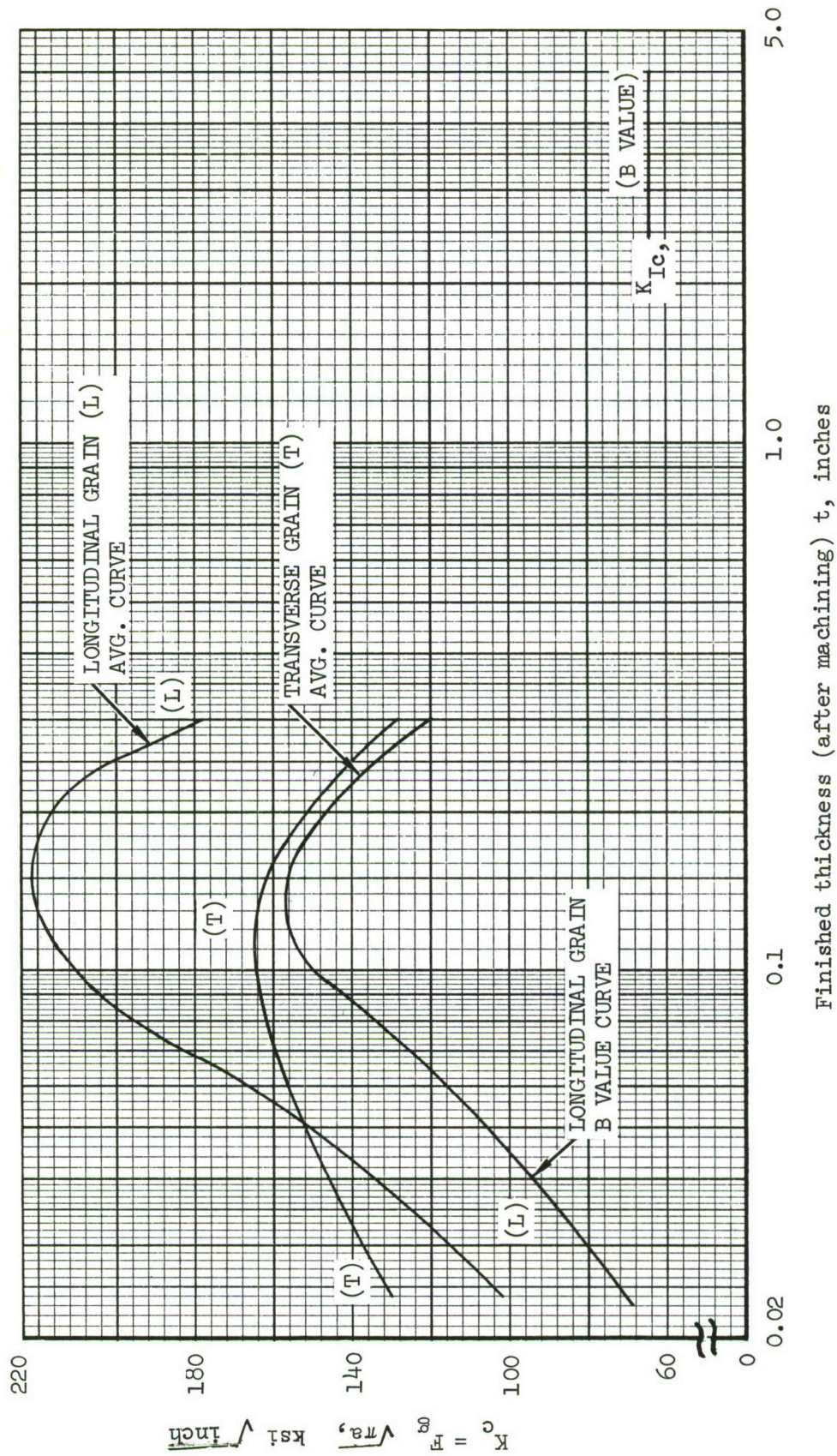


FIGURE 5-7 FRACTURE TOUGHNESS OF Ti-6Al-4V, MILL ANNEALED SHEET AND PLATE

The environment has little effect on the sustained load crack growth properties of aluminum alloys and therefore the B-basis  $K_{Ic}$  value given in Figure 5-6 is applicable for the sustained load crack growth analysis.

#### Crack Growth Properties

Constant-amplitude crack propagation rate allowables for the two materials are given in Tables 5-4 and 5-5. The rates are estimated average values; the assumed environment is laboratory air. These allowables were developed by combining applicable data on 7075-T6 and 7075-T76 aluminum, and Ti-6Al-4V and Ti-8Al-1Mo-1V titanium from References 5-6 through 5-11.



TABLE 5-4

CONSTANT AMPLITUDE RATE OF GROWTH OF ONE END OF A CRACK, 7075-T76\*

Effective Stress Intensity <sup>(1)</sup> ksi x sq. rt. of inches	Crack Growth Rate, da/dN <sup>(2)</sup> microinches/cycle
2.000	.040
7.800	1.000
10.000	2.500
12.500	5.000
17.500	13.000
25.000	50.000
35.000	190.000
70.000	17999.075

\*  $m = .5$ ,  $R_c = -.12$ 

TABLE 5-5

CONSTANT AMPLITUDE RATE OF GROWTH OF ONE END OF A CRACK, Ti-6Al-4V\*\*

Effective Stress Intensity <sup>(1)</sup> ksi x sq. rt. of inches	Crack Growth Rate, da/dN <sup>(2)</sup> microinches/cycle
3.800	.001
4.000	.030
4.500	.048
5.500	.090
7.500	.300
13.500	2.400
15.500	4.000
20.500	9.000
25.000	18.000
29.000	30.000
75.000	369.999
140.000	600,000.000

\*\*  $m = .75$ ,  $R_c = -1.0$ (1)  $K = K_{\max} (1-R)^m$ . If  $R < R_c$ , replace  $R$  in this equation by  $R_c$ .(2) Linear interpolation is used on  $K$  vs.  $\log(da/dN)$  to calculate intermediate  $da/dN$  values.

## 5.4 PRELIMINARY DESIGN

### 5.4.1 Stress Assumptions

The integrally stiffened and zee-stiffened wing upper surfaces were initially optimized for compression loading using the Emero and Spundt wide-column techniques (Reference 5-12).

The multi-spar plate wings were designed so that the upper surfaces were non-buckling under compression at limit load. Various spar spacings were considered up to a total of eleven spars. The eleven spar configuration was finally selected as giving reasonable stress levels and practical spacing.

The lower surfaces for all designs were initially sized by ratioing down the upper surface sizes using data from comparably loaded wings to meet the tension allowable stress requirements.

The wing designs were analyzed at wing stations spaced at 35-inch intervals from the wing root to the wing tip. The section properties and stresses were calculated at each selected wing station. Reiterations were performed until the wing upper surface was stable as a column and in local crippling.

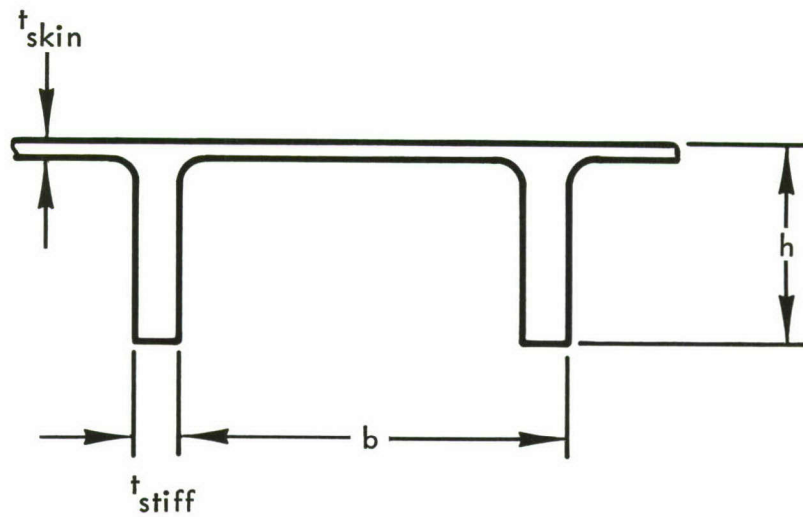
### 5.4.2 Integrally Stiffened Wing

A schematic of the cross section of the integrally stiffened skin is shown in Figure 5-8. A constant stiffener spacing was selected and the skin and stiffener thicknesses and stiffener heights were varied to provide sections as close to optimum as was reasonably possible without complicated machining.

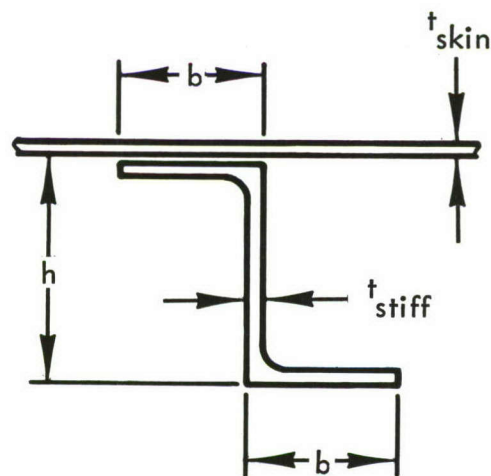
Minimum skin thicknesses of 0.02 inch for D6AC steel, 0.03 inch for titanium and 0.04 inch for aluminum were used for compression stability. The preliminary sizing and stress levels are summarized in Tables 5-6, 5-7 and 5-8.

### 5.4.3 Zee-Stiffened Wing

A schematic of the zee-stiffened cross section is shown in Figure 5-8. A constant stiffener depth was selected over the inboard section of the wing and a second constant depth over the outboard section of the wing. The stiffeners were placed on constant chord lines to avoid excessive forming and alternate



a. INTEGRALLY STIFFENED CROSS SECTION



b. ZEE-STIFFENED CROSS SECTION

NOTE: 30 INCH RIB SPACING TYPICAL FOR ALL DESIGNS.

FIGURE 5-8 . SCHEMATIC CROSS SECTIONS OF STIFFENED SKIN DESIGNS



TABLE 5-6

D6AC STEEL 220 ksi 3 SPAR INTEGRALLY STIFFENED WING SIZING  
(REFERENCE FIGURE 5-8)

BUTT LINE	UPPER SURFACE					LOWER SURFACE				
	t <sub>skin</sub>	h	t <sub>stiff</sub>	b	f <sub>max</sub> *	t <sub>skin</sub>	h	t <sub>stiff</sub>	b	f <sub>max</sub> *
45 (Root)	.08	1.0	.23	2.0	-97000	.07	1.0	.20	2.0	106000
80	.07	↑	.22	↑	-88000	.06	↑	.19	↑	98000
115	.06	↑	.21	↑	-78000	.05	↑	.18	↑	92000
150	.05	↑	.20	↑	-68000	.04	↑	.16	↑	83000
185	.04	↑	.18	↑	-57000	.03	↑	.15	↑	70000
220	.03	↑	.16	↑	-42000	.03	↑	.14	↑	44000
255	.03	↑	.14	↑	-22000	.02	↑	.12	↑	28000
280	.02	↑	.12	↑	-6000	.02	↑	.10	↑	6500
323 (Tip)	.02	1.0	.10	2.0	0	.02	1.0	.10	2.0	0

TABLE 5-7

Ti-6Al-4V ANNEALED 3 SPAR INTEGRALLY STIFFENED WING SIZING  
(REFERENCE FIGURE 5-8)

BUTT LINE	UPPER SURFACE					LOWER SURFACE				
	t <sub>skin</sub>	h	t <sub>stiff</sub>	b	f <sub>max</sub> *	t <sub>skin</sub>	h	t <sub>stiff</sub>	b	f <sub>max</sub> *
45 (Root)	.09	1.5	.25	2.0	-67000	.08	1.50	.24	2.0	71000
80	.08	1.4	.23	↑	-67000	.07	1.35	.22	↑	72000
115	.07	1.3	.21	↑	-63000	.06	1.20	.20	↑	71000
150	.06	1.2	.20	↑	-57000	.05	1.05	.20	↑	65000
185	.05	1.1	.20	↑	-45000	.04	1.00	.20	↑	51000
220	.04	1.0	.20	↑	-33000	.04	1.00	.20	↑	33000
255	.04	1.0	.18	↑	-17000	.03	1.00	.18	↑	20000
280	.04	1.0	.16	↑	-3700	.03	1.00	.16	↑	4200
323 (Tip)	.04	1.0	.14	2.0	0	.03	1.00	.14	2.0	0

TABLE 5-8

7075-T76 ALUMINUM 3 SPAR INTEGRALLY STIFFENED WING SIZING  
(REFERENCE FIGURE 5-8)

BUTT LINE	UPPER SURFACE					LOWER SURFACE				
	t <sub>skin</sub>	h	t <sub>stiff</sub>	b	f <sub>max</sub> *	t <sub>skin</sub>	h	t <sub>stiff</sub>	b	f <sub>max</sub> *
45 (Root)	.12	2.0	.250	2.0	-49000	.10	2.0	.240	2.0	54000
80	.11	1.9	.225	↑	-48000	.09	1.9	.215	↑	53000
115	.10	1.8	.200	↑	-44000	.08	1.8	.190	↑	49000
150	.09	1.7	.175	↑	-41000	.07	1.7	.170	↑	46000
185	.08	1.6	.150	↑	-35000	.06	1.6	.140	↑	40000
220	.07	1.5	.125	↑	-28000	.06	1.5	.130	↑	31000
255	.06	1.4	.125	↑	-14000	.05	1.4	.120	↑	15000
280	.05	1.3	.125	↑	-2600	.04	1.3	.120	↑	3000
323 (Tip)	.04	1.2	.125	2.0	0	.04	1.2	.100	2.0	0

\* f<sub>max</sub> are stresses for ultimate design loads

stiffeners were dropped off outboard when the stiffener spacing became too small. The skin and stiffener thicknesses were chosen to provide near optimum dimensions without complicated machining. The preliminary sizing and stress levels are summarized in Tables 5-9, 5-10, and 5-11.

#### 5.4.4 Multi-Spar Plate Wing

Once the skins were sized, the spar caps were sized to give the required stress levels. Preliminary sizing and stress levels are summarized in Tables 5-12, 5-13 and 5-14.

#### 5.4.5 Resizing for Final Design Stress Allowables

Two concepts required resizing to meet the design allowable stresses for fatigue. These were the zee and integrally stiffened aluminum wings. The resizing was performed by ratioing the equivalent thicknesses of the lower surfaces and then distributing the additional material into the structural details. Sizing and stress levels are summarized in Tables 5-15 and 5-16.

TABLE 5-9 D6AC STEEL 220 ksi 3 SPAR ZEE-STIFFENED WING SIZING  
(REFERENCE FIGURE 5-8)

BUTT LINE	UPPER SURFACE					LOWER SURFACE					SPACING
	t <sub>skin</sub>	h	t <sub>stiff</sub>	b	f <sub>max</sub> *	t <sub>skin</sub>	h	t <sub>stiff</sub>	b	f <sub>max</sub> *	
45 (Root)	.10	1.25	.09	1.00	-102000	.09	1.00	.09	1.00	110000	4.00
80	.08	↑	.09	1.00	-93000	.07	1.00	.09	1.00	103000	3.65
115	.07	↑	.08	1.00	-81000	.06	↑	.08	1.00	96000	3.30
150	.06	↑	.07	1.00	-67000	.05	↑	.07	1.00	79000	2.95
185	.05	↑	.06	1.00	-56000	.04	↑	.06	.75	65000	2.60
220	.04	↑	.06	.75	-42000	.03	↑	.06	.75	44000	2.25
255	.03	↑	.06	.75	-28000	.02	↑	.06	.75	30000	3.80
290	.03	↓	.05	.75	-5000	.02	↓	.05	.75	5500	3.45
323 (Tip)	.03	1.25	.04	.75	0	.02	1.0	.04	.75	0	3.10

TABLE 5-10 Ti-6Al-4V ANNEALED 3 SPAR ZEE-STIFFENED WING SIZING  
(REFERENCE FIGURE 5-8)

BUTT LINE	UPPER SURFACE					LOWER SURFACE					SPACING
	t <sub>skin</sub>	h	t <sub>stiff</sub>	b	f <sub>max</sub> *	t <sub>skin</sub>	h	t <sub>stiff</sub>	b	f <sub>max</sub> *	
45 (Root)	.125	1.5	.10	1.00	-82000	.10	1.25	.10	1.00	92000	4.00
80	.100	↑	.10	1.00	-73000	.09	↑	.10	1.00	79000	3.65
115	.080	↑	.10	1.00	-63000	.07	↑	.10	1.00	70000	3.30
150	.060	↑	.10	1.00	-52000	.06	↑	.08	1.00	62000	2.95
185	.050	↑	.08	1.00	-44000	.04	↑	.06	1.00	51000	2.60
220	.040	↑	.06	1.00	-31000	.04	↑	.06	.75	39000	2.25
255	.03	↑	.06	.75	-25000	.03	↑	.06	.75	27000	3.80
290	.03	↓	.06	.75	-4300	.03	↓	.06	.75	4800	3.45
323 (Tip)	.03	1.5	.06	.75	0	.03	1.25	.06	.75	0	3.10

TABLE 5-11 7075-T76 ALUMINUM 3 SPAR ZEE-STIFFENED WING SIZING  
(REFERENCE FIGURE 5-8)

BUTT LINE	UPPER SURFACE					LOWER SURFACE					SPACING
	t <sub>skin</sub>	h	t <sub>stiff</sub>	b	f <sub>max</sub> *	t <sub>skin</sub>	h	t <sub>stiff</sub>	b	f <sub>max</sub> *	
45 (Root)	.18	1.5	.17	1.00	-59000	.16	1.25	.15	1.00	65000	4.00
80	.16	↑	.15	1.00	-54000	.14	↑	.14	1.00	60000	3.65
115	.14	↑	.13	1.00	-48000	.12	↑	.13	.90	54000	3.30
150	.12	↓	.11	.75	-42000	.10	↓	.12	.75	46000	2.95
185	.10	1.5	.09	.75	-35000	.08	1.25	.10	↑	40000	2.60
220	.08	1.0	.10	.75	-24000	.06	1.00	.08	↓	28000	2.25
255	.06	↑	.08	.75	-12000	.05	↑	.07	↓	13000	1.90
290	.04	↓	.06	.75	-4000	.04	↓	.055	↓	4500	3.10
323 (Tip)	.04	1.0	.04	.75	0	.04	1.00	.04	.75	0	2.50

\* f<sub>max</sub> are stresses for ultimate design loads



TABLE 5-12

D6AC STEEL 220 ksi 11-SPAR UNSTIFFENED SKIN WING SIZING

BUTT LINE	UPPER SURFACE			LOWER SURFACE			SPAR SPACING
	$t_{\text{skin}}$	SPAR AREA PER CAP	$f_{\text{max}}^*$	$t_{\text{skin}}$	SPAR AREA PER CAP	$f_{\text{max}}^*$	
45 (Root)	.20	.9	-65900	.18	.9	70900	11.7
80	.17	.8	-64400	.15	.8	69600	10.7
115	.14	.7	-61200	.12	.7	67400	9.8
150	.11	.6	-52500	.09	.6	58400	8.9
185	.09	.5	-46600	.07	.5	53200	7.9
220	.07	.4	-35400	.05	.4	41500	7.0
255	.05	.2	-24800	.03	.2	32100	6.1
290	.03	.1	-7800	.02	.1	9600	5.1
323 (Tip)	.02	.1	0	.02	.1	0	4.2

TABLE 5-13

Ti-6Al-4V ANNEALED 11 SPAR UNSTIFFENED SKIN WING SIZING

BUTT LINE	UPPER SURFACE			LOWER SURFACE			SPAR SPACING
	$t_{\text{skin}}$	SPAR AREA PER CAP	$f_{\text{max}}^*$	$t_{\text{skin}}$	SPAR AREA PER CAP	$f_{\text{max}}^*$	
45 (Root)	.25	1.5	-48500	.22	1.5	52400	11.7
80	.22	1.2	-47400	.19	1.2	52200	10.7
115	.19	1.0	-44300	.16	1.0	49000	9.8
150	.16	0.8	-40000	.14	0.8	43000	8.9
185	.13	0.6	-34800	.11	0.6	38300	7.9
220	.10	0.4	-28700	.09	0.4	30500	7.0
255	.07	0.2	-19600	.06	0.2	21600	6.1
290	.04	0.1	-6500	.03	0.1	7700	5.1
323 (Tip)	.03	0.1	0	.03	0.1	0	4.2

TABLE 5-14

7075-T76 ALUMINUM 11 SPAR UNSTIFFENED SKIN WING SIZING

BUTT LINE	UPPER SURFACE			LOWER SURFACE			SPAR SPACING
	$t_{\text{skin}}$	SPAR AREA PER CAP	$f_{\text{max}}^*$	$t_{\text{skin}}$	SPAR AREA PER CAP	$f_{\text{max}}^*$	
45 (Root)	.35	1.5	-42000	.30	1.5	45000	11.7
80	.32	1.3	-38000	.27	1.3	41000	10.7
115	.29	1.1	-34000	.24	1.1	37000	9.8
150	.26	0.9	-29000	.21	0.9	34000	8.9
185	.22	0.7	-24000	.17	0.7	28000	7.9
220	.18	0.5	-19000	.14	0.5	23000	7.0
255	.14	0.3	-13000	.11	0.3	15000	6.1
290	.10	0.3	-3000	.08	0.3	3500	5.1
323 (Tip)	.08	0.3	0	.08	0.3	0	4.2

\*  $f_{\text{max}}$  are stresses for ultimate design loads

TABLE 5-15

RESIZED 7075-T76 ALUMINUM INTEGRALLY STIFFENED  
STRUCTURE (REFERENCE FIGURE 5-8)


LOWER SURFACE					
BUTT LINE	$t_{\text{skin}}$	$h$	$t_{\text{stiff}}$	$b$	$f_{\text{max}}^*$
45 (Root)	.150	2.0	.280	2.0	44500
80	.125	1.9	.260		43900
115	.100	1.8	.220		44400
150	.090	1.7	.180		43600
185	.060	1.6	.140		40000
220	.060	1.5	.130		31000
255	.050	1.4	.120		15000
280	.040	1.3	.120		3000
323 (Tip)	.040	1.2	.100	2.0	0

TABLE 5-16

RESIZED 7075-T76 ALUMINUM ZEE-STIFFENED STRUCTURE  
(REFERENCE FIGURE 5-8)

LOWER SURFACE						
BUTT LINE	$t_{\text{skin}}$	$h$	$t_{\text{stiff}}$	$b$	$f_{\text{max}}^*$	SPACING
45 (Root)	.24	1.50	.20	1.20	44500	4.00
80	.20	1.50	.18	1.00	44100	3.65
115	.15	1.50	.14	1.00	44500	3.30
150	.10	1.50	.11	1.00	44400	2.95
185	.08	1.25	.10	.75	40000	2.60
220	.06	1.00	.08	.75	28000	2.35
255	.05	1.00	.07	.75	13000	1.90
280	.04	1.00	.055	.75	4500	3.10
323 (Tip)	.04	1.00	.04	.75	0	2.50

\*  $f_{\text{max}}$  are stresses for ultimate design loads with a fatigue cutoff of 44,500 psi

## 5.5 DESIGN STRESS ALLOWABLES

### 5.5.1 Fatigue Analysis

The fatigue analysis has been performed using the methods described in Section 4.2. The allowables in the form of constant-life diagrams used in performing the analysis are given in Section 5.3. The fatigue loading spectra applicable to the wing structure are given in Section 5.2. In performing the analysis, various ratios of ultimate design load to ultimate design stress were assumed to determine the relationship between ultimate design stress and design fatigue life.

The results of the fatigue analysis are plotted in Figure 5-9 for the aluminum structure and Figure 5-10 for the titanium structure. These figures show the relationship between ultimate design tension stress and design fatigue life for the two types of loading spectra being considered, a typical spectrum representing normal operational usage and a spectrum representing the most severe operation anticipated. As indicated in these figures, the selected fatigue allowable stresses are based on the results for a composite spectrum consisting of 25% severe operation and 75% typical operation. These design stresses reflect use of a design life of 16,000 hours (4000 hours x 4) and fatigue quality indices consistent with current design and manufacturing practices.

A fatigue quality index of 4.0 was selected as representative of the fatigue quality that can be achieved in aluminum structure. A fatigue quality of 4.0 has been used as a basis for selecting design stress allowables for various types of aircraft at Lockheed for many years. Correlations between analysis and fatigue test results, as shown in Figure 5-11, indicate that structures designed to a fatigue quality of 4.0 have a high probability of meeting or exceeding the fatigue test requirements.

The fatigue properties of titanium material are generally affected more by fabrication and processing than aluminum materials are and, therefore, a fatigue quality index of 5.0 was selected. Fatigue tests conducted on titanium structure in connection with the SST program (Reference 5-13) indicate a fatigue quality level of 5.0 can be achieved.



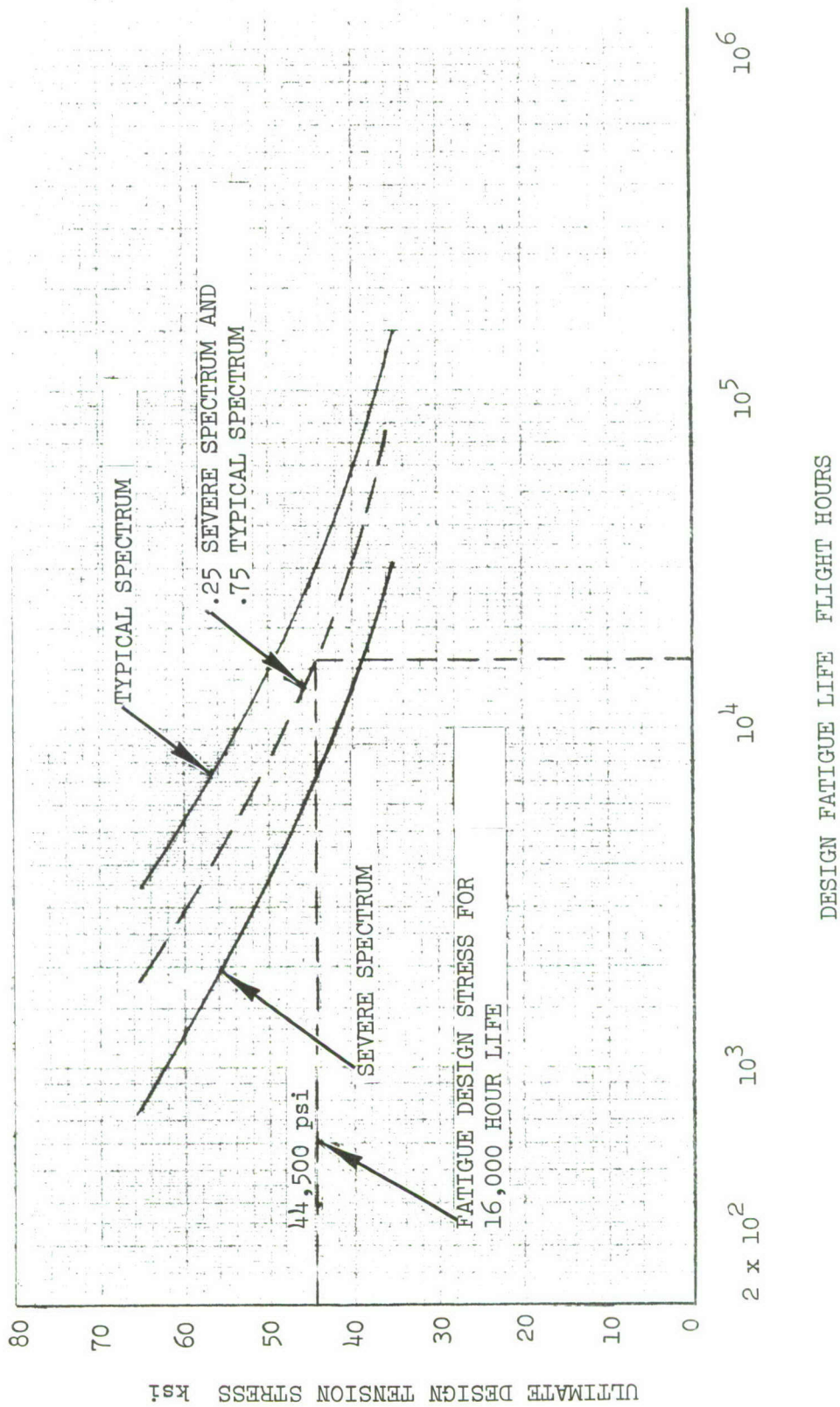


FIGURE 5-9 ULTIMATE DESIGN TENSION STRESS ALLOWABLE FOR 7075-T76 ALUMINUM STRUCTURE AND FATIGUE QUALITY INDEX = 4.0



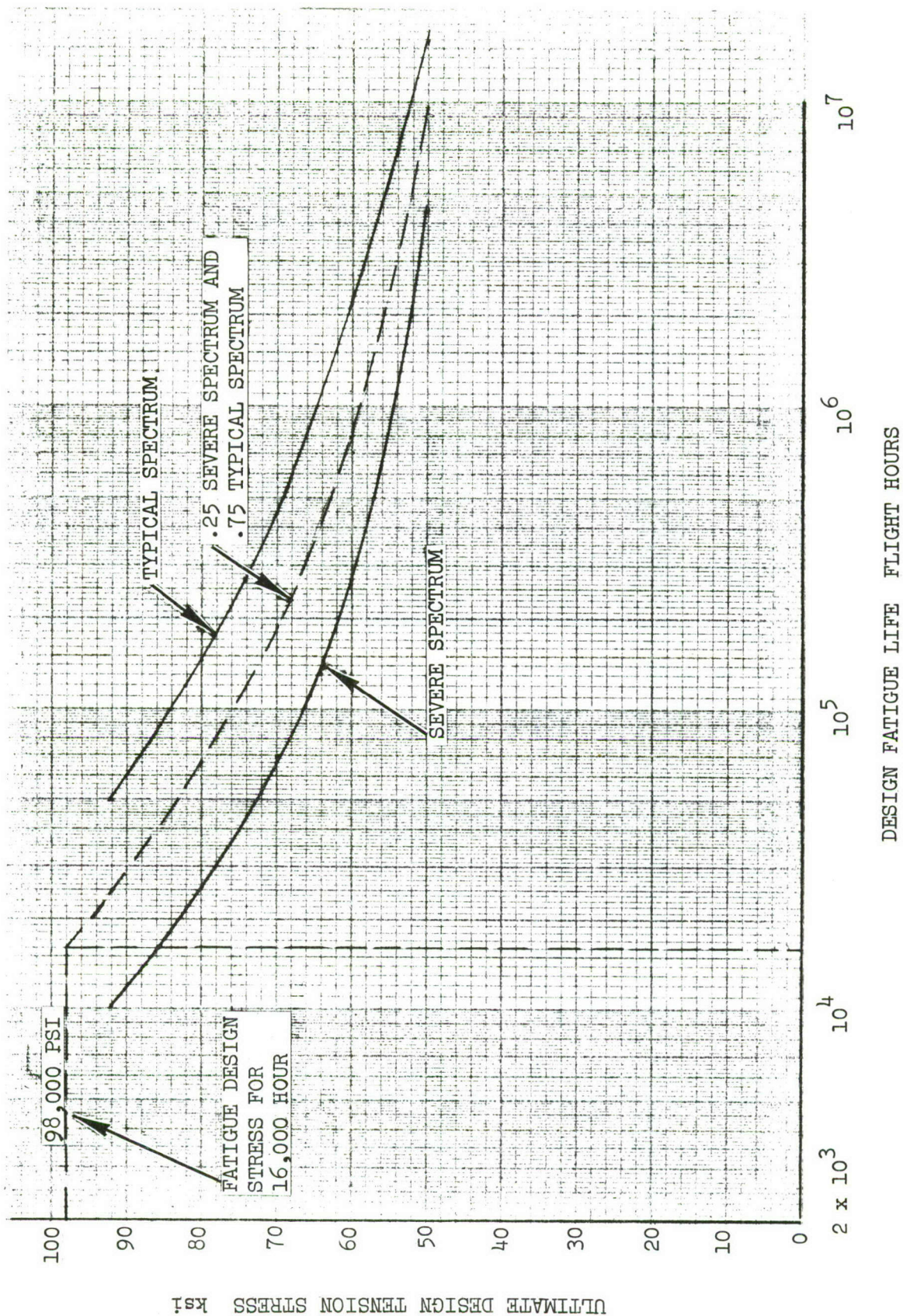


FIGURE 5-10 ULTIMATE DESIGN TENSION STRESS ALLOWABLE FOR Ti-6AL-4V STRUCTURE AND A FATIGUE QUALITY INDEX = 5.0

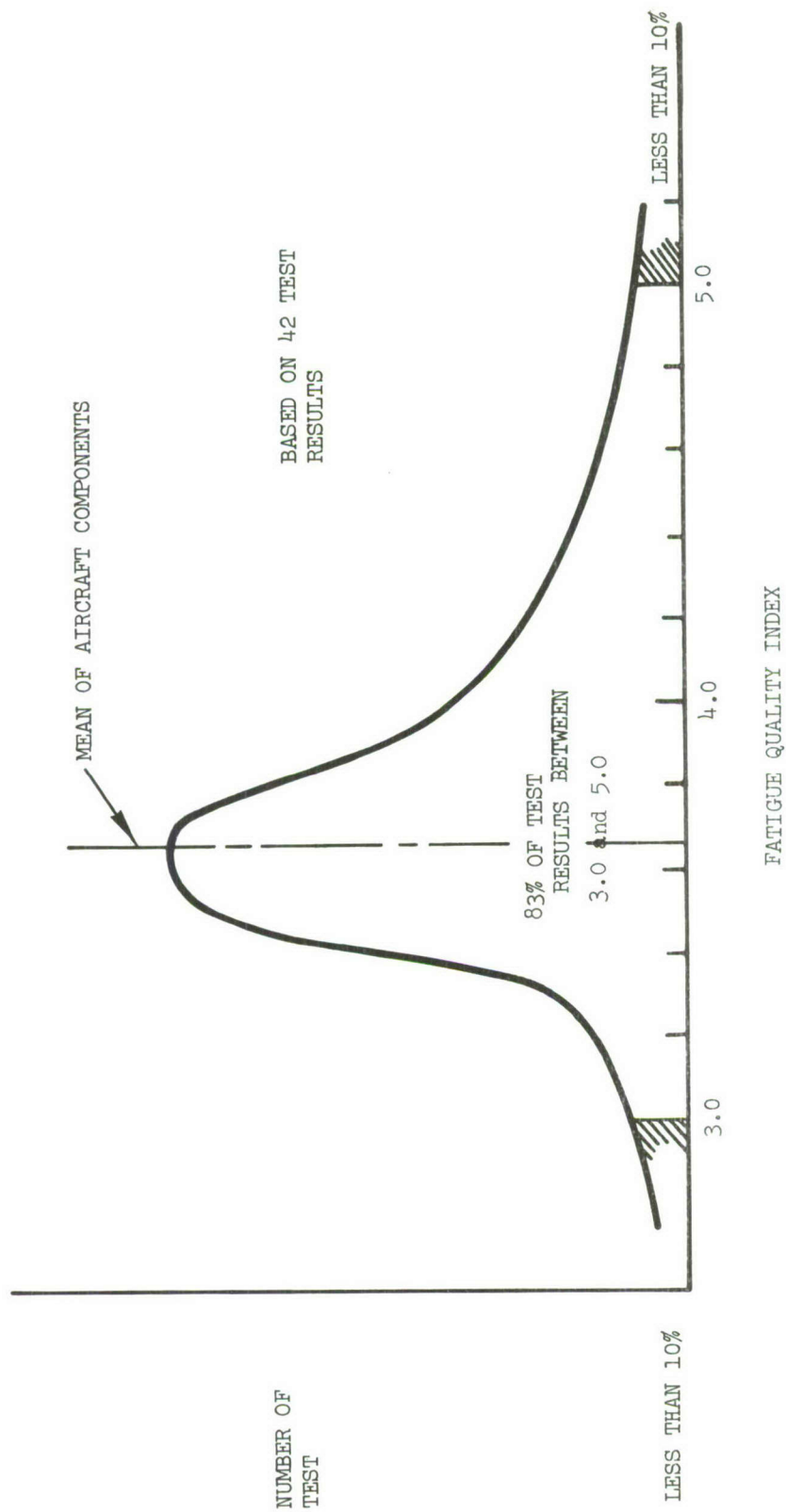


FIGURE 5-11 DISTRIBUTION CURVE FOR AIRCRAFT STRUCTURAL COMPONENT TEST VALUES OF FATIGUE QUALITY INDEX (REFERENCE 5-14)



As noted, the maximum design tension stresses were selected for a composite mission mix consisting of 25% severe spectrum and 75% typical spectrum. The maximum design tension stress of 39,000 psi for 100% of the severe maneuver spectrum was too low compared to maximum tension stresses for current fighter/attack type aircraft, which are of the order of 50,000 psi. The severe spectrum covers the highest maneuver loading anticipated for this type of aircraft, and is, therefore, too severe to use for design which should represent an average anticipated usage. In service the aircraft may be rotated to some extent so that no single aircraft is likely to receive the most severe usage 100% of the time. According to the latest Air Force Policy (Reference 5-15) a fatigue monitoring program will be conducted for any new aircraft design. Therefore, aircraft accumulating damage at a high rate could be rotated to average out the usage or be given more thorough and frequent inspections to detect fatigue cracking before it occurs fleetwide. To meet these service life requirements, the structure was resized for a maximum design tension stress of 44,500 psi as discussed in Section 5.4.

Using the composite mission spectrum for titanium structure, the maximum design tension stress was calculated to be 98,000 psi as shown in Figure 5-10. Since this stress was above the maximum ultimate tension stress achieved from static design considerations, no resizing was necessary for the titanium structural concepts.

#### 5.5.2 Fatigue Crack Growth

The fatigue crack growth analysis procedure is described in Section 4.4. The method does not take possible crack retardation effects into account, as has been discussed, because retardation may not occur on aircraft in service to the extent observed in the laboratory. Constant-amplitude crack growth rate allowables for Ti-6Al-4V and 7075-T76 aluminum are presented in Tables 5-4 and 5-5. Maneuver and taxi load spectra representing typical and severe usage are plotted in Figure 5-3.

These loading spectra have been converted from continuous spectra to discrete load levels, described in terms of a maximum load factor and a number of occurrences per 1000 hours.

A sample sequence of 2 flights is shown in Figure 5-12 to illustrate how the ground-air-ground (GAG) cycles are defined for the crack growth analysis. The largest positive load in each flight is combined with the negative taxi load to identify a peak-to-peak GAG cycle for each flight. The remaining positive loads are treated normally as excursions from the flight mean load,  $N_Z = 1$ . The sequence of cycles for this example are shown in Table 5-17.

For simplicity it is assumed that the peak positive loads for GAG cycles are the 1333 or 1530 highest positive loads to occur in 1000 hours for the typical and severe spectrum, respectively. On this basis, the two spectra, typical and severe, are given in Table 5-18 in terms of maximum and minimum load factors and number of occurrences per 1000 hours.

Using these tabulated values and the crack growth rate curves for titanium and aluminum, crack growth rates per flight-hour versus  $\alpha_s$  are calculated using Equations (4-17) thru (4-20), with  $N_Z$  replacing  $Z_1$ . These spectrum crack growth rate curves, applicable to any<sup>i</sup> configuration and value of  $S$ , are plotted in Figure 5-13 for the two materials and the two loading spectra.

The crack growth calculations have been made based on the severe spectrum. Crack growth due to the typical spectrum loadings are estimated directly from the severe spectrum calculation for the same configuration; i.e., a factor on load or stress is used to convert from the one to the other.

To check this procedure and to obtain the value of these factors, one calculation has been made using the typical spectrum and a surface flaw in unreinforced structures, Figures D-3 and D-4 in Appendix D. The values of design stress level giving equal crack growth periods for identical initial and final flaw sizes were compared against results for the severe spectrum, Figures D-1 and D-2 in Appendix D. This comparison is summarized in Table 5-19. If a particular value of the load-stress conversion factor  $S = S_1$  gives a crack growth period,  $N$ , under the severe spectrum, then an  $S$ -value of  $C$  times  $S_1$  gives approximately the same crack growth period  $N$  for the typical spectrum, where

$$C = 1.29 \text{ for Ti-6Al-4V}$$

$$C = 1.32 \text{ for 7075-T76 aluminum}$$



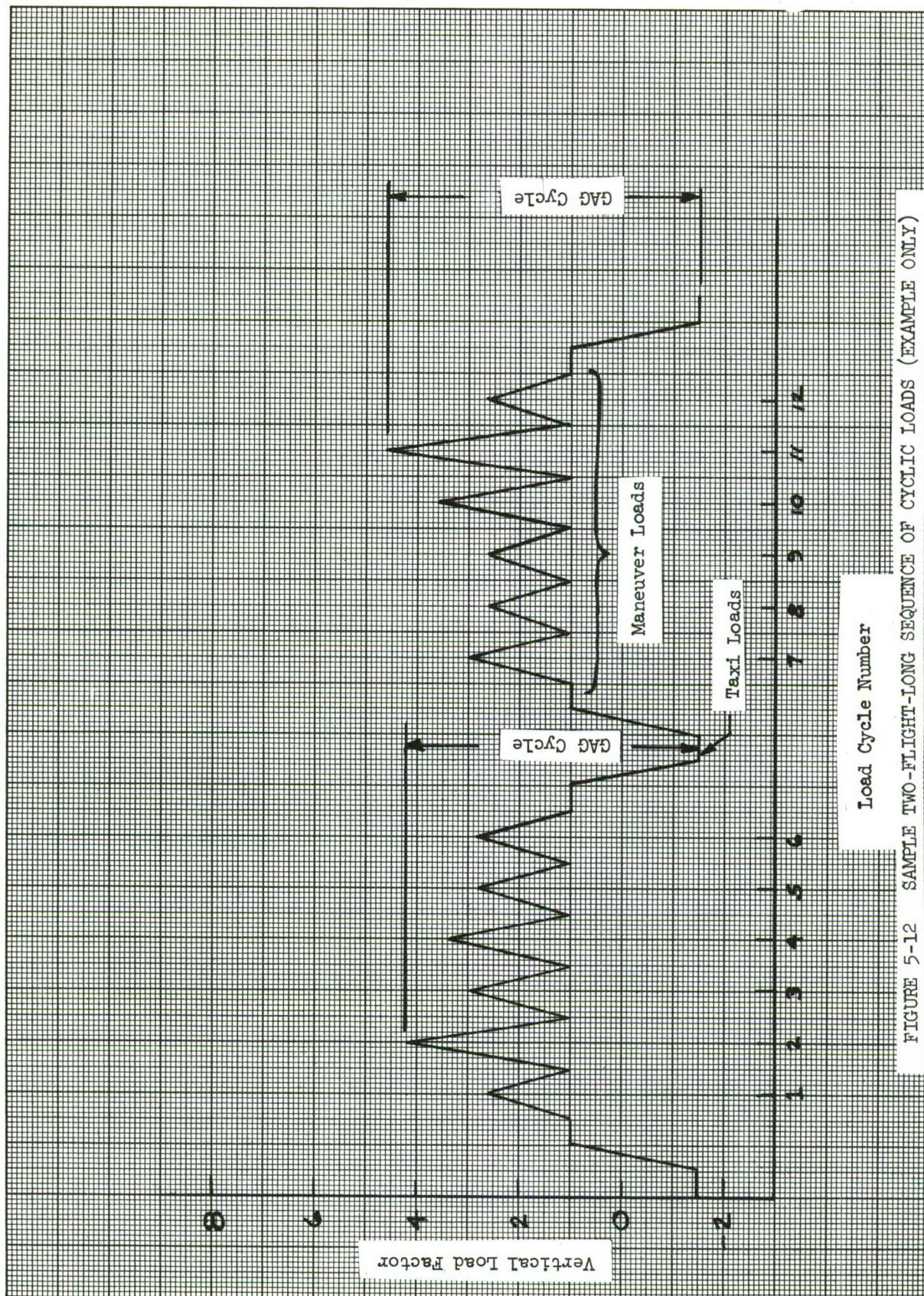


FIGURE 5-12 SAMPLE TWO-FLIGHT-LONG SEQUENCE OF CYCLIC LOADS (EXAMPLE ONLY)



TABLE 5-17  
Sequence of Cycles for the Sample Load History of Figure 5-12  
(Example Only)

Cycle Number	Maximum $N_z$	Minimum $N_z$
1	2.6	1.0
2	4.2	-1.5
3	3.0	1.0
4	3.4	1.0
5	2.8	1.0
6	2.8	1.0
7	3.0	1.0
8	2.6	1.0
9	2.6	1.0
10	3.6	1.0
11	4.6	-1.5
12	2.6	1.0

TABLE 5-18

## TYPICAL AND SEVERE LOAD SPECTRA

Typical Spectrum *			Severe Spectrum **		
Load	Factor, $N_z$	Cycles per 1000 hrs.	Load Factor, $N_z$		Cycles per 1000 hrs.
Max.	Min.		Max.	Min.	
8.0	-1.5	1.0	8.2	-1.5	1.2
7.8		.5	8.0		.7
7.6		.7	7.8		.9
7.4		1.0	7.6		1.4
7.2		1.5	7.4		1.6
7.0		2.1	7.2		3.4
6.8		3.2	7.0		6
6.6		5	6.8		11
6.4		6	6.6		16
6.2		10	6.4		29
6.0		9	6.2		51
5.8		24	6.0		65
5.6		28	5.8		100
5.4		38	5.6		160
5.2		60	5.4		250
5.0		70	5.2		300
4.8		90	5.0		400
4.6		130	4.8		133
4.4		140	4.8	-1.5	367
4.2		180	4.6	1.0	550
4.0		250	4.4		750
3.8	-1.5	17	4.2		800
3.8	1.0	283	4.0		1000
3.6		450	3.8		1100
3.4		600	3.6		1100
3.2		800	3.4	1.0	1800
3.0		1200			
2.8		1600			
2.6	1.0	2200			

\* 45 Minute Flights

\*\* 39-minute flights

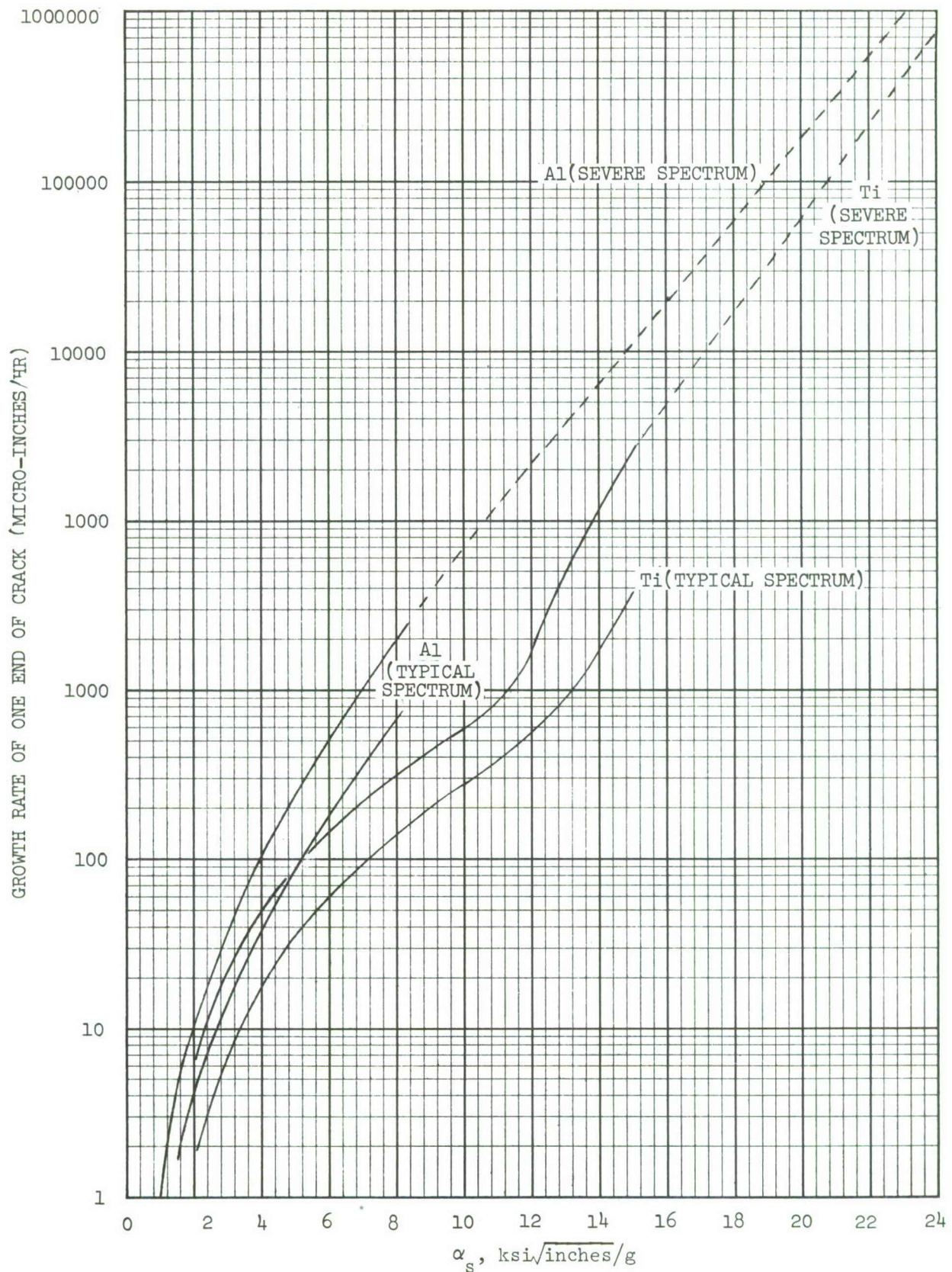


FIGURE 5-13 GROWTH RATE,  $da/dF$ , versus  $\alpha_s$  FOR SPECTRUM LOADING



TABLE 5-19 CONVERSION FACTORS TO APPLY ANALYSIS TO TYPICAL SPECTRUM

Material	Spectrum	S (ksi/g)	a <sub>o</sub> (inch)	a <sub>final</sub> (inch)	"Life" (hours)	Obtained by Interpolation on Figure	$C = \frac{S_{\text{typical}}}{S_{\text{severe}}}$
<div>Aluminum</div> <div>↑</div> <div>↓</div> <div>Aluminum</div>	Severe	4.66	.025	.075	30,600	D-1	1.33
	Typical	6.20	.025	.075	30,600	D-3	
	Severe	4.66	.075	.150	8,400	D-1	1.33
	Typical	6.20	.075	.150	8,400	D-3	
	Severe	5.72	.100	.500	6,300	D-1	1.32
	Typical	7.55	.100	.500	6,300	D-3	
							1.32
<div>Titanium</div> <div>↑</div> <div>↓</div> <div>Titanium</div>	Severe	7.00	.025	.075	18,600	D-2	1.26
	Typical	8.84	.025	.075	18,600	D-4	
	Severe	7.00	.075	.150	5,900	D-2	1.27
	Typical	8.90	.075	.150	5,900	D-4	
	Severe	9.08	.060	.500	5,730	D-2	1.35
	Typical	12.26	.060	.500	5,730	D-4	
							1.29

The composite spectrum used for fatigue analysis, consisting of a mix of 75% of the typical spectrum and 25% of the severe spectrum, would be handled similarly. For the composite spectrum the value of the conversion factor  $S$  giving the same value of crack growth period  $N$  as the severe spectrum at  $S = S_1$  would be  $C' \times S_1$ , where

$$C' = 1 + \frac{3}{4} (C-1)$$

hence

$$C' = 1.22 \text{ for Ti-6Al-4V}$$

$$C' = 1.24 \text{ for 7075-T76 aluminum.}$$

Crack growth calculations have been conducted at various  $S$  values for the several basic configurations sketched in Figure 5-14. The initial crack is shown darkened, and the assumed growth is shown by the striation-type lines.

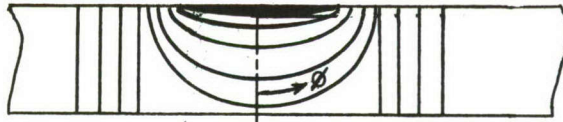
As discussed in Section 4.33, cracks depicted in cases I through IV of Figure 5-14 are assumed to grow as part-thru cracks with  $\alpha_b = 1.0$  until the flaw depth,  $a$ , is equal to the sheet thickness,  $t$ . At that point a thru-the-thickness crack of length equal to the surface length  $2c$  of the crack is assumed.

In the cases I and III the part-thru crack is assumed to maintain its (circular) shape until  $a = t$ . For case II however, the shape changes during crack growth. Under in-plane tension loading the local stress intensity near the surface ( $\phi = 90^\circ$  in II, Figure 5-14) is substantially lower than the local stress intensity at the deepest point ( $\phi = 0^\circ$  in II, Figure 5-14). Therefore, the growth in the depth direction is faster than the growth along the surface until a nearly semi-circular shape is attained (Reference 5-16).

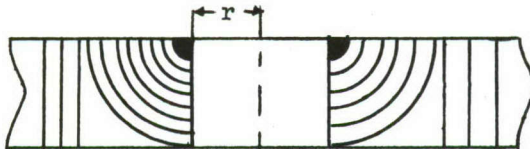
(The presence of the front and back surfaces, not accounted for in the discussion in Reference 5-16, have opposing effects on the stable shape of part-thru cracks. Growth rate in the surface direction is increased due to the front surface, whereas growth rate in the depth direction is increased due to the back surface.)



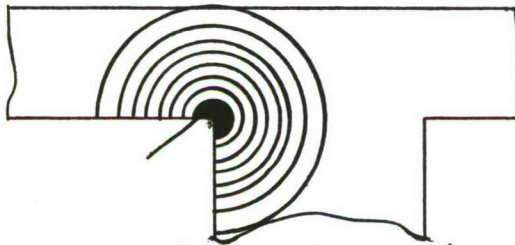
I. SEMI-CIRCULAR PART-THRU CRACK/THRU CRACK



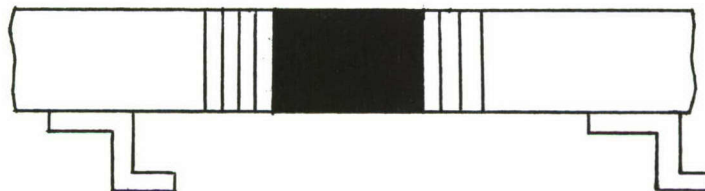
II. SHALLOW PART-THRU CRACK/THRU CRACK



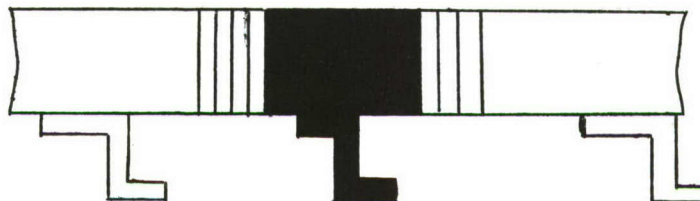
III. DOUBLE CORNER CRACK AT A HOLE



IV. TYPE II CORNER CRACK (INTEGRAL STIFFENER)



V. THRU-THICKNESS CRACK BETWEEN REINFORCEMENTS



VI. THRU-THICKNESS CRACK AT A REINFORCEMENT

FIGURE 5-14 ELEMENTARY GEOMETRIES FOR THE CRACK PROPAGATION ANALYSIS



Considering the sparseness of applicable quantitative knowledge it would be of questionable usefulness to attempt to devise a complex analysis procedure to account for change in crack shape. Therefore, the simple assumption is made that  $da/dN = dc/dN$  (where  $c$  is the surface half-length and  $a$ , the depth) which underestimates the rate of change in the shape of the crack. By this assumption, the initial value of  $(c-a)$  is maintained until  $a = t$ , the end-point of the part-thru crack analysis.

Once having predetermined the crack shape history, the procedures of Section 4.3 can be applied to obtain the geometry factor  $\alpha$  as a function of crack length. For a part-thru crack Equation (4-8) yields

$$\alpha = \sqrt{\pi a} \quad \frac{M_1'}{\phi} \cdot \alpha_b \quad (5-1)$$

where  $\alpha_b = 1.0$  and  $M_1'/\phi$  is obtained from Figure 4-9. For the semi-circular crack  $M_1'/\phi = 0.71$ . For the shallow crack growing in the manner described above,  $M_1'/\phi$  values are given in Table 5-20 as a function of crack depth  $a$  and surface crack length  $2c$ .

TABLE 5-20 VALUE OF  $M_1'/\phi$  FOR A SHALLOW PART-THRU CRACK, CASE II

$a$	$2c$	$a/2c$	$M_1'/\phi$
0.015	0.090	0.17	0.92
0.020	0.100	0.20	0.89
0.030	0.120	0.25	0.84
0.045	0.150	0.30	0.78
0.070	0.200	0.35	0.72
0.120	0.300	0.40	0.69
0.270	0.600	0.45	0.69

The value of  $\alpha$  for case III is, from Equation(4-14),

$$\alpha = \sqrt{2a} \cdot \alpha_b \cdot F\left(\frac{L}{r}\right)/1.12 \quad (5-2)$$

where  $\alpha_b = 1.0$  and  $F\left(\frac{L}{r}\right)$  is obtained from Figure 4-12 with  $L = a/\sqrt{2}$ . Values of  $F(L/r)$  are given in Table 5-21, assuming the radius  $r$  of the fastener hole is 0.125 inch.

TABLE 5-21 BOWIE CORRECTION FOR CORNER CRACK (r = 0.125 Inch)

Corner Crack Depth	L	L/r	One Crack F(L/r)	Two Cracks • F(L/r)
0	0	0	3.37	3.37
0.018	0.0125	0.1	2.73	2.73
0.035	0.025	0.2	2.30	2.33
0.053	0.0375	0.3	2.04	2.12
0.088	0.0625	0.5	1.73	1.85
0.124	0.0875	0.7	1.55	1.64
0.159	0.1125	1.0	1.41	1.51
0.208	0.175	1.4	1.20	1.32
0.354	0.25	2.0	1.06	1.2
0.530	0.375	3.0	0.94	1.125
-	0.625	5.0	0.81	1.06
-	1.25	10.0	0.75	1.03
-	$\infty$	$\infty$	0.71	1.0

After  $a = t$  the semi-elliptical part-thru cracks (case I and II) have become thru-the-thickness cracks and Equation (4-6a) applies. Thus

$$\alpha = \sqrt{\pi c} \phi_1 \quad (5-3)$$

where  $c$  is the half-length of the crack and  $\phi_1 = 1.0$  because no plate edge effects are assumed. For case III and  $a \geq t$ , from Equation (4-10),

$$\alpha = \sqrt{\pi a} \cdot \phi_1 \cdot F(L/r) \quad (5-4)$$

where  $\phi_1 = 1.0$  and  $L = a$ . Columns 2, 4 and 5 of Table 5-21 can be used again for  $F(L/r)$  if  $r = 0.125$  inch is assumed.

The value for  $\alpha$  for case IV was assumed to be mid-way between that of an embedded penny-shaped crack and that of a semi-circular part-thru crack. Hence

$$\alpha = \frac{1.12 + 1.00}{2} \left[ \frac{2}{\pi} \sqrt{\pi a} \right] \quad (5-5)$$

For cracks in the vicinity of reinforcements, cases V and VI of Figure 5-14,  $\alpha = \lambda \sqrt{\pi a}$  and the dimensionless geometric coefficient  $\lambda$  must be determined as

discussed in Section 4.3.6. The calculated values of  $\lambda$  for the design configurations of the present study are presented in Tables 4-1 thru 4-3.

The load-stress conversion factor  $S$  at a particular location in a particular design is given by

$$S = \frac{f_{\max}}{1.5 \times 7.33 \text{ g}} \quad (5-6)$$

where  $f_{\max}$  is the gross area tensile stress at the particular structural location that would result from the application of the ultimate design load factor. Values of  $f_{\max}$  are given in Tables 5-6 thru 5-16. A series of values of  $S$  were selected, enclosing the range of all feasible designs, and each calculation of  $a$  vs.  $N$  was repeated for these various  $S$  values.

Results of the fatigue crack growth calculations are plotted as crack length vs. flight-hours for various values of the load-stress conversion factor  $S$  in Appendix D. These calculations are then used as the basis for "piecing together" damage sequences for design considerations of criteria for durability, growth of cracks in non-inspectable areas, and inspection intervals for inspectable areas.

#### Durability

The durability criterion requires that an initial crack (flaw) of surface length 0.25 inch does not grow to a critical size in two lifetimes, in this case 8000 hours. The spectrum used for this analysis is the same as that used for the fatigue analysis, which is a 75% - 25% mix of the typical and the severe spectra, respectively.

Figures 5-15 and 5-16 show the growth of a 0.25 inch initial crack (flaw) due to the severe spectrum. Two lifetimes correspond to the stress levels shown in Table 5-22 for the severe spectrum. The factor for converting from the severe to the composite (fatigue) spectrum is 1.24 for aluminum and 1.22 for titanium (see page 5-37). Therefore the stress cutoffs for durability are as indicated in the last column in Table 5-22 corresponding to the fatigue spectrum.



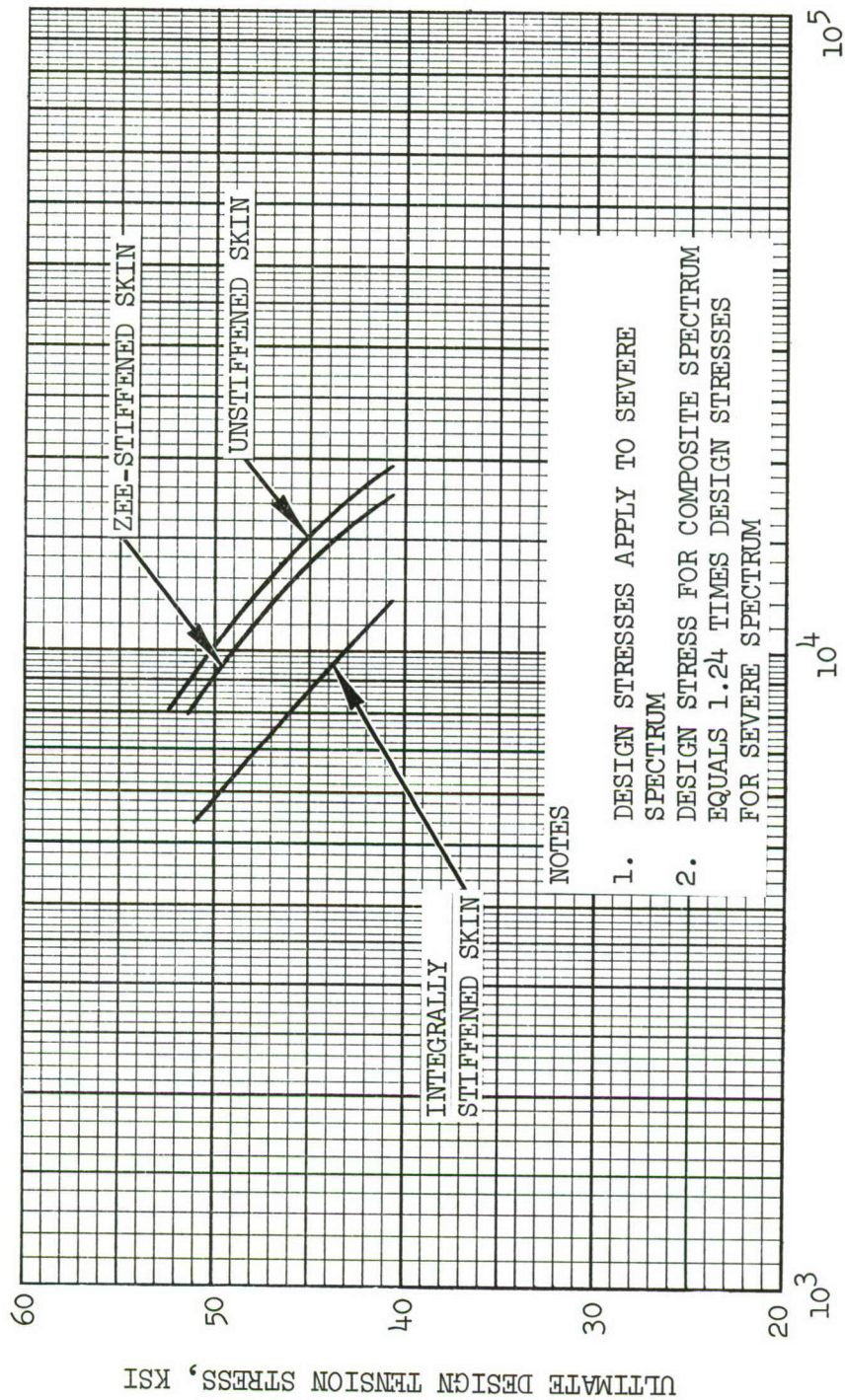
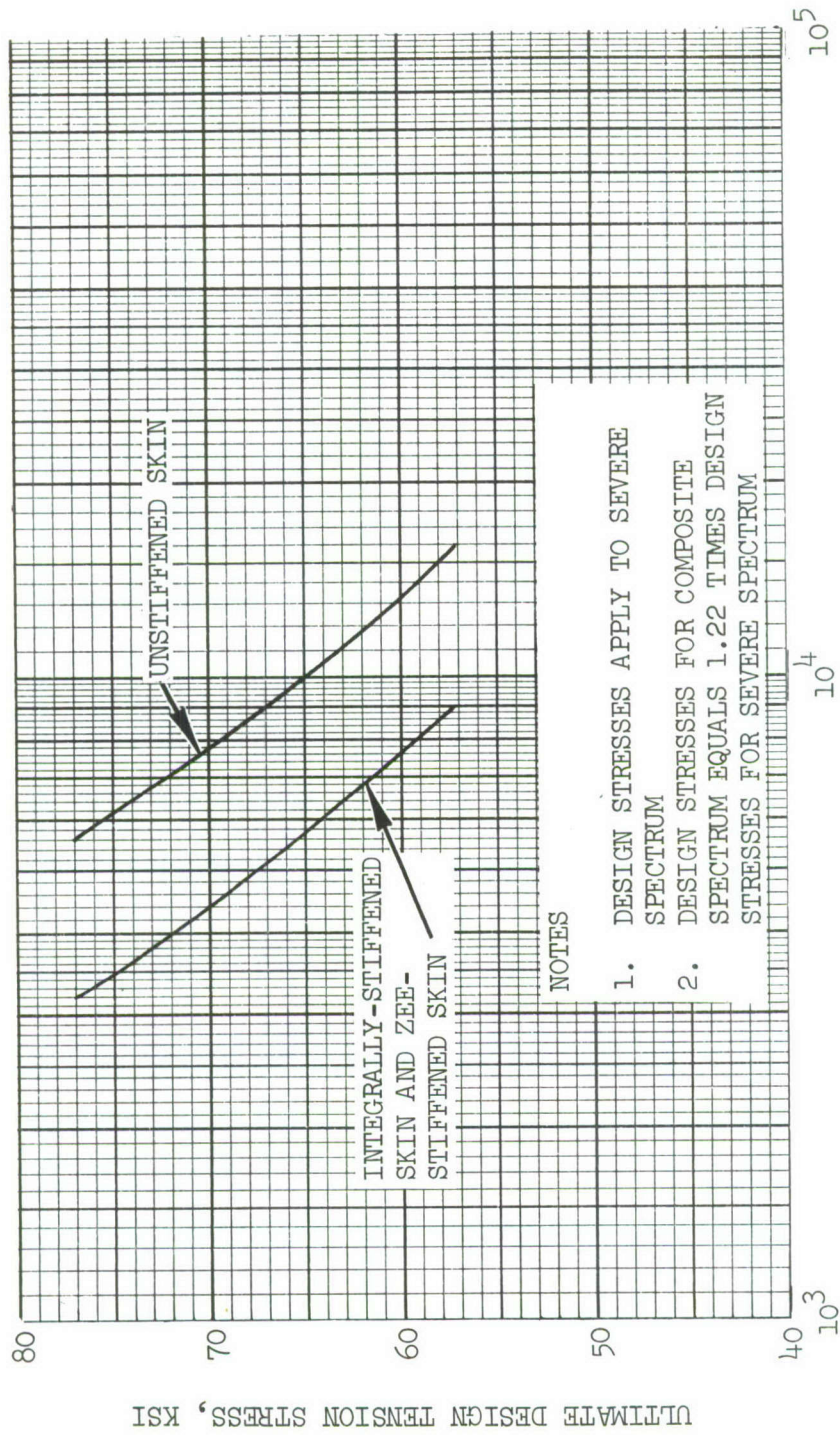


FIGURE 5-15. ULTIMATE DESIGN TENSION STRESS ALLOWABLES FOR DURABILITY REQUIREMENT - ALUMINUM STRUCTURE



FLIGHT HOURS FROM  $a_0 = 0.125$  IN. TO FAILURE

FIGURE 5-16. ULTIMATE DESIGN TENSION STRESS ALLOWABLES FOR DURABILITY REQUIREMENT - TITANIUM STRUCTURE



TABLE 5-22 SUMMARY OF ULTIMATE DESIGN TENSION STRESS ALLOWABLES TO MEET DURABILITY REQUIREMENT

Material	Structure	Severe Spectrum*	Composite Spectrum *
Aluminum	Zee Stiffened	51.3	63.6
	Integrally Stiffened	46	57
	11-Spar Unstiffened	52.5	65.1
Titanium	Zee Stiffened	59.2	72.2
	Integrally Stiffened	59.2	72.2
	11-Spar Unstiffened	69.5	84.8

\* Ultimate Design Tension Stress Allowable, ksi

#### Non-inspectable Structure

The criterion for non-inspectable structure requires that an initial crack or flaw located at the most critical point should not grow to catastrophic failure in two lifetimes. The most critical initial crack is a double corner crack in the skin at the edge of a fastener hole at a reinforcement, case III of Figure 5-14. The reinforcement may be a zee-stiffener or a spar, depending upon the type of construction. Since integrally stiffened structure does not have fastener holes along the reinforcements, a different critical damage must be defined for integrally stiffened structure. Two possibilities have been identified. One is a double corner crack at a fastener hole at a skin splice, case III of Figure 5-14. The other is an internal corner crack at the internal radius of the integral stiffener, case IV of Figure 5-14. The initial crack size assumed in all cases was  $a_0 = 0.05$  inch as indicated in Table 5-2.

Having defined initial cracks, the next decision is the growth sequence. Some time during the growth process the skin crack located at the reinforcement fastener hole will initiate a crack in the reinforcement. The time when this will occur is unpredictable, yet it will profoundly affect the crack propagation period that is calculated. If the skin crack and reinforcement crack were to initiate simultaneously and propagate in parallel, the crack growth period would be extremely short. To presume that this unlikely case occurs, however, would be to penalize fastener-attached reinforced structure, rather than giving credit for its having separate members. On the other hand, to assume that initiation of a crack in the reinforcing member occurs only after the skin crack is very long would be too unconservative.



As a reasonable compromise the following crack growth sequence is assumed for the zee-stiffened and multi-spar unstiffened structure. The initial skin crack is assumed to grow as a double corner crack ( $a_o = 0.05$  inch) until  $a = t$ . At this point a double corner crack ( $a_o = 0.05$  inch) originates in the stiffener and grows until  $a = t_s$  (thickness of stiffener). At this point the stiffener breaks. Now the skin crack, which remained stationary while the stiffener crack was propagating, begins to grow again. Its growth is now quite rapid, since the stress field is magnified by the broken stiffener.

For the integrally stiffened cases, there is no problem with crack growth sequence because we are dealing with continuous structure. The corner crack is assumed to grow radially until  $a = t$ , and then a as thru-the-thickness crack. As mentioned in Section 4.3.6 the thru-crack, upon reaching the integral stiffener, also grows "radially"; that is, at equal rates in all directions, along the skin and up the integral stiffener.

On the basis of the above assumptions, crack growth periods for non-inspectable areas are calculated. The results of these calculations are given in Figures 5-17 and 5-18 for an initial crack size of  $a_o = 0.05$  inch. The calculations consist of adding the growth periods for all phases of the growth sequence. For example, consider zee-stiffened titanium structure at a maximum design tension stress level of 60.4 ksi ( $S = 5.49$  ksi/g). Using Figure D-6 in Appendix D, an initial 0.05 inch corner crack in the skin at the fastener hole gives

$$N_1 = N(0.1) - N(0.05) = 3300 - 1650 = 1650 \text{ hours}$$

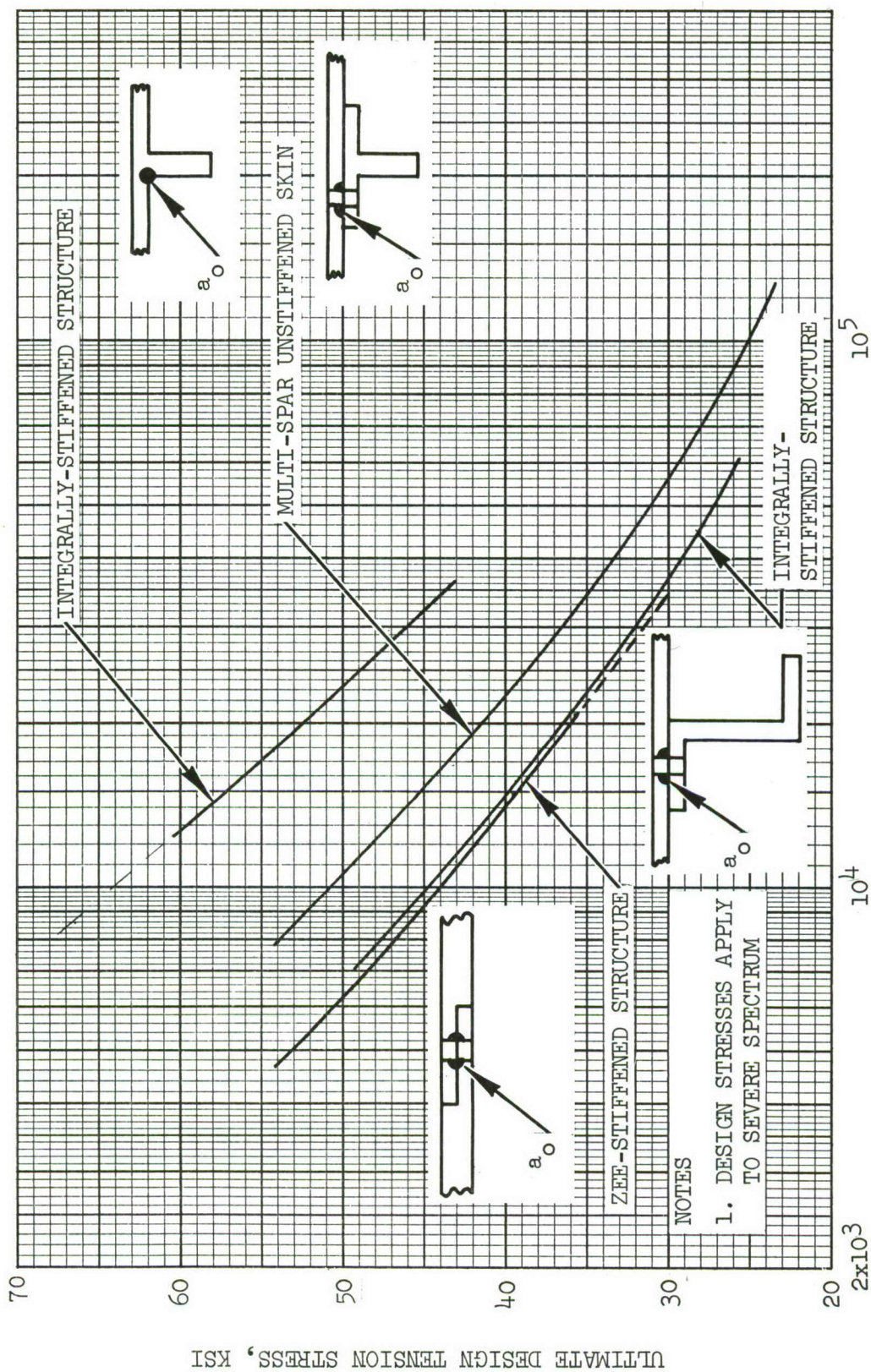
to grow until  $a = t = 0.1$  inch. The next growth period, the growth of a 0.05 inch double corner crack at the reinforcement, yields

$$N_2 = N(0.1) - N(0.05) = 3300 - 1650 = 1650 \text{ hours}$$

to grow through the reinforcement thickness. Finally, the growth of the skin crack adjacent to the broken zee-stiffener is, from Figure D-8 in Appendix D

$$N_3 = N(6.0) - N(0.100 + 0.125) = 200 \text{ hours}$$

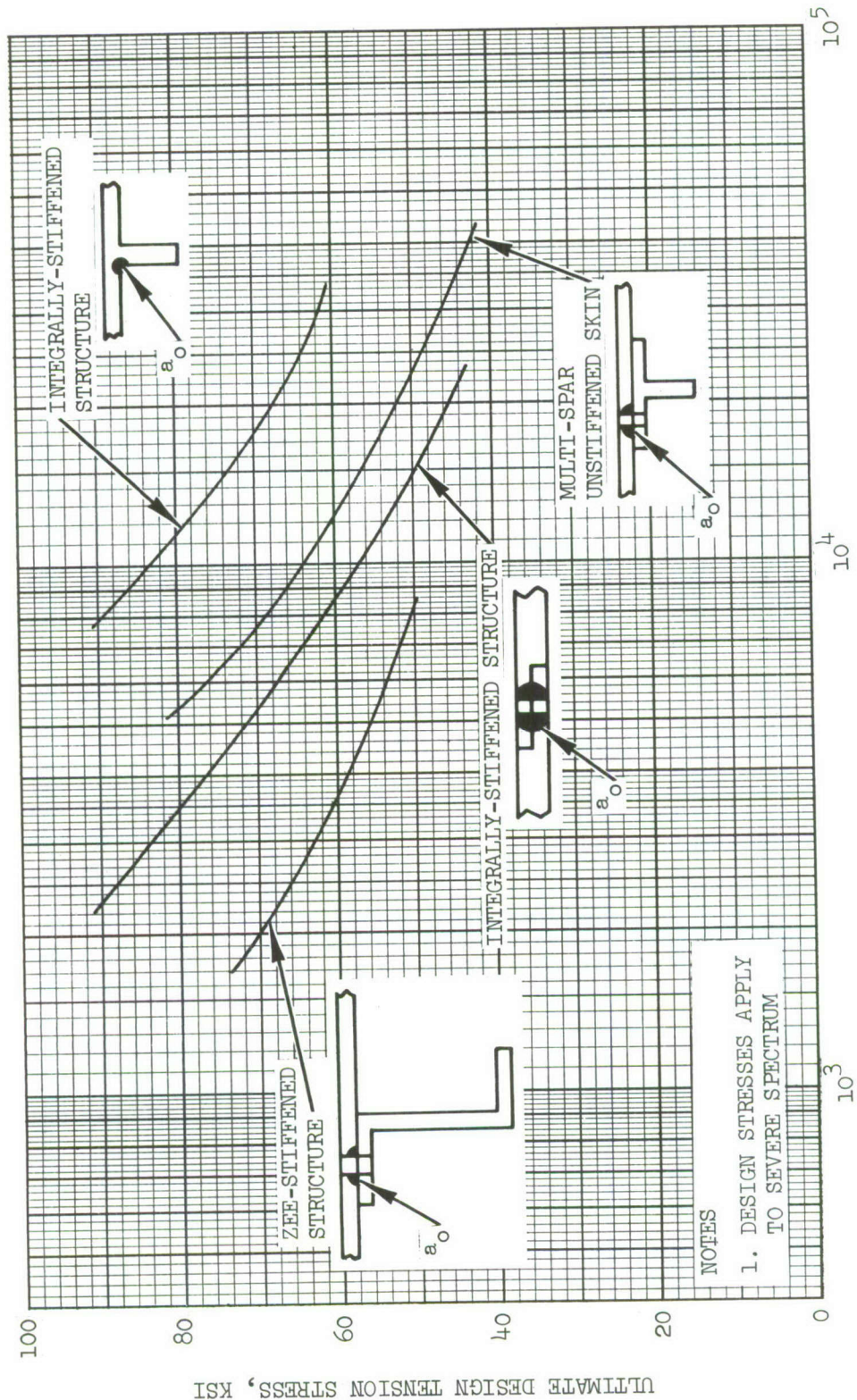
to grow from an effective half-length,  $a$ , of 0.225 inch (which includes the hole radius) to catastrophic failure. Then the total crack growth period for this



FLIGHT HOURS FROM  $a_o = 0.050$  IN. TO FAILURE

FIGURE 5-17. ULTIMATE DESIGN TENSION STRESS ALLOWABLES FOR ALUMINUM NON-INSPECTABLE STRUCTURE





FLIGHT HOURS FROM  $a_o = 0.050$  IN. TO FAILURE

FIGURE 5-18. ULTIMATE DESIGN TENSION STRESS ALLOWABLES FOR TITANIUM NON-INSPECTABLE STRUCTURE



stress level and initial crack size is

$$N (S = 60.4) = N_1 + N_2 + N_3 = 3500 \text{ hours}$$

which is a point on Figure 5-18.

The ultimate design tension stress allowables are summarized in Table 5-23 below.

TABLE 5-23 SUMMARY OF STRESS ALLOWABLES FOR NON-INSPECTABLE STRUCTURE

Material	Type of Structure	Ultimate Design Tension Stress Allowables, ksi	
		Severe Spectrum *	Composite Spectrum *
Aluminum	Zee-Stiffened Skin	46.8	58.0
	Integrally Stiffened Skin	47.7	59.1
	Unstiffened Skin	53.9	66.8
Titanium	Zee-Stiffened Skin	50.4	61.5
	Integrally Stiffened Skin	61.5	75.0
	Unstiffened Skin	69.0	84.2

\* Based on 8000 flight hours (2 lifetimes)

The values for the severe spectrum were obtained from Figures 5-17 and 5-18 for a service life of 8000 hours ( $S_1 = 2.0$  from Table 5-2). To obtain the values for the typical spectrum, the severe spectrum values are multiplied by 1.24 for aluminum and 1.22 for titanium as discussed on page 5-37.

#### NDI In-Service Inspectable Structure

The design criteria for this classification specify that an initial crack located at the most critical point should not grow to catastrophic failure in one inspection period.

For the zee-stiffened and ll-spar unstiffened structure, the most critical location of the initial flaw is a through-the-thickness crack at the edge of a fastener hole adjacent to a broken zee-stiffener or spar, respectively; see Figures D-7, D-8, D-13 and D-14 of Appendix D. For the integrally stiffened structure the most critical initial flaw is a thru-the-thickness crack under a partially broken integral stiffener, see Figures D-11 and D-12 of Appendix D.

Using the appropriate figures in Appendix D, maximum ultimate design tension stress level vs. crack growth period curves are plotted for each structure and for initial crack sizes of 0.25, 0.50, and 1.0 inch in Figures 5-19 thru 5-24.

The inspection interval in this case is a relatively short time. In addition, it is possible that any given aircraft may experience severe service usage over a period of one inspection interval. Therefore, the severe spectrum was considered applicable for the problem of determining IRAN inspection intervals, rather than the milder composite spectrum used for fatigue.

The ultimate design tension stresses for the NDI in-service inspectable structure are summarized in Table 5-24 for the applicable crack sizes and inspection intervals of 500 hours and 1000 hours. Except for the integrally stiffened structure, the initial crack size was taken to be  $(r + t_s)$ , where  $t_s$  is the skin thickness at butt line 45 from Tables 5-10, 5-13, 5-15, and 5-16. A one-inch crack was taken for the integrally stiffened skin structure since this case is more comparable to the other cases, i.e., approximately a 3 to 4-inch crack length.



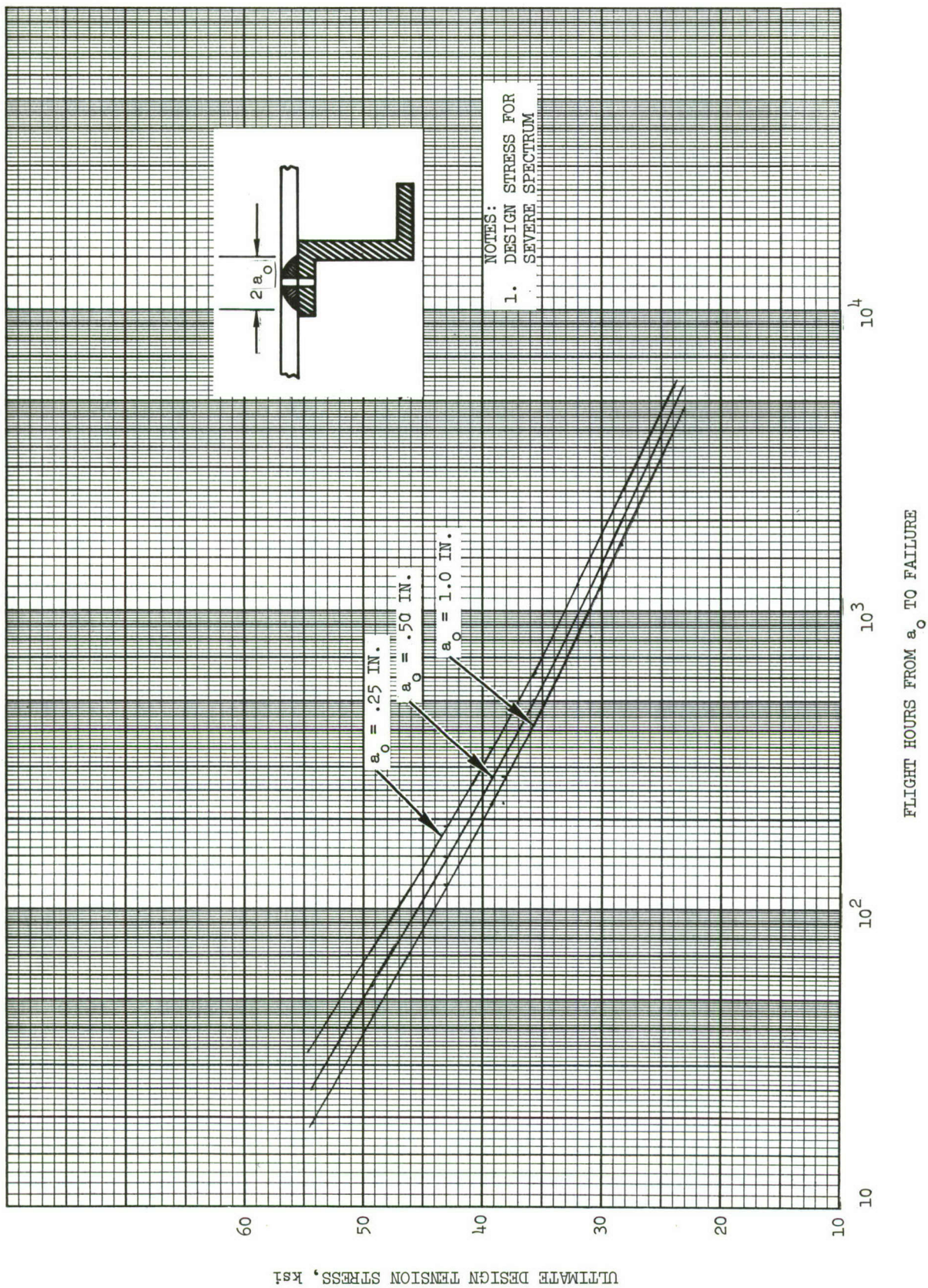


FIGURE 5-19 ULTIMATE DESIGN TENSION STRESS ALLOWABLES FOR A BROKEN ZEE-STIFFENER AND THRU-THICKNESS CRACK IN 7075-T76 ALUMINUM



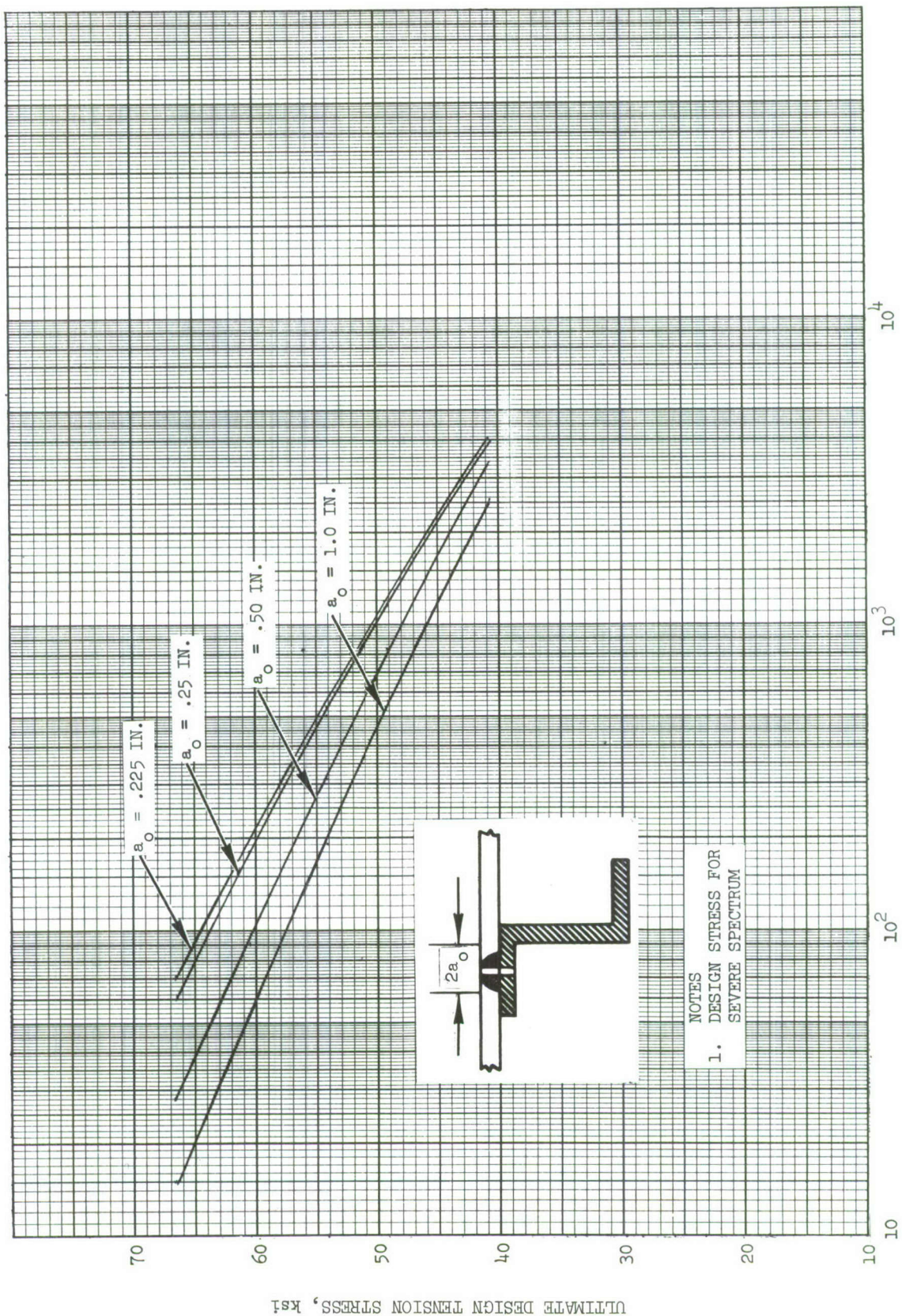


FIGURE 5-20 ULTIMATE DESIGN TENSION STRESS ALLOWABLES FOR A BROKEN ZEE-STIFFENER AND THRU-THICKNESS CRACK IN Ti-6AL-4V



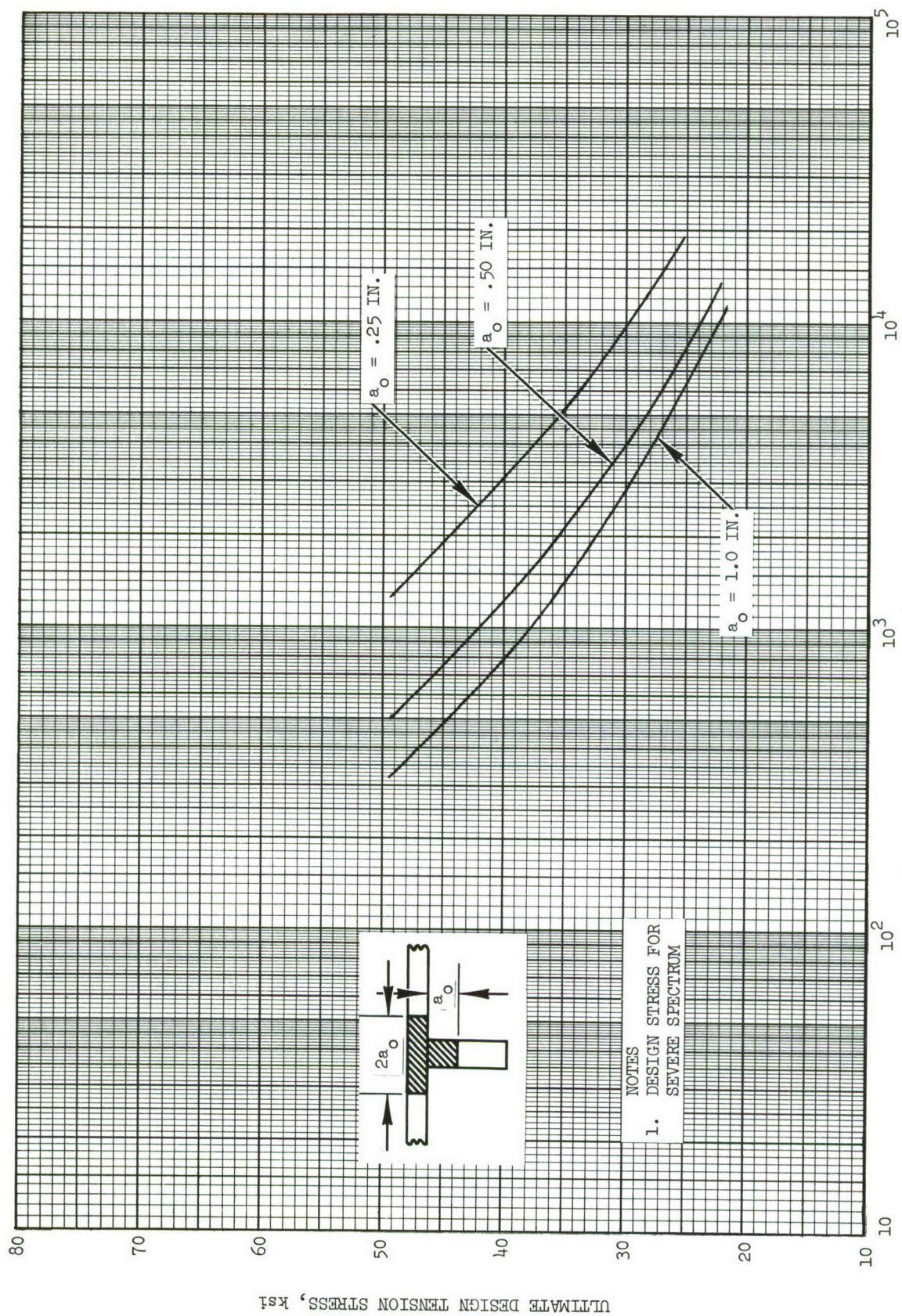


FIGURE 5-21 ULTIMATE DESIGN TENSION STRESS ALLOWABLES FOR A CRACKED RISER AND THRU-THICKNESS SKIN CRACK IN 7075-T76 ALUMINUM



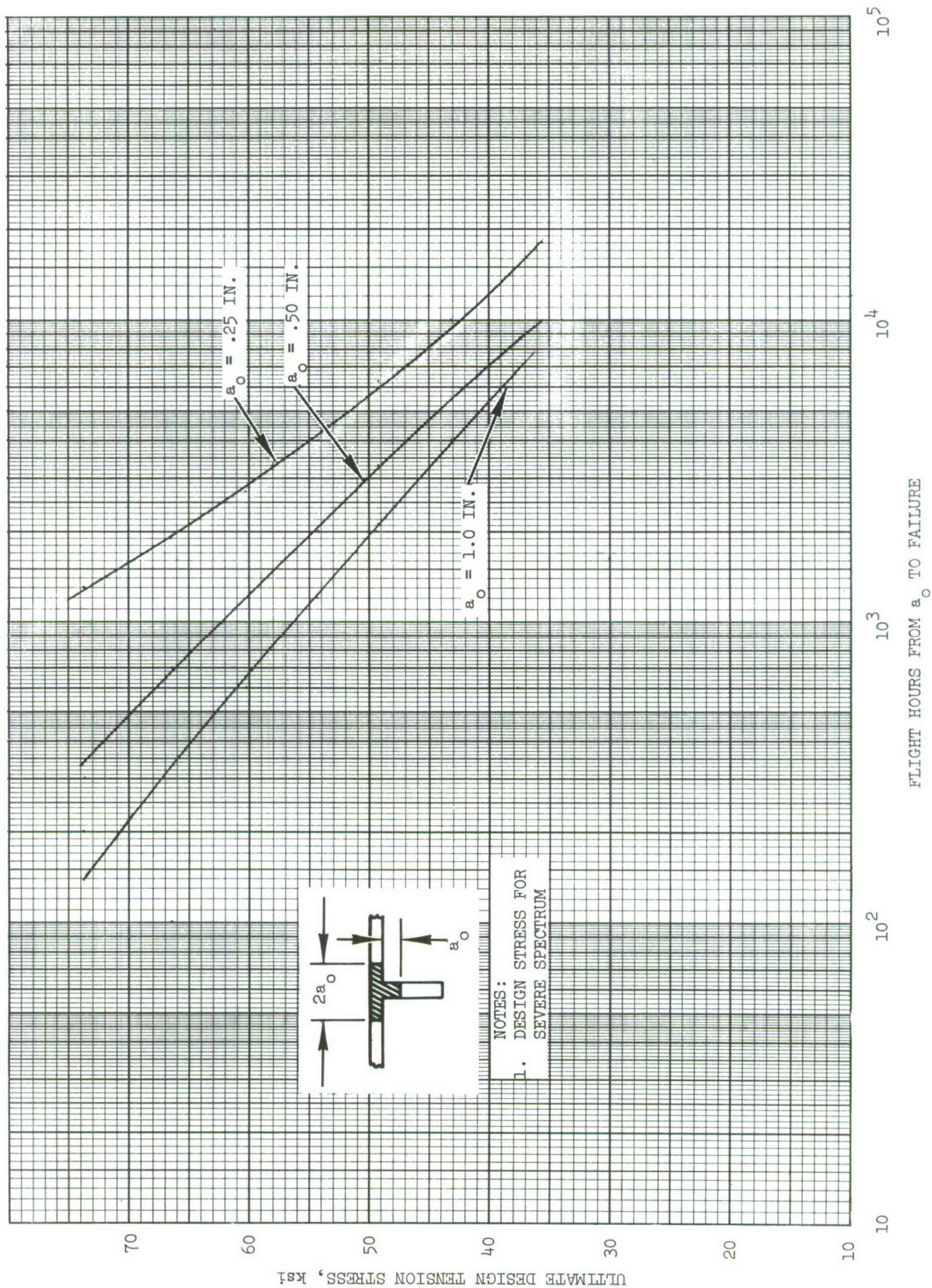


FIGURE 5-22 ULTIMATE DESIGN TENSION STRESS ALLOWABLES FOR A CRACKED RISER AND THRU-THICKNESS SKIN CRACK IN Ti 6AL-4V



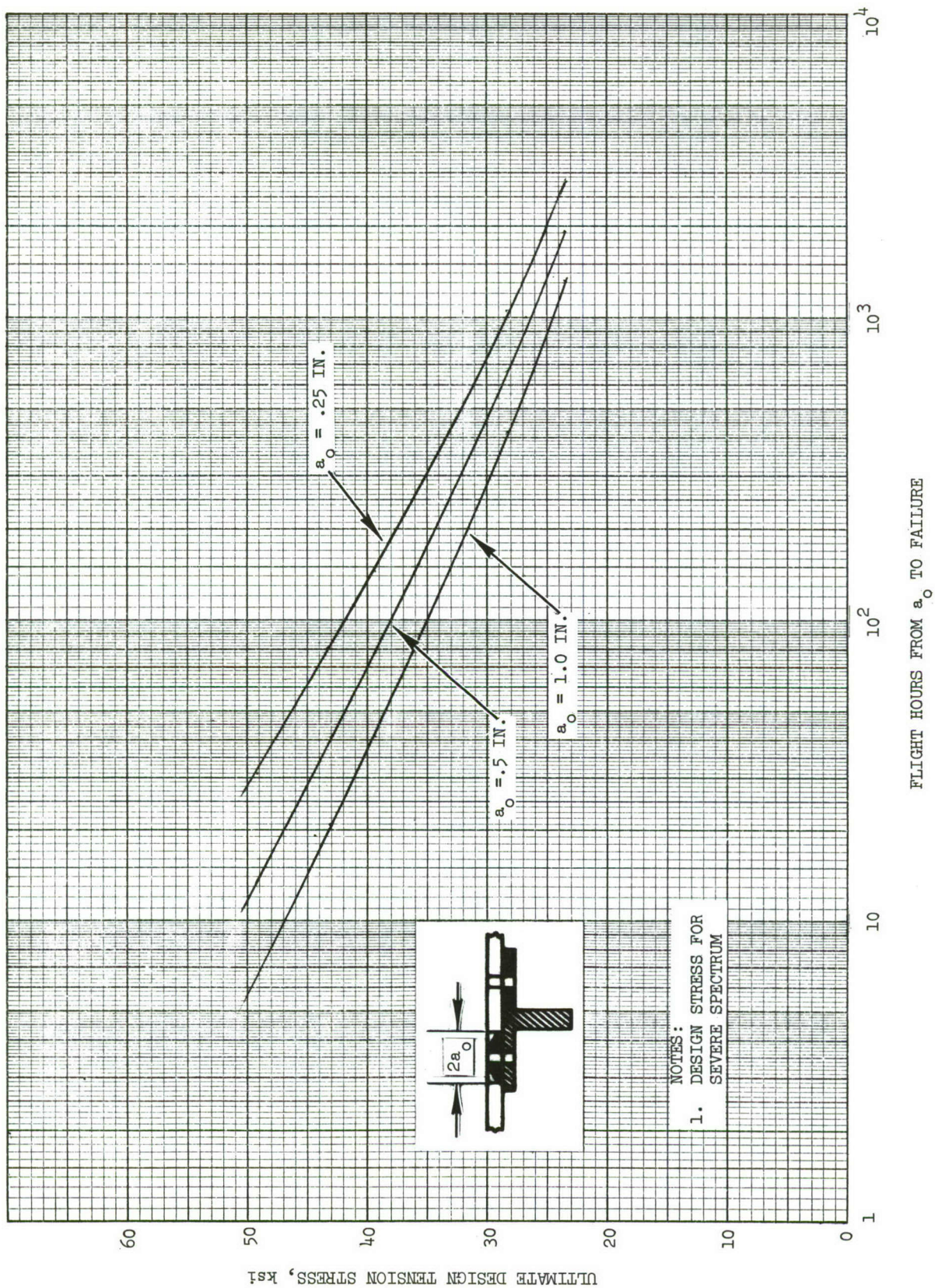


FIGURE 5-23 ULTIMATE DESIGN TENSION STRESS ALLOWABLES FOR A BROKEN SPAR CAP AND THRU-THICKNESS CRACK IN 7075-T76 ALUMINUM



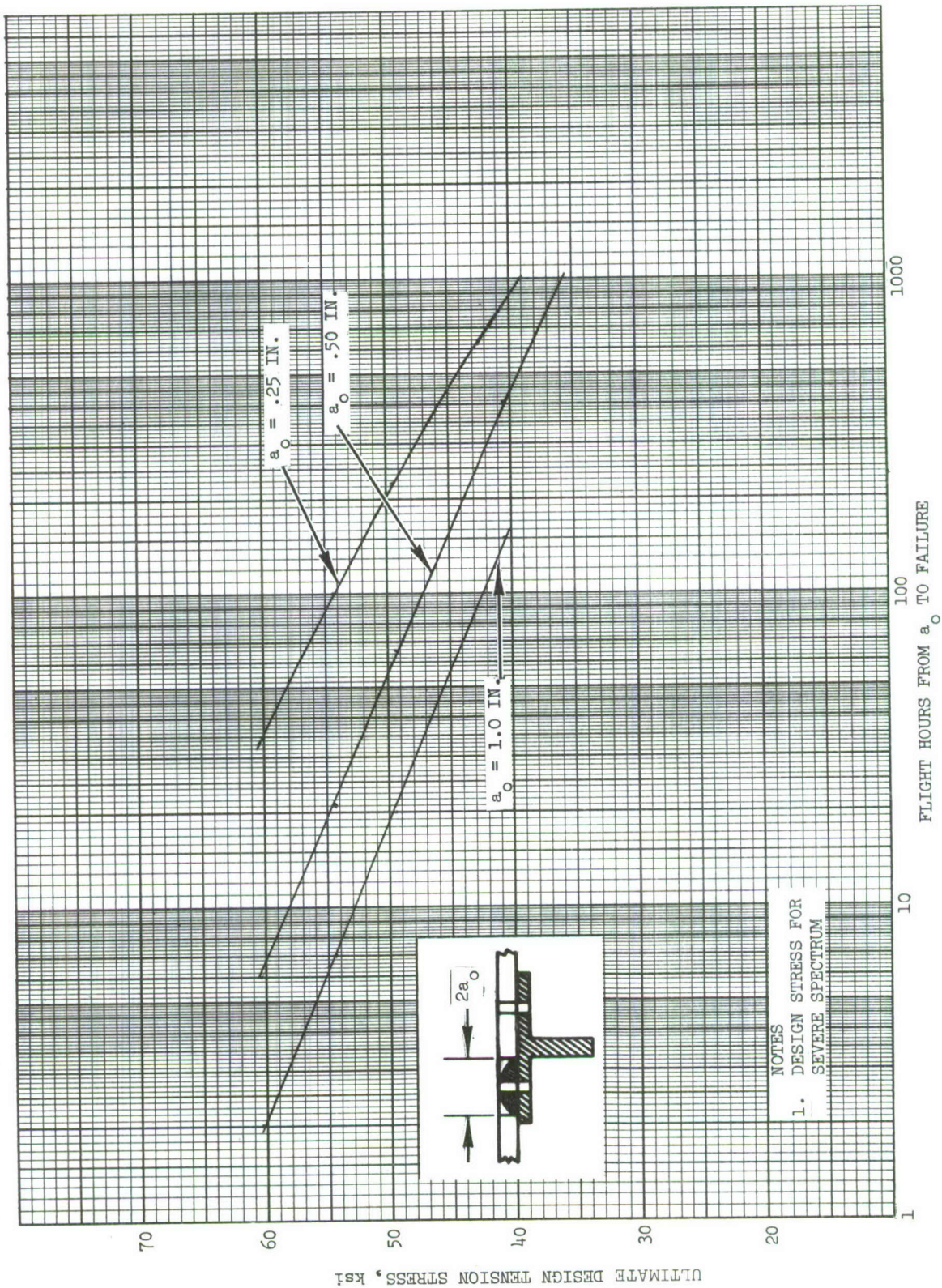


FIGURE 5-24 ULTIMATE DESIGN TENSION STRESS ALLOWABLES FOR A BROKEN SPAR CAP AND THRU-THICKNESS SKIN CRACK IN Ti-6AL-4V

TABLE 5-24      ULTIMATE DESIGN TENSION STRESS ALLOWABLES FOR NDI IN-SERVICE  
INSPECTABLE STRUCTURE

Type of Structure	Inspection Interval, Flight Hours	Ultimate Design Stress Allowables, psi	
		7075-T76 Aluminum	Ti-6Al-4V
Zee-Stiffened	1000	32,500 for $a_o = .365$ in.	50,500 for $a_o = .225$ in.
	500	36,300 for $a_o = .365$ in.	54,900 for $a_o = .225$ in.
Integrally Stiffened	1000	38,000 for $a_o = 1.0$ in.	56,200 for $a_o = 1.0$ in.
	500	44,500 for $a_o = 1.0$ in.	62,800 for $a_o = 1.0$ in.
Multi-Spar Unstiffened	1000	26,700 for $a_o = .425$ in.	38,000 for $a_o = .345$ in.
	500	30,200 for $a_o = .425$ in.	42,300 for $a_o = .345$ in.



### Walk-Around Inspectable Structure

No direct life requirement is placed upon a structure containing a damage of the size that would be found in a walk-around inspection. As shown in Section 3.3, any direct life calculation is unreliable due to the many uncertainties in the analysis, particularly those introduced by the large effect of variations in stresses. The residual strength requirement indirectly results in an assurance of survival for some number of flights, since a structure capable of sustaining one extremely high load in residual strength would be capable of sustaining several slightly less severe load cycles in low cycle fatigue crack growth.

#### 5.5.3 Residual Strength Analysis

Appendix F describes a residual strength analysis approach using crack growth resistance curves. That type of material property information was not available for this application study. It is possible, however, to use a fracture mechanics based analysis using  $K_c$  values to predict the residual strength of reinforced structure. As indicated in Appendix F a reasonable failure prediction using the local minimum applied K value ( $K_m$  in Figure F-6) can be made by equating it to the wide panel  $K_c$  value. The necessary stress intensity analyses are described in Section 4. For all cases which were considered, this approach was within 10% of the residual strength allowable determined by the methods of analysis described in Section 4.6.

Residual strength analyses were performed using the methods of analysis described in Section 4.6. The analyses for various types of assumed damage are discussed below.

##### 1. A Broken Reinforcing Member and a Skin Crack to Adjacent Intact Stiffeners

The method of analysis described in Section 4.6 is used to calculate the residual strength for this damage case. The section properties used for the analysis are taken from the appropriate tables in Section 5.4. The calculation procedure for this case can be summarized as follows:

- a) The stress in the cracked skin without the effect of the reinforcement is

$$F' = \frac{0.80 K_c}{\sqrt{W'}} \quad (5-7)$$

- b) The effective area of the reinforcement

- o For zee-stiffeners and spar caps

$$A_e = \frac{A}{[1 + (y/\rho)^2]} \quad (5-8)$$

- o For integral stiffeners the effective area,  $A_e$ , is taken to be 1/5 of the cross-sectional area. Because the crack will progress up the riser while it is growing across the skin, the effective area is assumed to be similar to that used for fuselage frames with cut-outs for stringers.
- o The spar caps for the multi-spar unstiffened skin are assumed to be extruded tee-sections, two inches on the skin side and an outstanding leg one inch long with a thickness all around of 0.50 inch for both the aluminum and titanium structure.

- c) The lumped stiffening parameter is determined from

$$\Sigma \frac{\bar{A}_e}{t} = \frac{2A_e}{t} \quad (5-9)$$

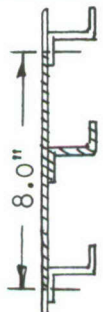
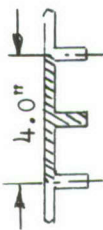
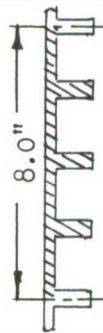
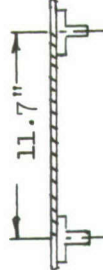
- d) The structural efficiency  $\gamma$  of the reinforcement is calculated from Figure 4-23.

- e) The residual strength is then calculated from the following equation:

$$F_g = \gamma F' \quad (F-10)$$

The results of these calculations are summarized in Table 5-25. For the integrally stiffened structure two sizes of damage are assumed, a 4-inch skin crack with one riser broken and an 8-inch skin crack with three risers broken.

TABLE 5-25 SUMMARY OF RESIDUAL STRENGTH CALCULATIONS FOR SKIN CRACKS BETWEEN EFFECTIVE REINFORCEMENTS

Assumed Damage *	Item								
		Aluminum	Titanium	Aluminum	Titanium	Aluminum	Titanium	Aluminum	Titanium
Skin Thickness, inches $K_c$ , ksi/inch $W'$ , inches $F'$ , ksi (without reinforcements)		0.24	0.10	0.15	0.08	0.15	0.08	0.30	0.22
		75.7	208	82.5	193	82.5	193	72	208.5
		8.0	8.0	4.0	4.0	8.0	8.0	11.7	11.7
		21.4	58.8	33.0	74.2	23.3	54.6	16.8	48.8
<u>Stiffener Section Properties</u> Area, in. <sup>2</sup> $\rho$ , inches $I$ , in. <sup>4</sup> $Y$ , inches $A_e$ , in. <sup>2</sup> $\Sigma \bar{A}_e/t$									
		0.70	0.305	0.560	0.341	0.560	0.341	1.5	1.5
		0.569	0.498	-	-	-	-	0.408	0.408
		0.2265	0.0758	-	-	-	-	0.25	0.25
		0.75	0.625	-	-	-	-	0.50	0.50
		0.212	0.118	0.112	0.0681	0.112	0.0681	0.600	0.600
		1.765	2.37	1.49	1.70	1.49	1.70	4.0	5.45
		1.37	1.327	1.235	1.25	1.30	1.325	1.57	1.637
$F_g$ , ksi (with Reinforcements)		29.4	81.2	40.7	92.7	30.3	72.3	26.4	79.8

\* Damage indicated by cross-hatched areas in sketches



## 2. Residual Strength for Skin Cracks - Crack Tips Not in the Vicinity of Reinforcements

For this damage case, the residual strength is solely determined by the fracture toughness properties of the material. Broken reinforcements across the cracked area will tend to increase the stress intensity somewhat at the crack tip; however, this is not taken into account in this analysis. The residual strength is calculated simply by the following equation:

$$F' = \frac{0.8 K_c}{\sqrt{W'}} = \frac{0.8 K_c}{\sqrt{2a_o}} \quad (5-11)$$

The B-basis  $K_c$  values which are used for predicting the residual strength are obtained from Figures 5-6 and 5-7. The results of the residual strength analysis are summarized in Table 5-26.

## 3. One Plank Broken

To meet the walk-around inspectable criteria, a 8-inch skin crack is assumed to occur anywhere in the skin surface. The most critical location is where the skin crack is centered over a reinforcing member, i.e., a riser, zee-stiffener or spar cap. For the zee-stiffened and integrally-stiffened structures, risers or stiffeners are spaced such that the tips of an 8-inch crack are centered over a riser or zee-stiffener. Therefore, the reinforcement is considered effective in determining the residual strength for these two classes of structure. However, for a 8-inch crack centered over a spar cap, there is no effective reinforcement at the crack tip. In this case, the residual strength is based solely on the fracture toughness properties of the skin material, unless a skin splice is placed midway between spar caps. Therefore, for the multi-spar structure, a multi-plank skin construction was considered with the skin splices spaced midway between spar caps, i. e., 11.7 inch wide skin planks.

The residual strength of a multi-plank structure can be determined once a joint has been designed. For this analysis it is assumed that the following fastener systems are used; one row of 1/4-inch diameter steel Hi-Loks with a shear strength of 4650 lbs. for the aluminum structure and two rows of the same

TABLE 5-26 SUMMARY OF RESIDUAL STRENGTH CALCULATIONS FOR 8-INCH  
SKIN CRACK NOT INFLUENCED BY REINFORCEMENTS

ITEM	Zee Stiffened Skin		Integrally Stiffened Skin		Multi-Spar Unstiffened Skin	
	Aluminum	Titanium	Aluminum	Titanium	Aluminum	Titanium
Skin Thickness, inches	0.24	0.10	0.15	0.08	0.30	0.22
B-Basis $K_c$ , Ksi $\sqrt{\text{inch}}$	53	146	57.8	135	50	146
$W'$ , inches	8.0	8.0	8.0	8.0	8.0	8.0
$\sqrt{W'}$ , $\sqrt{\text{inches}}$	2.83	2.83	2.83	2.83	2.83	2.83
$F'$ , ksi	15	41.1	16.3	38.2	14.5	41.3

fasteners for the titanium structure. A fastener spacing of four diameters is used for both designs. For these assumed joint designs, the residual strength is calculated using the following procedure (based on the analysis given in Section 4.6.1):

- (1) Assume values for the applied stress,  $f_g$ .
- (2) Calculate the effective length,  $L_t$ , required for the attachments to transfer the load from the broken plank to the adjoining planks from

$$L_t = \frac{f_g A_{cut} S}{2 P_A} \quad (5-12)$$

- (3) For the aluminum material enter Figure 4-19 and determine the effective width,  $W_e$ , using the curve for 7075-T6 material. This curve is probably conservative for 7075-T76 material since the lower strength 2024-T3 aluminum alloy curve is above the curve for 7075-T6 in Figure 4-19. For titanium assume  $W_e = L_t/3$ . As shown in Figure 4-19, the material curves for 2024-T3 and 7075-T6 become asymptotic to the  $W_e = L_t/3$  curve which is independent of the material properties. This should yield conservative results for the titanium structure also.

- (4) Calculate  $\beta = \frac{2 W_e}{W} = \frac{2 W_e}{n W_m}$

For both titanium and aluminum multi-spar unstiffened skin structures  $n = 10$ .

- (5) Enter Figure 4-20 with  $\beta$  and  $n = 10$  to determine  $F_g/F_{tu}$ .
- (6) Calculate the allowable gross area stress where  $F_{tu} = 69$  ksi for 7075-T76 and 130 ksi for Ti-6Al-4V.
- (7) Repeat the above calculation procedure until a solution is obtained that gives  $f_g = F_g$ . This will give the allowable stress that yields a margin of safety of zero.



Following the above analysis procedure gives allowable stresses of 36,000 psi for 7075-T76 aluminum structure and 50,000 psi for Ti-6Al-4V structure. The allowable stress for the titanium is based on an effective width of 3.67 inches. As shown in Figure 4-19 the effective widths for both 2024-T3 and 7075-T6 are significantly higher than the  $W_e = L_t/3$  curve for  $L_t$  values of 11 inches.

To determine the ultimate design tension stress allowables, the allowable stresses obtained by the above analyses must be related to the appropriate design load. Except for the broken plank case, the ultimate design tension stress allowables are obtained by relating the stress levels in Tables 5-25 and 5-26 to the once-per-700 flight load. This load occurs once per 455 flight hours or 2.2 times per 1000 flight hours for the 39-minute flights. From Figure 5-3, this load level corresponds to  $N_Z = 7.8$  g which is approximately 106 percent limit load. The ultimate design tension stress allowables were then obtained by multiplying the  $F_g$  stresses in Table 5-25 and the  $F'$  stresses in Table 5-26 by  $150/106 = 1.415$  and are summarized in Table 5-27 for various types of assumed damage.

For the broken plank case a factor was applied to the loads to account for the dynamic effect of suddenly breaking a plank, as discussed in Section 3.2.2. There presently is no theoretical analysis available to account for dynamic effects of a propagating crack arresting at a reinforcement. The factor developed for the broken plank case is not applicable for crack arrest situations, and therefore was not applied to the above cases. In general, cracks will grow gradually under fatigue loads, and therefore no dynamic effect would occur. However, in the event the damage is induced suddenly, as for example battle damage, some dynamic effect may occur. To account for this, tests should be conducted on the structure by suddenly cutting the structure while the structure is subjected to load. Tests of this kind conducted in the past on aluminum shell structure indicates that the decrease in failure load due to dynamic effects is small. (References 5-17 and 5-18).

For the broken plank case, it is assumed that the entire cut load goes into the two adjacent planks; then the redistributed load in these planks is approximately 50 percent of the original load in the broken plank. Inclusion of the 10 percent dynamic factor gives an effective redistributed load of  $[100 + 50 + 0.150(50)]/150 = 1.033$ . Therefore, for the broken plank case, the ultimate design tension

stresses were obtained by multiplying the stresses given on page 5-63 by  $1.50/1.033 \times 1.06 = 1.37$ . The resulting ultimate design tension stress allowables are summarized in Table 5-27.

The design stress allowable for the multi-spar unstiffened skin structure given in Table 5-27 depends on whether the skin surface is planked or monolithic. If the skin structure is monolithic, then the allowables are 20,500 psi for the aluminum structure and 58,400 psi for the titanium structure. If the skins are planked, so that the splices occur midway between spar caps, then the design stress allowables could be increased to 37,400 psi for the aluminum structure and 68,500 psi for the titanium structure. In this case the structure would be good for a 11.7 inch broken plank centered over a broken spar cap and a 11.7 inch crack between spar caps. Therefore, the final design stress allowables for multi-spar unstiffened skin structure are 37,400 psi for the aluminum structure and 68,500 psi for the titanium structure.

#### 5.5.4 Environmental Effects

The effect of environment on crack propagation has been considered in the two ways discussed in Section 4.5.

All of the life calculations for fatigue crack propagation utilized fatigue crack propagation data representative of ambient laboratory air conditions. This probably represents the level of detrimental environment a fighter would encounter. Had this application been real (rather than a study) more information would have been available on anticipated environments and data could be generated for the exact condition desired. The use of higher humidity data would have been more conservative, but it was not available.

The values of the stresses required to produce a stress intensity factor greater than  $K_{Isc}$  for the damage sizes used in the life calculations were computed. These are summarized for each damage size, material and structural configuration in Table 5-28. In all cases these stresses are above the flight one-g stress level (one-g ground stress is compressive). It is therefore concluded that environmental crack growth due to sustained loads is not significant for the configurations and materials under consideration.



TABLE 5-27 ULTIMATE DESIGN TENSION STRESS ALLOWABLES FOR WALK-AROUND INSPECTABLE DAMAGE



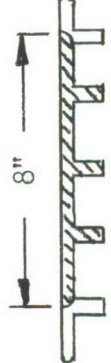
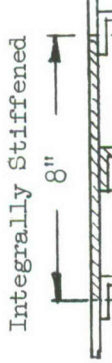
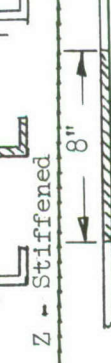
Type of Structure  Assumed Damage	Ultimate Design Tension Stress, psi					
	Aluminum Structure			Titanium Structure		
	Z-Stiffened Skin	Integrally Stiffened Skin	Multi-Spar Unstiffened Skin	Z-Stiffened Skin	Integrally Stiffened Skin	Multi-Spar Unstiffened Skin
One out of 10 planks broken plus a broken spar cap. 	49,300	49,300	49,300	>68,500	>68,500	>68,500
 Multi-Spar  Integrally Stiffened  Z-Stiffened  Multi-Spar	41,600	42,900	37,400	115,000	102,000	113,000
			20,500			58,400



TABLE 5-28 SUMMARY OF SUSTAINED LOAD CALCULATIONS

Material	Structure	Thick. in.	Durability	Non-inspectable	NDI In-service Inspectable (Equivalent of a 3-in. crack)				
			$\frac{\alpha}{\sqrt{\text{in.}}}$	$K_{\text{Iscc}}/\alpha$ ksi	$\frac{\alpha}{\sqrt{\text{in.}}}$	$K_{\text{Iscc}}/\alpha$ ksi	$\lambda$	$\frac{\alpha}{\sqrt{\text{in.}}}$	$K_{\text{Iscc}}/\alpha$ ksi
Aluminum $K_{\text{Ic}} = 26.5$ $= K_{\text{Iscc}}$	Zee Stiff.	0.24	0.442	60.0	0.677	39.1	2.4	2.6	10.2
	Int. Stiff.	0.15	↓	↓	↓	↓	1.7	3.0	8.8
	Multi-Spar	0.30	0.442	60.0	0.677	39.1	2.3	2.65	10.
Titanium $K_{\text{Ic}} = 63.5$ $K_{\text{Iscc}} = 28.5$	Zee Stiff.	0.10	0.627	45.5	0.677	42.0	2.5	2.1	13.5
	Int. Stiff.	0.06	0.627	45.5	↓	↓	1.7	3.0	9.5
	Multi-Spar	0.22	0.442	64.5	0.677	42.0	2.55	2.65	10.

① Equation (5-1) if  $t > a$  and Equation (5-3) if  $t < a$ .

② Equation (5-2)

③ Section 4.3.6

④  $\alpha = \lambda \sqrt{\pi a}$

#### 5.5.5 Summary of Design Stress Allowables

The ultimate design tension stress allowables obtained in Section 5.4 and 5.5 above are summarized in Table 5-29. Each design must meet the static, fatigue and durability requirements and one of the structural integrity requirements. The design stress allowable that meets these minimum requirements is indicated by an asterisk. The fatigue requirement sizes the aluminum structure and the static and durability requirement sizes the titanium structures. None of the structures are sized by the structural integrity requirements. This is no doubt due to the fact that both materials used for the example design have good fracture toughness and crack growth properties.

TABLE 5-29 SUMMARY OF ULTIMATE DESIGN TENSION STRESS ALLOWABLES TO MEET VARIOUS DESIGN CRITERIA

Maximum Ultimate Design Tension Stress Allowables at Lower Wing Surface at Butt Line 45 in ksi								
Material	Type of Structure	Structural Integrity Requirements						
		Static	Fatigue	Durability	Non-In-spectable	NDI In-Service Inspection Interval		Walk-Around Inspectable
						500 hours	1000 hour	
Aluminum	Zee-Stiffened Skin	65.0	44.5*	63.6	58.0	36.3	32.5	41.6
	Integrally Stiffened Skin	54.0	44.5*	57.0	59.1	44.5	38.0	42.9
	Unstiffened Skin	45.0	44.5*	65.1	66.8	30.2	26.7	37.4
Titanium	Zee-Stiffened Skin	92.0	98.0	72.2*	61.5	54.9	50.5	115
	Integrally Stiffened Skin	71.0*	98.0	72.2	75.0	62.8	56.2	102
	Unstiffened Skin	52.4*	98.0	84.8	84.2	42.3	38.0	68.5

\* Maximum design stress levels that meet all requirements



## 5.6 STRUCTURAL WEIGHT COMPARISON

This section presents the estimated baseline wing weights for the various structural concepts and materials analyzed. The baseline weights reflect design sizing of the wing structure considering both ultimate strength and fatigue allowable stresses. The optimum weight of the surfaces and spars are calculated from the thicknesses and areas in Section 5.4. Statistically derived factors account for non-optimum items such as joints and fasteners, control surfaces, etc. These non-optimum weight increments are essentially the same as for the initial weight estimate presented in Section 5.2.

Table 5-30 presents wing weights based on the ultimate strength design sizing alone for Ti-6Al-4V annealed and D6AC (220 ksi) steel. In titanium, the 11-spar unstiffened skin wing concept is the heaviest, 7740 lbs., with an allowable lower surface stress of 52,400 psi. The 3-spar zee-stiffened skin concept is the lightest, 6080 lbs., with an allowable stress of 92,000 psi. The 3-spar integrally stiffened skin weighs 6,627 lbs., with an allowable stress of 72,000 psi.

The weights for the aluminum concepts are summarized in Table 5-31 which also shows the impact of fatigue on the design weights. The lower surfaces for the zee and the integrally stiffened concepts were resized to reflect a fatigue allowable stress of 44,500 psi. The aluminum 11-spar unstiffened skin is again the heaviest concept, 6713 lbs., with an allowable stress of 45,000 psi. The lightest concept is the 3-spar integrally-stiffened structure, 5864 lbs., after resizing for fatigue. The 3-spar zee-stiffened wing weighs 5990 lbs.

Figure 5-25 illustrates the lower surface wing weight variation as a function of the allowable lower surface stress. The point analysis data from Tables 5-30 and 5-31 are represented by the circles. The remaining weight trends are obtained by ratioing the stress levels and surface weights for each spanwise section.

The lower surface weights required to meet the various design criteria are summarized in Table 5-32. The wing weights were obtained from Figure 5-25 for the various design stress levels given in Table 5-29. No weights were calculated if the design stresses were considerably over the static design stress allowables.

TABLE 5-30 BASELINE TITANIUM AND STEEL ESTIMATED WING WEIGHTS

Item	Ti 6Al-4V, Ann. (1) (2)				D6AC STEEL (1)		
	11-Spar Unstiffened	3-Spar Zee- Stiffened	3-Spar Integrally Stiffened	3-Spar Integrally Stiffened	11-Spar Unstiffened	3-Spar Zee Stiffened	3-Spar Integrally Stiffened
Upper Surfaces (Incl. Joints)	2401	1533	1795	1795	3143	2255	2381
Lower Surfaces	2192	1338	1623	1623	2826	1965	2051
Beam Caps	(incl.in, surf.)	206	206	206	(incl.in, surf.)	268	268
Beam Webs	1327	508	508	508	2160	768	768
Ribs	None	675	675	675	None	940	940
Leading & Trailing Edges	450	450	450	450	450	450	450
Fairings & Access Doors	300	300	300	300	300	300	300
Ailerons	170	170	170	170	170	170	170
Leading & Trailing Edge Flaps	800	800	800	800	800	800	800
Spoilers	100	100	100	100	100	100	100
Total Wing Weight (lbs.)	7740	6080	6627	6627	9949	8016	8228

(1) Sized for ultimate strength

(2) No resizing required to meet fatigue requirements

TABLE 5-31 BASELINE ALUMINUM ESTIMATED WING WEIGHTS

Item	Al 7075-T76 (1)			Al 7075-T76 (2)		
	11-Spar Unstiffened	3-Spar Zee- Stiffened	3-Spar Integrally Stiffened	3-Spar Zee- Stiffened	3-Spar Integrally Stiffened	
Upper Surfaces (Incl. Joints)	2073	1381	1507	1381 (2)	1507 (2)	
Lower Surfaces	1817	1240	1375	1564	1564	
Beam Caps	(incl. in. surf.)	160	160	160	160	
Beam Webs	1003	354	354	354	354	
Ribs	None	585	585	585	585	
Leading & Trailing Edges	450					
Fairings & Access Doors	300					
Ailerons	170	1820			1820	
Leading & Trailing Edge Flaps	800					
Spoilers	100					
Total Wing Weight (Lbs.)	6713	5540	5801	5864	5990	

(1) Sized for ultimate strength alone.

(2) Resized to include effect of a fatigue allowable stress of 44,500 psi.



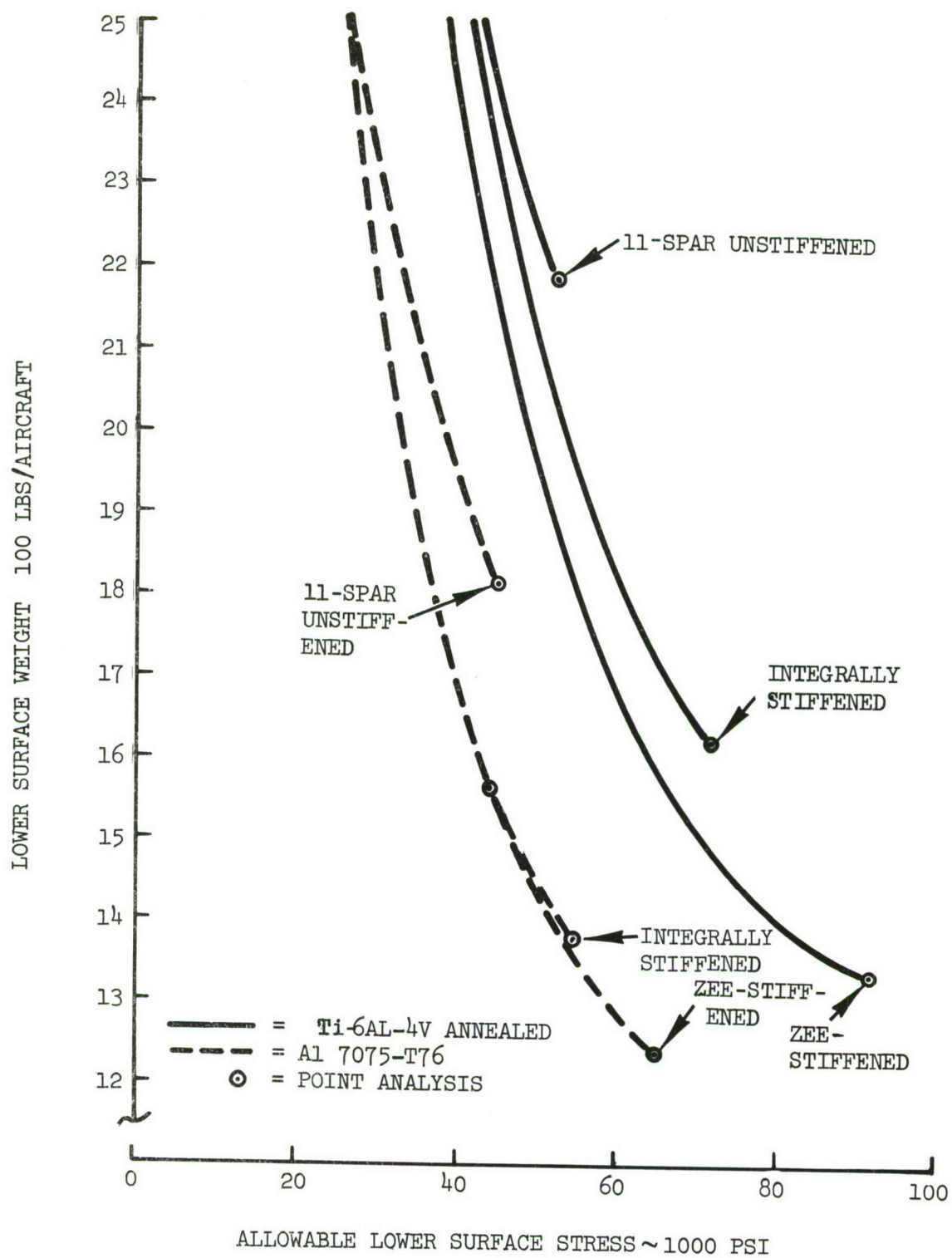


FIGURE 5-25 LOWER SURFACE WING WEIGHT VARIATIONS

TABLE 5-32 SUMMARY OF LOWER SURFACE WING WEIGHTS TO MEET VARIOUS CRITERIA

Lower Wing Surface Weight to Meet Various Design Criteria (Ref. Table 5-29), lbs.								
Material	Type of Structure	Structural Integrity Requirements						
		Static	Fatigue	Durability	Non-In-spectable	NDI In-Service Inspection Interval		Walk-Around Inspectable
						500 hours	1000 hours	
Aluminum	Zee-Stiffened Skin	1240	1564*	1255	1310	1850	2040	1650
	Integrally Stiffened Skin	1375	1564*	1325	1300	1564	1775	1610
	Unstiffened Skin	1817	1830*	①	①	2335	2500	2060
Titanium	Zee-Stiffened Skin	1338	①	1480*	1655	1825	1955	①
	Integrally Stiffened Skin	1623*	①	1615	1590	1775	1930	①
	Unstiffened Skin	2192 *	①	①	①	2530	2770	①

\* Weights that meet all requirements

(1) Weights less than required for static strength

The minimum weight lower surface that meet all the design criteria is the titanium zee-stiffened skin structure at 1480 lbs. The next lightest designs, the integrally stiffened and zee-stiffened aluminum skin structure, are 5.7 percent heavier. The other three designs considered were 9.7, 24, and 49 percent heavier than the lightest design. The weight impact of the various design criteria is discussed in Section 5.7.



## 5.7 EVALUATION

### 5.7.1 Durability Requirement

All the structures must meet the durability criteria, i.e., an initial crack  $a_o = 0.125$  inch shall not grow to a critical size in 8000 hours (2 service lives) for the average usage. The ultimate design tension stress allowables and wing lower surface weights to meet the durability requirement are summarized in Tables 5-29 and 5-32, respectively. For the aluminum structures the design stress allowables are all above the fatigue ultimate tension stress allowable of 44.5 ksi. This indicates that the capabilities of current production inspection techniques, as summarized in Section 3.2.3, are satisfactory for this material and application. A larger stress (weight) impact could be expected for some other aluminum alloys whose crack propagation properties and fracture toughness are not as good as those for 7075-T76 material.

The design allowable stress to meet the durability requirement for the titanium integrally stiffened and unstiffened skin structures are above the static design stress allowables (see Table 5-29).

For zee-stiffened titanium structure, the durability requirement reduces the design stress level from 92 ksi (static and fatigue considerations) to 72.2 ksi. This is about a 21 percent reduction in stress and an 11 percent weight penalty as shown in Table 5-32. In this case it might be cost effective to improve the inspection capabilities and demonstrate that initial flaws smaller than the  $a_o = 0.125$  inch can be found with a high degree of reliability provided the higher stresses also meet the structural integrity requirements discussed below.

### 5.7.2 Structural Integrity Requirements

To meet the recommended criteria, the structure must be designed for one of the three inspectability classifications, i.e., walk-around inspectable, non-inspectable, or NDI in-service inspectable structure. A discussion of the stress and weight impact for each of these three classifications follows:

### Walk-Around Inspectable Structure

The zee-stiffened and integrally stiffened aluminum structure can meet the walk-around inspectable criterion with slight reductions in the 44,500 psi ultimate design stress levels, 6.5 percent and 3.6 percent respectively. This corresponds to weight penalties of 5.5 percent and 2.9 percent. The aluminum multi-spar unstiffened skin structure would require a 16 percent reduction in stress level and 12.5 percent weight penalty.

All the titanium structures can meet this requirement without any weight penalty, since the allowable stresses are above those required to meet the static, fatigue and durability requirements.

### NDI In-Service Inspectable Structure

All the titanium and aluminum structures would have to pay a rather large weight penalty (between 13.5 percent and 36.5 percent) to meet these criteria for a 1000-hour inspection interval. The integrally stiffened aluminum structure is the only structure that meets the criteria without a weight penalty for a 500-hour inspection interval.

Since the selected design stress levels are all above the design stress level for NDI in-service inspection intervals greater than 500 hours, the IRAN inspections cannot be relied on as a means of preventing catastrophic failure. For this criterion to be weight competitive with the other structural integrity requirements, in-service inspection capabilities have to be demonstrated to be better than the data to date indicates, i.e., initial crack sizes considerably smaller than 3 to 4 inches can be detected with a high degree of confidence.

### Non-Inspectable Structure

Although the lower wing surfaces can be readily inspected in-service, it is conceivable that the structure could be designed to meet the non-inspectable criteria for less weight than the NDI in-service inspectable or walk-around inspectable criteria if the initial crack size was assumed to be  $a_0 = 0.05$  in. However, as discussed later, one of the difficulties in applying the criteria to a design application is the uncertainty of the sequence of events which must be assumed to perform the crack growth analysis. For this design study, crack



growth curves were developed for each of the classes of structure assuming a flaw or crack,  $a_0 = 0.050$  in., was present at the most critical design detail at the wing root station. The results of these analyses are plotted in Figures 5-17 and 5-18 which show the relation between maximum design tension stress and flights to failure starting with the initial crack size. The life requirement in this case is one service lifetime of the severe service usage.

For a 4000-hour service life the design stress allowable for integrally stiffened and zee-stiffened aluminum structure is 59,100 and 58,000 psi respectively, and greater than this for the multi-spar unstiffened skin structure. Therefore, the aluminum structure can meet the criteria without affecting the design stress allowable and the structural weight.

For the titanium structure the corresponding allowables are 61.5 ksi for zee-stiffened structure, 75 ksi for the integrally stiffened structure, and approximately 84.2 ksi for the multi-spar unstiffened structure. The only structure that would be affected by this criterion is the zee-stiffened titanium structure. Therefore, it might be better to design the zee-stiffened titanium structure to meet the walk-around inspectable criteria.

The reason the multi-spar structure looks the best is because the skin and reinforcing member (spar cap) are thicker than the zee stiffened structure or the integrally stiffened skin. Recall that the sequence of cracking assumed was the growth of an 0.05 in. flaw to a thru-the-thickness crack in the skin, then the growth of an 0.05 in. flaw to a thru-the-thickness crack in the reinforcement, and finally the growth, after the reinforcement is broken, of the thru-the-thickness skin crack to failure. Most of the crack growth time is contributed by the first two phases, which are artificially long in duration for large thicknesses. Based on the uncertainty of the assumed sequence of events occurring in an actual structure, the design stresses obtained for the non-inspectable classification can not be considered as reliable as those obtained for the other classifications. Because of the difficulty in calculating the crack growth period of complex structure starting with a small initial crack size, it is recommended that some representative testing be conducted to establish more reliable design stress allowables. Tests could be conducted by pre-flawing representative design details and applying fatigue loadings to the specimens to failure at various stress levels. A more reliable preliminary design analysis procedure could be developed by analyzing the



results of various crack growth tests, similar to what is done to establish fatigue allowables.

### 5.7.3 Structural Weight Evaluation

As shown in Table 5-32, the lightest structure to meet the static and fatigue requirements is the zee-stiffened titanium structure. The next lightest structures are the aluminum zee and integrally stiffened structures which are about 17 percent heavier. To meet the durability requirements, the weight of the zee-stiffened titanium structure must be increased 10.6 percent, but it is still 6.4 percent lighter than the next lightest structure. All the structures can meet one of the three structural integrity requirements without an additional weight penalty. Therefore, based on the results of this study, a 7075-T76 aluminum zee or integrally stiffened skin structure could be designed to meet the proposed criteria without a weight penalty. A zee-stiffened Ti-6Al-4V structure that meets all the requirements is about 7 percent lighter than the lightest aluminum structure. All the other types of structures considered would be heavier. The multi-spar unstiffened skin structure is not weight competitive with either the zee-stiffened skin or the integrally stiffened skin for this application.

## 6.0 REFERENCES

### 3.0 REFERENCES

- 3-1 Tiffany, C. F., "Fracture Control of Metallic Pressure Vessels," NASA SP-8040, May 1970.
- 3-2 Federal Aviation Agency (FAA) Federal Aviation Regulations (FAR) Part 25, Airworthiness Standards: Transport Category Airplanes.
- 3-3 FAA, FAR, Part 27, Airworthiness Standards: Normal Category Rotorcraft.
- 3-4 FAA, FAR, Part 29, Airworthiness Standards: Transport Category Rotorcraft.
- 3-5 MIL-A-8866(ASG), "Airplane Strength and Rigidity - Reliability Requirements, Repeated Loads, and Fatigue," 18 May 1960.
- 3-6 MIL-A-8861(ASG), "Airplane Strength and Rigidity - Flight Loads," 18 May 1960.
- 3-7 The Air Force Airplane Structural Integrity Program (ASIP) Program Requirements, Technical Report ASD-TR-66-57, May 1970.
- 3-8 Wood, Howard A., "Fracture Control Procedures for Aircraft Structural Integrity," AFFDL-TR-71-89, July 1971.
- 3-9 CP 621L2002 and NA70-76 Requirements for B-1 Aircraft as of January 1971.
- 3-10 Fitch, George E., Jr., "Application of Fracture Mechanics to Aircraft Structures," presented at 1972 Western Metal and Tool Exposition, 13-17 March 1972, Los Angeles, California.
- 3-11 Mullins, D. W., "Maneuver Load Data from F-104C and D Aircraft," ASD-TR-62-363, April 1962.
- 3-12 Berens, A. P., "Load Factor Data for F-5A and F-105D Aircraft in Weapon Passes," AFFDL-TR-68-47, May 1968.
- 3-13 Taylor, J., "Manual on Aircraft Loads," Pergamon Press, 1965, p 103.
- 3-14 Clay, L. E. and Duke, G. L., "Structural Flight Loads Data from T-38 Aircraft Using A/A24U-10 Recording Sets," ASD-TR-69-99, August 1969.

- 3-15 "F-105D Statistical Flight Loads Program," SEG-TR-66-16, June 1966.
- 3-16 Wei, R. P. and Landes, J. C., "Correlation Between Sustained Load and Fatigue-Crack Growth in High-Strength Steels," Materials Research and Standards, July 1969, pp. 25-27, 44, 46.
- 3-17 Bucci, R., Ph-D Dissertation, Lehigh University, 1970.
- 3-18 Barsom, J. M., "Effect of Cyclic-Stress Form on Corrosion-Fatigue Crack Propagation Below  $K_{ISCC}$  in a High Yield Strength Steel," paper presented at the International Conference on Corrosion Fatigue, University of Connecticut, Storrs, Conn., June 14-18, 1971.
- 3-19 MIL-A-8866(ASG), p. 4.
- 3-20 King, T. T., "Some Developments in the Air Force Aircraft Structural Integrity Program (ASIP)," in Proceedings of the Air Force Conference on Fatigue and Fracture, AFFDL-TR-70-144, Sept. 1970, pp. 701-721.
- 3-21 Ravera, R. J., and Sih, G. C., "Transient Analysis of Stress Waves Around Cracks Under Antiplane Strain," J. Acoustic Soc. of America, 47, pp. 875-881, 1970.
- 3-22 Embley, G. T., and Sih, G. C., "Response to a Penny Shaped Crack To Impact Waves," Proceedings of 12th Mid-Western Conference, 1971.
- 3-23 Enearl, R. O., "Wing Fail-Safe Tests," Lockheed-California Company, LR 11251, February 28, 1956.
- 3-24 Packman, P. F., Pearson, H. S., Marchese, G. B., and Owens, J. S., "The Applicability of a Fracture Mechanics - Non-Destructive Testing Design Criterion," AFML-TR-68-32, 1968.
- 3-25 Sattler, F. J., "Non-Destructive Flaw Detection Techniques for Critical Defect Determination," NASA CR-72602, January 1970.
- 3-26 Bryan, David F., "The B-52G-H Wing Cycle Test Program," Proceedings of the Air Force Conference on Fatigue and Fracture of Aircraft Structures and Materials AFFDL TR 70-144, September 1970.



- 3-27 Fitch, G. E., Jr., Jackman, R. E. and Horsfall, W. P., "The F-100 Aircraft Structural Integrity Program (ASIP)," Proceedings of the Air Force Conference on Fatigue and Fracture of Aircraft Structures and Materials, AFFDL TR 70-144, September 1970.
- 3-28 SMNAE, F-104 Special Projects Office, "F-104 Wing Program Final Report," Hq. SMAMA, McClellan, AFB, California, 1 December 1969.
- 3-29 "Tentative Method of Test for Plane-Strain Fracture Toughness of Metallic Materials," published by American Society for Testing and Materials, March 9, 1970.
- 3-30 Diamond, Patricia and Payne, A. O., "Reliability Analysis Applied to Structural Tests," presented at the Sixth International Committee on Aeronautical Fatigue Symposium, Miami Beach, Florida, May 12-14, 1971.
- 3-31 Payne, A. O. and Grandage, J. M., "A Probabilistic Approach to Structural Design", presented at Conference on Applications of Statistics and Probability to Soil and Structural Engineering, University of Hong Kong, September 1971.

#### 4.0 REFERENCES

- 4-1 Young, Louis, "Fatigue Analyses", Chapter 10, Metal Fatigue: Theory and Design, Edited by Angel F. Madayag, John Wiley and Sons, New York.
- 4-2 Stone, Melvin S., "Fatigue and Fail-Safe Design of a New Jet Transport Airplane," Fatigue Design Procedures, Proceedings of the Fourth ICAF Symposium, edited by E. Gassner and W. Shuz, Pergamon Press, London, pp 1-65.
- 4-3 Abelkis, P. R., and Bobovski, W. P., "Fatigue Strength Design and Analysis of Aircraft Structures, Part II - Fatigue Life Analysis Computer Program - Users Manual", AFFDL-TR-66-197, Part II, March 1967.
- 4-4 Paris, P. C., and Sih, G. C., "Stress Analysis of Cracks," in Fracture Toughness Testing and its Applications, page 30. Special Technical Publications No. 381, American Society for Testing and Materials, 1965.
- 4-5 Wilhem, D. P., "Fracture Mechanics Guidelines for Aircraft Structure Applications," AFFDL-TR-69-111, February 1970.
- 4-6 Orowan, E., "Fracture and Strength of Solids," Physical Society Progress Reports, Vol. 12, pp. 185-232, London, England (1949).
- 4-7 Irwin, G. R., "Fracture Dynamics," Fracturing of Metals, American Society for Metals, Cleveland, Ohio, pp 147-166 (1948).
- 4-8 Feddersen, C. E., Discussion to: Plane Strain Crack Toughness Testing, ASTM STP 410, 1967, p. 77.
- 4-9 Fichter, W. B., "Stress at the Tip of a Longitudinal Crack in a Plate Strip," Presented at the 5th U. S. National Congress of Applied Mechanics, University of Minnesota, Minneapolis, Minnesota, June 1966.
- 4-10 Smith, F. W., Emery, A. F., and Kobayashi, A. S., "Stress Intensity Factors for Semi-Circular Cracks (Part II - Semi-Infinite Solids)," Trans. ASME, Journal of Appl. Mech., Dec. 1967, pp. 953-959.

- 4-11 Liu, A. F., "Stress Intensity Factor for a Corner Flaw," Engineering Fracture Mechanics Journal, V. 4, 1972, pp 175-179.
- 4-12 Sneddon, I. N., "The Distribution of Stress in the Neighborhood of a Crack in an Elastic Solid," Proceedings, Royal Society of London, V. A-187, 1946, pp 229-260.
- 4-13 Bowie, O. L., "Analysis of an Infinite Plate Containing Radial Cracks Originating at the Boundary of an Internal Circular Hole," Journal of Math. and Physics, Vol. 35, 1956, pp 6-71.
- 4-14 Brussat, T. R., and Davis, C. S., "Crack Propagation Analysis," Lockheed-California Company LR 24917, December 1971.
- 4-15 Lockheed-California Company Structural Life-Assurance Manual, SIM No. 3a, "Fail-Safe and Damage Tolerant Design," October 25, 1971.
- 4-16 Poe, C. C., Jr., NASA Technical Report R-358, Stress-Intensity Factor for a Cracked Sheet with Riveted and Uniformly Spaced Stringers, Langley Research Center, May 1971.
- 4-17 Bloom, J. M. and Sanders, J. L., Jr., The Effect of a Riveted Stringer on the Stress in a Cracked Sheet, Journal of App. Mechanics, Sept. 1966.
- 4-18 Poe, C. C., Jr., Fatigue Crack Propagation in Stiffened Panels. Damage Tolerance in Aircraft Structures, American Society for Testing and Materials, ASTM STP 486, May 1971, pp 79-97.
- 4-19 Wheeler, O. E., "Spectrum Loading and Crack Growth," ASME Jl. of Basic Engineering, March 1972, pp 181-186.
- 4-20 Willenborg, J., Engle, R. M., and Wood, H. A., "A Crack Growth Retardation Model Using an Effective Stress Concept," AFFDL Technical Memorandum 71-1-FBR.
- 4-21 Jonas, O. and Wei, R. P., "An Exploratory Study of Delay in Fatigue Crack Growth," Int. Jl. of Fracture Mechs., Vol. 7, 1971, pp 116-118.
- 4-22 Raju, "Effect of Exposure to Elevated Temperatures on the Delay in Crack Growth Due to a High Stress Cycle," Int. Jl. of Fracture Mechs., V8, Mar. 1972, pp 99-102.



- 4-23 Brown, B. F. and Beachem, C. D., "A Study of the Stress Factor in Corrosion Cracking by the Use of the Pre-Cracked Cantilever Beam Specimens," Corrosion Science, Vol. 5, pp 745-750, 1965.
- 4-24 "Titanium Development Program," Document No. D6A10065-1, The Boeing Company, Seattle, Washington, (1966).
- 4-25 Steigerwald, E. A. and Benjamin, W. D., "Environmentally Induced Delayed Failures in Martensite High-Strength Steels," AFML-TR-68-80, 1968.
- 4-26 Johnson, H. H. "Environmental Cracking in High-Strength Materials," in Fracture, H. Kiebowitz (ed.), Vol. III, pp 679-720, Academia Press, New York, N.Y., 1971.
- 4-27 Wei, R. P. and Landes, J. D., "Correlation Between Sustained Load and Fatigue Crack Growth in High-Strength Steels," Material Research and Standards, Vol. 9, No. 7, pp 25-28, 1969.
- 4-28 Crichlow, W. J., "The Ultimate Strength of Damaged Structure - Analysis Methods with Correlating Test Data," in Full-Scale Fatigue Testing of Aircraft Structures, Pergamon Press, New York, 1960.
- 4-29 Romualdi, J. P., Frasier, J. T., and Irwin, G. R., "Crack Extension Force Near a Riveted Stringer," Report No. 4956, Naval Research Lab., May 1957.
- 4-30 Sanders, Jr., J. L., "Effect of a Stringer on the Stress Concentration Factor Due to a Crack in a Thin Sheet," NASA Tech. Rep. R-13, 1959.
- 4-31 Romualdi, J. P., "Fracture Arrest Design Considerations," in Proceedings of the Crack Propagation Symposium, Cranfield, England, September, 1961.
- 4-32 Isida, M., "Stress Concentration Due to a Central Transverse Crack in a Strip Reinforced on Either Side," Journal, Japan Soc. Aero-Space Sciences, Vol. 10, 1962.

- 4-33 Terry, T., "Analysis of a Reinforced Infinite Plate Containing a Single Crack," Ph.D. Dissertation, Lehigh University, September, 1963.
- 4-34 Leybold, H. A., "A Method for Predicting the Static Strength of a Stiffened Sheet Containing a Sharp Notch," NASA Technical Note D-1943, Aug. 1963.
- 4-35 "Crack Propagation Prediction and Crack-Stopper Techniques for Stiffened and Unstiffened Flat Sheet in a Supersonic Transport Environment," ASD-TDR-63-773, Air Force Systems Command, Wright-Patterson Air Force Base, Ohio, Sept. 1963.
- 4-36 Grief, R., and Sanders, J. L., Jr., "The Effect of a Stringer on the Stress in a Cracked Sheet," Journal of Applied Mechanics, Trans. ASME, Series E, Vol. 32, 1965.
- 4-37 Bloom, J. M. and Sanders, J. L., Jr., "The Effect of a Riveted Stringer on the Stress in a Cracked Sheet," Journal of Applied Mechanics, Trans. ASME, Series E, Vol. 33, 1966.
- 4-38 Vlieger, H., and Broek, D., "Residual Strength of Cracked Stiffened Panels," National Aerospace Laboratory NLR-TN-653, The Netherlands, Dec. 1967.
- 4-39 Wang, D. Y., "An Investigation of Fatigue Crack Propagation and Fail-Safe Design of Stiffened Large Aluminum Alloy Panels with Various Crack Stoppers," in Proceedings, 10th ASME/AIAA Structures, Structural Dynamics and Materials Conference, New Orleans, La., April 14, 1969.
- 4-40 Poe, C. C., Jr., "The Effect of Uniformly Spaced Stringers on the Stress Intensity Factor of a Cracked Sheet," Presented at the Air Force Conference on Fatigue and Fracture of Aircraft Structures and Materials, Miami Beach, Florida, Dec., 1969.
- 4-41 Crichlow, W. J., "The Optimum Design of Shell Structure for Static Strength, Stiffness, Fatigue and Damage Tolerance Strengths," in Symposium on Structural Optimization, AGARD-CP-36-70, North Atlantic Treaty Organization, 1970.

- 4-42 Liu, A. F., and Ekvall, J. C., "Material Toughness and Residual Strength of Damage Tolerant Aircraft Structures," Damage Tolerance in Aircraft Structures, ASTM STP 486, May 1971, pp 98-121.
- 4-43 Liu, A. F., "Residual Strength of Flat Panels Reinforced with Riveted Flat Straps," LR 22819, Rev. A., Lockheed-California Company, Burbank, California, December 1970.
- 4-44 Creager, M., and Liu, A. F., "The Effect of Reinforcements on the Slow Stable Tear and Catastrophic Failure of Thin Metal Sheet," AIAA paper No. 71-113, presented at the AIAA 9th Aerospace Sciences Meeting, New York, N. Y., Jan. 25 27, 1971.
- 4-45 Swift, T., and Wang, D. Y., "Damage Tolerant Design Analysis Methods and Test Verification of Fuselage Structure," Proceedings of the Air Force Conference on Fatigue and Fracture of Aircraft Structures and Materials, December 1969, Miami Beach, Florida, AFFDL-TR 70-144.
- 4-46 Bluhm, J. I., "Fracture Arrest," in Fracture, H. Liebowitz, (Ed.), Vol. 5, Academia Press, (1969).
- 4-47 Kobayashi, A. S. and Naiden, D. E., "Stress Intensity Factor for a Straight Crack Approaching a Circular Hole," Proceedings of the Air Force Conference on Fatigue and Fracture of Aircraft Structures and Materials, December 1969, Miami Beach, Florida, AFFDL TR-70-144
- 4-48 Yoffe, E. H., "The Moving Griffith Crack," Philosophical Magazine, Series 7, Vol. 42, 1954.
- 4-49 Craggs, J. W., Journal of Mechanics and Physics of Solids, Vol. 8, pp 66 - 76 (1960).
- 4-50 Broberg, K., "The Propagation of a Brittle Crack," Arkiv for Fysik, Vol. 18, p 159, 1960.
- 4-51 Baker, B. R., Journal of Applied Mechanics, Vol. 29, p 449, 1962.
- 4-52 Erdogan, F., "Crack Propagation Theories," in Fracture, H. Liebowitz (Ed.), Vol. 2, Academia Press, 1968.



- 4-53 Rice, J. R., "Mathematical Analysis in the Mechanics of Fracture," in Fracture, H. Liebowitz (Ed.), Vol. 2, Academia Press, 1968.
- 4-54 Sih, G. C., "Dynamic Aspects of Crack Propagation," Inelastic Behavior of Solids, edited by M. F. Kanninen, et al, McGraw-Hill, New York, 1970.
- 4-55 Embley, G. T. and Sih, G. C., "Response of a Penny-Shaped Crack to Impact Waves," Proceedings of 12th Mid-Western Mechanics Conference, 1971.
- 4-56 Glennie, E. B. and Willis, J. R., "An Examination of the Effects of Some Idealized Models of Fracture on Acceleration Cracks," in J. Mech. Phys. Solids, 1971, Vol. 19, pp 11 to 30.
- 4-57 Steverding, B., and Lehnigk, S. H. "The Propagation Law of Cleavage Fracture," Int'l. Journal of Fracture Mechs. Vol. 6, No. 3, pp 223-232, September 1970.

## 5.0 REFERENCES

- 5-1 King, T. T. "Some Developments in the Air Force Aircraft Structural Integrity Program (ASIP)," in Proceedings of the Air Force Conference on Fatigue and Fracture, AFFDL-TR-70-144, Sept. 1970, pp 701-721.
- 5-2 MIL-HDBK-5B, "Metallic Materials and Elements for Aerospace Vehicle Structures," 1 September 1971.
- 5-3 Lockheed-California Company Structural Life-Assurance Manual, SLM No. 16 and 17, "Constant Life Diagrams for Aluminum and Titanium", Revised November 30, 1971.
- 5-4 Lunde, T., "Fatigue Allowable Stresses for S-3A Materials," Lockheed-California Company LR 24526, 12 August, 1971.
- 5-5 Liu, A. F., "Statistical Variation in Fracture Toughness Data of Air-frame Materials," Proceedings of the Air Force Conference on Fatigue and Fracture of Aircraft Structures and Materials, AFFDL-TR-70-144, held at Miami Beach, Florida 15-18 December 1969.
- 5-6 Paris, P. C., Weiss, W., Wessel, E. T., and Anderson, A. F.; "On the Threshold for Fatigue Crack Growth,". To be submitted for publication.
- 5-7 Johnson, H. H. and Paris, P. C. "Sub-Critical Flaw Growth". Engineering Fracture Mechanics, vi, 1968, pp 3-45.
- 5-8 Van Orden, J. M. and Liu, A. F., "Evaluation of X7475-T61 Clad Sheet," Lockheed-California Report LR 24951, February 1972.
- 5-9 Lockheed-California Company Structural Life-Assurance Manual, SLM No. 3a, "Fail-Safe and Damage Tolerant Design," October 25, 1971.
- 5-10 Hudson, C. M., "Fatigue Crack Propagation in Several Titanium and Stainless Steel Alloys and One Superalloy," NASA TN-D2331, Oct. 1964.
- 5-11 "Fuselage Fail-Safe Design Data and Bomb-Resistant Analysis for the Supersonic Transport," FDL-TDR-64-80, June 1964.

- 5-12 Emero, D. H. and Spundt, L., "Optimization of Multirib and Multiweb Wing Box Structures Under Shear and Moment Loads," AIAA 6th Structures and Materials Conference, Palm Springs, April 5-7, 1965.
- 5-13 "Supersonic Transport Development Program Phase III Proposal," Volume II-C Airframe Design Report, Book 5 of 5, Lockheed Report No. LR 19838, September 1966.
- 5-14 Ekvall, J. C., "Fatigue-Relating Past Experience to Design," Interface of Material and Structures Including Proceedings of Monterey Symposium, U. S. Naval Postgraduate School Report NPS-57Hp 7111A, October 1971.
- 5-15 King, Troy T., "Some Developments in the Air Force Structural Integrity Program (ASIP)," Proceedings of the Air Force on Fatigue and Fracture of Aircraft Structures and Materials held at Miami Beach, Florida, 15-18 December, 1969, AFFDL-TR-70-144.
- 5-16 Westmann, R. A., "Note on Estimating Critical Stress for Irregularly Shaped Planar Cracks," International Journal of Fracture Mechanics, v. 2, 1966, pp 561-563.
- 5-17 Enearl, R. O., "Wing Fail-Safe Tests," Lockheed-California Company Report, LR 11251, February 28, 1956.
- 5-18 Lutz, H. W., "Crack Propagation of Dynamically Produced Cracks," Lockheed-California Company Report No. LR 12923, July 1958.



## APPENDIX B REFERENCES

- B-1 "Tentative Method of Test for Plane-Strain Fracture Toughness of Metallic Materials" ASTM Designation E399-70T, Annual Book of ASTM Standards, Part 31, pp. 911-927 (1970).
- B-2 "Military Standardization Handbook Metallic Materials and Elements for Aerospace Vehicle Structures," MIL-HDBK-5B, September 1971.
- B-3 "Titanium Development Program," Commercial Supersonic Transport Program, Phase II-C Report, Contract FA-SS-66-5, D6A10065-1, Boeing Company, Seattle, Washington, 1966.
- B-4 Piper, D. E., Smith, S. H., and Carter, R. V., "Corrosion Fatigue and Stress-Corrosion Cracking in Aqueous Environment," presented at the 1966 ASM National Congress, Chicago, Oct. 31, 1966.
- B-5 "Progress Report on Delayed Fracture Characteristics of Titanium Alloys," LR 19741, Lockheed-California Company, Burbank, Calif. 1966.
- B-6 "SST Development Program," Phase III Proposal, Vol. II-C, Book 4, LR 19839, Lockheed-California Company, Burbank, Calif. 1966.
- B-7 Liu, A. F., "Statistical Variations in Fracture Toughness of Airframe Materials," D6-15784TN, Boeing Co., Seattle, Washington, pp 33, 1968.
- B-8 "Development of Engineering Data on Titanium Extrusion for Use in Aerospace Design," AFML-TR-67-189, Air Force Materials Laboratory, Wright-Patterson AFB, Ohio, 1967.
- B-9 Liu, A. F., "Statistical Variation in Fracture Toughness Data of Airframe Materials," presented at the Air Force Conference on Fatigue and Fracture of Aircraft Structures and Materials, December 1969, Miami Beach, Florida.
- B-10 Jones, R. E., "Comparison of Fracture Toughness Values Obtained Using Semi-Infinite Aluminum Plates with Values Obtained Using Laboratory Size Specimens," AFML-TR-69-58 Air Force Materials Laboratory, Wright-Patterson AFB, Ohio (1969).

- B-11 Allen, F. C., "Effect of Thickness on the Fracture Toughness of 7075-Aluminum in the T6 and T73 Conditions," in Damage Tolerance in Aircraft Structures ASTM STP 486, American Society for Testing and Materials, May 1971, pp 16-38.
- B-12 Feddersen, C. E., and Moon, D. P., "A Compilation and Evaluation of Crack Behavior Information on D6AC Steel Plate and Forging Materials for the F-111 Aircraft." Defense Metals Information Center, Battelle, Columbus Laboratories, Columbus, Ohio, June 25, 1971.
- B-13 Communication between C. M. Garcia (Lockheed-California Company) and C. D. Little and Jim Shultz (General Dynamics, Fort Worth) 8-27-71.
- B-14 "Fracture Toughness and Tear Tests," AFML-TDR-64-238, Air Force Materials Laboratory, 1964, Wright-Patterson Air Force Base, Ohio.
- B-15 Figge, I. E., "Residual Static Strength of Several Titanium and Stainless-Steel Alloys and One Superalloy at -109°F, and 550°F," NASA TN D-2045, December 1963.
- B-16 Feddersen, C. E., "Evaluation of the Residual Strength of Center Cracked Tension Panels," Damage Tolerance in Aircraft Structures, ASTM STP 486, American Society for Testing Materials, 1971, pp. 50-78,
- B-17 "Fracture Toughness and Tear Tests," AFML-TDR-64-238, Air Force Materials Laboratory, 1964, Wright-Patterson Air Force Base, Ohio.
- B-18 "Notch Resistance and Fracture Toughness Characteristics of High Strength Metals," ASD-TDR-63-494, Air Force Materials Laboratory, Wright-Patterson AFB, Ohio, 1963.
- B-19 Liu, A. F., "Fail-Safe Allowables L-1011 Materials," LR 22652, Lockheed-California Company, January 1970.
- B-20 Feddersen, C. E., A Task Report on Determination of the Effectively Infinite Width of Center-Cracked Tension Panels to MIL-HDBK-5 Residual Strength Task Group, March 18, 1970 - Battelle Memorial Institute, Columbus Laboratories, Columbus, Ohio.

B-21    Schwartz, R. D., "L-1011 Structural Materials Evaluation," LR 22008,  
Lockheed-California Company, 20 November 1970.



## APPENDIX E - REFERENCES

- E-1 Irwin, G. R., "The Crack Extension Force for a Part Through Crack in a Plate," Transactions ASME, Journal of Applied Mechanics, 1962, pp 651, 654.
- E-2 Rice, J. C., and Levy, N., "The Part-Through Surface Crack in an Elastic Plate," Technical Report NGL 40-002-080/3 to the National Aeronautics and Space Administration, Brown University, Providence R.I., September 1970.
- E-3 Smith, F. W., Emery, A. F., and Kobayashi, A. S., "Stress Intensity Factors for Semi-Circular Cracks (Part II - Semi-Infinite Solid)," Trans. ASME, Journal of Appl. Mech., Dec. 1967, pp. 953-959.
- E-4 Thresher, R. W., and Smith, F. W., "Stress-Intensity Factors for a Surface Crack in a Finite Solid," ASME Paper No. 71-APM-6, presented at the Applied Mechanics Western Conference, University of Southern California, Los Angeles, Calif., August 23-25, 1971.
- E-5 Smith, F. W., and Alavi, M. J., "Stress-Intensity Factors for a Part-Circular Surface Flaw," ASME, Proceedings of the First International Conference on Pressure Vessel Technology, 1969. pp 793-800.
- E-6 Kobayashi, A. S., and Moss, W. L., "Stress Intensity Magnification Factors for Surface-Flawed Tension Plate and Notched Round Tension Bar," in Fracture 1969, Chapman and Hall, Ltd., London, 1969.
- E-7 Wigglesworth, L. A., "Stress Distribution in a Notched Plate," Mathematika, Vol. 4, 1957, pp. 76-96.
- E-8 Irwin, G. R., "Plastic Zone Near a Crack and Fracture Toughness," Seventh Sagamore Ordnance Materials Research Conference, Racquette Lake, New York, August 16-19, 1960.
- E-9 McClintock, F. A., and Irwin, G. R., "Plasticity Aspects of Fracture Mechanics," in Fracture Toughness Testing and Its Applications, Special Technical Publication #381, American Society for Testing and Materials, 1965, pp 84-113.
- E-10 Gross, B., et al, "Stress-Intensity Factors for a Single-Edge-Notch Tension Specimen by Boundary Collocation of a Stress Function," NASA TN-2395, 1964.

- E-11 Tiffany, C. F., et al, "Extended Loading of Cryogenic Tanks," NASA CR-72252, December 1966.
- E-12 Masters, J. N., Haese, W. P., and Finger, R. W., "Investigation of Deep Flaws in Thin Walled Tanks," NASA CR-72606, Report on Contract NAS 3-10290, March 1969.
- E-13 Forman, R. G., and Kobayashi, A. S., "On the Axial Rigidity of a Perforated Strip and the Strain Energy Release Rate in a Centrally Notched Strip Subjected to Uniaxial Tension," J1. of Basic Engineering, ASME Trans., December 1964.
- E-14 Isida, M., "Stress Intensity Factors for the Tension of an Eccentrically Cracked Tip," J. Appl. Mech. Trans. ASME, Series E., Vol. 33, pp 674-675, (1966).
- E-15 Dixon, J., "Stress Distribution Around Edge Slits in a Plate Loaded in Tension - Effect of Finite Width of Plate," J1. of Royal Aeronautical Society, (TN), V. 66, No. 617, May 1962.
- E-16 "Fracture Testing of High-Strength Sheet Materials," Bulletin No. 243, ASTM, January 1960, pp 29-40.

## APPENDIX A PROPOSED AIR FORCE SERVICE LIFE REQUIREMENTS

Pertinent requirements from the proposed MIL Std. XXX (USAF) "Aircraft Structural Integrity Program (ASIP): Airplane Requirements", dated 15 October 1971 are given in the sections below. This document is currently in the draft review and approval cycle of the Air Force.



## 1.0 SERVICE LIFE REQUIREMENTS

The primary structure shall incorporate materials, stress levels, and structural configurations which (1) allow routine in-service inspection, (2) minimize crack initiation, and (3) minimize the probability of loss of the aircraft due to propagation of undetected fatigue cracks, flaws, or other damage. A durable structural design which is resistant to crack initiation shall be a primary requirement in order to achieve low structural maintenance needs. In addition, damage tolerant design is required for primary structure to ensure structural safety since undetected flaws or damage can and sometimes do exist in critical structural components despite the design, fabrication, and inspection efforts expended to eliminate their occurrence.

### 1.1 DURABILITY

Areas of the airframe that could be susceptible to fatigue, corrosion, or other crack initiation mechanisms shall be identified by analyses and tests. The airframe shall be designed to withstand four (4) structural service lifetimes without fatigue cracking. The design service load spectrum shall be derived from the service life criteria specified in paragraph 1.0 and MIL-A-8866. In addition it shall be an objective for the structural airframe to withstand one (1) service lifetime without general corrosion, or crack initiation due to mechanisms other than fatigue.

### 1.2 DAMAGE TOLERANCE

Damage tolerant design concepts are categorized into two general categories: (1) those where unstable crack propagation is locally contained through the use of multiple load paths, crack stoppers and/or fail-free structural components (i.e., these concepts are referred to as "fail-safe"), and (2) those monolithic structures where flaws or defects are not allowed to attain the critical size required for unstable rapid propagation (i.e., these are referred to as "slow crack growth" concepts). Both design approaches shall assume the presence of initial damage (i.e., undetected flaws and defects) and shall have a specified minimum residual strength level both during and at the end of a specified period of unrepaired service usage. The required residual strengths, unrepaired period of service use and initial damage assumptions shall be as specified in paragraphs 1.2.1 thru 1.2.3.

### 1.2.1 Residual Strength Requirements

Except in the case where the damage is of such a nature that it is obvious to the pilot and/or crew, while the airplane is airborne, the specified minimum residual strength shall be either the limit design load or the maximum spectrum load, whichever is larger. In addition the damage shall not endanger safety of flight due to loss of control or by reduction of the flutter speed below  $V_D$ . For the above case of "in-flight detectable" damage, the airplane shall retain sufficient strength to safely return to its operational base. Also, in the case of a "fail-safe" design the remaining structure shall be capable of withstanding the dynamic overloads resulting from the failure of a single member plus the design limit load or maximum spectrum load whichever is larger.

### 1.2.2 Period of Unrepaired Service Use

The minimum required period of unrepaired service usage shall depend upon in-service damage detectability.

1.2.2.1 This period shall be one scheduled inspection interval if the damage can be detected by a visual "walk-around" inspection. The scheduled inspection interval shall not be less than one-fourth ( $1/4$ ) of the design service lifetime.

1.2.2.2 This period shall be two scheduled inspection intervals if the damage can be detected during normal scheduled service inspections using USAF approved non-destructive inspection procedures (i.e., X-ray, visual, penetrant, proof test, etc.). For "fail-safe" designs it shall be shown that the selected in-service inspection procedures will detect any failed members in multiple load path structures and/or arrested crack propagation in single load path structures. Monolithic "slow crack growth" designs shall be considered to be in-service inspectable if the critical flaw size (at limit load or max spectrum load whichever is larger) is a through the thickness crack of a length equal to or greater than two (2) inches and is located in an accessible and inspectable area of the structure. Surface and subsurface flaws or defects shall be considered in-service inspectable in monolithic "slow crack growth" designs only if proof testing is used as the scheduled in-service inspection technique.



1.2.2.3 The minimum period of unrepaired service usage shall be one lifetime if the damage cannot be easily detected during in-service inspections. This applies to "fail-safe" designs where because of the detailed structural arrangement in-service inspection either will not or cannot be readily performed. Except as noted above, it also applies to all monolithic "slow crack growth" design concepts.

### 1.2.3 Initial Damage Assumptions and Damage Growth Requirements

The assumed initial damage sizes and damage growth requirements depend upon the type of damage tolerant design approach selected.

#### 1.2.3.1 Monolithic "Slow Crack Growth" Designs

1.2.3.1.1 It shall be assumed that an initial flaw or defect of the maximum undetectable size exists in the structure and it is located in the area of highest tensile stress and is the most unfavorably oriented with respect to the stress fields and the fracture properties of the materials.

1.2.3.1.2 This maximum undetectable size ( $a/Q$  value) shall be assumed to be 0.10 inch except as follows:

a. A smaller initial flaw size may be assumed subsequent to a demonstration that all flaws larger than the selected size have at least a 90% probability of detection with a 95% confidence using the selected production inspection procedures, equipment, and personnel. This demonstration shall be subject to USAF approval.

b. A smaller initial size may be assumed if proof test inspection is used. In this case the maximum undetectable initial size shall be the calculated critical size at the proof test stress levels and temperature using the upper bound of the material  $K_{IC}$  data.

1.2.3.1.3 Except for those structures which have been shown to be in-service inspectable per the requirements in paragraph 1.2.2 it shall be shown by analysis and test that the maximum undetectable initial flaw size will not grow to critical size (at limit load or maximum spectrum load, whichever is larger) in one lifetime.



1.2.3.1.4 For those structures which have been shown to be in-service inspectable per the requirements of paragraph 1.2.2 the maximum undetectable initial flaw size shall not grow to critical size in either one or two inspection intervals depending upon the degree of inspectability as specified in paragraph 1.2.2.

#### 1.2.3.2 Fail Safe Designs

1.2.3.2.1 It shall be assumed that an initial defect or flaw of the maximum undetectable size exists in the structure in the area of highest tensile stress and is most unfavorably oriented with respect to the stress field and the fracture properties of the material. In multiple load path fail-safe structure, an initial flaw shall be assumed to exist in each of the primary load carrying members. The maximum undetectable flaw size(s) (i.e.,  $a/Q$  values) shall be assumed to be not less than 0.033 inch except as follows:

a. A smaller initial flaw size may be assumed subsequent to a demonstration that all flaws larger than this size have at least a 90% probability of detection with a 50% confidence using the selected production inspection procedures, equipment, and personnel. This demonstration shall be subject to USAF approval.

1.2.3.2.2 For structure which is "in-service" inspectable per the requirements of paragraph 1.2.2 it shall be shown by analysis and test that subsequent to the failure of a single member or load path (at the most critical time during the service life) the maximum possible flaw size in the remaining structure (i.e., the size at time of failure) will not grow to critical size (at limit or maximum spectrum load whichever is larger) in either one or two scheduled inspection intervals depending upon the degree of inspectability as specified in paragraph 1.2.2.

1.2.3.2.3 For structure which is not "in-service" inspectable per the requirements of paragraph 1.2.2 it shall be shown by analysis and test that subsequent to failure of a single member or load path (at the most critical time during the service life) the maximum possible flaw size in the

remaining structure will not grow to critical size (at limit or maximum spectrum load whichever is larger) during the remaining life of the structure.

### 1.3 FRACTURE MECHANICS ANALYSIS

The contractor shall analyze those applicable areas of primary structure established under the provisions of paragraph 1.1. This analysis shall identify the character and dimensions of the smallest initial crack which could grow to critical size during the anticipated lifetime and cause failure at the maximum service spectrum stress or limit load stress whichever is greater. The analysis shall assume the presence of a crack-like defect, placed in the most unfavorable orientation with respect to the applied stress and the material properties, and shall predict the growth behavior in the chemical, thermal, and sustained and cyclic stress environment to which that portion of the component will be subjected. In addition to these factors,  $da/dt$  and  $da/dn$ , the interaction effects of variable loading, will be considered. The complete analysis for each component shall be supplied for review and approval including that portion of the analysis which identifies whether the critical areas are under plane strain, plane stress or mixed mode conditions at the onset of rapid crack propagation and including all crack growth rate and critical crack length test data on which the analysis was based.

### 1.4 TESTING

#### 1.4.1 Specimen Testing.

Valid fracture data shall be determined on a statistical basis in accordance with the procedures set forth in the 1968 ASTM Standards, Part 31, entitled "Proposed Method of Test for Plane Strain Fracture Toughness of Metallic Materials", the 1970 ASTM Standards Test Method E399-70T, AFFDL-TR-69-11 or by alternate methods approved by the procuring agency. The materials from which the structures identified in paragraph 1.1 are to be fabricated shall be controlled by a system of procedures and/or specifications which are sufficient to preclude the utilization in fracture critical areas of materials possessing  $K_{IC}$  values inferior to those assumed in design. Tests will be conducted on all billets, forgings, extrusions, plates, or other forms (from which final parts are finished) to evaluate the plane strain fracture toughness, where thicknesses permit. A



slice will be cut from these items, or integral projections thereof, a receiving inspection, so that specimens from each slice may be tested. These specimens shall have been heat treated with the same material from which they were cut.

#### 1.4.2 Component Testing

Damage tolerance tests will be conducted on that structure which is considered to be damage tolerant to verify that the failure of the critical component will not result in catastrophic loss of the structure. Tests will be performed during the preproduction design verification component test program and the full scale qualification test program. These tests will be conducted by pre-cracking a particular member to the critical crack length and applying a load corresponding to the maximum stress obtainable during the lifetime of the aircraft, or limit load, whichever is greater.

Tests will be conducted on selected critical structure, particularly safe-life components, to verify the analysis crack propagation rates. Initial flaw size cracks will be initiated at the critical point and propagation rates measured. These tests will be performed during the production design verification test program and during the full scale qualification test program.

Wherever possible, the structural components used for static test and fatigue test will be used to perform these tests. If in certain cases, this is not possible, then additional components will be fabricated for testing.



## APPENDIX B FRACTURE TOUGHNESS PROPERTIES OF MATERIALS

Test methods for determining the fracture toughness properties,  $K_{Ic}$  and  $K_c$ , of materials has been under study by the American Society of Testing Materials (ASTM) for some time. Tentative testing methods for obtaining valid  $K_{Ic}$  values are given in Reference B-1. Testing methods for obtaining valid,  $K_c$ , plane stress and mixed mode fracture toughness values are under investigation by MIL-HDBK-5 Residual Strength Task Group. Mr. Charles Feddersen, Battelle Memorial Institute, is the Task Group Leader. Since no readily published allowables for fracture toughness properties of materials are available, some limited data on Ti-6Al-4V annealed, 7075-T6 aluminum and D6AC steel were reviewed. These data are presented in this appendix and provide the basis for establishing design allowable stresses for the fracture toughness properties of materials used in the application analysis. These data are considered representative only since sufficient data are not available to establish allowables according to the guidelines given in Chapter 9 of Reference B-2.

### 1.0 $K_{Ic}$ Data

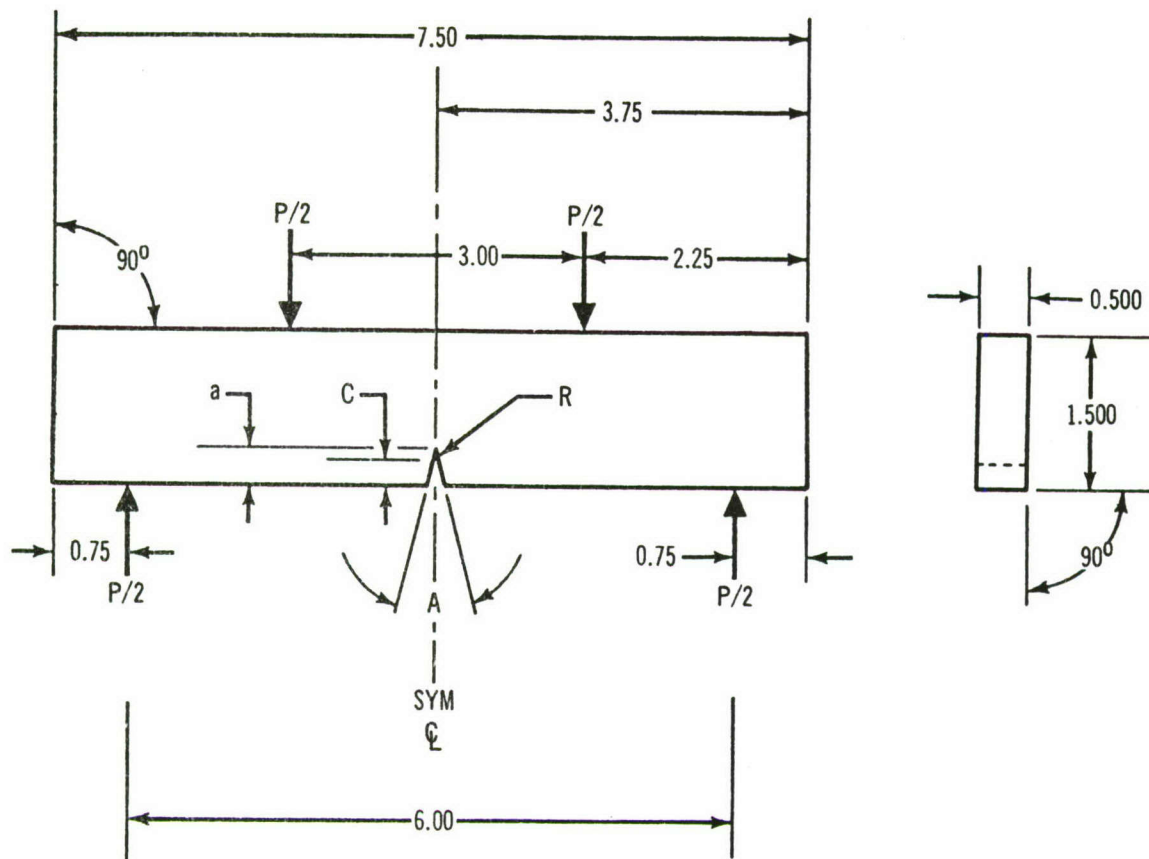
The  $K_{Ic}$  data for Ti-6Al-4V annealed and 7075-T6 aluminum compiled and discussed in this appendix were obtained from four point notch-bend type specimens as shown in Figure B-1. The data for D6AC Steel were obtained from compact tension specimens. The data obtained from these specimens will generally provide valid data if the applicable requirements of Reference B-1 are satisfied.

#### 1.1 Ti-6Al-4V Mill Annealed

Data obtained from References B-3 thru B-8 are summarized in Table B-1 and plotted in Figure B-2 as a function of tensile yield strength. The scatter of data in Figure B-2 can be considered representative for titanium.

Two groups of data from Table B-1 were selected for statistical analysis.

Since the fracture toughness properties vary with tensile yield strength, each data group was selected to include data with approximately the same tensile yield strength, i.e. 125-130 KSI and 144-148.6 KSI. Plotting these two groups of data on probability paper in Figure B-3 shows that the data exhibit log-normal distribution. Therefore, the statistical properties can be computed



A = 45° NOTCH ANGLE  
 R = 0.011 MAX. NOTCH RADIUS  
 C = 0.225 ± 0.001 NOTCH DEPTH  
 a = 0.300 ± 0.001 NOTCH PLUS FATIGUE CRACK DEPTH  
 B = 0.500 ± 0.001 SPECIMEN WIDTH  
 W = 1.500 ± 0.001 SPECIMEN DEPTH  
 L = 1.50 MOMENT ARM  
 ALL DIMENSIONS IN INCHES

$$K = \frac{PL}{BW^{3/2}} \left[ \left( \frac{1}{17.2} \right) \left( 34.7 \frac{a}{W} - 55.2 \left( \frac{a}{W} \right)^2 + 196 \left( \frac{a}{W} \right)^3 \right) \right]^{1/2}$$

FIGURE B-1 NOTCHED-BEND SPECIMEN

TABLE B-1 FOUR POINT NOTCHED-BEND  $K_{Ic}$  DATA FOR Ti-6Al-4V MILL ANNEALED

REF. NO.	PRODUCT	GRAIN DIRECTION	$F_{ty}$ KSI	$K_{Ic}$ KSI $\sqrt{IN.}$	REMARKS
B-3	PLATE	T	148.6	54.2	1200°F, 2 HOURS, A.C. $\triangle_2$
B-3	PLATE	T	148.6	54.5	1200°F, 2 HOURS, A.C. $\triangle_2$
B-3	PLATE	T	144.1	60.7	1300°F, 2 HOURS, A.C. $\triangle_2$
B-3	PLATE	T	144.1	61.7	1300°F, 2 HOURS, A.C. $\triangle_2$
B-3	PLATE	T	144.9	65.3	1400°F, 2 HOURS, A.C. $\triangle_2$
B-3	PLATE	T	144.9	65.7	1400°F, 2 HOURS, A.C. $\triangle_2$
B-3	PLATE	T	145.4	76.3	1500°F, 2 HOURS, A.C. $\triangle_2$
B-3	PLATE	T	145.4	74.5	1500°F, 2 HOURS, A.C. $\triangle_2$
B-3	PLATE	T	145	63.8	1300°F, 6 HOURS, A.C. $\triangle_2$
B-3	PLATE	T	145	58.4	1300°F, 6 HOURS, A.C. $\triangle_2$
B-3	PLATE	T	146.2	65.2	1300°F, 24 HOURS, A.C. $\triangle_2$
B-3	PLATE	T	146.2	64.3	1300°F, 24 HOURS, A.C. $\triangle_2$
B-4	PLATE	T	135 $\triangle_3$	85	$\triangle_4$
B-5	PLATE	T	133	73	1350°F, 8 HOURS, F.C.
B-6	PLATE	T	141	72	1350°F, 8 HOURS, F.C.
B-6	PLATE	T	137 $\triangle_3$	83	1325°F, 1 HOURS, F.C. $\triangle_4$
B-5	PLATE	L	130	78	1350°F, 8 HOURS, F.C. $\triangle_1$
B-7	PLATE	L	$\triangle_3$	85.2	$\triangle_5$
B-5	L - EXTRUSION	L	130	80	1350°F, 1 HOURS, A.C. $\triangle_1$
B-5	L - EXTRUSION	L	130	83	1350°F, 2 HOURS, A.C. $\triangle_1$
B-5	L - EXTRUSION	L	130	83	1350°F, 4 HOURS, A.C. $\triangle_1$
B-5	L - EXTRUSION	L	130	76	1450°F, 1 HOURS, A.C. $\triangle_1$
B-5	L - EXTRUSION	L	130	79	1450°F, 2 HOURS, A.C. $\triangle_1$
B-5	L - EXTRUSION	L	130	74	1450°F, 4 HOURS, A.C. $\triangle_1$
B-5	L - EXTRUSION	L	130	73	1250°F, 1 HOURS, A.C. $\triangle_1$
B-5	L - EXTRUSION	L	130	72	1250°F, 2 HOURS, A.C. $\triangle_1$
B-7	J - EXTRUSION	L	128	92	1300°F, 1 HOURS, F.C.
B-8	T - EXTRUSION	L	125-130	77	1300°F, 1 HOURS, A.C. $\triangle_1$
B-8	T - EXTRUSION	L	125-130	81	1300°F, 1 HOURS, A.C. $\triangle_1$
B-8	T - EXTRUSION	L	125-130	79	1300°F, 1 HOURS, A.C. $\triangle_1$
B-8	T - EXTRUSION $\triangle_6$	L	125-130	74	1300°F, 1 HOURS, A.C. $\triangle_7$
B-8	T - EXTRUSION	L	125-130	72	1300°F, 1 HOURS, A.C. $\triangle_7$
B-8	T - EXTRUSION	L	125-130	74	1300°F, 1 HOURS, A.C. $\triangle_7$
B-8	T - EXTRUSION	L	125-130	73	1300°F, 1 HOURS, A.C. $\triangle_7$
B-8	T - EXTRUSION	L	125-130	70	1300°F, 1 HOURS, A.C. $\triangle_7$
B-8	T - EXTRUSION	L	125-130	61	1300°F, 1 HOURS, A.C. $\triangle_7$
B-8	T - EXTRUSION	L	125-130	61	1300°F, 1 HOURS, A.C. $\triangle_7$
B-8	T - EXTRUSION	L	125-130	71	1300°F, 1 HOURS, A.C. $\triangle_7$
B-8	T - EXTRUSION	L	125-130	66	1300°F, 1 HOURS, A.C. $\triangle_7$

NOTES:

- $\triangle_1$  GROUP NO. 1 FOR STATISTICAL ANALYSIS  
 $\triangle_2$  GROUP NO. 2 FOR STATISTICAL ANALYSIS  
 $\triangle_3$   $F_{tu}$  (ESTIMATED  $F_{ty} = 125$  KSI)

- $\triangle_4$  MAY BE AN AVERAGE OF SEVERAL TEST POINTS  
 $\triangle_5$  AVERAGE OF 5 TEST POINTS (77.8 - 90.3)  
 $\triangle_6$  THIN SECTION  
 $\triangle_7$  SUB-SIZE SPECIMEN, CONSERVATIVE VALUE



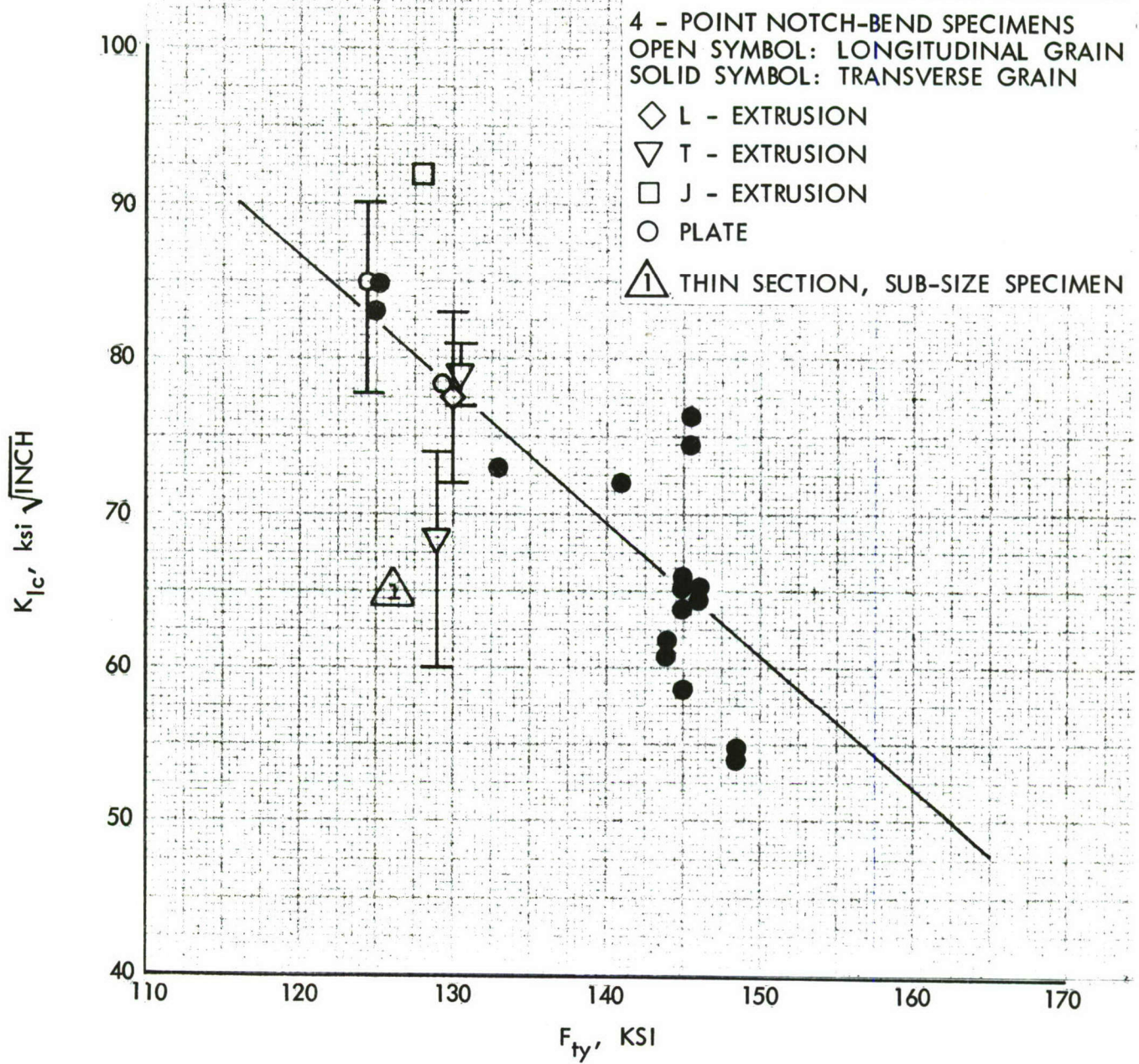


FIGURE B-2  $K_{Ic}$  VERSUS TENSILE YIELD STRENGTH, Ti-6Al-4V MILL ANNEALED

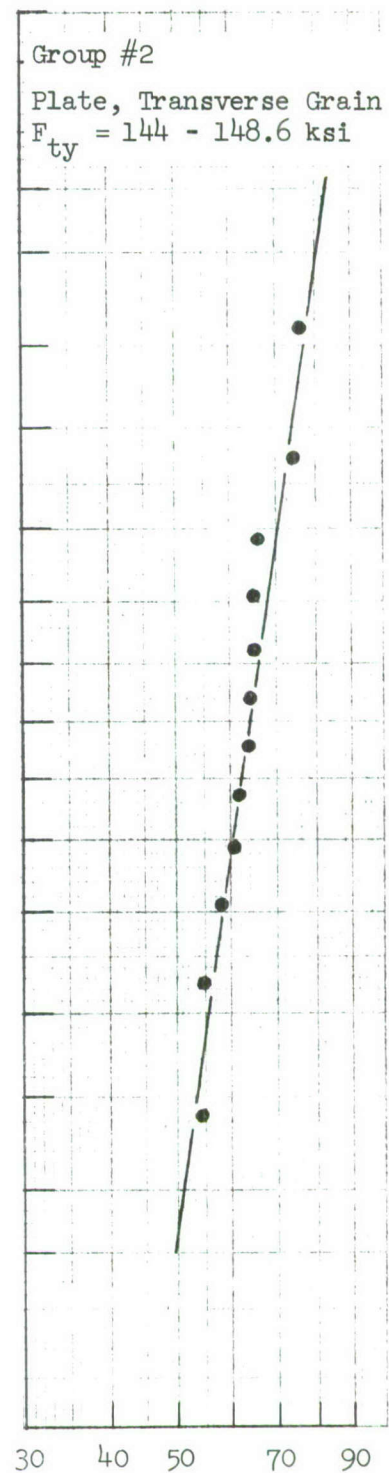
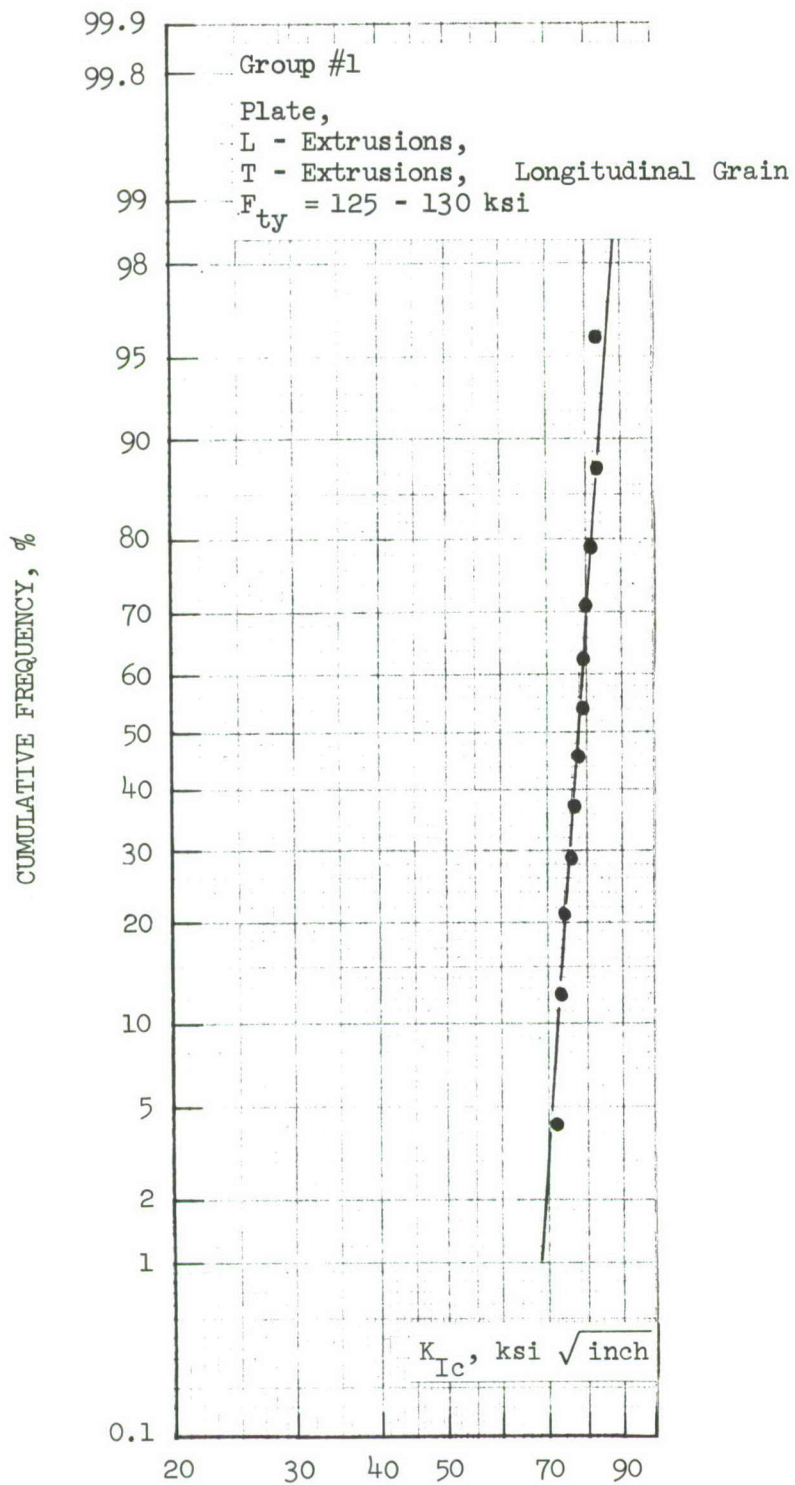


FIGURE B-3 FOUR-POINT NOTCHED-BEND  $K_{Ic}$  DATA FOR Ti-6Al-4V MILL ANNEALED, LOG-NORMAL DISTRIBUTION

from the following equations:

- (1) The sample mean

$$\bar{X} = 10^{1/n \sum \log X_i} \quad (B-1)$$

where  $X_i$  are single observations equivalent to  $K_{Ic}$ .

- (2) The tolerance for the mean (the lower limit of confidence band containing the true or population mean) is

$$\bar{X}_{\alpha/S} = \bar{X} \cdot 10^{-\left(\log S \cdot \frac{t_{\alpha, n-1}}{\sqrt{n}}\right)} \quad (B-2)$$

where  $n$  = sample size

$$\log S = \sqrt{\frac{1}{n-1} \sum (\log X_i - \log \bar{X})^2}$$

- (3) The minimum value is

$$\log X_{\min} = \log \bar{X}_{\alpha/S} - \log S \cdot t_{\alpha', n-1} \quad (B-3a)$$

or

$$X_{\min} = \bar{X} \cdot 10^{-(t_{\alpha', n-1} + \frac{t_{\alpha, n-1}}{\sqrt{n}}) \log S} \quad (B-3b)$$

- (4) If the population standard deviation ( $\sigma$ ) is known, Equations B-2 and B-3b become:

$$\bar{X}_{\alpha/\sigma} = \bar{X} \cdot 10^{-(\log \sigma \cdot K_{\alpha})/\sqrt{n}} \quad (B-4)$$

- (5) and

$$X_{\min} = \bar{X} \cdot 10^{-(K_{\alpha'} + \frac{K_a}{\sqrt{n}}) \log \sigma} \quad (B-5)$$



Using the above equations, the sample statistics and the statistics based on an assumed value for the log  $\sigma$  were calculated and summarized in Table B-2. The value of log  $\sigma = 0.05$  is considered typical for the Ti-6Al-4V material based on statistical analysis of data given in Reference B-9. For comparison purposes the  $K_{Ic}$  allowables were calculated using MIL-HDBK-5 B values basis (Reference B-2) and  $\bar{X} - 3$  sigma basis. The  $\bar{X} - 3$  sigma values are somewhat lower than MIL-HDBK-5B values. The data were not considered sufficient to calculate A basis values, i.e.,  $\alpha = 0.99$ ,  $\alpha' = 0.95$ .

The effect of loading rate on the plain strain fracture toughness properties is shown in Figures B-4 and B-5 for two titanium alloys. These data indicate that the loading rate effect on  $K_{Ic}$  is rather small at room temperature but is significant at a reduced temperature of  $-65^{\circ}\text{F}$  for loading rates less than 2 ksi/sec.

### 1.2 7075-T6 Aluminum Alloy

The fracture toughness data of 7075-T6 aluminum were reviewed to provide an indication of the scatter characteristics on the fracture toughness properties of aluminum alloys, since very little data was available for 7075-T6 aluminum alloy. The plane strain,  $K_{Ic}$  data from two sources are summarized in Table B-3. The  $K_{Ic}$  data for the longitudinal and transverse grain directions plotted in Figure B-6 shows that a log normal distribution provides a good fit to the data. The average  $K_{Ic}$  values are 31.12 and 28.94 ksi  $\sqrt{\text{inch}}$  for the longitudinal and transverse grain directions, respectively.

Statistical analysis of the data is summarized in Table B-4. For this analysis it was assumed the log  $S = \log \sigma = 0.04$ . This analysis gives MIL-HDBK-5 B basis  $K_{Ic}$  values of 26.48 and 23.68 ksi  $\sqrt{\text{inch}}$  for the longitudinal and transverse grain directions, respectively.

### 1.3 D6AC Steel Alloy

Compact tension  $K_{Ic}$  data were obtained from Reference B-1 which compiled all the D6AC data generated under a multilaboratory experimental program. The specimens were machined from either plates or forgings of two different sizes (either 0.8 or 1.5 to 1.8 inches thick). The plates or forgings were heat-treated to obtain

TABLE B-2 SUMMARY OF Ti-6Al-4V MILL ANNEALED  $K_{Ic}$  ALLOWABLE DATA

TEST GROUP	$K_{Ic}$ - Data (ksi $\sqrt{\text{in.}}$ )			Sample Statistics				Statistics for $\text{Log } \sigma = .05$				$K_{Ic}$ Allowables	
	Min.	$\bar{X}$	Max.	Log S	$\bar{X}_{.9/S}$ ksi $\sqrt{\text{in.}}$	$X_{\text{min.}}$ (S) ksi $\sqrt{\text{in.}}$	Log $\sigma$	$\bar{X}_{.9/\sigma}$ ksi $\sqrt{\text{in.}}$	$X_{\text{min.}}$ ( $\sigma$ ) ksi $\sqrt{\text{in.}}$	MIL-HDBK-5 B Value * ksi $\sqrt{\text{in.}}$	$\bar{X} - 3 \text{ Sigma}$ ksi $\sqrt{\text{in.}}$		
#1 $F_{ty} = 125-130$ ksi	72.0	77.9	83.0	.0204	76.6	70.5	0.05	74.6	61.8	69.84	67.0		
#2 $F_{ty} = 144-148.6$ ksi	54.2	63.7	76.3	.0435	61.3	51.2	0.05	61.1	50.5	48.8	43.5		

\*  $\alpha = 0.90$ ,  $\alpha' = 0.95$

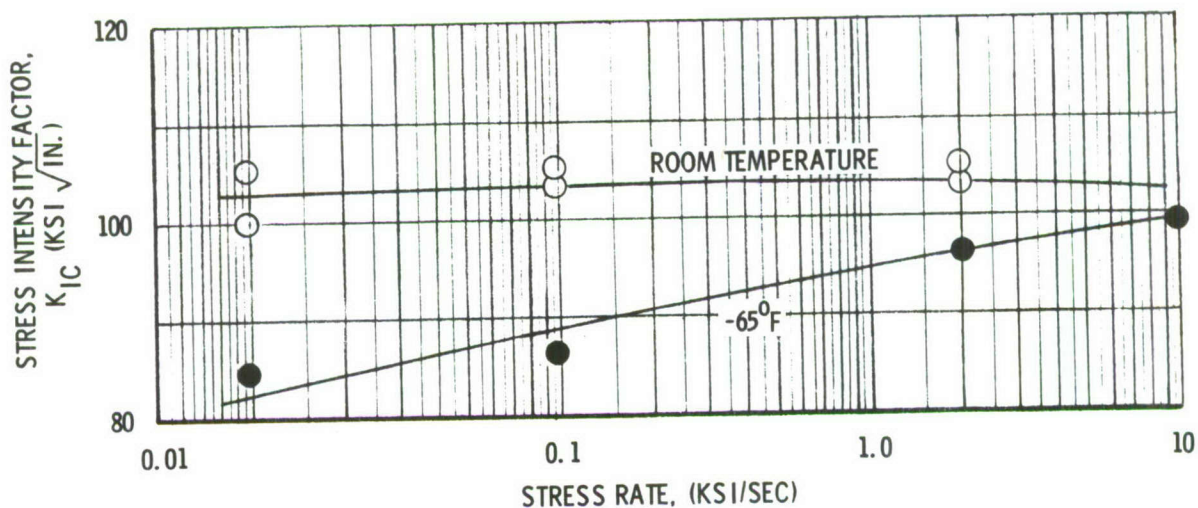


FIGURE B-4 EFFECT OF STRESS RATE ON  $K_{IC}$  FOR Ti-6Al-4V, Beta-STA-1250 (REFERENCE B-3)

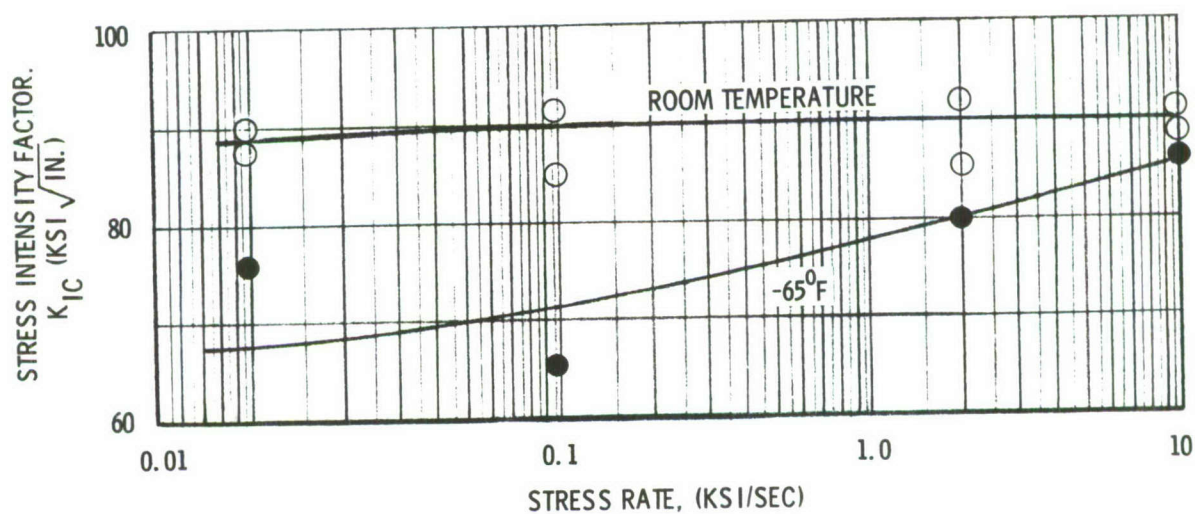


FIGURE B-5 EFFECT OF STRESS RATE ON  $K_{IC}$  FOR Ti-4Al-3 Mo-1V, Beta-STA-1150 (REFERENCE B-3)



TABLE B-3 FOUR-POINT NOTCHED-BEND  $K_{Ic}$  VALUES FOR 7075-T6 ALUMINUM ALLOY

Ref. No.	PRODUCT	GRAIN DIRECTION	$F_{ty}$ ksi	$K_{Ic}$ (ksi $\sqrt{\text{inch}}$ )	REMARKS
B-10	1-3/8" Plate	L	76.6	33.08	Lot No. 1
			76.6	33.12	Lot No. 1
			76.6	32.64	Lot No. 1
			80.3	29.51	Lot No. 2
			80.3	27.88	Lot No. 2
			80.3	26.21	Lot No. 2
			78.5	28.62	Lot No. 3
			78.5	32.36	Lot No. 3
			78.5	31.74	Lot No. 3
		T	73.6	29.14	Lot No. 1
			73.6	27.50	Lot No. 1
			73.6	27.95	Lot No. 1
			73.6	28.67	Lot No. 1
			77.4	32.98	Lot No. 2
			77.4	31.83	Lot No. 2
			77.4	29.64	Lot No. 2
			77.4	31.76	Lot No. 2
B-10	1-3/8" Plate	T	76.0	26.80	Lot No. 3
			76.0	27.31	Lot No. 3
			76.0	24.77	Lot No. 3
B-11	Clad Plate	L	74	31	Heat No. 55109
			↓	31	Heat No. 55109
			74	28	Heat No. 55109
				31	Heat No. 55109
			76	29	Heat No. 93034
			↓	33	Heat No. 93034
				35	Heat No. 93034
B-11	Clad Plate	L	76	34	Heat No. 93034
				33	Heat No. 93034

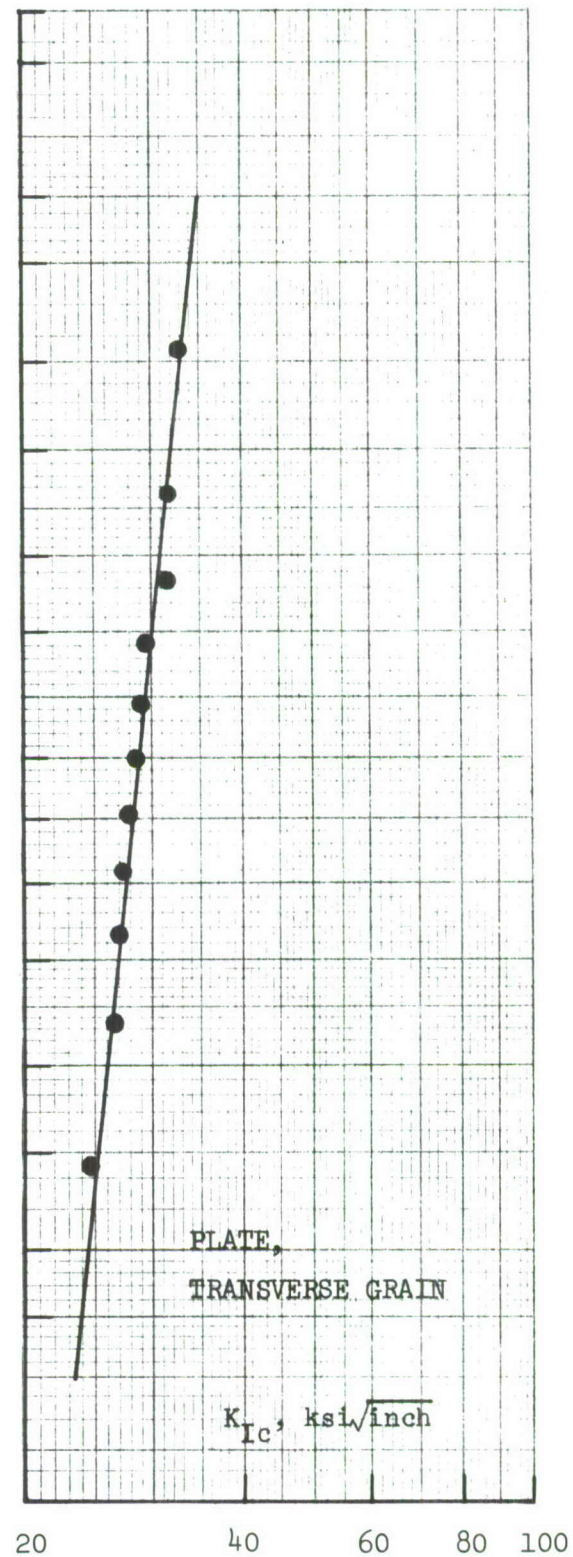
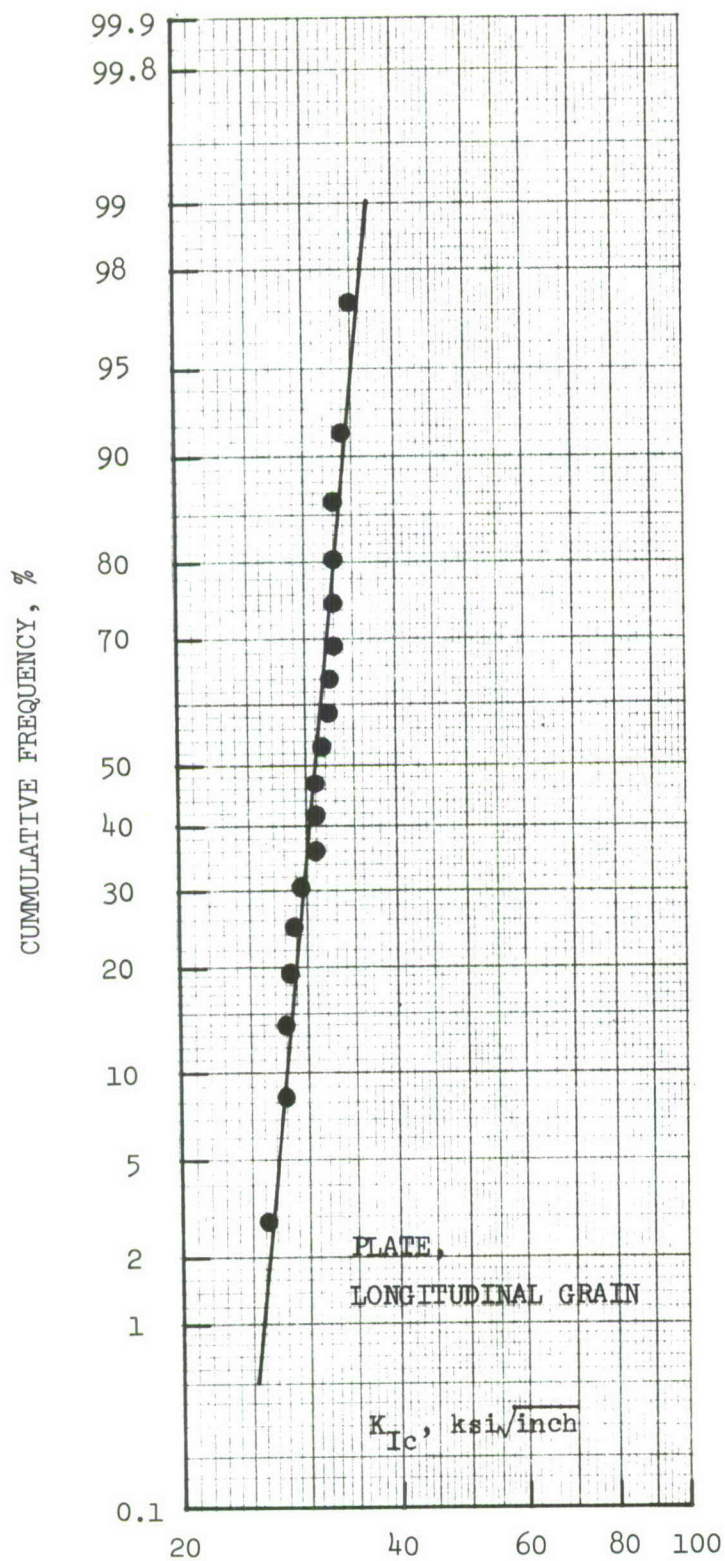


FIGURE B-6. FOUR-POINT NOTCHED-BEND  $K_{Ic}$  DATA FOR 7075-T6 ALUMINUM ALLOY, LOG-NORMAL DISTRIBUTION

TABLE B-4 7075-T6 ALUMINUM  $K_{Ic}$  ALLOWABLE DATA

GRAIN DIR.	$K_{Ic}$ - Data ( $\text{ksi}\sqrt{\text{in.}}$ )			Sample Statistics				$K_{Ic}$ Allowables	
	Min.	$\bar{X}$	Max.	Log S = Log $\sigma$	$X_{.9/S} = X_{.9/\sigma_2}$ $\text{ksi}\sqrt{\text{inch}}$	$X_{\min}(S) = X_{\min}(\sigma)$ $\text{ksi}\sqrt{\text{inch}}$	MIL-HDBK-5 B Value $\text{ksi}\sqrt{\text{inch}}$	X - 3 Sigma $\text{ksi}\sqrt{\text{inch}}$	
L	26.21	31.12	35.00	0.04 **	30.3	26.0	26.48	24.07	
T	24.77	28.94	32.98	0.04 *	27.95	24.0	23.68	22.01	

\*\* Computed Log S = 0.0384

\* Computed Log S = 0.03585



### 1.3 D6AC Steel Alloy (Continued)

the same tensile strength properties by eight different operational procedures. Summaries of the heat-treat methods and the  $K_{IC}$  data are listed in Tables B-5 and B-6, respectively.

In reviewing Table B-6 data it was observed that the variation in the  $K_{IC}$  values were mainly attributed to the effects of material thicknesses and the two distinguishable quenching methods, 140°F oil versus 325° - 400°F salt. It was also shown that differences in  $K_{IC}$  values between product forms (plate or forging) were probably insignificant. With this in mind, the 12 sets of data listed in Table B-6 were grouped in 7 groups and new average values, and statistically based MIL-HDBK-5 B-scale values were computed. The results are listed in Table B-7 and are also plotted in Figure B-7.

### 2.0 $K_C$ Data

Currently the MIL-HDBK-5 Residual Strength Task Group recommends guidelines for obtaining plane stress and mixed mode fracture toughness properties from tests conducted on center cracked panels. Generally valid data will be obtained if the crack size is approximately 1/4 to 1/3 of the panel width and the width of the panel is sufficiently large (generally 24 inches wide or more) so that the stress across the net section at failure is less than the yield strength of the material. The  $K_C$  data obtained for Ti-6Al-4V annealed and 7075-T6 aluminum are presented and discussed below.

#### 2.1 Ti-6Al-4V Mill Annealed

Some typical  $K_C$  fracture toughness data are plotted in Figures B-8 and B-9 for two panel widths. The data display technique shown on Figures B-8 and B-9 are discussed in Reference B-16 and are in agreement with that being proposed by the MIL-HDBK-5 Residual Strength Task Group. The  $K_C$  value is obtained by finding the best fit  $K_C$  curve over the region from  $F_g = 2/3 F_{ty}$  to  $2a = W/3$ . The data outside these limits will generally fall approximately on the lines drawn from these tangency points on the  $K_C$  curve to  $F_g = F_{ty}$  and  $2a = W$  as shown in the figures.

TABLE B-5 HEAT TREAT METHODS VS. HEAT TREAT OPERATIONS  
FOR DCAC STEEL

Heat Treat Operation △2	Heat Treat Methods △1							
	A	B	C	D	E	F	G	H
Austenitizing	1700 ± 25°F △3		1650 ± 25°F △3			1650 ± 25°F △3		
Ausbay (Interrupted) Quenching	Cooled from austenitizing temperature to 975 ± 25°F in austenitizing furnace and held at 975 ± 25°F until material stabilized at this temperature. (Note: Cooling rate between 1350 and 1150°F must not be less than 6°F per minute.)							
Quenching	140°F Oil △4 (a) △4 (a)		Salt △4 325°F   325°F   400°F (b) △4 (c) △4 (b)			Salt △4 400°F   400°F   375°F (c) △4 (b) △4 (b)		
Tempering	Double tempered at 1025°F; held at temperature for 2 hours per cycle.							

NOTES:



Methods reported in Reference (B-12) for correlating fracture toughness as a function of quenching medium material thickness and quench medium circulation rate.



Detail heat treat operations per Reference (B-13)



Held at temperature for 1 hour per inch of thickness.



The quench medium circulation rates described in Reference (B-12) have the following conotation:

- a. "Good" denotes test material heat treated without a fixture.
- b. "Fair" denotes test material heat treated in a fixture with 1/2-inch spacers between the test material and the fixture.
- c. "Poor" denotes test material heat treated in a fixture with 1/4-inch spacers between the test material and the fixture.

TABLE B-6 SUMMARY OF D6AC STEEL  $K_{Ic}$  DATA

Thickness (inch)	Product Form	Quench Medium	Avg. $K_{Ic}$ (ksi $\sqrt{\text{inch}}$ )	Number of Specimens
.8	Forging	E 400°F Salt	65.3	60
.8	Plate	E 400°F Salt	64.5	100
.8	Plate	C 325°F Salt + Agitation	81.8	4
.8	Plate	F 400°F Salt	53.8	12
.8	Plate	A 140°F Oil	94.6	25
.8	Forging	A 140°F Oil	96.9	26
1.5 - 1.8	Forging	G 400°F Salt	43.8	6
"	Forging	H 375°F Salt + Agitation	49.4	14
"	Plate	H 375°F Salt + Agitation	61.3	20
"	Plate	D 325°F Salt + Agitation	47.0	3
"	Plate	B 140°F Oil	79.1	5
"	Forging	B 140°F Oil	89.6	8



TABLE B-7 D6AC STEEL  $K_{Ic}$  ALLOWABLE DATA

Thickness (inch)	Heat Treat Method	Prod. Form	No. of Heats	Number of Specimens	$K_{Ic}$ Max. ksi $\sqrt{\text{in.}}$	$K_{Ic}$ Avg. ksi $\sqrt{\text{in.}}$	$K_{Ic}$ Min. ksi $\sqrt{\text{in.}}$	S*	$K_{Ic}$ MIL-HDBK-5 ksi $\sqrt{\text{in.}}$	B Scale
.8	A	P	3	25	101.69	94.56	83.27	3.76	87.65	
1.5-1.8	B	P&F	2	13	98.47	85.64	64.09	9.88	64.35	
.8	C, E, F	P	6	116	89.45	63.95	37.81	12.63	44.92	
1.5-1.8	D, H	P	3	23	81.07	59.47	40.16	14.07	33.17	
.8	A	F	7	26	109.40	96.93	84.79	5.66	86.61	
.8	E	F	2	60	96.34	65.25	50.30	11.86	46.17	
1.5-1.8	G, H	F	3	20	75.74	47.68	39.28	7.73	32.79	

\* S = Sample standard deviation.

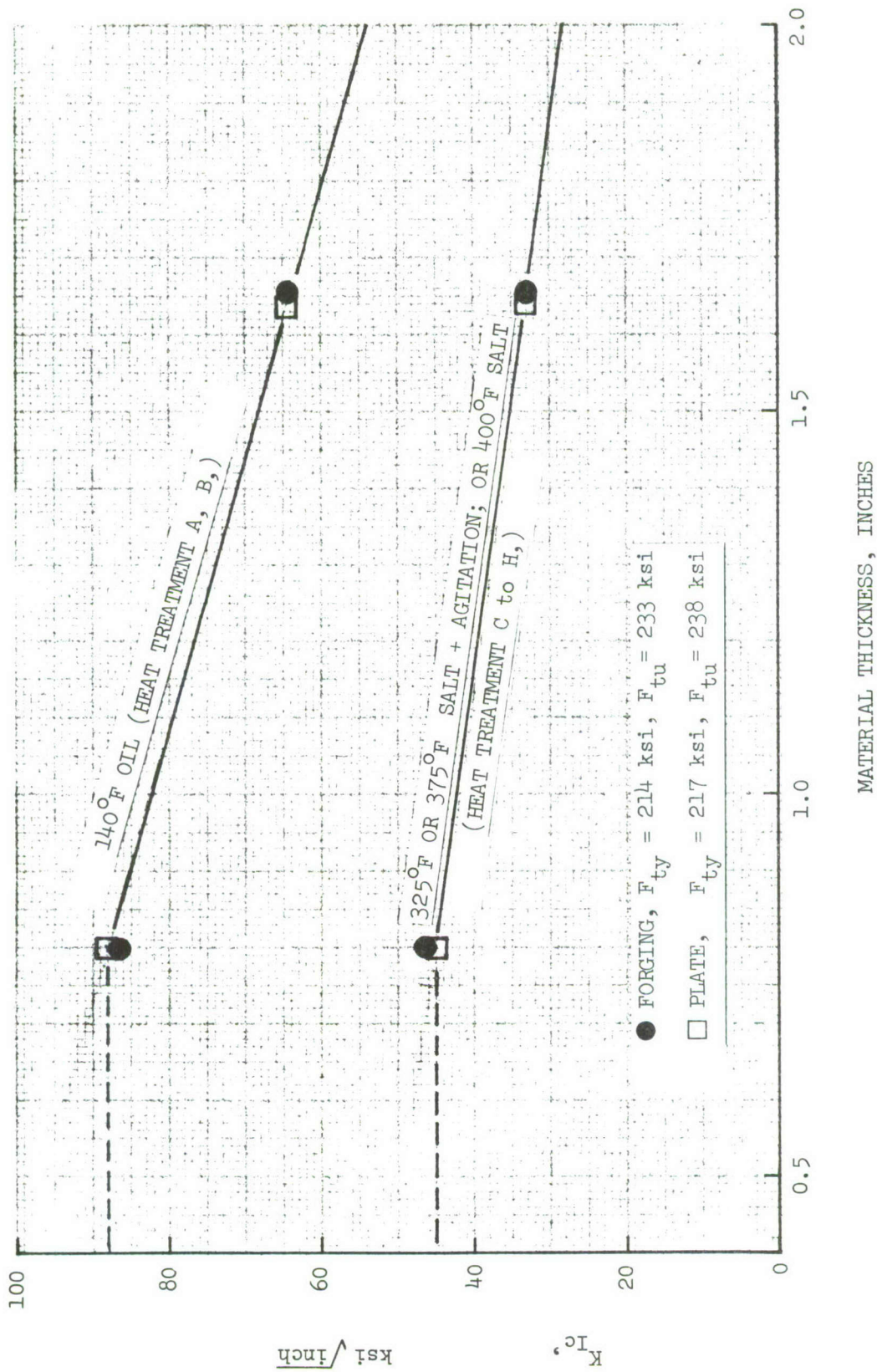


FIGURE B-7. MIL-HDBK-5 B-SCALE  $K_{Ic}$  VALUES FOR D6AC STEEL AS A FUNCTION OF HEAT TREATMENT



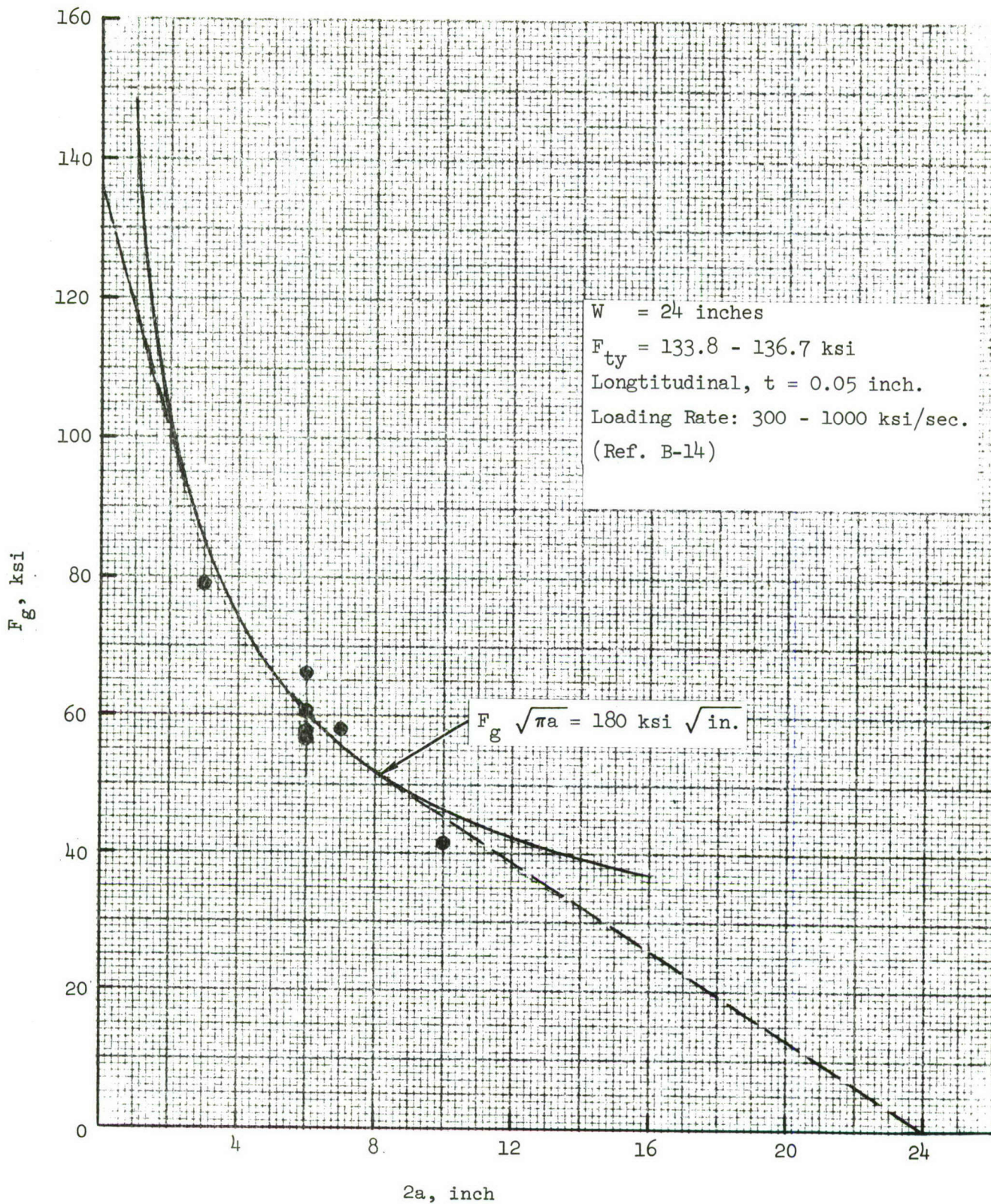


FIGURE B-8 RESIDUAL STRENGTH FOR Ti-6Al-4V MILL ANNEALED,  $W = 24 \text{ IN.}$



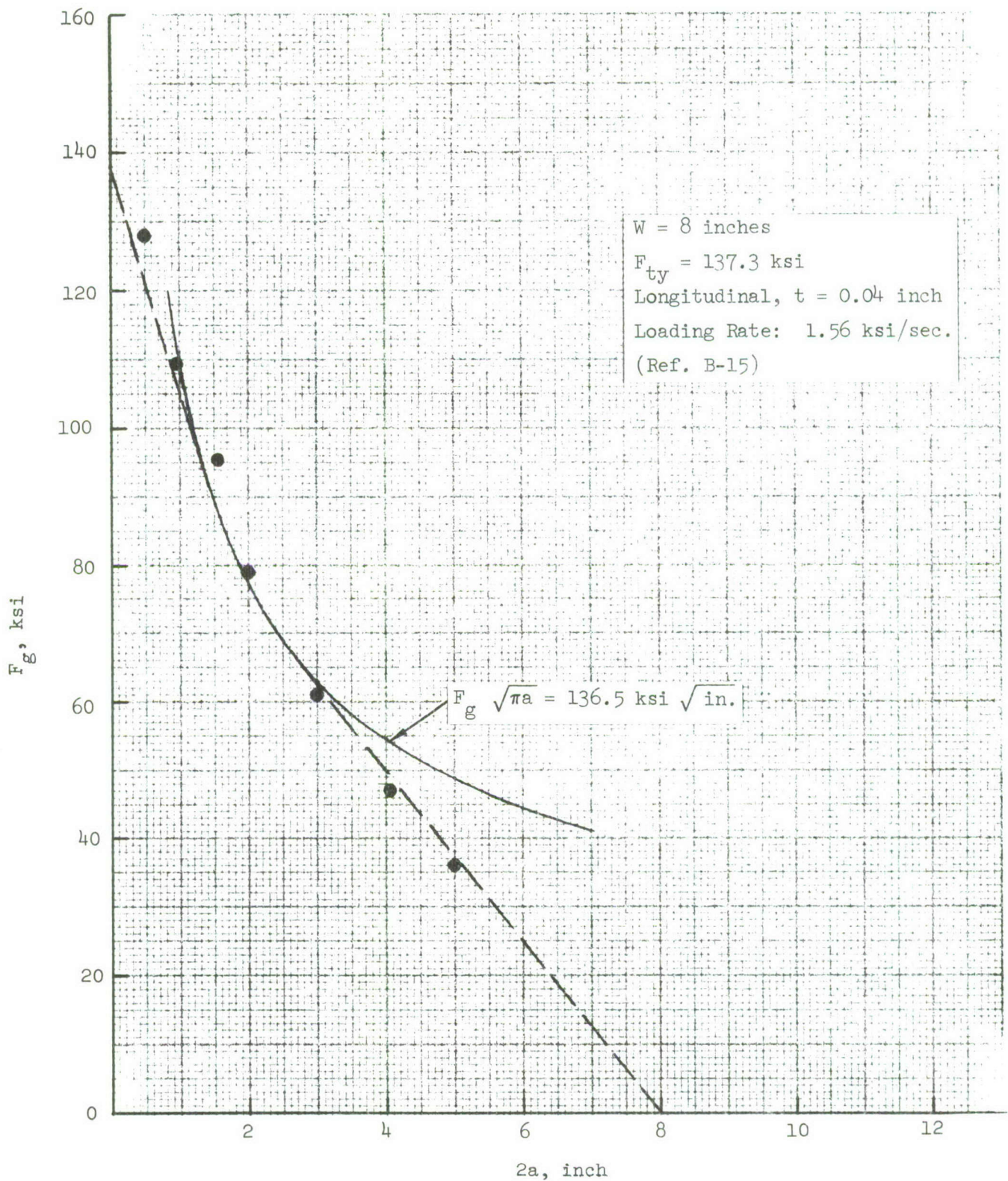


FIGURE B-9. RESIDUAL STRENGTH FOR Ti-6AL-4V MILL ANNEALED,  $W = 8$  IN.

$K_C$  data for various thicknesses of materials are summarized in Table B-8. The data includes four nominal gage thicknesses, 0.025, 0.05 (0.05 - 0.063), 0.125 and 0.21 inch tested over a wide range of loading rates (from 100 psi/sec to  $10^6$  psi/sec). The effect loading rate has on the  $K_C$  value is illustrated in Figures B-10 thru B-13. These figures show that  $K_C$  values generally increased as the loading rate increased. However, for the majority of the data the effect of loading rate was negligible up to a loading rate of 100,000 psi/sec. Therefore, the data can be conveniently divided into two groups; i.e.,  $K_C$  for  $\dot{f}_g > 100$  ksi/sec. and  $K_C$  for  $\dot{f}_g \leq 100$  ksi/sec.

The data in Table B-8 was separated into four groups ( $\dot{f}_g > 100$  ksi/sec,  $\dot{f}_g \leq 100$  ksi/sec, longitudinal grain, and transverse grain) and plotted in Figure B-14 as a function of thickness. The curves were extrapolated to a  $K_{IC}$  values of 74 and 63.5 ksi  $\sqrt{\text{inch}}$ . These B values of  $K_{IC}$  were determined by interpolation for a tensile yield strength of 135 ksi which is considered typical for the test panels. The maximum  $K_C$  values are obtained in the thickness range of 0.1 - 0.2 inch. The scatter in data is considered typical except for the 0.024 inch transverse grain,  $\dot{f}_g \leq 100$  ksi/sec which is rather large. The data for thin gages is not considered to be as reliable because localized bending in the vicinity of the crack tip may have affected the results even though buckling guides were utilized during testing.

## 2.2 7075-T6 Aluminum Alloy

$K_C$  data for clad and bare 7075-T6 aluminum alloy data are given in Tables B-9 and B-10 for various thicknesses of material. The data for the various thicknesses of material are plotted in Figures B-15 and B-16 with typical curves drawn thru the data points. The curves were drawn to  $K_{IC}$  values of 30 and 27.5 ksi  $\sqrt{\text{inch}}$  for the longitudinal and transverse grain directions, respectively. These  $K_{IC}$  values are approximately equal to the  $\bar{X}_{0.9/S}$  values given in Table B-4. The scatter of data shown in Figures B-15 and B-16 can be considered typical for 7000 series aluminum alloys.



TABLE B-8  $K_c$  DATA FOR Ti-6Al-4V MILL ANNEALED

3

Ref. No.	t (inch)	W (inch)	GRAIN DIR.	$f_g$ (psi/sec)	2a (inch)	$F_g$ (ksi)	$F_{ty}$ (ksi)	$F_g \sqrt{\pi a}$ (ksi√in.)	REMARKS
B-17	.022	24	L	$1.42 \times 10^6$	6.0	60.337	136.6	184.63	
B-18	.025	8	L	$1.2 \times 10^3$	2.01	57.2	141.7	101.	Heat D2963
"	"	"	L	"	2.00	56.4	"	100.	"
"	"	"	L	"	2.01	58.9	"	104.	Heat D2963
								102 Avg.	
B-17	.025	8	T	$.76 \times 10^6$	1.98	75.584	127.0	133.78	
"	.026	"	"	$.83 \times 10^6$	2.0	76.332	127.0	135.10	
								133.4 Avg.	
B-17	.025	8	T	$1.25 \times 10^3$	1.27	110.0	129.9	155.10	Heat M5900
					1.49	109.9		167.04	"
					2.77	82.8		172.22	"
					3.03	77.3		167.74	"
					1.27	70.6	138.2	99.54	Heat D2963
					1.52	79.9		123.04	"
					2.52	53.4		105.73	"
					3.01	53.7		116.52	"
					1.32	76.8	139.0	109.82	Heat D2133
					1.51	65.7		100.52	"
					2.64	52.8		107.18	"
					3.01	45.4		98.51	"
B-18	.025	8	T	$1.25 \times 10^3$	2.01	102.2	129.9	180.89	Heat M5900
				"	2.02	96.8		172.30	"
				$.835 \times 10^2$	2.01	92.2		163.19	"
				$1.67 \times 10^4$	1.99	93.8		166.02	"
				$.835 \times 10^2$	2.0	56.8	138.2	100.53	Heat D2963
				"	2.01	54.6	139.0	96.64	Heat D2133
				$1.67 \times 10^4$	2.01	64.6	138.2	114.34	Heat D2963
				"	2.01	55.8	139.0	98.76	Heat D2133
				$1.25 \times 10^3$	2.0	66.1	138.2	116.99	Heat D2963
				"	1.99	66.0	138.2	116.82	"
				"	2.01	61.8	139.0	109.38	Heat D2133
				"	2.0	60.9	139.0	107.79	"
								129.00 Avg.	
B-18	.025	8	T	Fatigue Cycle to Failure	5.8	25	138.2	75.25	
					5.2		138.2	71.25	
					5.0		139.0	70.00	
					4.8		139.0	68.50	
					5.6	25	138.2	74.00	
					6.0		138.2	76.50	
					5.4		139.0	72.75	
					6.0		139.0	76.50	
B-19	.04	8	L	$1.56 \times 10^3$	2.02	78.7	137.3	140.0	
				"	3.03	61.2	137.3	133.0	
								136.5 Avg.	

1

R = 0.1

3

Guided

B-21

2


R = 0.6




TABLE B-8 (Cont'd.)

Ref. No.	t (inch)	W (inch)	GRAIN DIR	$\dot{f}_g$ (psi/sec)	2a (inch)	$F_g$ (ksi)	$F_{ty}$ (ksi)	$F_g \sqrt{\pi a}$ (ksi $\sqrt{\text{in.}}$ )	REMARKS
B-19	.04	8	L	1.56x10 <sup>3</sup>	0.48 0.952 1.55 4.05 5.02	128.0 109.5 95.5 47.2 36.2	137.3 " " " "	111.0 133.5 148.5 118.5 101.5	
B-3	.063 .060 .065	12	T	1.0x10 <sup>3</sup> .97x10 <sup>3</sup> .175x10 <sup>3</sup> .152x10 <sup>3</sup> 9.92x10 <sup>3</sup> 9.98x10 <sup>3</sup>	4.22 4.20 4.18 4.22 4.22 4.19	60.0 56.0 59.3 59.0 68.7 68.0	137.7 " 136.0 " " "	154.1 143.5 150.0 151.5 176.2 174.0	Heat D7166 " Heat D7658 " " "
								158.1 Avg.	
B-17	.05	24	T	4.99x10 <sup>3</sup> 4.93x10 <sup>3</sup> 4.75x10 <sup>3</sup> 4.86x10 <sup>3</sup>	6.0 6.0 6.0 6.01	51.467 52.125 47.0 51.448	133.8 133.8 136.0 136.0	157.48 159.50 142.82 157.43	Heat D5257 " Heat D5256 "
								154.56 Avg.	
B-18	.05	8	T	1.25x10 <sup>3</sup>	2.04 2.01 2.03 2.04	69.8 68.2 66.4 68.4	139.9 139.9 138.3 138.3	124.24 120.71 118.19 121.75	
								121.22 Avg.	
B-17	.05	24	T	.52x10 <sup>6</sup> .57x10 <sup>6</sup> 1.02x10 <sup>6</sup> .97x10 <sup>6</sup> 1.04x10 <sup>6</sup>	6.0 6.0 6.0 6.01 6.0	55.527 51.937 58.777 57.131 59.425	133.8 133.8 136.0 136.0 132.2	169.91 158.92 179.85 174.82 181.84	Heat D5257 " Heat D5256 " Heat D4949
								173.1 Avg.	
B-17	.05	8	T	1.02x10 <sup>6</sup> .96x10 <sup>6</sup> " " .94x10 <sup>6</sup> .97x10 <sup>6</sup> 1.12x10 <sup>6</sup> 1.14x10 <sup>6</sup> 1.15x10 <sup>6</sup>	1.98 2.0 1.99 2.0 2.0 2.0 2.0 2.0 2.0	88.02 95.341 92.765 86.335 86.845 88.123 87.35 87.92 91.957	133.8 136.0 132.2 132.2 132.2 132.2 132.2 132.2 132.2	154.91 168.75 164.19 152.81 153.71 155.97 154.60 155.61 162.76	Heat D5257 Heat D5256 Heat D4949 " " " " " "
								158.2 Avg.	
B-17	.05	24	L	.94x10 <sup>5</sup> 4.96x10 <sup>3</sup> .96x10 <sup>3</sup> 4.92x10 <sup>3</sup> 1.05x10 <sup>5</sup> 4.86x10 <sup>3</sup> .54x10 <sup>3</sup> 4.97x10 <sup>3</sup>	5.99 5.99 6.0 6.0 6.0 6.01 5.99 6.01	47.3 47.5 47.5 49.6 53.2 51.8 54.2 51.4	136.5 136.5 136.5 136.5 136.7 136.7 136.7 136.7	144.73 145.4 145.35 152.0 162.7 154.2 165.85 155.5	Heat D5257 " " " Heat D5256 " " "
								153.2 Avg.	

TABLE B18 (Cont'd.)

Ref. No.	t (inch)	W (inch)	GRAIN DIR.	$\dot{f}_g$ (psi/sec)	2a (inch)	$F_g$ (ksi)	$F_{ty}$ (ksi)	$F_g/\sqrt{2a}$ (ksi/ $\sqrt{\text{in.}}$ )	REMARKS
B-17	.05	24	L	$.76 \times 10^6$	6.0	60.7	136.5	185.74	Heat D5257
				$.78 \times 10^6$	6.0	56.6	136.5	173.19	"
				$.83 \times 10^6$	6.0	66.1	136.7	202.26	Heat D5256
				$.33 \times 10^6$	6.0	57.3	136.7	175.33	"
								184.13 Avg.	
B-17	.05	24	L	$.36 \times 10^6$	7.16	57.9	134.2	193.96	Heat D4949
				$.81 \times 10^6$	10.0	41.6	136.5	164.73	Heat D5257
				$1.12 \times 10^6$	3.0	78.8	136.5	170.99	"
	.1235	24	L	$1.04 \times 10^6$	6.04	80.58	134.6	247.38	
	.1267	8	T	$1.09 \times 10^6$	1.98	103.726	139.7	183.59	
	.127	12	T	$.74 \times 10^3$	4.20	63.6	133.0	163.0	
	.129			$1.02 \times 10^3$	4.19	62.6	133.0	160.5	
	.126			$.91 \times 10^3$	4.20	63.6	133.0	163.0	
								162.2 Avg.	
B-17	.212	24	L	$4.1 \times 10^3$	6.01	70.55	129.3	216.57	Heat D4949
	.208			$4.47 \times 10^3$	6.01	66.055	129.3	202.78	
	.2045			$1.07 \times 10^5$	6.01	73.95	129.3	227.03	
	.204			$.90 \times 10^5$	6.01	69.63	129.3	213.74	
								215.03 Avg.	
B-17	.212	24	L	$.72 \times 10^6$	6.0	80.96	129.3	247.74	Heat D4949
	.2175			$.65 \times 10^6$	6.0	76.41	129.3	233.81	
								240.80 Avg.	
B-17	.2115	24	L	$.8 \times 10^6$	3.01	93.105	129.3	202.03	Heat D4949
	.22			$.58 \times 10^6$	10.0	55.325	129.3	219.08	
	.2152	8	T	$.99 \times 10^6$	2.27	81.206	139.6	152.66	
	.211			$.63 \times 10^6$	2.01	87.45	139.6	154.78	
								153.72 Avg.	
B-17	2.16	8	T	$4.6 \times 10^3$	2.12	33.679	139.6	61.29 	

 Data questionable



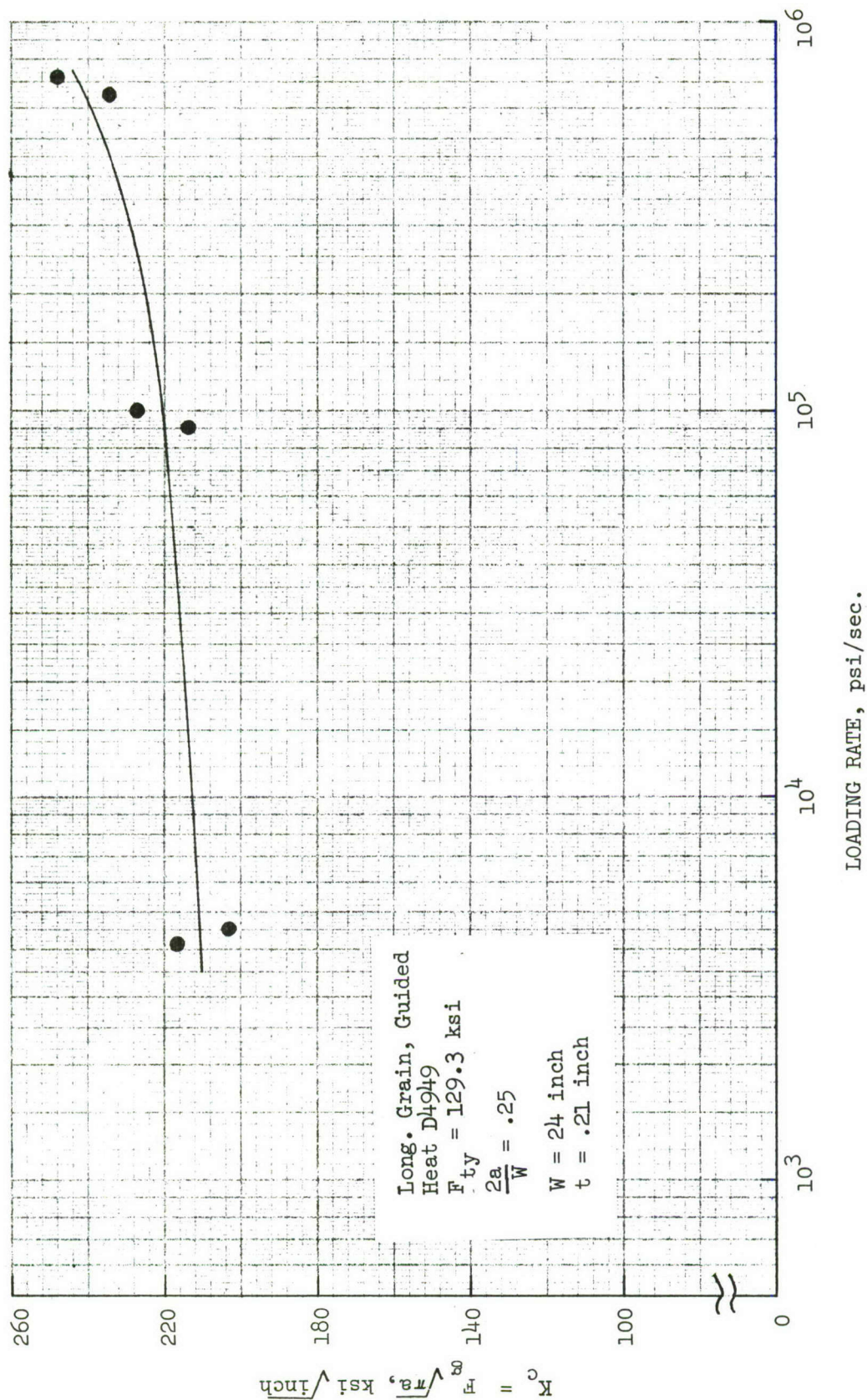


FIGURE B-10. EFFECT OF LOADING RATE ON RESIDUAL STRENGTH OF Ti-6Al-4V MILL ANNEALED, 0.21 INCH THICKNESS PLATE, LONGITUDINAL GRAIN DIRECTION



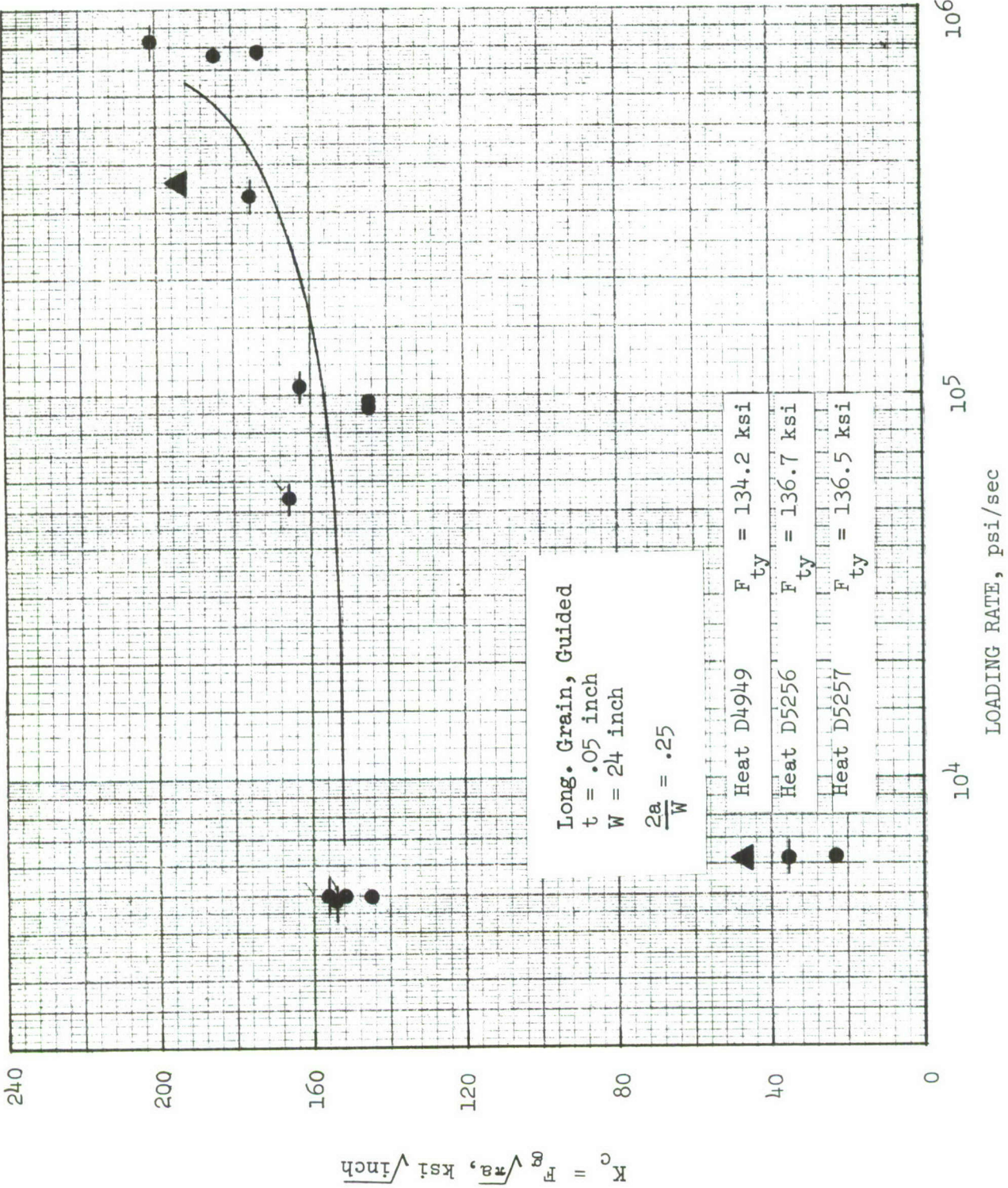


FIGURE B-11. EFFECT OF LOADING RATE ON RESIDUAL STRENGTH OF Ti-6Al-4V MILL ANNEALED, 0.05 INCH THICKNESS SHEET, LONGITUDINAL GRAIN DIRECTION



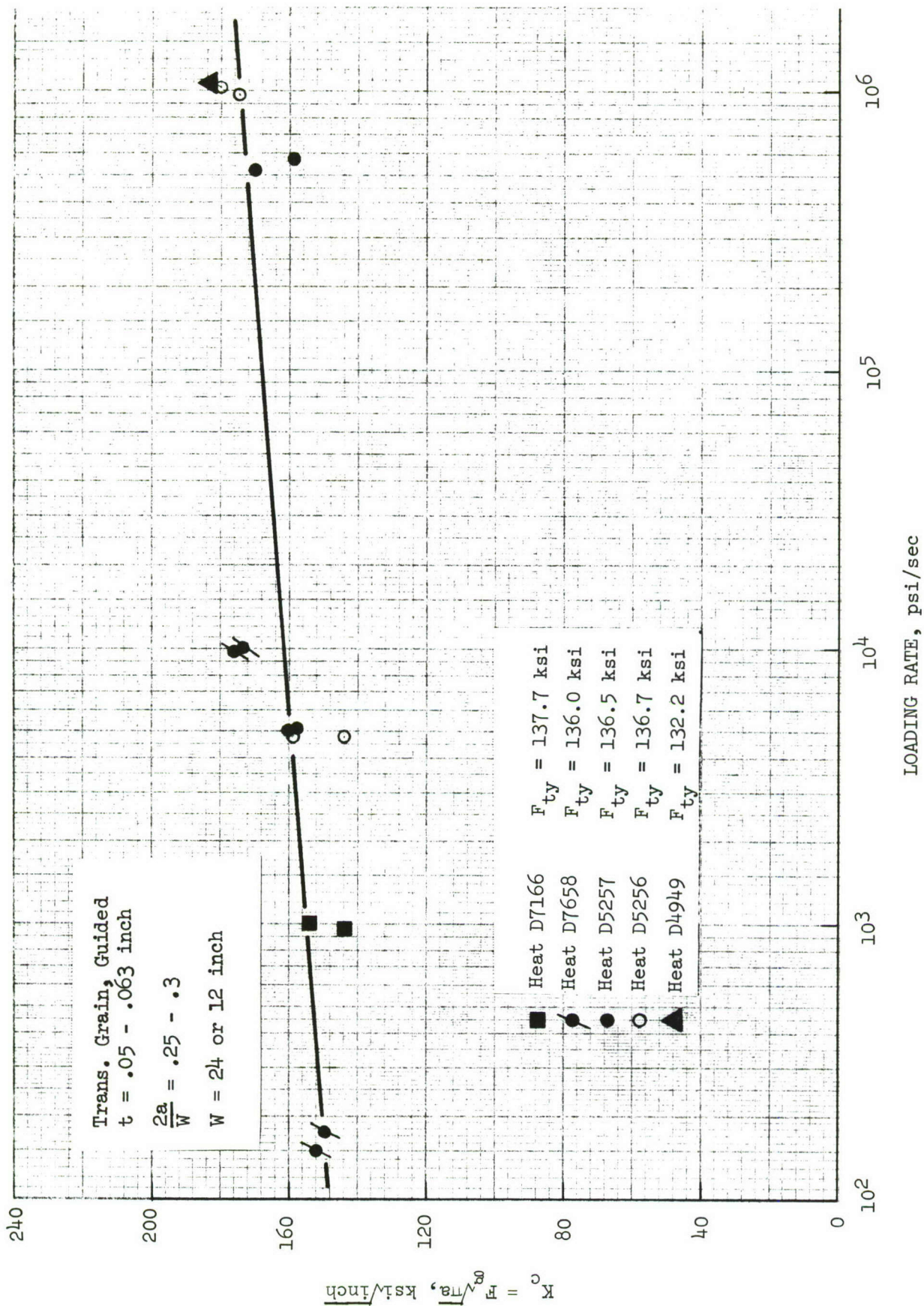


FIGURE B-12. EFFECT OF LOADING RATE ON RESIDUAL STRENGTH OF Ti-6Al-4V MILL ANNEALED, 0.05 - 0.063 INCH THICKNESS SHEET, TRANSVERSE GRAIN DIRECTION

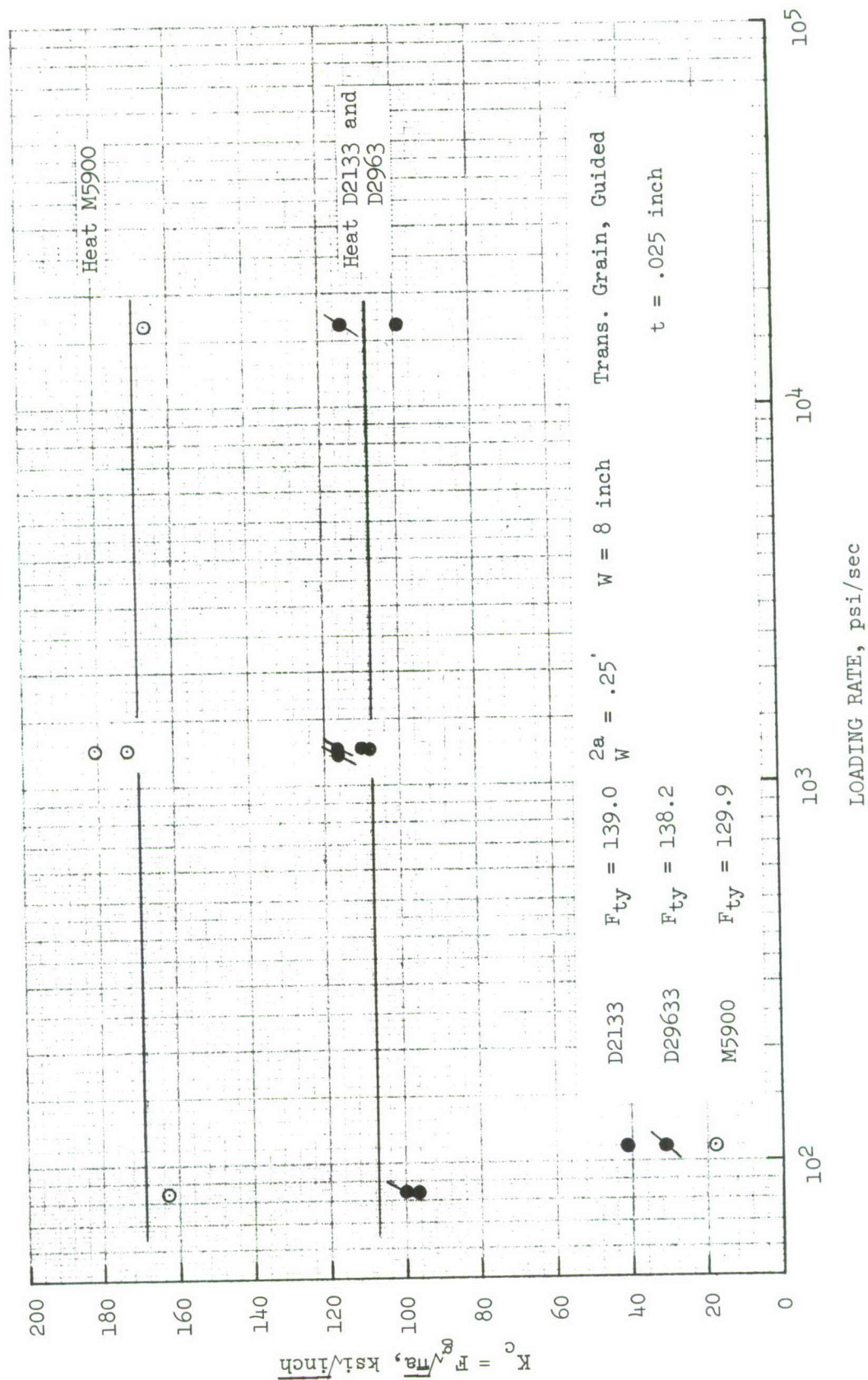


FIGURE B-13. EFFECT OF LOADING RATE ON RESIDUAL STRENGTH OF Ti-6Al-4V MILL ANNEALED, 0.025 INCH THICKNESS SHEET, TRANSVERSE GRAIN DIRECTION



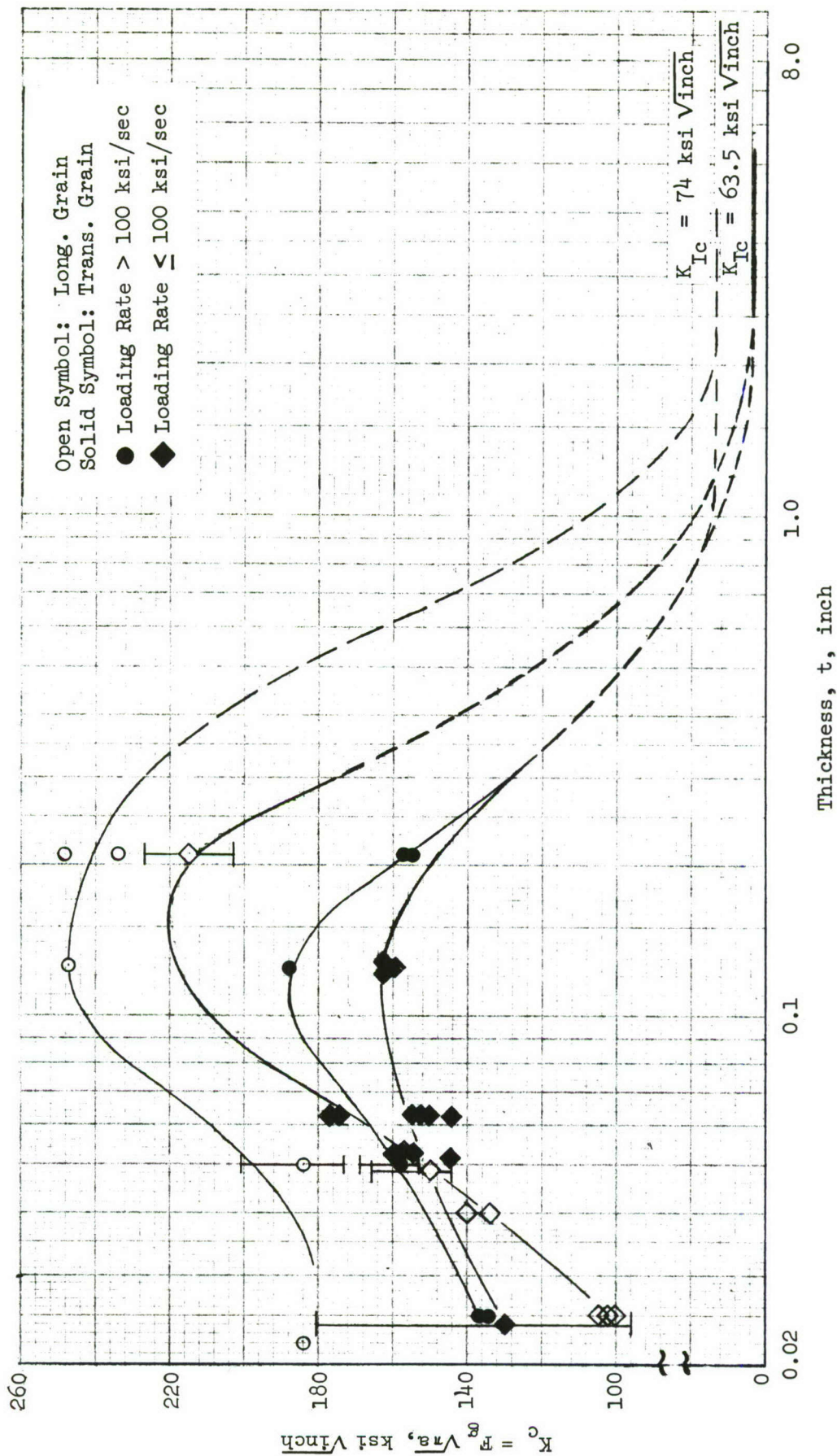


FIGURE B-14 EFFECT OF THICKNESS ON FRACTURE TOUGHNESS OF Ti-6Al-4V MILL ANNEALED

TABLE B-9  $K_c$  DATA FOR 7075-T6 CLAD ALUMINUM ALLOY

Ref. No.	t (inch)	W (inch)	GRAIN DIR.	GUIDED	2a (inch)	$F_g$ (ksi)	$F_{ty}$ (ksi)	$F_g \sqrt{\pi a}$ (ksi $\sqrt{\text{in.}}$ )	REMARKS
B-19	.051	24.0	L	Yes	8.00	22.9		81.1	Heat 1 <span style="border: 1px solid black; padding: 0 2px;">1</span>
	.049		L		8.05	21.1		74.9	Heat 2
	.051		T		8.13	16.5		58.9	Heat 1
	.050		T		7.96	17.6		62.3	Heat 2
	.071		L		8.08	16.4		58.4	Heat 1
	.071		L		8.00	18.2		64.4	Heat 2
	.071		T		8.60	15.1		55.4	Heat 1
	.070		T		8.05	17.8		63.2	Heat 2
	.101		L		8.05	22.1		78.5	Heat 1
	.100		L		8.07	17.5		62.1	Heat 2
	.101		T		7.99	18.2		64.4	Heat 1
	.102		T		8.05	20.8		73.8	Heat 2
B-20	.09	12.0	<span style="border: 1px solid black; padding: 0 2px;">2</span>	Yes	3.44	27.7	75.9	64.3	
					3.18	28.2		62.9	
					3.06	28.2		61.3	
					3.52	28.0		65.5	
					3.02	36.1		78.3	
					3.56	25.1		59.2	
	.1	36.0	<span style="border: 1px solid black; padding: 0 2px;">2</span>	Yes	9.93	17.5	75.9	69.0	
B-21	.125	24.0	L	Yes	5.98	26.0	75.0	79.6	Heat No. 55109
					6.03	26.0		79.6	
					8.70	22.0		81.2	
					8.04	22.0		78.1	
					6.00	28.0	71.0	85.7	Heat No. 93034
					5.96	26.0		79.6	
					7.96	23.0		81.4	
					8.00	22.0		77.8	
B-19	.254	11.9	T	No	4.10	25.9	70.1	65.5	<span style="border: 1px solid black; padding: 0 2px;">3</span>
	.260	12.1	T		4.12	26.2		66.5	
	.252	12.1	T		4.06	26.9		67.8	
	.254	12.0	T		4.01	22.6		56.5	
	.251	12.0	L	No	4.20	25.4	73.8	65.0	<span style="border: 1px solid black; padding: 0 2px;">3</span>
	.252	12.0	L		3.95	25.7		64.3	
	.254	12.0	L		5.13	21.7		61.4	
	.251	12.0	L		4.05	23.5		59.2	
	.255	16.0	L		4.90	23.0		63.7	
	.254	16.0	L		4.70	19.4		52.6	

## NOTES:

- 1 Fatigue precracked in 100% humidity
- 2 Grain direction not identified
- 3 Fatigue precracked in 3.5% NaCl solution

TABLE B-10  $K_c$  DATA FOR 7075-T6 BARE ALUMINUM ALLOY

Ref No.	t (inch)	W (inch)	GRAIN DIR.	GUIDED	2a (inch)	$F_g$ (ksi)	$F_{ty}$ (ksi)	$F_g \sqrt{\pi a}$ (ksi $\sqrt{\text{in.}}$ )	REMARKS
B-21	.316	8.0	L	No	2.36	29.2	82.1	56.1	①
	.316	8.0	L	No	3.31	28.8	81.3	54.7	①
	.603	8.0	L	No	2.44	22.7	80.5	44.3	①
	.603	8.0	L	No	2.45	22.2	78.2	43.3	①

① Bare, machined from 3/4-inch plate





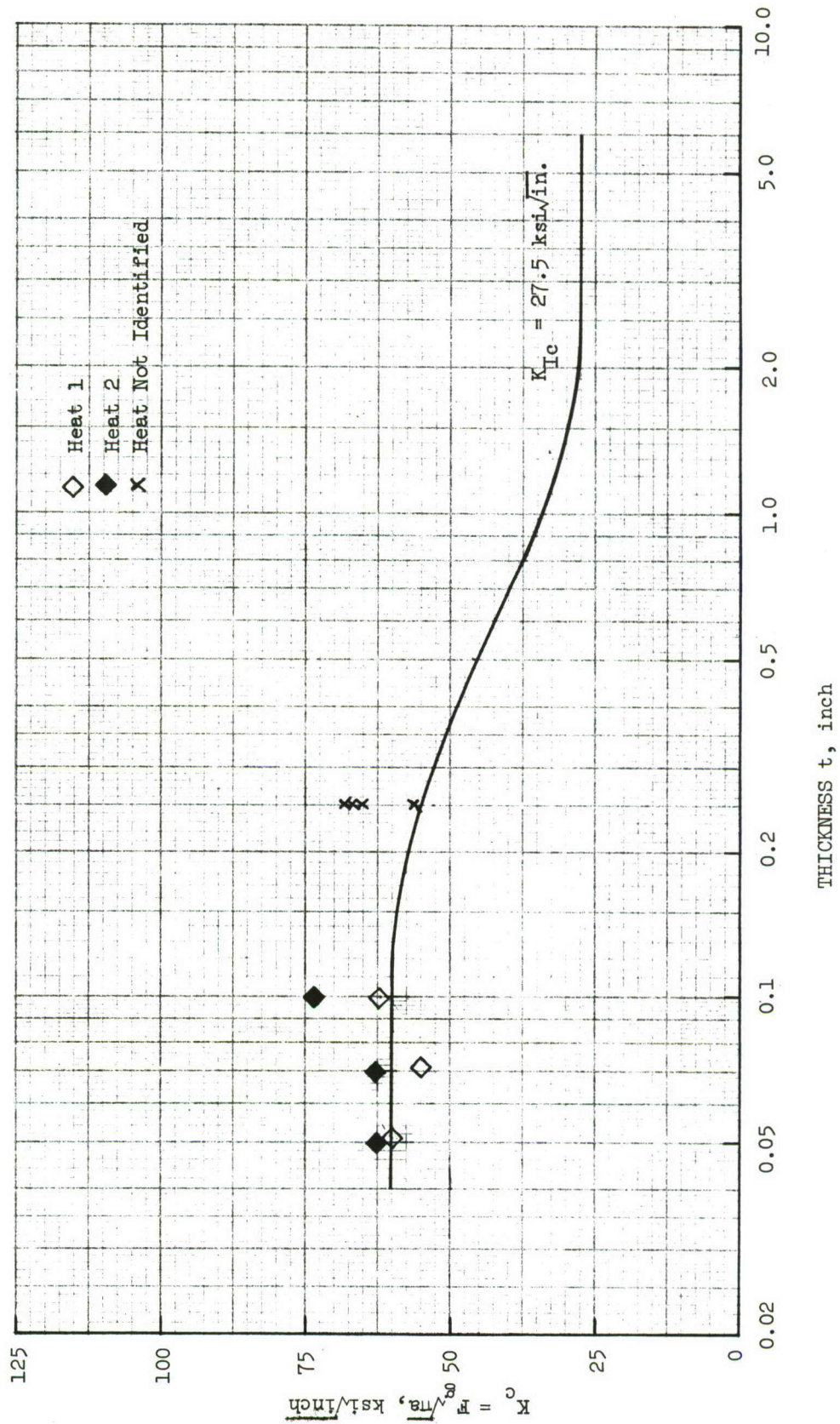


FIGURE B-16. FRACTURE TOUGHNESS PROPERTIES FOR 7075-T6 ALUMINUM, TRANSVERSE GRAIN



## APPENDIX C    SUSTAINED-LOAD SPECTRUM

It is desired to characterize the time at high load for the wing of a typical fighter or trainer. Then, based on this characterization, it is desired to develop a so-called "sustained load spectrum", a plot of load vs. cumulative time exceeding that load.

In the following discussion, a sustained load spectrum is developed from limited experimental data and presented in two forms:

- (1) In terms of a representative sinusoidal cyclic frequency. The low frequency is used to account for the time at high load. This is intended to apply to any fighter or trainer.
- (2) In terms of a plot of load factor level vs. cumulative time above that level. This is developed from a given cyclic spectrum using the frequency plot (1), and is therefore specifically applicable only for that spectrum.

For maneuver-critical aircraft, high wing loads tend to arise from either sharp pullouts or tight turns. In either case the maneuver consists of a change in angular direction, and the high forces arise from centrifugal acceleration.

At constant velocity  $v$  and constant centrifugal acceleration, the time required to change angular direction through an angle  $\theta$  is inversely proportional to load factor  $N_Z$ :

$$t = \frac{v\theta}{2N_Z g} = \frac{c}{N_Z} \quad (C-1)$$

where  $c$  is a constant (this formula ignores the velocity loss during the maneuver and the load factor component due to gravity, and assumes constant  $n$ ).

Based on this equation it is possible to estimate the length of time a particular load factor is maintained in a typical high -  $g$  maneuver if the value of the proportionality constant  $c$  is known.

To obtain appropriate empirical estimates for the constant  $c$ , flight test data were utilized. Time records for eighteen high load-factor pullout maneuvers were analyzed to determine the cumulative time above some chosen load factor,  $N_Z^*$ .



Choosing  $N_Z^*$  to be 90%, 75%, and 50% of  $N_{Z_{\max}}$  (the peak load factor for each maneuver), cumulative times  $T(0.90)$ ,  $T(0.75)$ , and  $T(0.50)$  were found. Correspondingly, 18 values for each of the constants  $c(0.90)$ ,  $c(0.75)$  and  $c(0.50)$  were estimated from the equation

$$c(r) = N_{Z_{\max}} T(r) \quad (C-2)$$

where  $r$  is the ratio of  $N_Z^*$  to  $N_{Z_{\max}}$  and takes the values 0.9, 0.74, and 0.5.

The three average values of  $c(r)$  are calculated in Table C-1.

The intent now is to represent time at load by assigning a selected slow cyclic frequency to the most severe cyclic loading events. Based on the above discussion, the frequency should be proportional to load factor, i.e.,

$$f = AN_{Z_{\max}} \quad (C-3)$$

where  $A$  is a constant. This constant can be found in terms of the empirical constants  $c(r)$ , as follows.

Assuming load cycling between zero and  $N_{Z_{\max}}$  (see Figure C-1) the load factor at any time is given by

$$N_Z(t) = \frac{N_{Z_{\max}}}{2} + \frac{N_{Z_{\max}}}{2} \cos(2\pi ft) \quad (C-4)$$

where  $f$  is the frequency. Written in another form,

$$f \times t = \frac{1}{2\pi} \cos^{-1} \left( \frac{N_Z(t)}{N_{Z_{\max}}} - 1 \right) \quad (C-5)$$

If we limit our consideration to the first half cycle, then  $t$  in Equation (C-5) is half the value of time per cycle above load level  $N_Z^* = N_Z(t)$ , i.e.,

$$t = \frac{1}{2} T \quad (C-6)$$

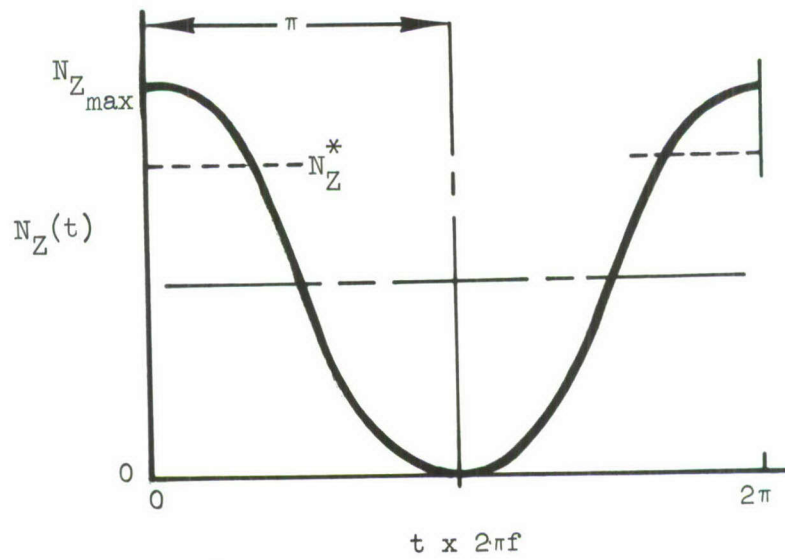


FIGURE C-1 ZERO-TO- $N_{Z_{max}}$  LOAD CYCLE

TABLE C-1 CALCULATION OF  $c(r)$  FROM FLIGHT TEST DATA ON PULLOUT  
MANEUVERS OF A TYPICAL FIGHTER AIRCRAFT

MANEUVER CASE	$N_{Z_{max}}$	TIME ABOVE LOAD, Seconds			$c = T N_{Z_{max}}$		
		T(.50)	T(.75)	T(.90)	c(.50)	c(.75)	c(.90)
1	8.85	5.5	3.2	1.5	48.6	28.3	13.3
2	8.1	3.5	1.7	0.6	28.3	13.8	4.9
3	8.6	8.85	6.7	0.8	76.0	57.6	6.9
4	6.0	4.0	4.0	3.8	24.0	24.0	22.8
5	5.3	2.65	2.55	1.1	14.0	13.5	5.8
6	3.5	2.15	1.2	0.6	7.5	4.2	2.1
7	5.8	5.5	4.8	2.4	31.9	27.8	13.9
8	5.9	2.7	2.5	0.96	15.9	14.8	5.7
9	5.5	4.0	4.0	2.1	22.0	22.0	11.6
10	5.22	3.08	2.62	0.9	16.1	13.7	4.7
11	5.7	7.0	4.6	3.4	39.9	26.2	19.4
12	4.35	4.0	3.86	2.34	17.4	16.8	10.2
13	5.7	4.2	2.2	1.7	23.9	12.5	9.7
14	5.5	2.4	2.1	0.52	13.2	11.5	2.9
15	4.0	7.7	7.25	6.65	30.8	29.0	26.6
16	3.73	3.5	2.6	1.35	13.0	9.7	5.0
17	3.47	3.1	2.87	2.2	10.7	9.9	7.6
18	5.2	3.75	1.85	1.0	19.5	9.6	5.2
Total					452.7	344.9	178.3
Divided by					18	18	18
Mean value of $c(r)$					25.15	19.16	9.9



Finally, combining Equations (C-2), (C-5) and (C-6), and letting  $N_Z(t) = N_Z^*$ , we obtain an expression for the frequency in terms of the maximum load factor  $n_{max}$  the empirical constant  $c(r)$ , and the ratio  $r = \frac{N_Z^*}{N_{Z_{max}}}$  (0.90, 0.75, or 0.50):

$$\begin{aligned} f &= \frac{1}{\pi T} \cos^{-1} \left( 2 \frac{N_Z^*}{N_{Z_{max}}} - 1 \right) \\ &= \frac{N_{Z_{max}}}{\pi c(r)} \cos^{-1} (2r - 1) \end{aligned} \quad (C-7)$$

Now utilizing Equation (C-3) we obtain the unknown proportionality constant A in terms of the empirical constants  $c(r)$ :

$$A = \frac{1}{\pi c(r)} \cos^{-1} (2r - 1) \quad (C-8)$$

Using Equation (C-8), three estimates of A were obtained:

From $c(90) = 9.9$ ,	$A = 0.0206$ cycle/(sec-g)
From $c(75) = 19.16$ ,	$A = 0.0174$ cycle/(sec-g)
From $c(50) = 25.15$ ,	$A = 0.0199$ cycle/(sec-g)

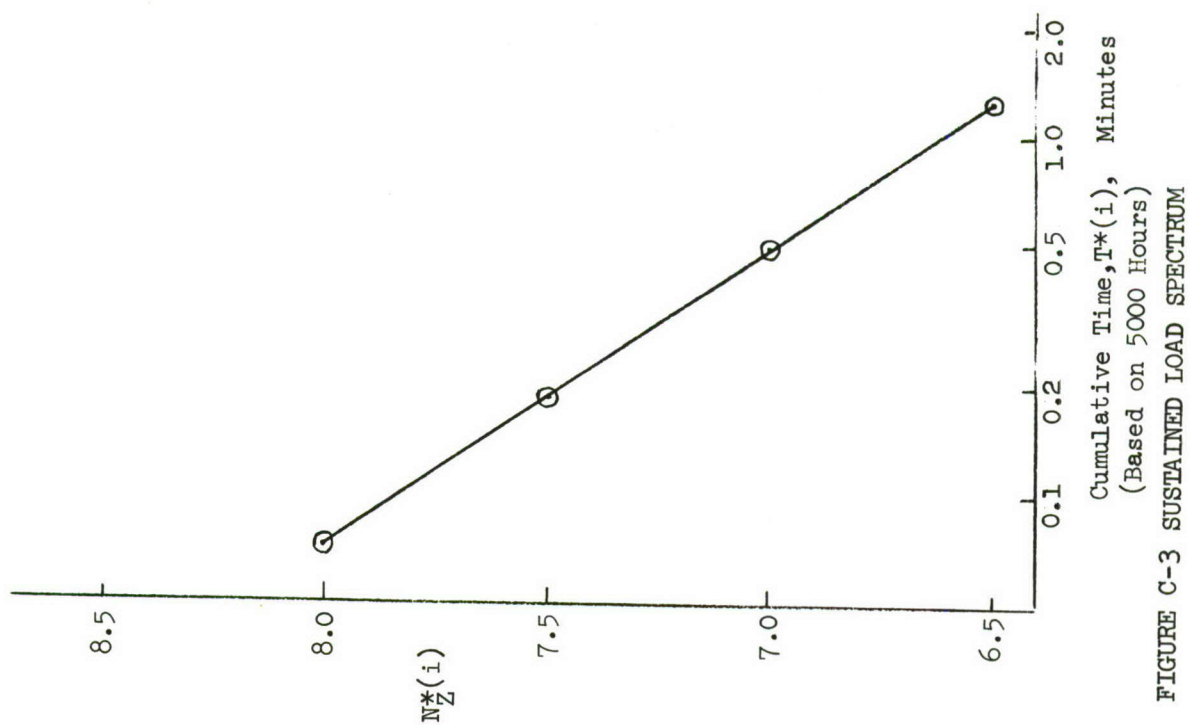
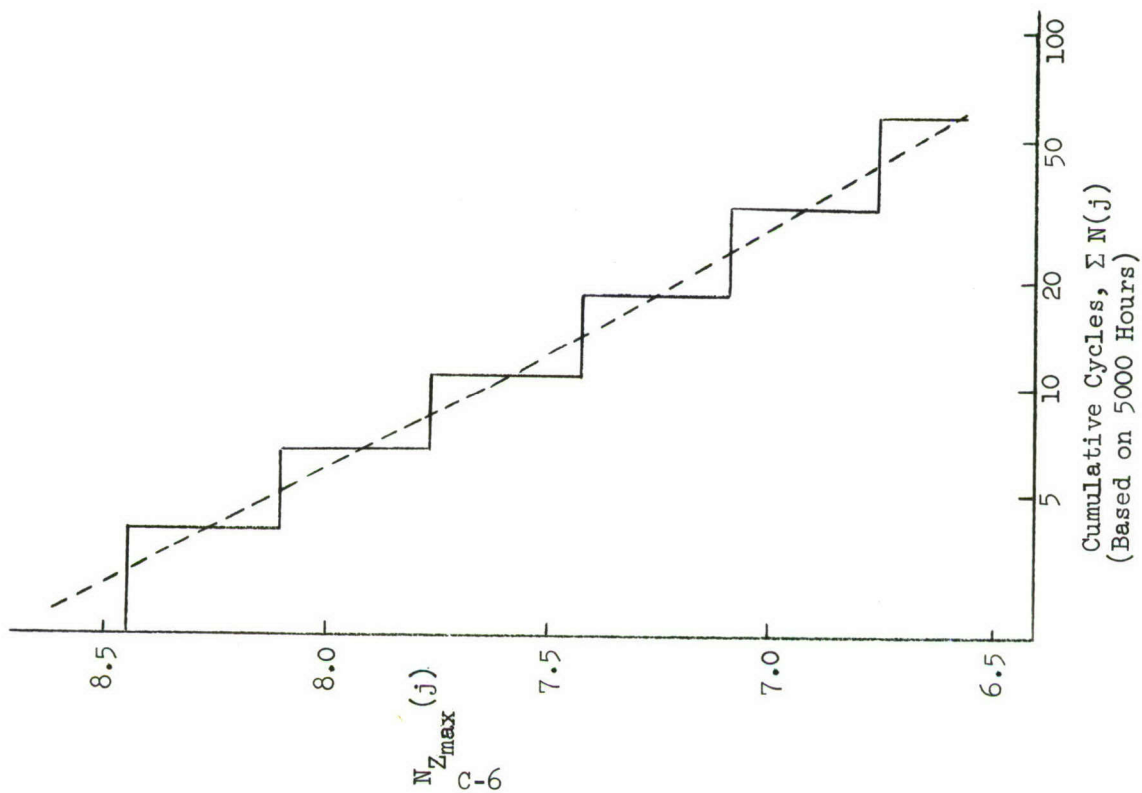
Based on this, a value of  $A = 0.02$  cycle/(sec-g) = 1.2 cycles/(minute-g) was chosen.

With "A" fixed, the representative frequency for a typical high - g pullout maneuver can be expressed in cycles per minute as

$$f = 1.2 \times N_{Z_{max}} \quad (C-9)$$

Besides this general equation it may be useful to display cumulative time at load vs. load factor for the design life of a specific aircraft. Such a plot can be constructed utilizing Equation C-9 in conjunction with a given cyclic load spectrum. An example of this construction is presented below.

The cyclic load spectrum selected for this example is given in Figure C-2. For brevity of the example, only load levels above  $N_Z = 6.5$  were considered. A lifetime of 5000 hours was selected.



The continuous cyclic spectrum (dotted line in Figure C-2) was converted to a discrete spectrum (solid lines in Figure C-2). For each peak load factor level  $n_{\max}(j)$  a number of occurrences  $N(j)$  in 5000 hours was obtained. Also from Equation C-9 the cyclic frequency  $f(j)$  was obtained.

Convenient values of load factor plateaus  $N_Z^*(i)$  were selected. For each load level in the spectrum, the time per cycle above any plateau is given by

$$T(i,j) = \frac{1}{\pi f(j)} \cos^{-1} \left( \frac{2N_Z^*(i)}{N_{Z_{\max}}(j)} - 1 \right) \quad (C-10)$$

This equation is obtained directly from Equations (C-5) and (C-6). Then the total time that the load factor is above plateau  $N_Z^*(i)$  in the 5000 hour life-time of the aircraft is given by

$$T^*(i) = \sum_j T(i,j) N(j) \quad (C-11)$$

This calculation is carried out in Table C-2 and the calculated cumulative sustained load spectrum for load factor levels above  $N_Z = 6.5$  are plotted in Figure C-3, page C-6.



TABLE C-2 EXAMPLE CALCULATION OF HIGH-LOAD PORTION OF A SUSTAINED-LOAD SPECTRUM

$N_{Z_{max}}(j)$ Fig. C-2	$N_Z^*(i)$	$\Sigma N(j)$ cycles	$N(j)$ cycles	$f(j)$ cpm	$\angle \alpha$ **	$\frac{N(j)}{f(j)180^\circ}$	$T(i,j)$ minutes Eqn. (3-9)	$T^*(i)$ minutes Eqn. (3-10)
8.44	8 7.5 7 6.5	3.9	3.9	10.13	26° 39° 49° 57°	.00213	.055 .083 .104 .121	0.072 0.182 0.483 1.220
8.10	8 7.5 7 6.5	6.4	2.5	9.72	12° 32° 43° 53°	.00143	.017 .047 .063 .078	
7.76	8 7.5 7 6.5	10.6	4.2	9.31	- 21° 36° 48°	.00250	- .052 .090 .120	
7.42	8 7.5 7 6.5	18.0	7.4	8.90	- - 24° 41°	.00462	- - .111 .189	
7.09	8 7.5 7 6.5	31.6	13.6	8.50	- - 13° 34°	.00890	- - .115 .302	
6.75	8 7.5 7 6.5	57.6	26.0	8.10	- - - 23°	.01785	- - - .410	

$$** \angle \alpha = \cos^{-1} \left[ 2 \left( \frac{N_Z^*(i)}{N_{Z_{max}}(j)} \right) - 1 \right]$$

## APPENDIX D      RESULTS OF CRACK GROWTH ANALYSIS

The discussion of the crack growth analysis in Section 5.3 first describes how to obtain plots of crack length vs. flight-hours for various damage cases. Secondly Section 5.3 describes how these curves are used to check the design stress levels against the durability and structural integrity criteria.

This appendix presents all the basic plots of crack length vs. cycles, as a function of assumed load factor-maximum spectrum stress relation, calculated in the analysis discussed in Section 5.3.



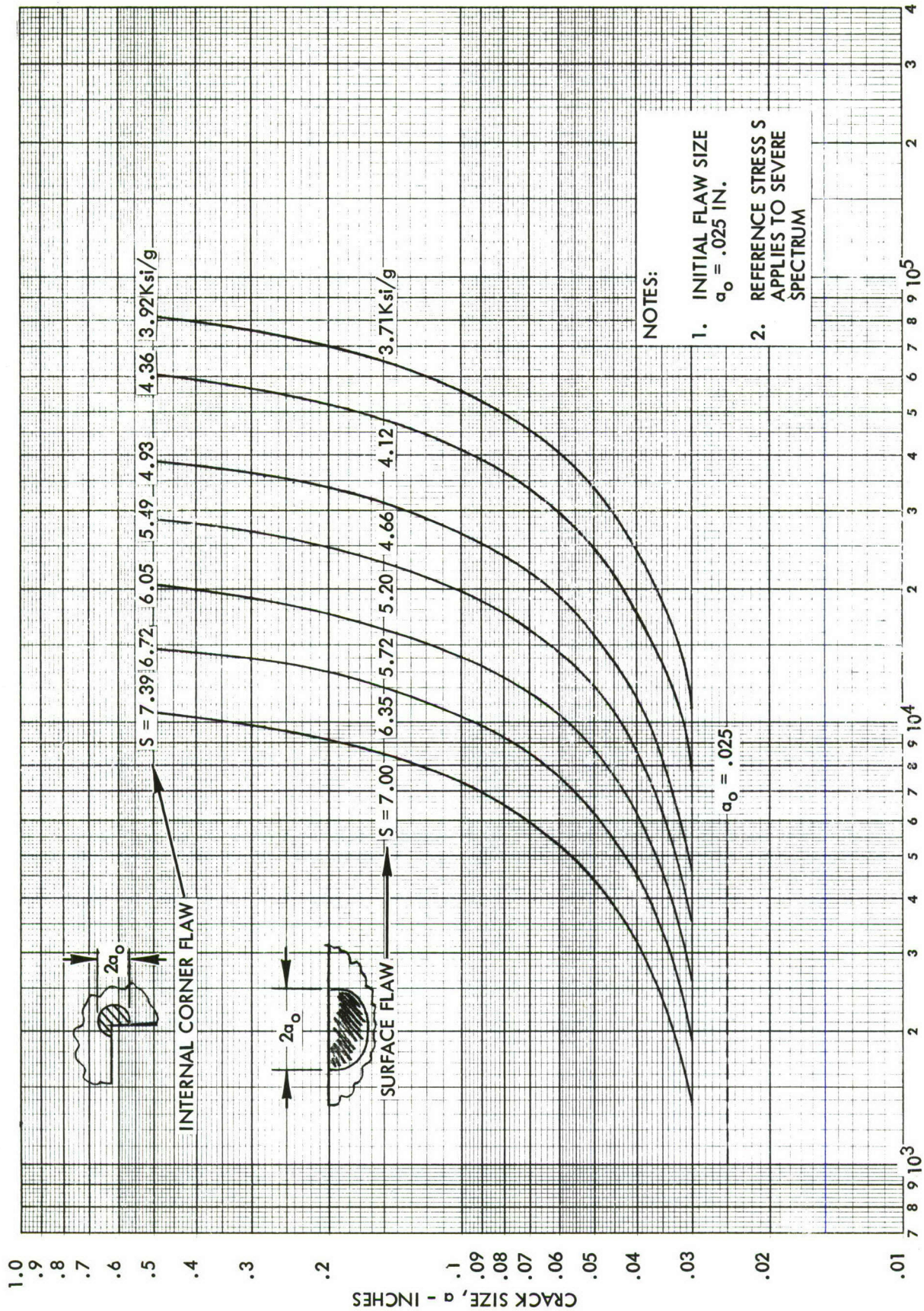


FIGURE D-1. CRACK GROWTH CURVES FOR SEMI-CIRCULAR FLAWS INITIATING AT A SURFACE OR INTERNAL CORNER IN 7075-T76 ALUMINUM - SEVERE SPECTRUM



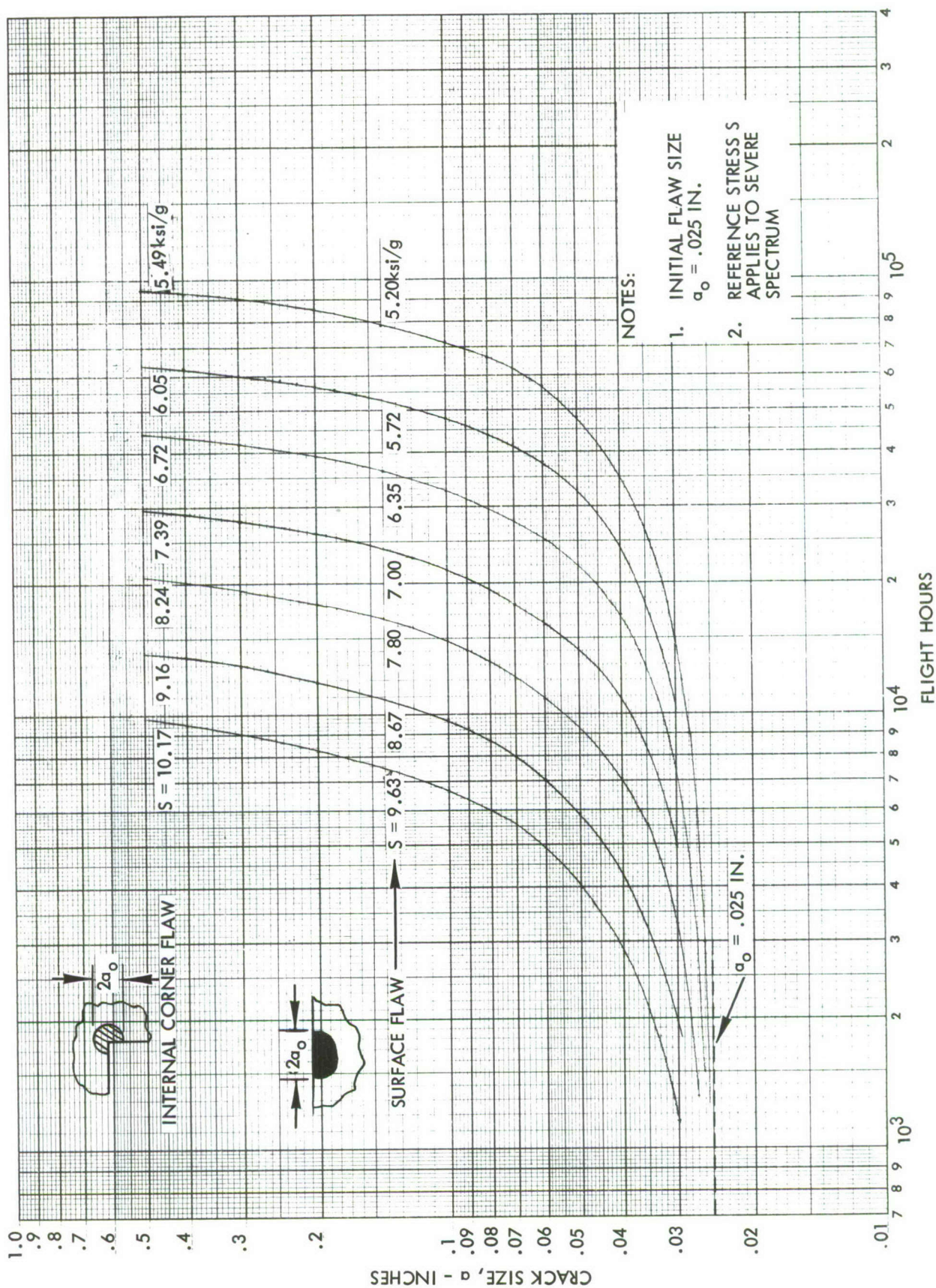


FIGURE D-2. CRACK GROWTH CURVES FOR SEMI-CIRCULAR FLAWS INITIATING AT A SURFACE OR INTERNAL CORNER IN Ti-6AL-4V - SEVERE SPECTRUM



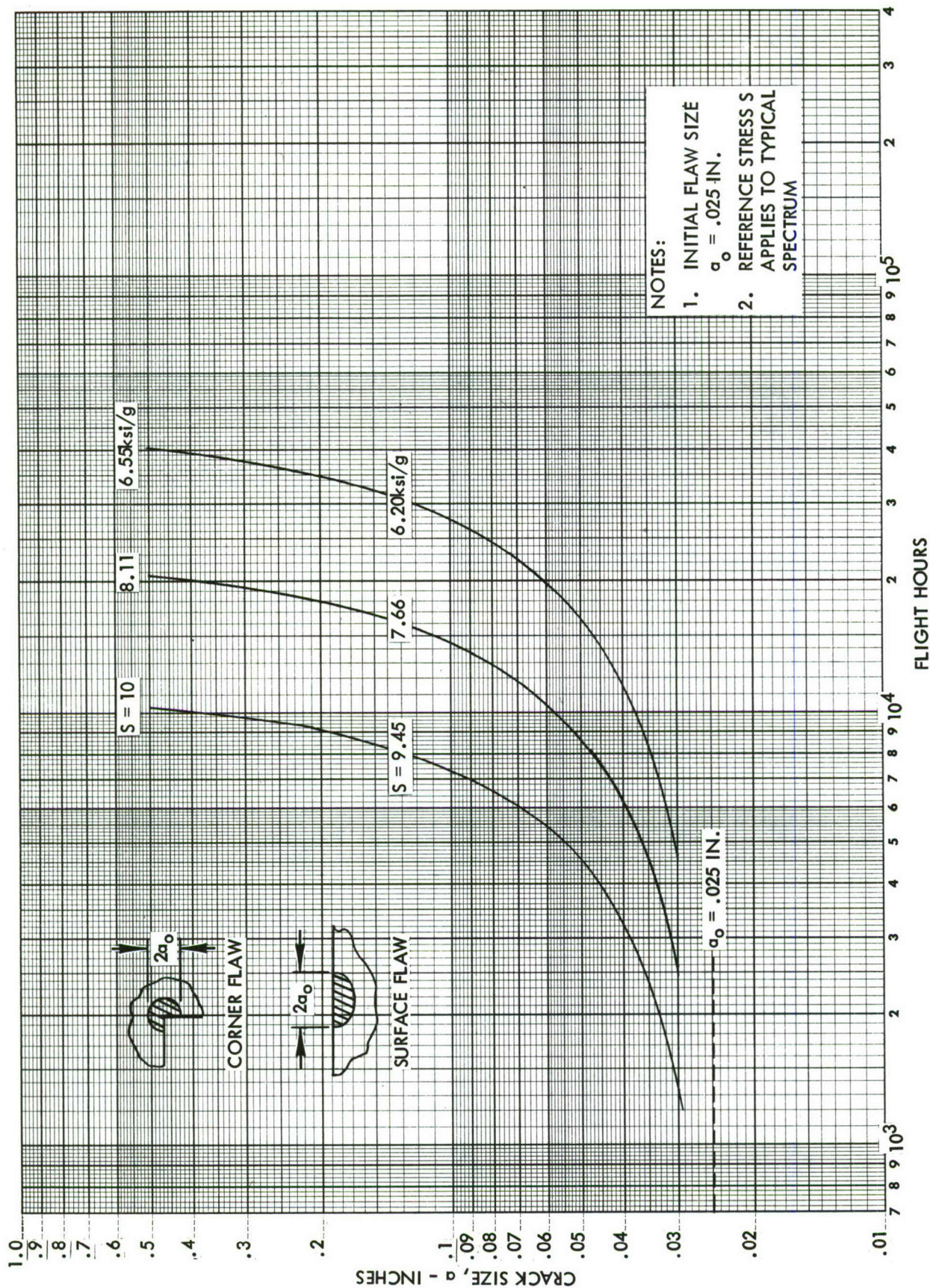


FIGURE D-3. CRACK GROWTH CURVES FOR SEMI-CIRCULAR FLAWS INITIATING AT A SURFACE OR INTERNAL CORNER IN 7075-T76 ALUMINUM - TYPICAL SPECTRUM



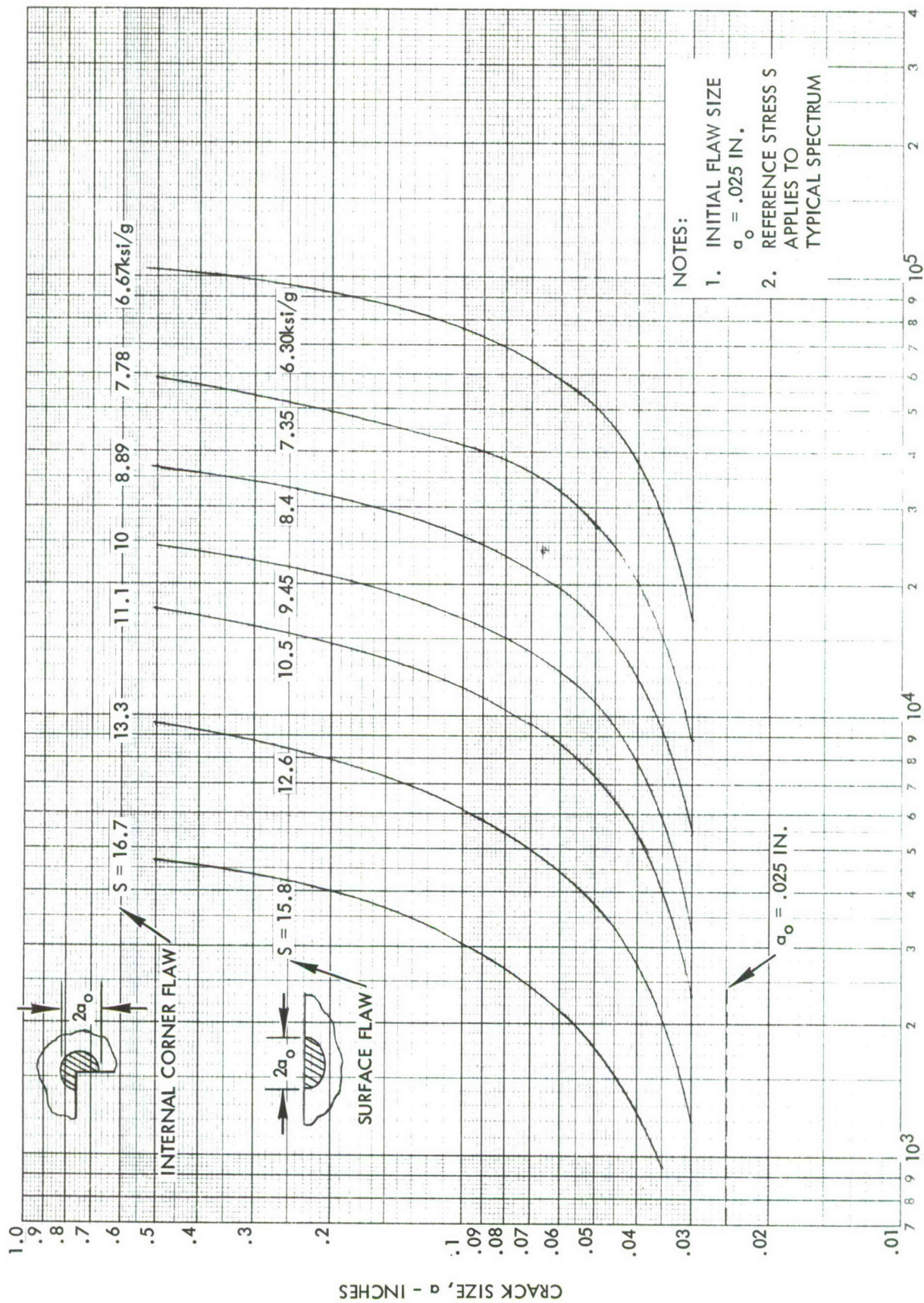


FIGURE D-4. CRACK GROWTH CURVES FOR SEMI-CIRCULAR FLAWS INITIATING AT A SURFACE ON INTERNAL CORNER IN T1 6AL-4V - TYPICAL SPECTRUM



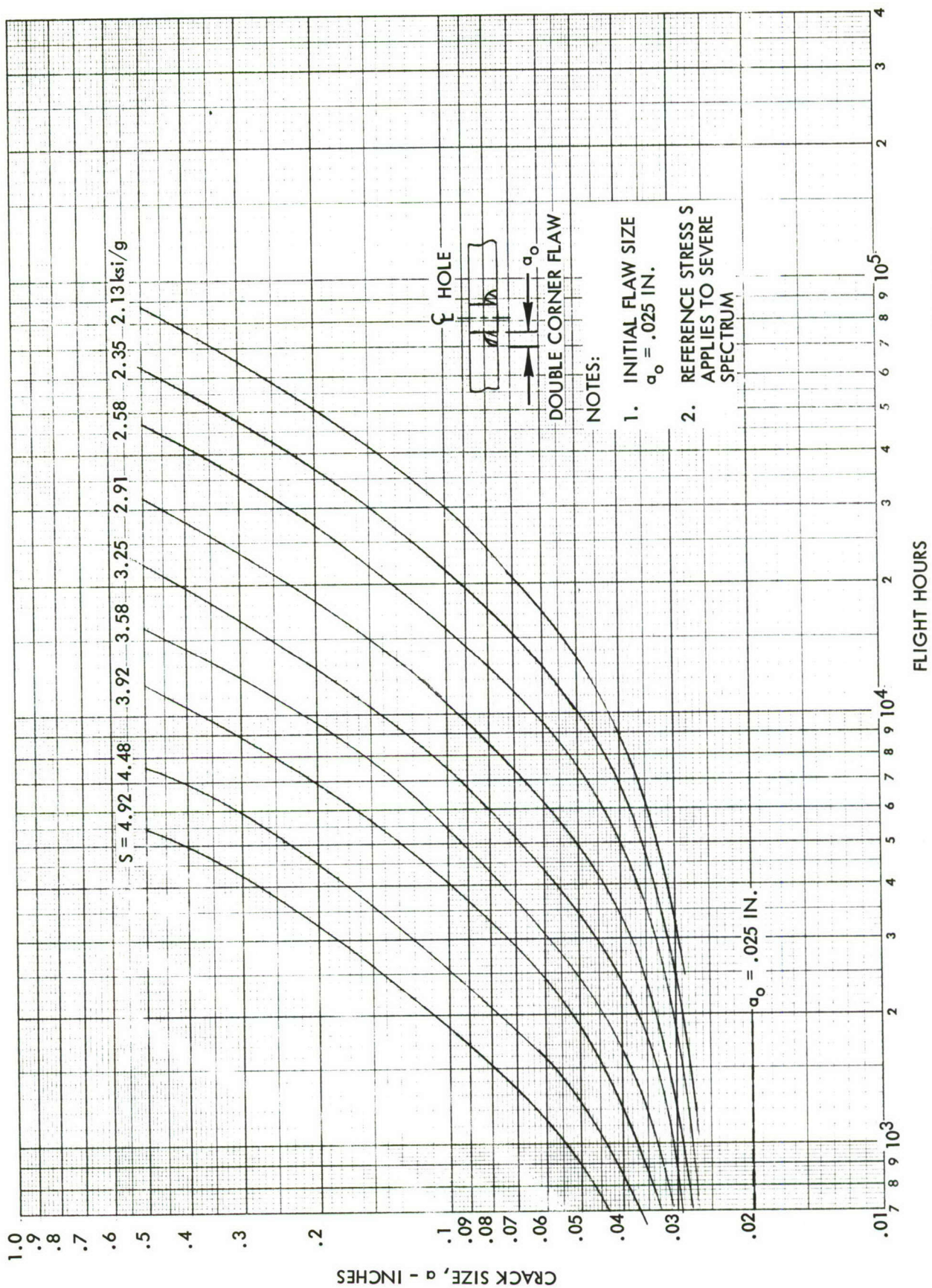


FIGURE D-5. CRACK GROWTH CURVES FOR DOUBLE CORNER FLAWS AT A HOLE IN 7075-T76 ALUMINUM



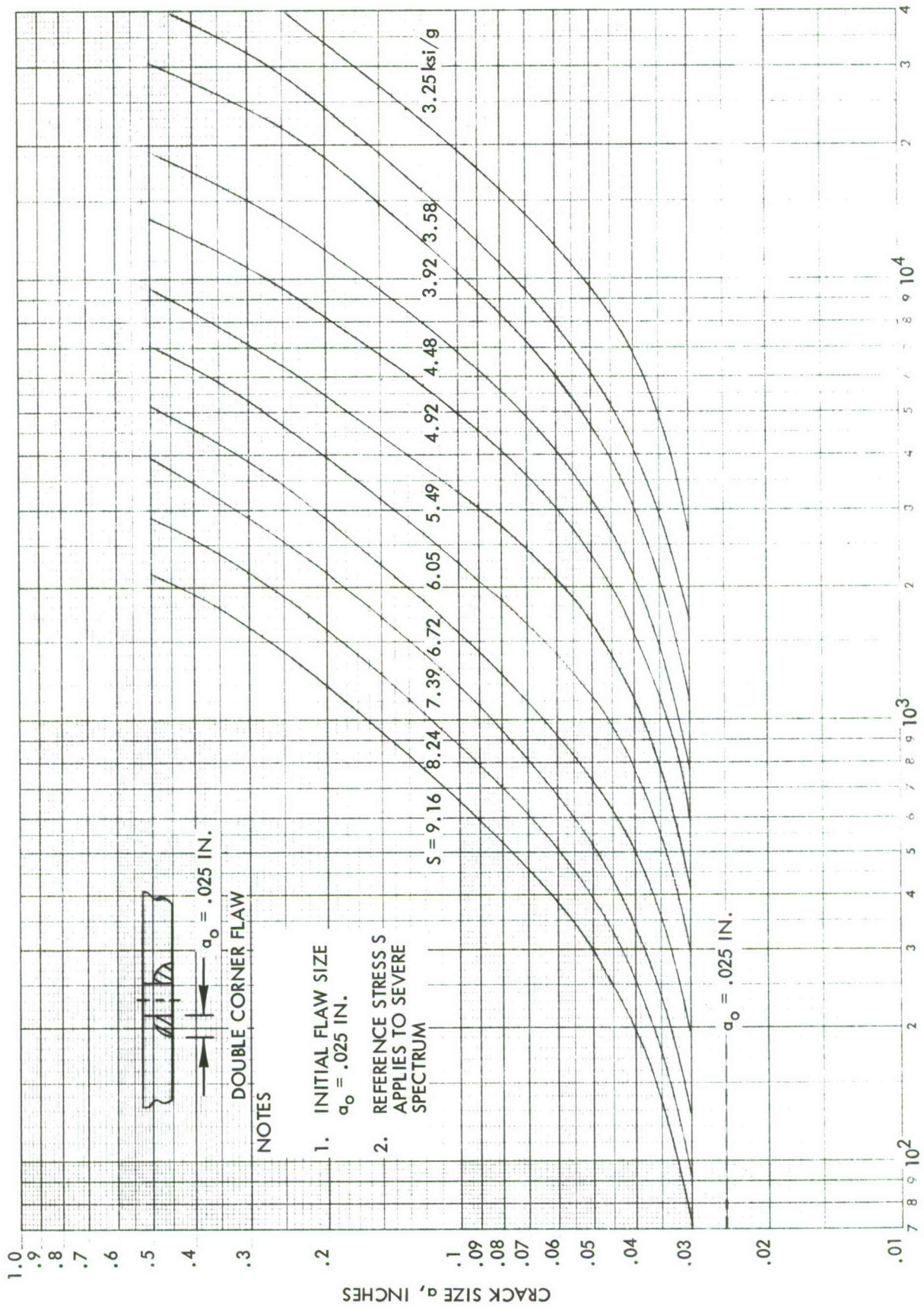


FIGURE D-6. CRACK GROWTH CURVES FOR DOUBLE CORNER FLAWS AT A HOLE IN Ti-6AL-4V



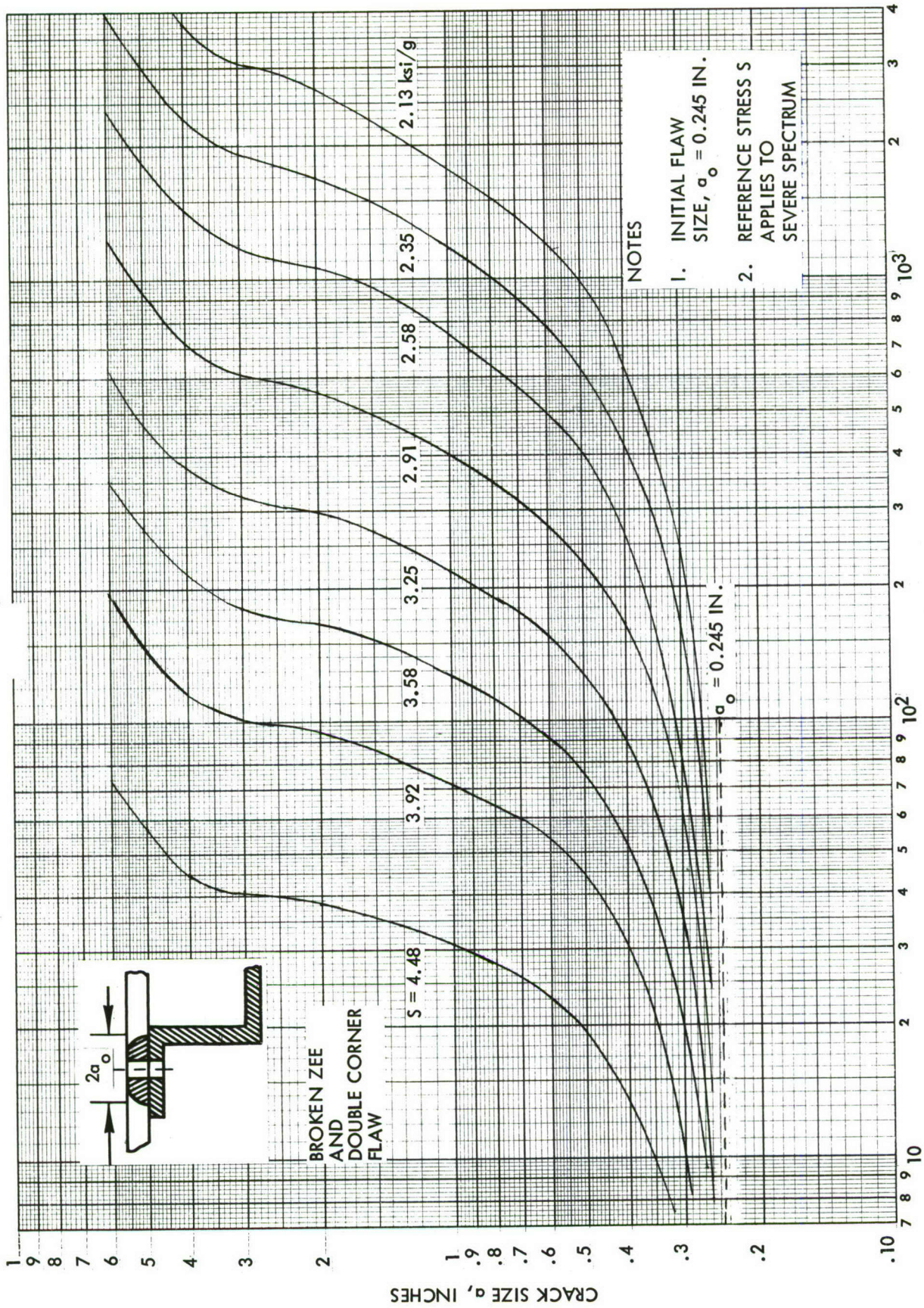


FIGURE D-7. CRACK GROWTH CURVES FOR A BROKEN ZEE STIFFENER AND A DOUBLE CORNER FLAW AT A HOLE IN 7075-T76 ALUMINUM



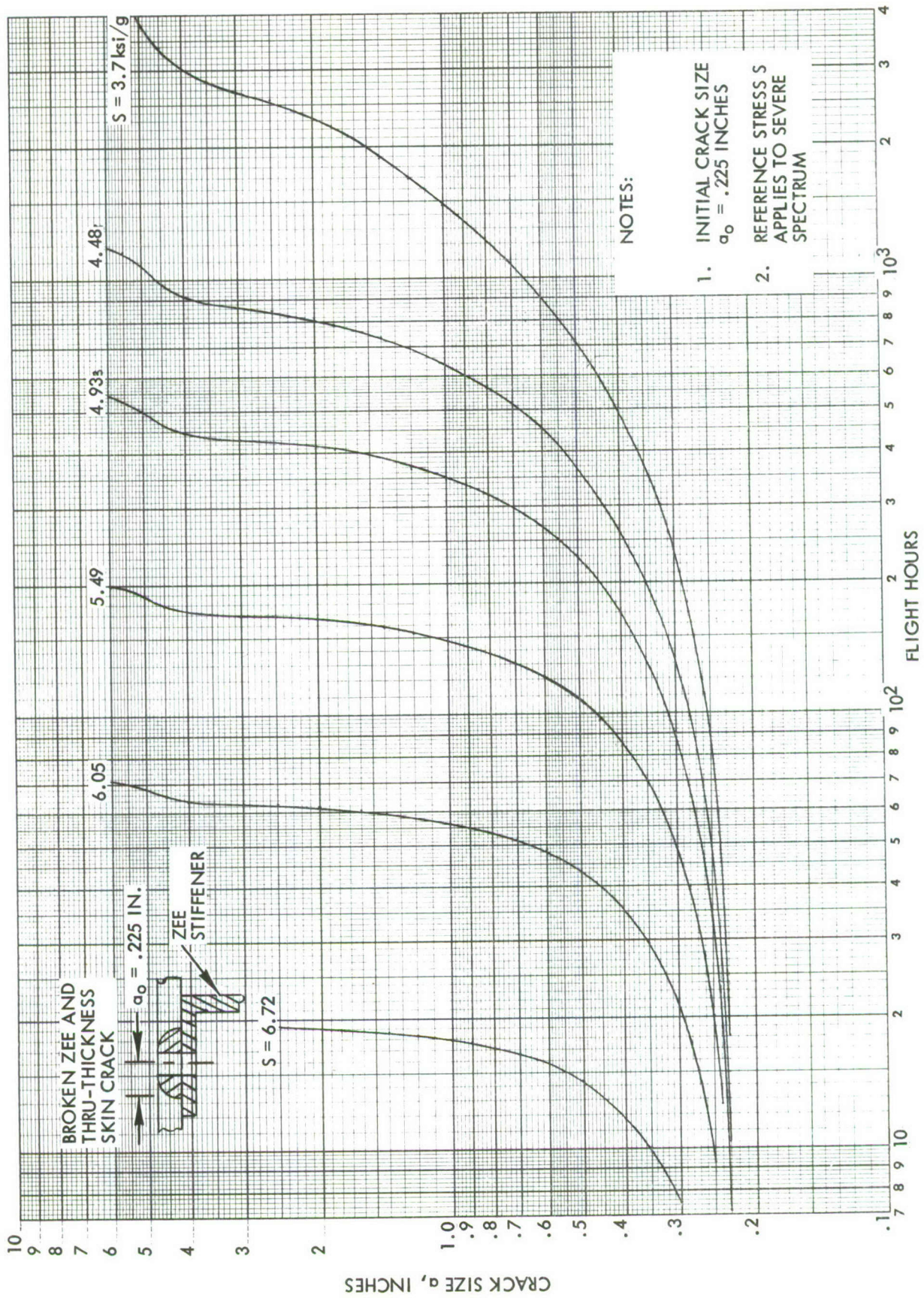


FIGURE D-8. CRACK GROWTH CURVES FOR A BROKEN ZEE STIFFENER AND THRU THICKNESS SKIN CRACK IN Ti-6AL-4V



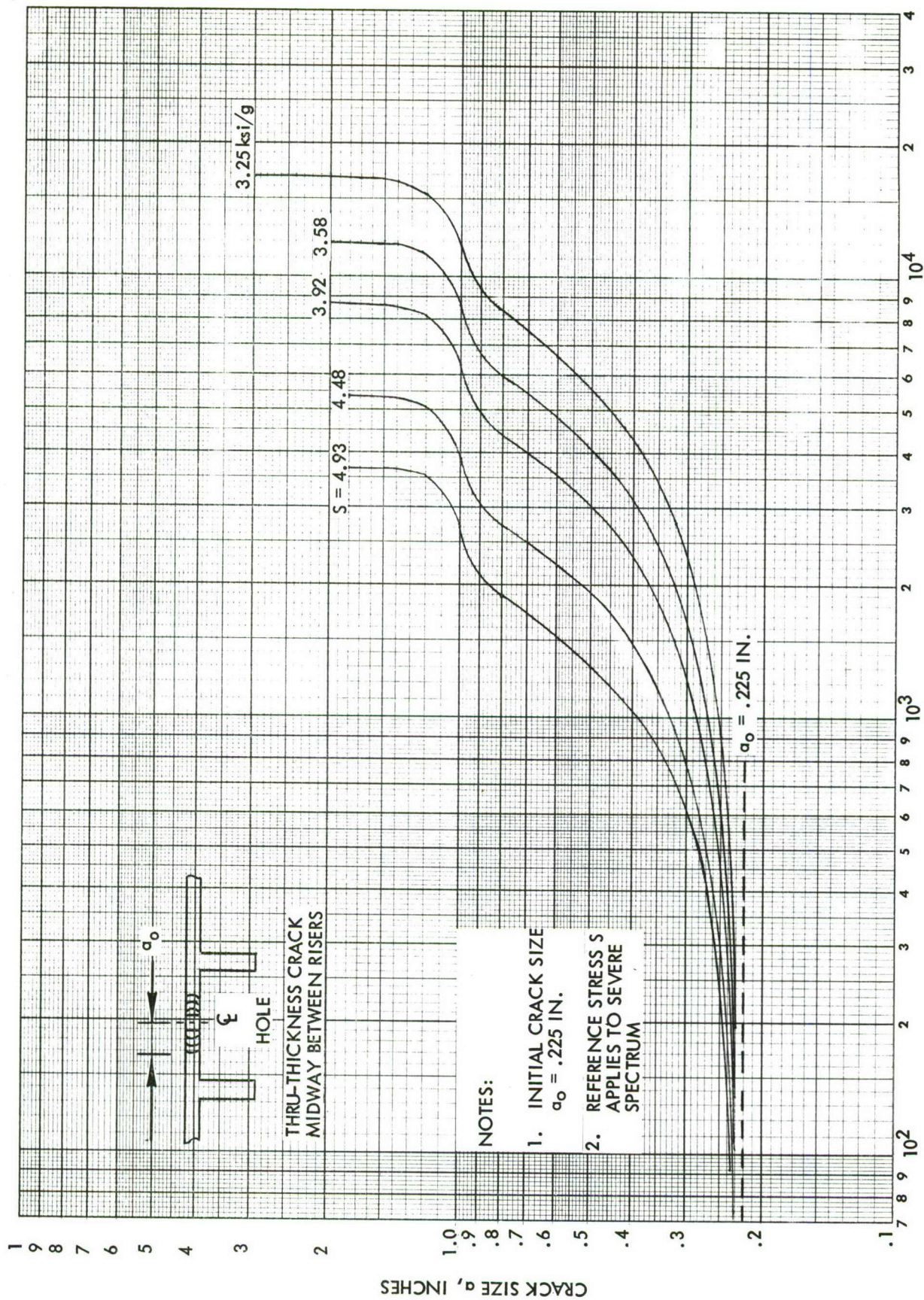


FIGURE D-9. CRACK GROWTH CURVES FOR THRU THICKNESS CRACK IN 7075-T76 ALUMINUM INTEGRALLY STIFFENED SKIN PLANKS



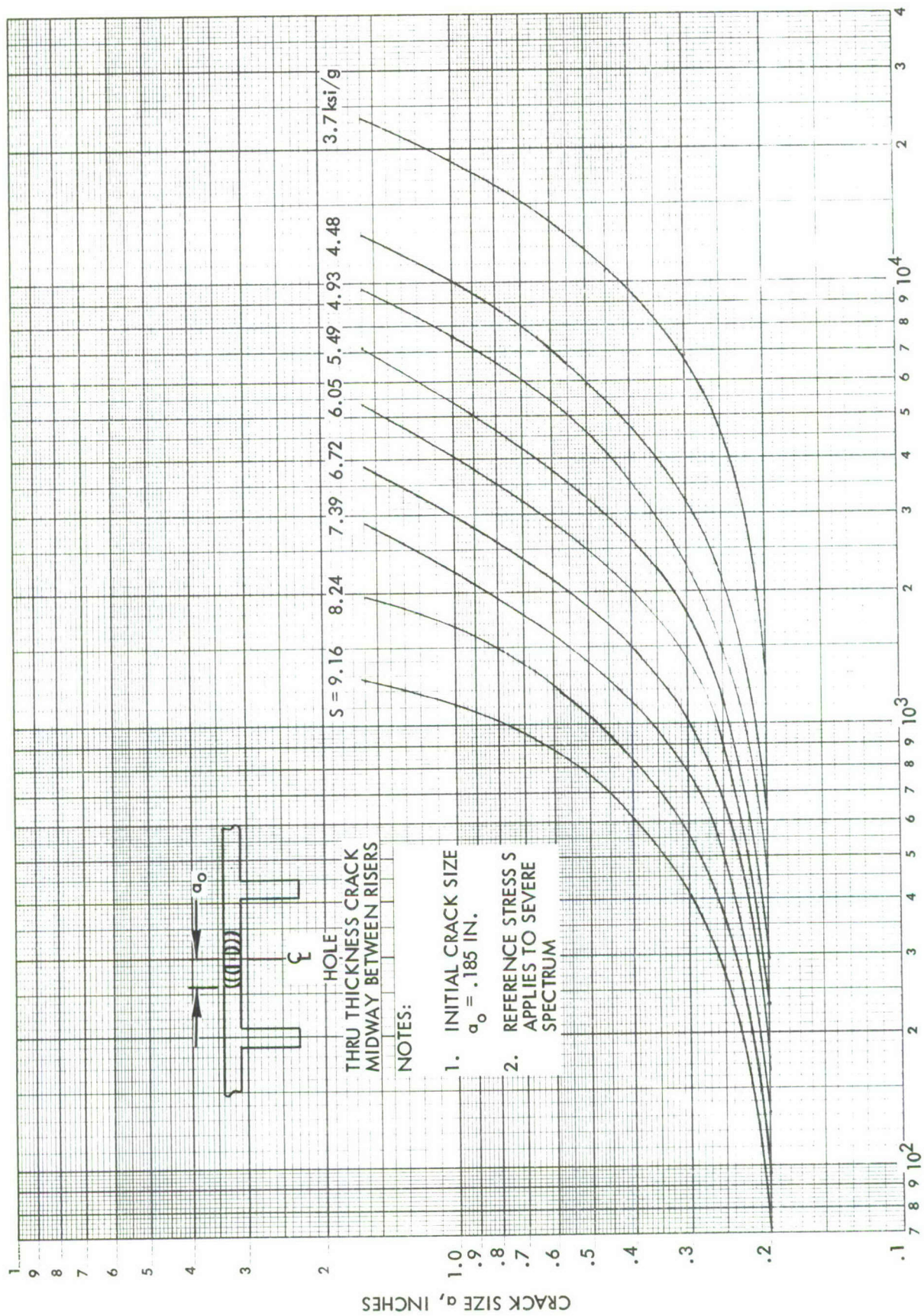


FIGURE D-10. CRACK GROWTH CURVES FOR THRU THICKNESS CRACK IN Ti-6Al-4V  
INTEGRALLY STIFFENED SKIN PLANKS



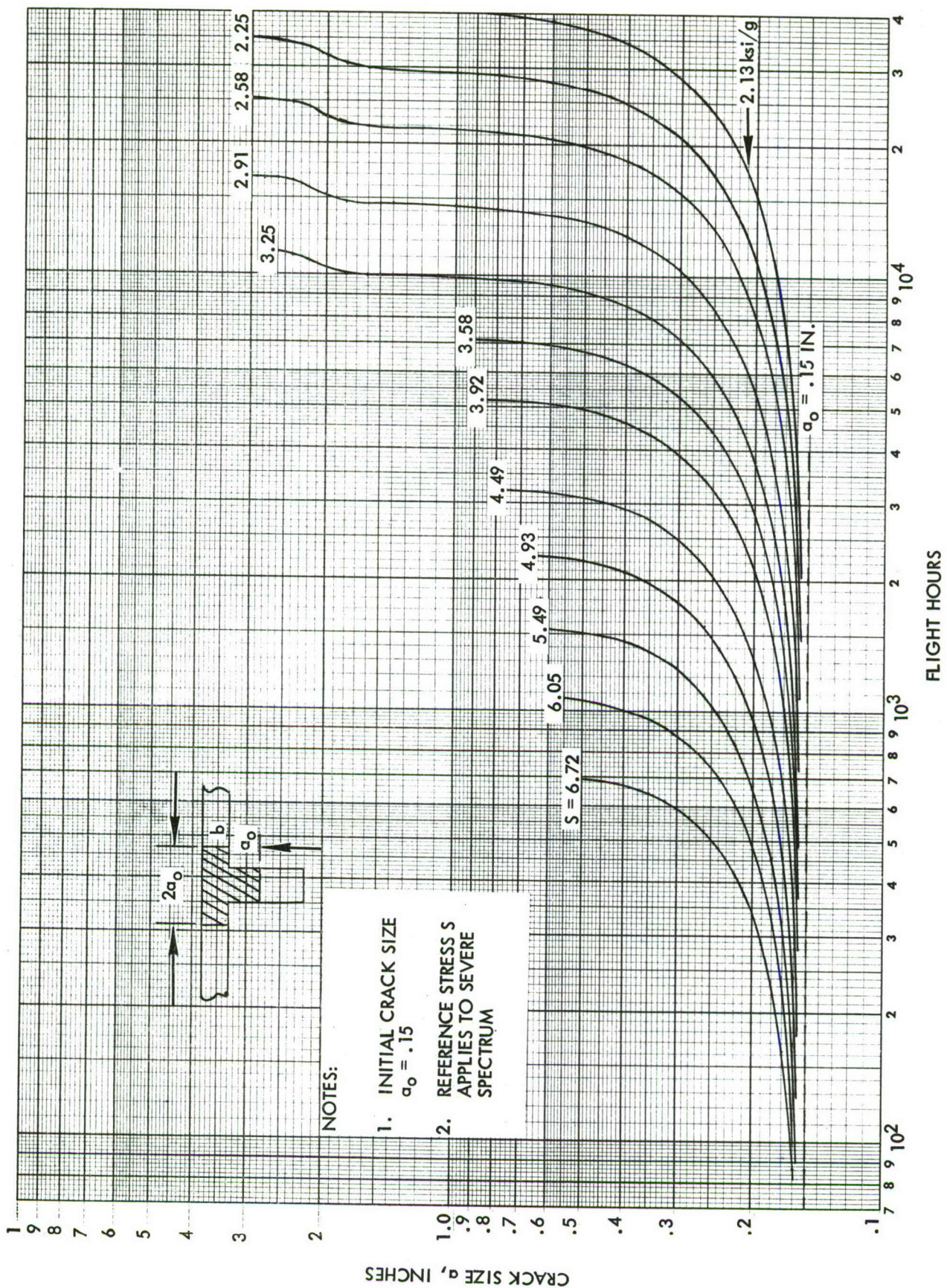


FIGURE D-11. CRACK GROWTH CURVES FOR CRACKED RISER AND THRU THICKNESS SKIN CRACK IN 7075-T76 ALUMINUM



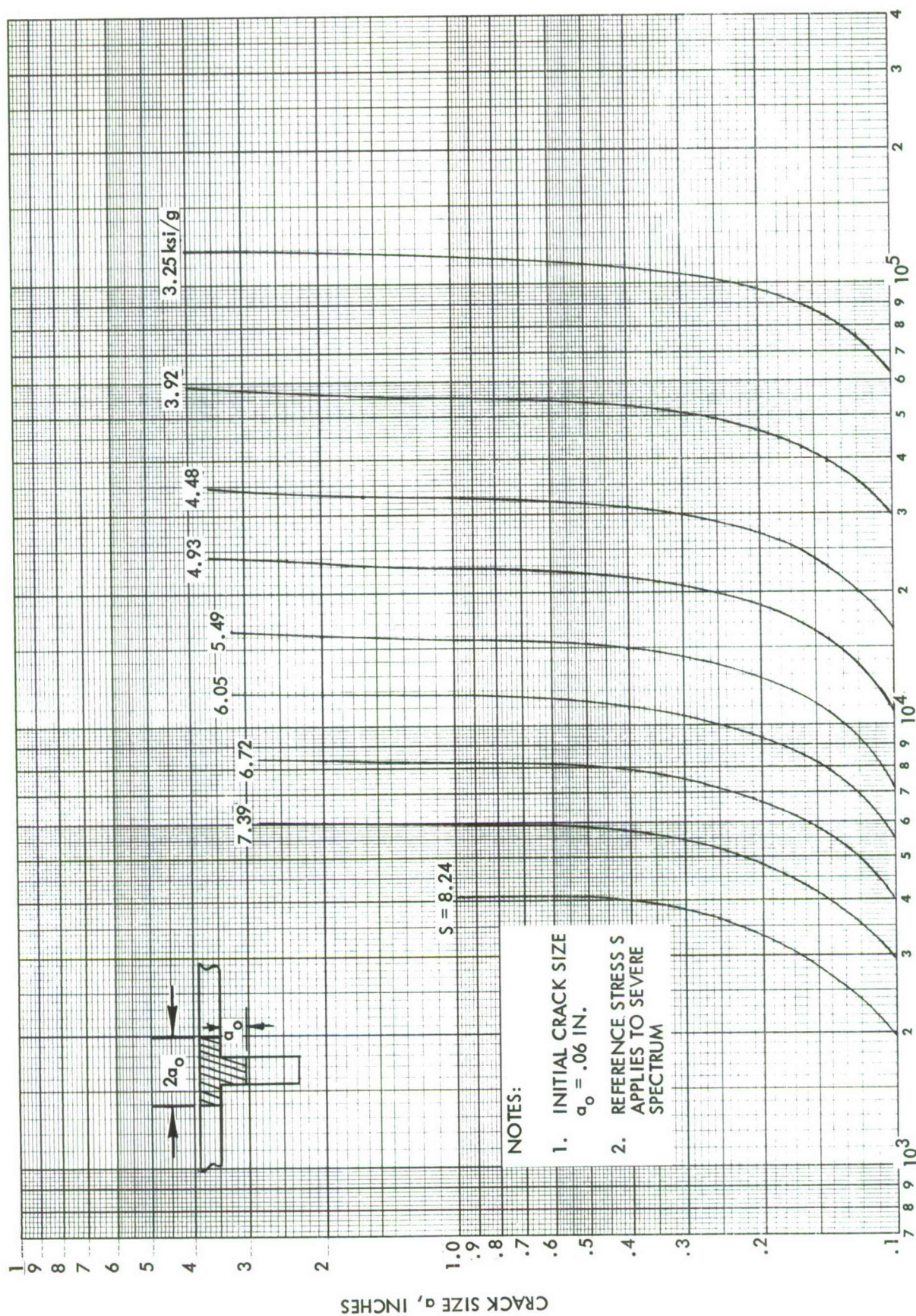


FIGURE D-12. CRACK GROWTH CURVES FOR CRACKED RISER AND THRU THICKNESS SKIN CRACK IN Ti-6Al-4V



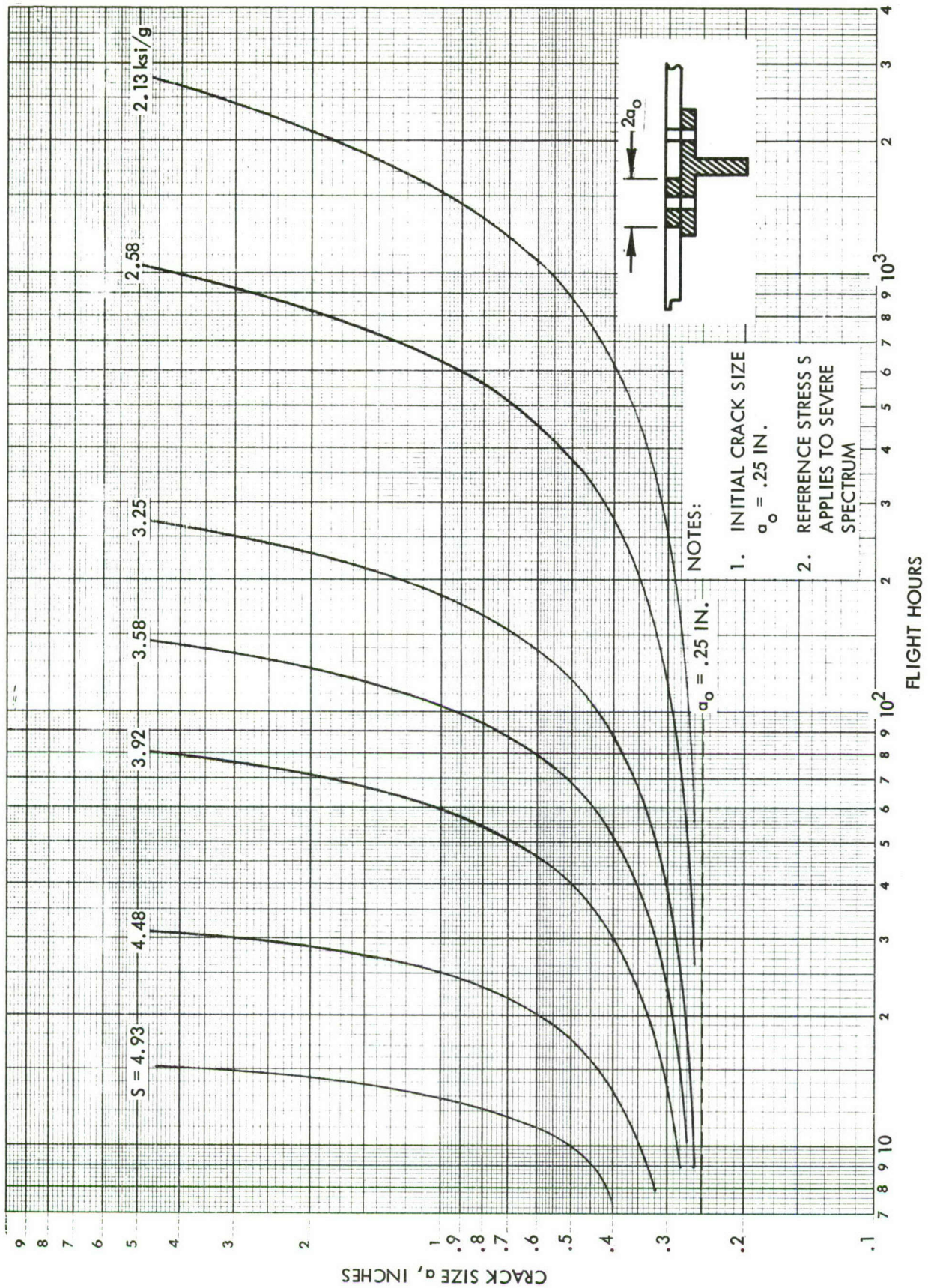


FIGURE D-13. CRACK GROWTH CURVES FOR A BROKEN SPAR CAP AND THRU-THICKNESS SKIN CRACK IN 7075-T76 ALUMINUM



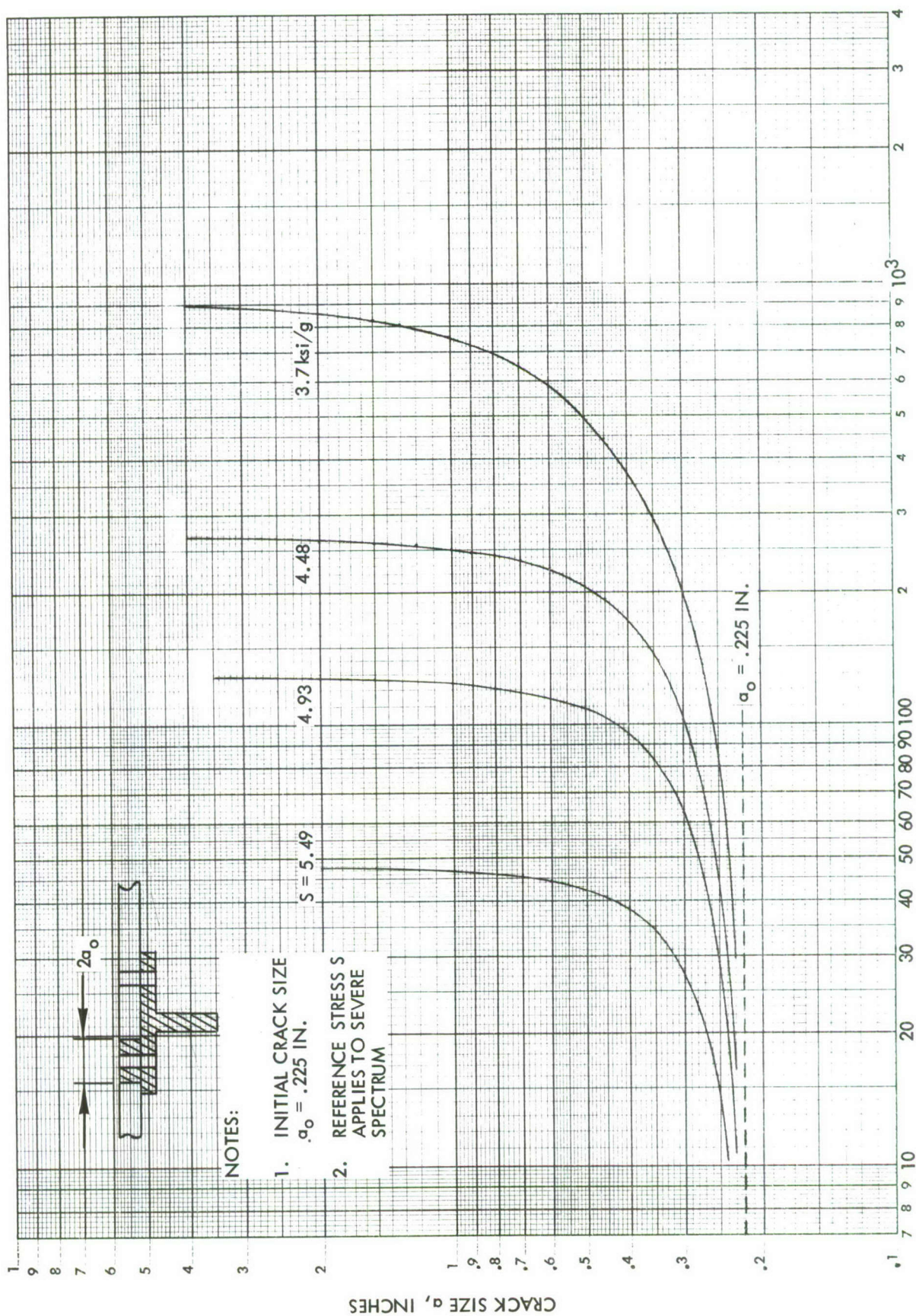


FIGURE D-14. CRACK GROWTH CURVES FOR A BROKEN SPAR CAP AND THRU THICKNESS SKIN CRACK IN Ti-6AL-4V



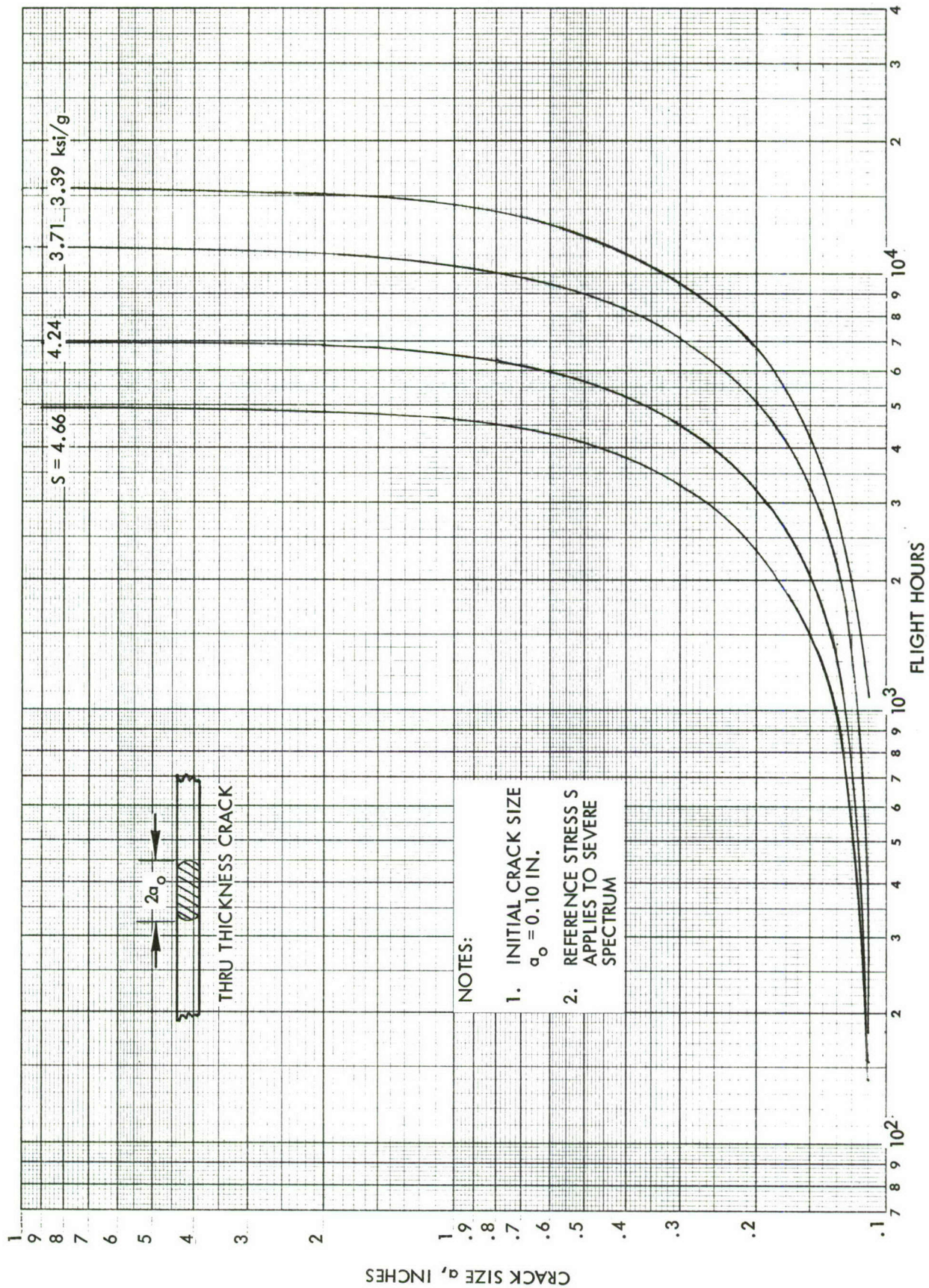


FIGURE D-15. CRACK GROWTH CURVES FOR THRU-THICKNESS CRACK IN UNSTIFFENED 7075-T76 ALUMINUM SKIN



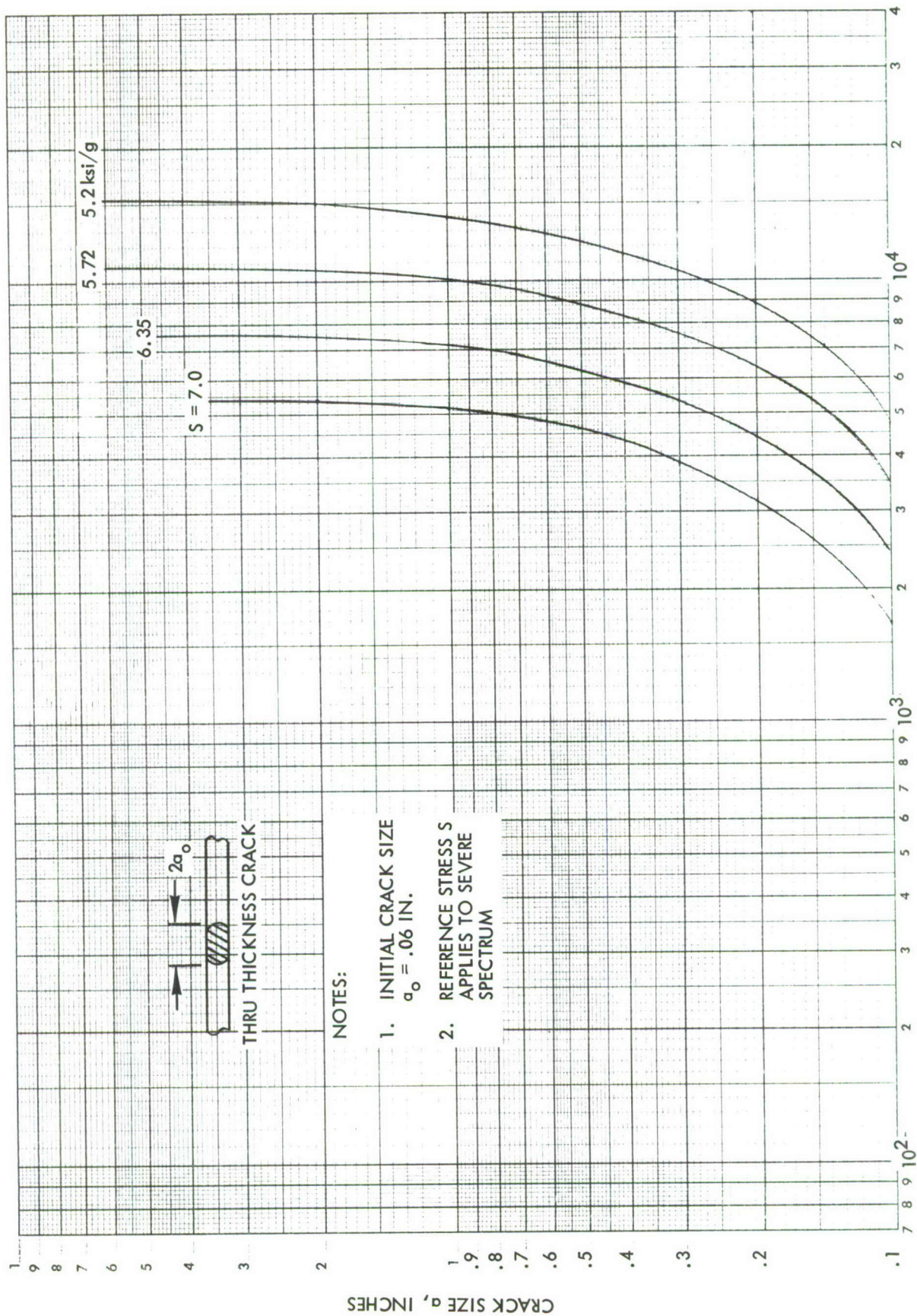


FIGURE D-16 CRACK GROWTH CURVES FOR THRU-THICKNESS CRACK IN UNSTIFFENED  
Ti-6Al-4V SKIN



## APPENDIX E

### STRESS INTENSITY FACTOR FOR A PART-THRU CRACK IN A PLATE

A great deal of attention has been given to the development of stress intensity factors for part-thru cracks (also called surface flaws.) In this appendix, the results of Irwin, Rice, Kobayashi and Smith (Reference E-1 to E-6) are adopted as a basis for constructing the geometric coefficients in the stress intensity expression. Generally, the shape of a part-thru crack emanating from one surface of a plate is assumed to be a half ellipse (Figure 4-8). Its shape can be described in terms of the ratio of one half of the minor axis to the major axis,  $a/2c$ , having the major axis coincident with the front surface of the plate. Two extreme cases,  $a/2c = 0$  (a scratch) and  $a/2c = 0.5$  (a semi-circle), constitute the upper and lower bounds of the crack shape. The stress intensity expression for some point on the periphery of such a crack is given by

$$K = f_g \sqrt{\pi a} \left[ \alpha_f \cdot \frac{M}{\phi} \cdot \alpha_b \quad M_p \right] \quad (E-1)$$

where

$a$  = crack depth, inches

$\alpha_f$  = a coefficient accounting for the influence of the front free surface (the free surface coincident with the visible length of the crack), dimensionless

$\alpha_b$  = coefficient accounting for the influence of the back free surface (the other side of the plate), dimensionless

$\frac{M}{\phi}$  = coefficient to account for the shape of the crack

where

$$M = \left[ \left( \frac{a}{c} \right)^2 \sin^2 \theta + \cos^2 \theta \right]^{1/4}, \text{ dimensionless}$$

$$\phi = \int_0^{\pi/2} \left[ 1 - \left( \frac{c^2 - a^2}{c^2} \right) \sin^2 \theta \right]^{1/2} \cdot d\theta, \text{ dimensionless}$$

$c$  = half crack length on the front surface, inches

and

$\theta$  = the angle locating a specific point on the crack front with respect to the axis of symmetry, radians

A numerical solution for the front surface influence factor,  $\alpha_f$ , was derived by Smith for a semi-circular crack shape ( $a/2c = 0.5$ ). From the plot of this solution, shown in Figure E-1, it is seen how the front surface geometric coefficient varies along the crack periphery. By linear interpolation between this numerical result for  $a/2c = 0.5$  and the classical limiting factor of 1.12 for  $a/2c = 0$  (Reference E-7), the front surface geometric coefficient  $\alpha_f$  as a function of  $\theta$  can be estimated for all intermediate  $a/2c$  values. The algebraic formula for this interpolation is

$$\alpha_f = 1.12 - [1.12 - \alpha_{f(a/2c = 0.5)}] \cdot \frac{a}{c} \quad (E-2)$$

Since both parameters,  $\alpha_f$  and  $M$ , are function of  $\theta$  and  $a/2c$ , a single parameter  $M_1 = M \cdot \alpha_f$  is defined and plotted in Figure E-2. It is seen from this figure that, temporarily neglecting the influence of the back surface, the maximum stress intensity is not always located at  $\theta = 0^\circ$ . The maximum  $K$  is at  $\theta = 90^\circ$  for  $a/2c$  greater than approximately 0.375. Conversely, maximum  $K$  is located at  $\theta = 0^\circ$  for  $a/2c$  less than 0.375. A stable crack shape probably occurs in the neighborhood of  $a/2c = 0.375$ . Defining  $M'_1$  to be the maximum value of  $M_1$  for the  $a/2c$  curves in Figure E-2 and assuming that the crack will grow in the direction of  $K_m$ , Equation (E-1) is then reduced to

$$K_{mx} = f_g \sqrt{\pi a} \left[ \frac{M'_1}{\phi} \cdot \alpha_b \right] M_p \quad (E-3)$$

A plot of  $M'_1/\phi$  versus  $a/2c$  is given in Figure 4-9. It is suggested that this plot be used in calculating stress intensities for part-thru cracks in design analysis.

So far we have discussed the geometric coefficients  $M$ ,  $\phi$  and  $\alpha_f$  and these are well defined. If the crack is shallow and the applied stress is low as compared to the yield strength of the material, the effects of the back surface and the plasticity at the crack tip are negligible. As the crack develops and propagates toward the back surface, excessive plastic yielding occurs in front of the crack. Although the  $M_p$  term will be deleted from the stress intensity expression, it is worthwhile to discuss its physical importance here. When the plastic zone ( $2r_p$ ) in front of the crack penetrates the thickness of the plate, the effect of this zone is altered. At this point the development of the crack front plastic zone

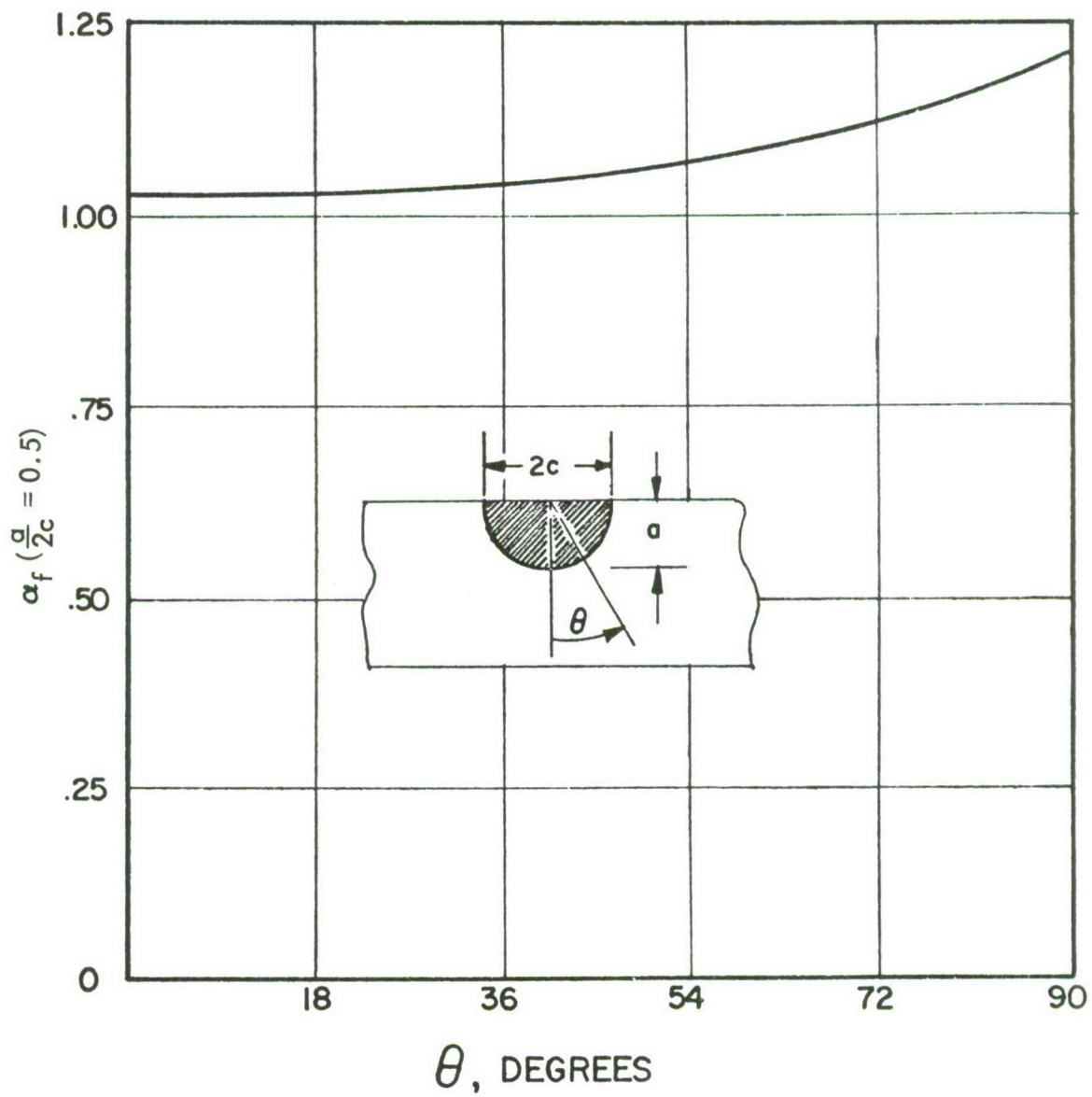


FIGURE E-1 FRONT SURFACE GEOMETRIC COEFFICIENT FOR A SEMI-CIRCULAR PART-THRU CRACK (REFERENCE E-3)



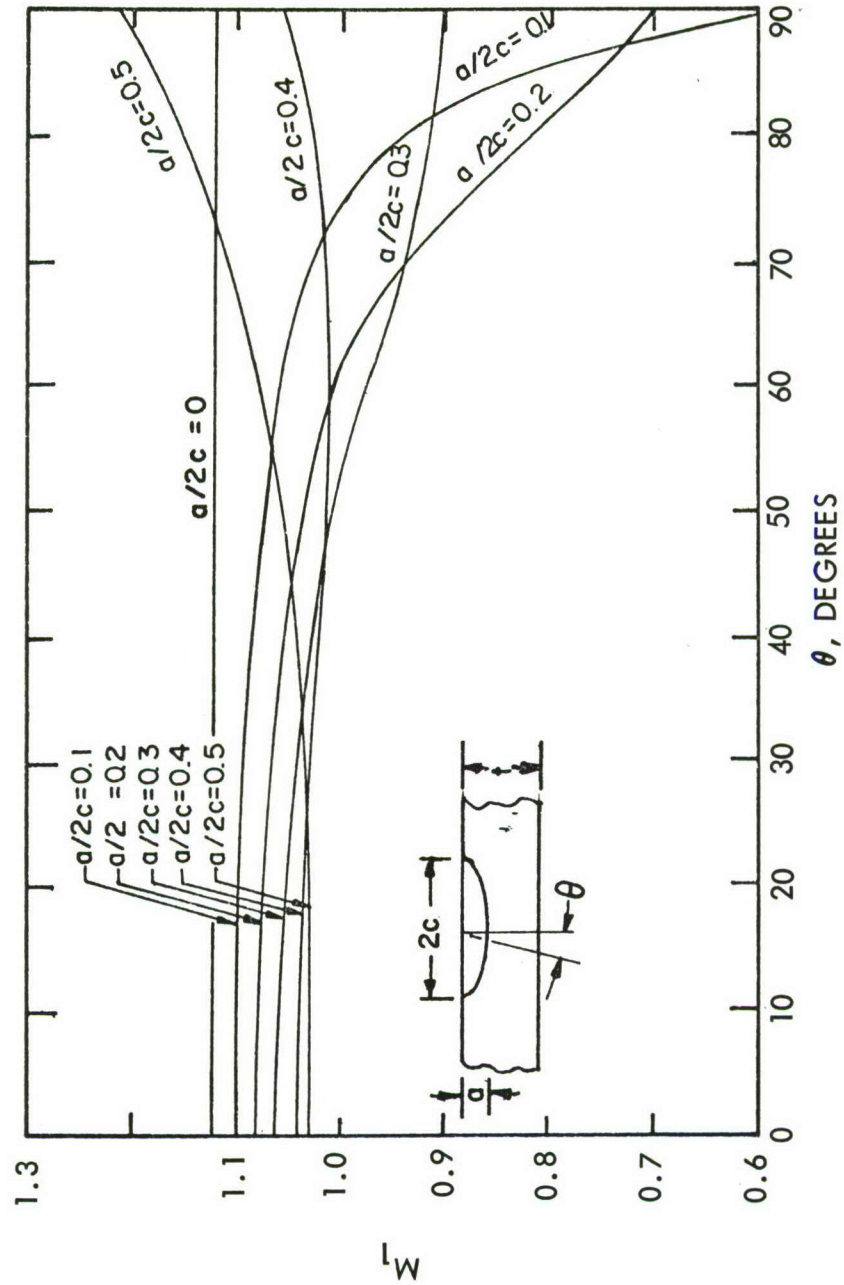


FIGURE E-2 FRONT SURFACE PARAMETER  $M_1$  FOR A SEMI-ELLIPTICAL PART-THRU CRACK

is limited by the fact that the available area in the crack front is bounded by the back surface.

The mechanics of crack growth just beyond this crack size is uncertain. One possibility is that fracture will be controlled by the stress intensity at or near the major axis of the semi-ellipse, and that the part-thru crack will behave like a thru-the-thickness crack. Certainly this must occur eventually as the crack size increases. Consider that the area between the crack and the back surface is undergoing plastic yielding; the load applied to the gross area is equal to  $f_g$  times  $2ct$ , and the maximum load applied to the net area is approximated by  $F_{ty}$  times  $(2ct - \pi ac/2)$ . By comparing these two loads, a criterion for the transition point can be estimated by

$$a_{et} = \frac{4t}{\pi} [1 - (f_g/F_{ty})] \quad (E-4)$$

where  $a_{et}$  is defined to be the crack depth for a crack equivalent to the thru-the-thickness crack. For crack depths larger than this, the stress intensity may be computed by the thru-the-thickness crack formula.

To define  $M_p$ , the effective crack depth is considered to be composed of apparent crack depth,  $a$ , and the half length of the plastic zone,  $r_p$ , in front of the crack tip. Equation (E-3) is then written as

$$K_{mx} = f_g \sqrt{\pi(a + r_p)} \cdot \alpha_b \cdot \frac{M_1'}{\phi} \quad (E-5)$$

For the point of maximum depth the state of stress at that point is plane strain. Therefore, from References E-8 and E-9,

$$r_p = \frac{1}{4\pi\sqrt{2}} \left( \frac{K}{F_{ty}} \right)^2 \quad (E-6)$$

Substituting Equation (E-6) into Equation (E-5) and solving for  $K_{mx}$ , gives

$$K_{mx} = f_g \sqrt{\pi a} \cdot \alpha_b \cdot M_1' [\phi^2 - 0.177 \alpha_b^2 \cdot M_1'^2 \left( \frac{f_g}{F_{ty}} \right)^2]^{-1/2} \quad (E-7)$$

Comparing Equations (E-3) and (E-7), it is seen that

$$M_p = \left[ 1 - 0.177 \alpha_b^2 \left( \frac{M_1'}{\phi} \right)^2 \cdot \left( \frac{f_g}{F_{ty}} \right)^2 \right]^{-1/2} \quad (E-8)$$

For a crack which is relatively shallow, Irwin (Reference E-1) has assumed that the combined effects of the front and the back surfaces would be approximately 10 percent. In other words, assuming  $\alpha_b \cdot M_1' = 1.1$ , Equation (E-8) reduces to

$$M_p = \left[ 1 - \frac{0.212}{\phi^2} \left( \frac{f_g}{F_{ty}} \right)^2 \right]^{-1/2} \quad (E-9)$$

Working curves for  $M_p$ , Equation (E-9) are plotted as solid lines in Figure E-3 as a function of  $a/2c$  and  $f_g/F_{ty}$ .

Alternatively, Kobayashi (Reference E-6) has proposed another crack tip plasticity factor. His  $M_p$  term is a function of  $f_g/F_{ty}$  and a material parameter  $m'$ . Note that the parameter  $m'$  is not a strain hardening exponent; however, for an elastic perfectly plastic material, the value of  $m'$  is also zero. Comparison of Kobayashi's and Irwin's  $M_p$  terms is shown in Figure E-3. Note that the  $M_p$  value for  $0.1 \leq m' \leq 0.2$  (the most common range of  $m'$ ) match the  $M_p$  values for  $0.2 \leq a/2c \leq 0.5$  (the most common range of the crack shape).

For the back surface coefficient  $\alpha_b$  there are three types of expressions available:

#### 1. Parametric Estimation

First, assume that the  $\alpha_b$  coefficient is a function of the crack depth to plate thickness ratio,  $a/t$ , and the crack geometry ratio,  $a/2c$ . Then the  $\alpha_b$  coefficient, in terms of  $a/t$ , can be estimated for any constant  $a/2c$  value. Second, assume that the effect of the back surface on the part-thru crack stress intensity is similar to the effect of the finite width (the edge) of a plate on the stress intensity of an edge crack or a center crack in a plate. Utilizing the available numerical solutions



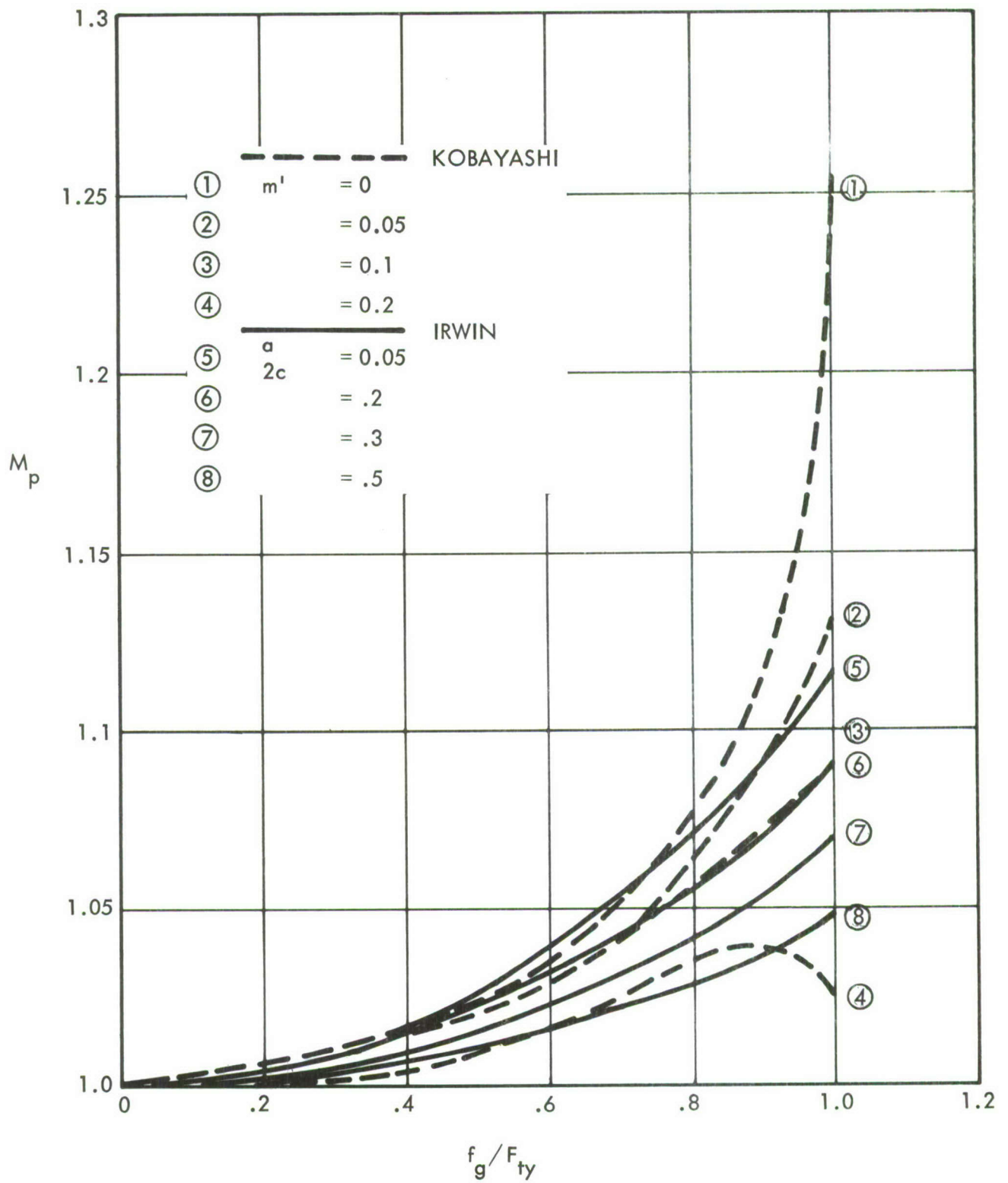


FIGURE E-3 COMPARISON OF KOBAYASHI'S AND IRWIN'S PLASTICITY FACTORS

for the two extreme crack shape ratios,  $a/2c = 0.5$  (a semi-circular crack, Reference E-6) and an  $a/2c = 0$  (an edge crack, Reference E-10), plus some intermediate functions for the middle values of  $a/2c$ , a complete series of  $\alpha_b$  factors can be estimated. Investigators at Boeing have found that the width correction factor of Forman and Kobayashi fits experimental data having intermediate  $a/2c$  values (References E-11 thru E-13). In this report, similar width correction factors for the center cracked panel configurations (References E-14 thru E-16) are employed for the intermediate values  $a/2c = 0.21, 0.23$  and  $0.25$ . Having these five  $a/t$  functions, for five  $a/2c$  ratios, a family of  $\alpha_b$  curves was constructed as shown in Figure E-4.

## 2. Numerical Solutions

Numerical solutions for  $\alpha_b$ , for  $a/2c = 0.2, 0.3, 0.4$  and  $0.5$  are given by Smith and Alavi (Reference E-5). Comparison between Smith's  $\alpha_b$  and the estimated  $\alpha_b$  are shown in Figure E-5. It is seen that these two  $\alpha_b$ 's agree with each other for  $a/2c$  ratios equal to, or greater than  $0.4$ .

Rice and Levy have solved the surface flaw problem as a whole without using separate geometric coefficients (See Reference E-2). Their stress intensity factor is plotted in Figure E-6 as a function of  $a/2c$ ,  $a/t$  and  $K_E$ . In Figure E-6, the parameter  $K_E$  is the edge crack stress intensity factor of Gross, et al; i.e.,  $K_E$  equals  $\sqrt{\pi}$  times  $M'_1/\phi$  times  $\alpha_b$ , in Figure 4-9 and E-4, respectively, for  $a/2c = 0$ . Rice has claimed that their numbers matched well with the numbers calculated using Smith and Alavi's solution.

Stress intensity factors calculated using  $M'_1/\phi$  and  $\alpha_b$  given in Figures 4-9 and E-4 were compared with values in Figure E-6. For  $a/2c$  ratios smaller than  $0.3$ , the estimated  $\alpha_b$  gave higher K-values as compared to the K-values of Rice and Levy. However, the K-values based on estimated  $\alpha_b$  agree well with the approximate solution given in Figure E-7 which was also worked out by Rice and Levy.

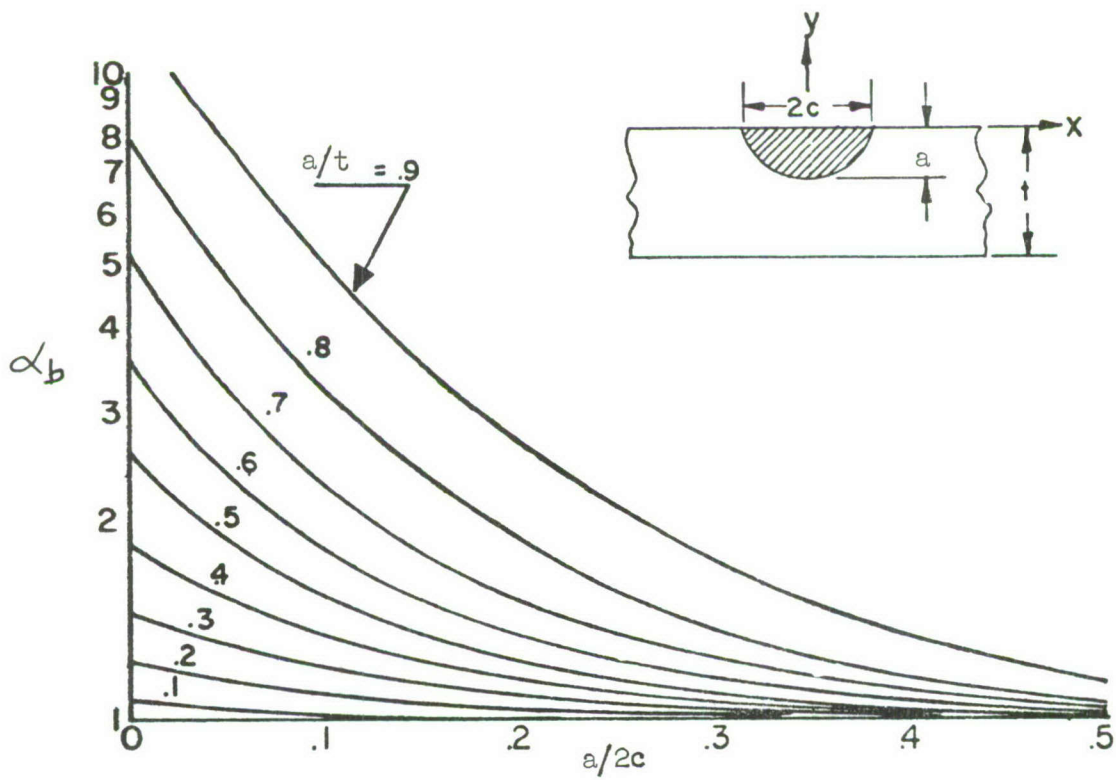


FIGURE E-4 ESTIMATED BACK SURFACE COEFFICIENT



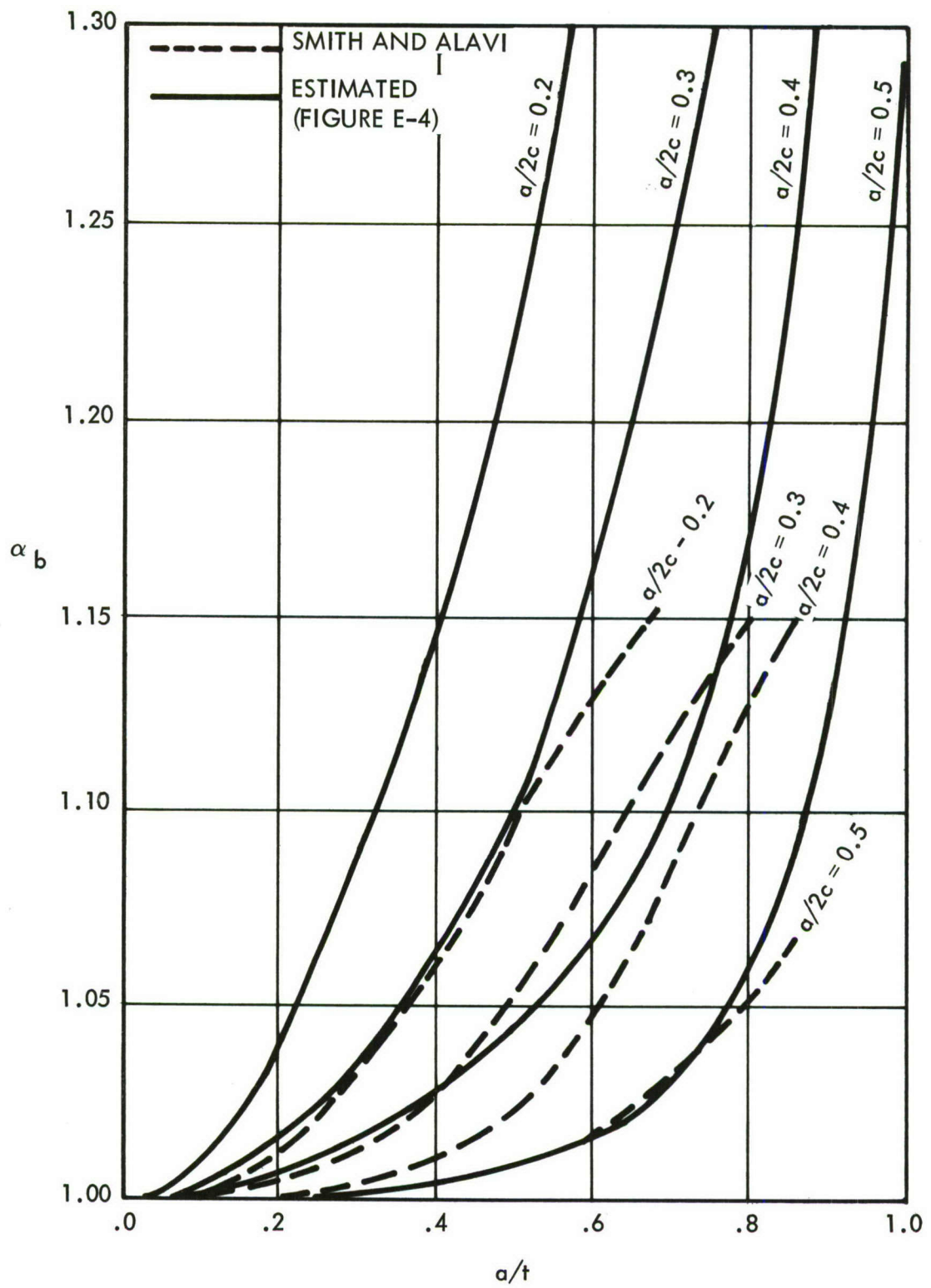


FIGURE E-5 COMPARISON OF BACK SURFACE COEFFICIENTS

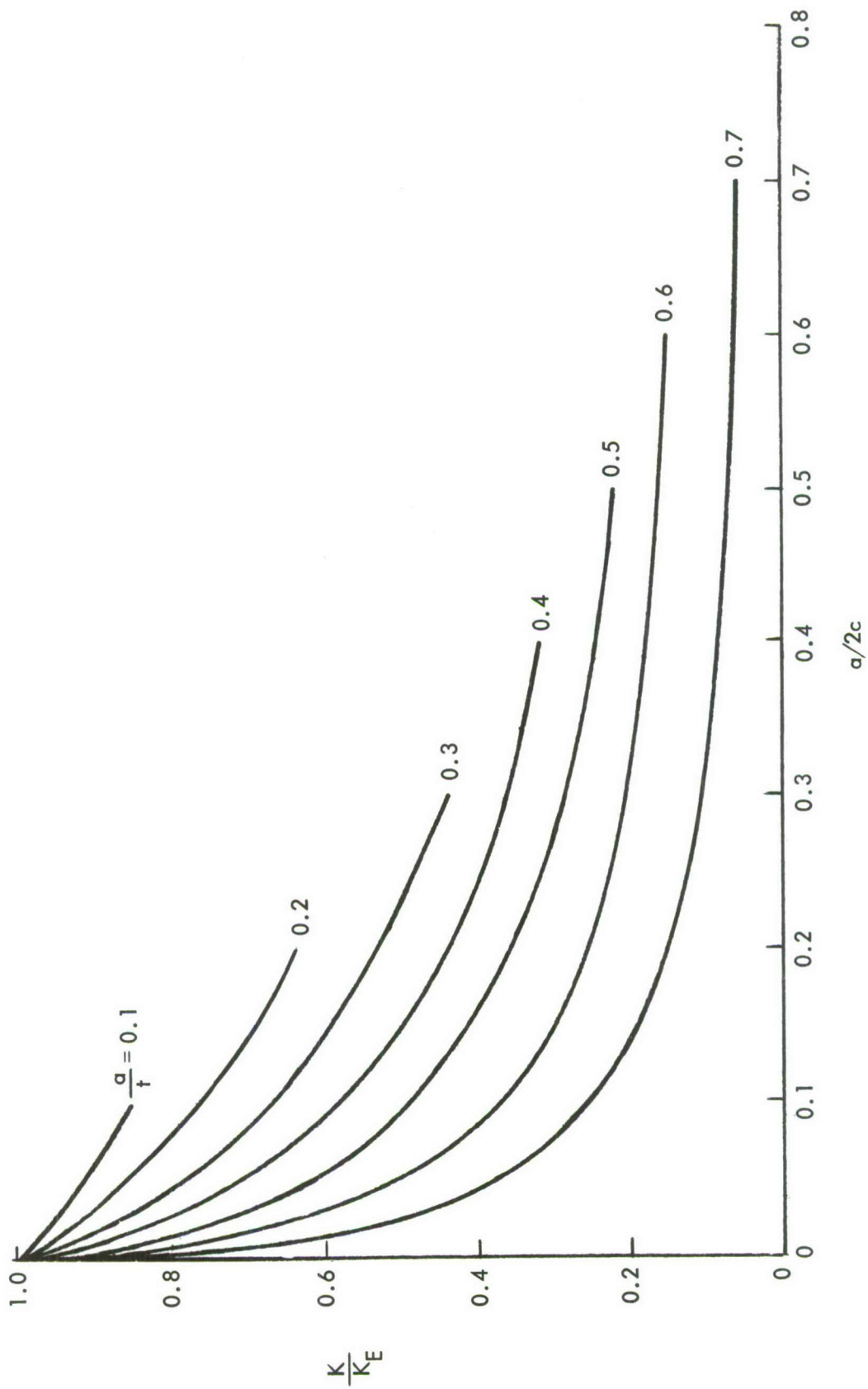


FIGURE E-6 RICE AND LEVY'S NUMERICAL SOLUTION FOR A PART-THRU CRACK (REFERENCE E-2)

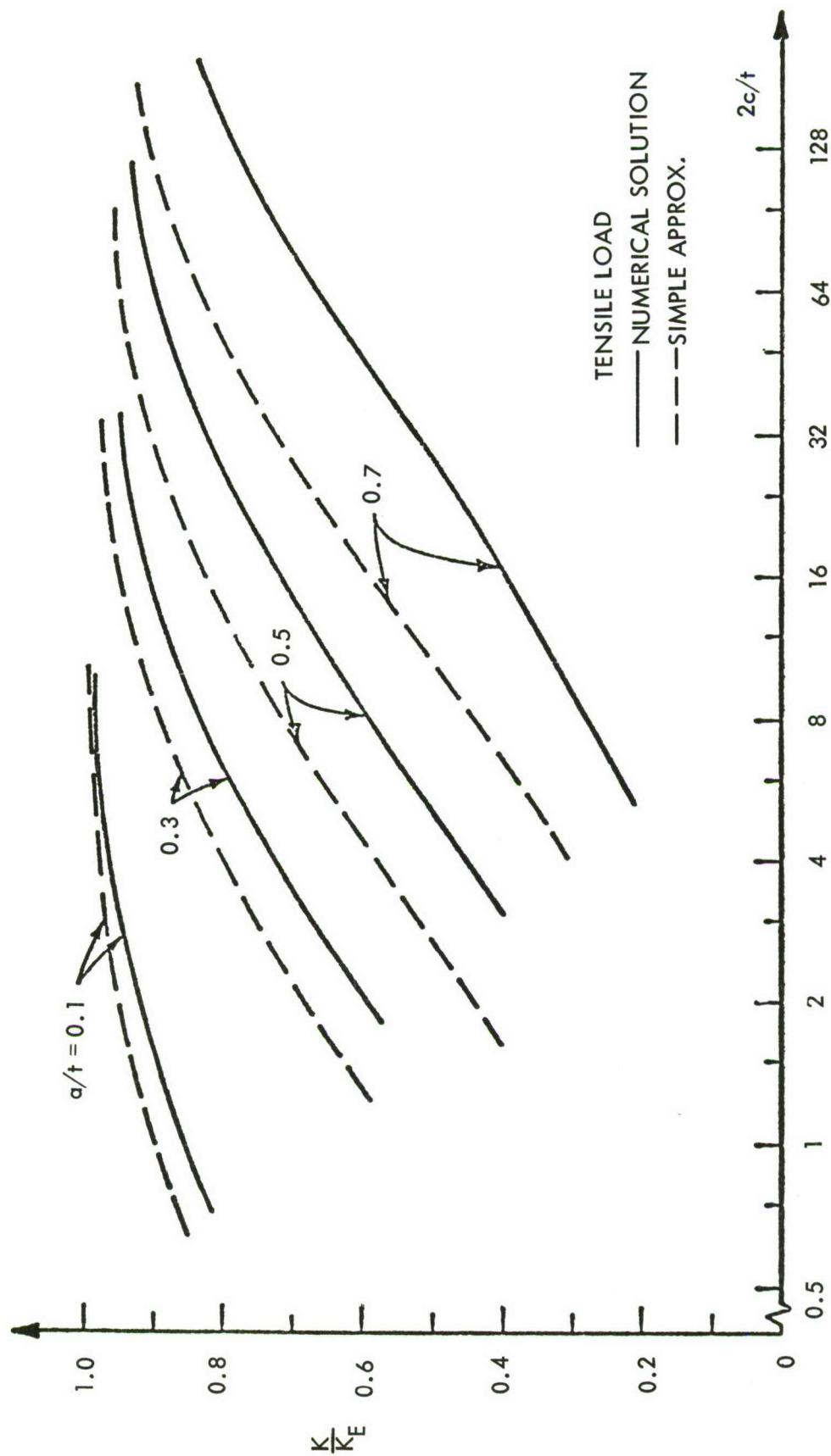


FIGURE E-7 COMPARISON OF RICE-LEVY'S APPROXIMATE AND NUMERICAL SOLUTIONS FOR A PART-THRU CRACK



### 3. Experimentally Determined $\alpha_b$ Factor

---

As shown in Figures E-8 and E-9, titanium and aluminum alloys exhibit a distinguishable susceptibility to the effect of the back free surface. Comparisons with Figure E-5 revealed that the estimated  $\alpha_b$  factors underestimate the back surface effect indicated by the data for titanium for  $a/2c > 0.2$ . However, comparing the data for aluminum, the estimated  $\alpha_b$  factor agrees well with the data for  $a/2c > 0.3$  but overestimates the effect of the back surface for  $a/2c < 0.3$ .

In summary, part-thru crack stress intensity factors calculated by Equation (E-3) with  $M_p$  set equal to unity and using the  $M'/\phi$  and  $\alpha_b$  coefficients given in Figures E-1 and E-4, are numerically equivalent to the K-values determined by the approximate solution of Rice and Levy. It is desirable to develop  $\alpha_b$  coefficients from experimental data; however, if the behavior for a given material is not known, either of the methods discussed in Items 1. and 2. above can be used as a first approximation.

Crack growth calculations carried out for the design of large scale structure require simplifications for the sake of expediency. In calculations for a part-thru crack, inclusion of the back surface correction in the stress intensity formulae would specialize each calculation to a given thickness. Therefore, in many design applications the back surface correction should not be included. Such an approach can be easily justified when one recognizes the myriad of other assumptions which cannot be avoided in analysis for design, and the heavy consequences of these assumptions on the reliability of the predicted structural integrity.

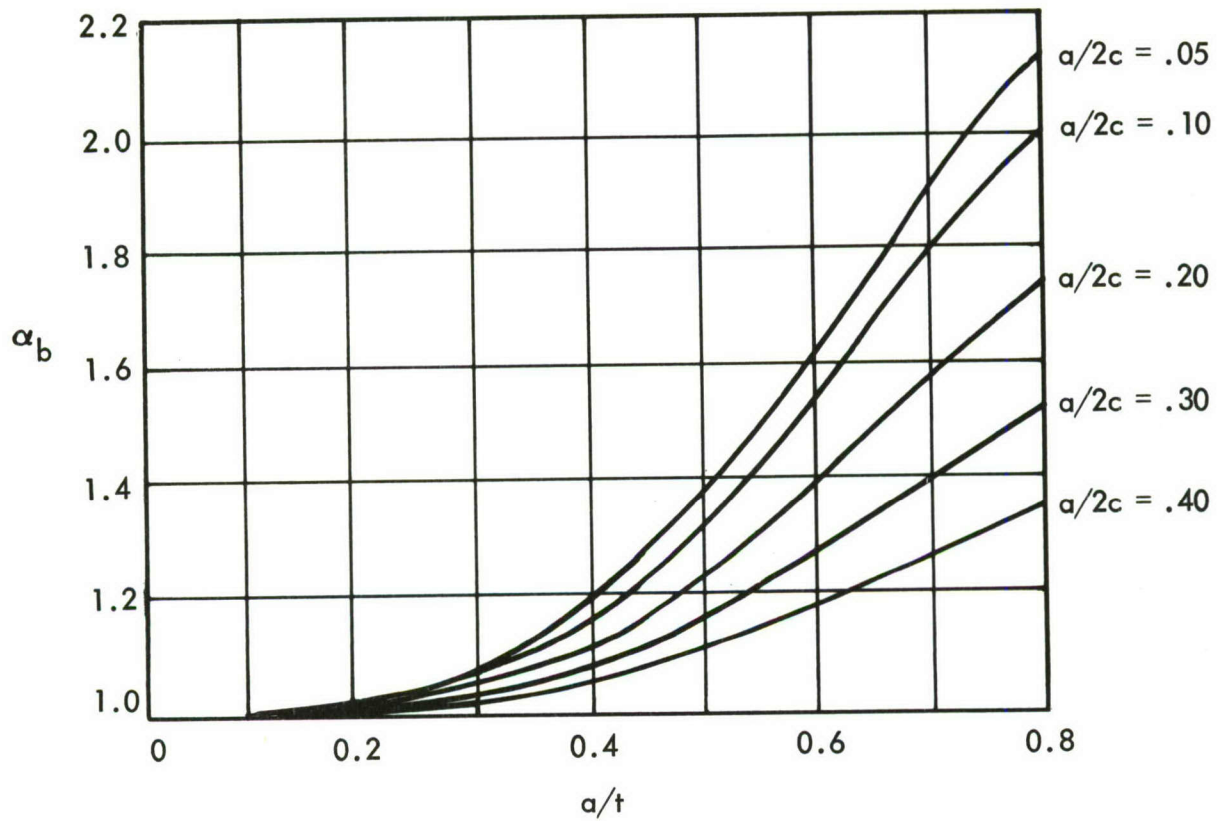


FIGURE E-8 BACK SURFACE COEFFICIENT FOR Ti-5Al-2.5Sn  
(ELI) BASE METAL AND WELDMENTS

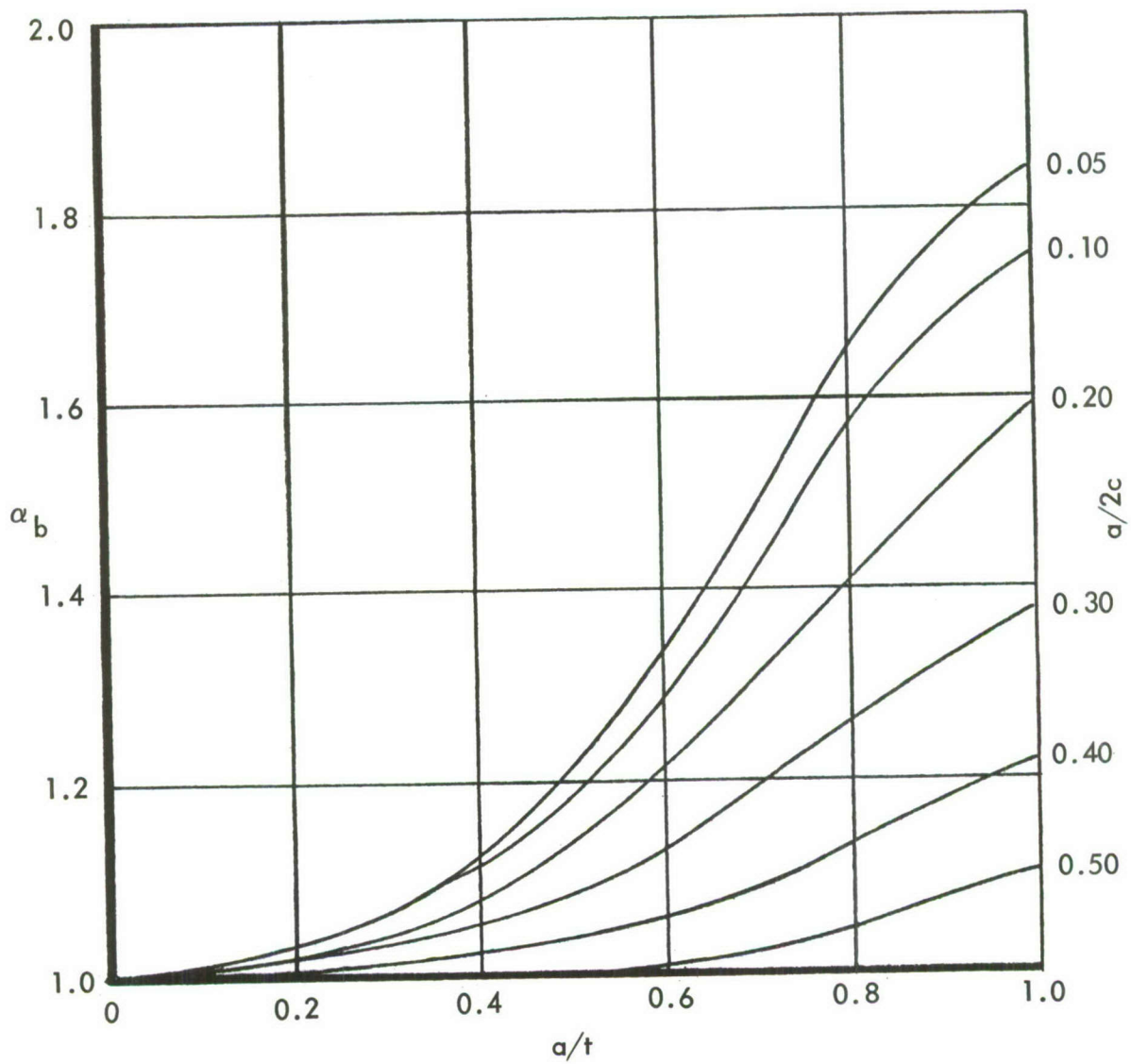


FIGURE E-9 BACK SURFACE COEFFICIENT  
FOR 2219-T87 ALUMINUM PLATE



## APPENDIX F

### THE CRACK GROWTH RESISTANCE CURVE APPROACH TO RESIDUAL STRENGTH PREDICTION

The  $K_c$  method presented in Section 4.6.2 for residual strength analysis of cracked reinforced structure is a highly effective empirically based technique. However, it is restricted to reinforced panels of specific geometry (regularly spaced reinforcements, no cutouts, etc.). A more general technique is one which is based on the crack growth resistance curve (R-curve) concept. In the R-curve approach it is assumed that the amount of incremental crack growth under monotonically increasing load is a function of the current value of the crack tip stress intensity factor only.

R-curves may properly be used over a wider range of configurations than the  $K_c$  approach. The only limitation is the existence of a meaningful stress intensity factor. R-curves may be generated using a variety of configurations, not necessarily similar to the configuration that is to be analyzed. For center-cracked panels, films showing the crack growth and load magnitude provide a straight forward method to define a R-curve. R-curves are of course, also thickness dependent and presently are available for only a few engineering materials. Up to now only the tensile mode (Mode I) has been investigated using this approach.

The failure criterion is

$$K = K_r \text{ and } \frac{\partial K}{\partial a} \geq \frac{\partial K_r}{\partial a} \quad (F-1)$$

That is, failure occurs when the applied K curve (dotted lines of Figure F-1 for various applied stresses) is tangent to the crack growth resistance curve (solid line of Figure F-1).

General design curves using these failure criteria are difficult to develop due to the complexity of the material property descriptions (a curve rather than a single data value, e.g.,  $K_c$ ). However, a simple graphical technique has been developed which makes the task of failure prediction easier. The technique works as long as an elastic analysis is appropriate. It will not work if there is yielding at locations other than at the crack tip (in a reinforcement for example).

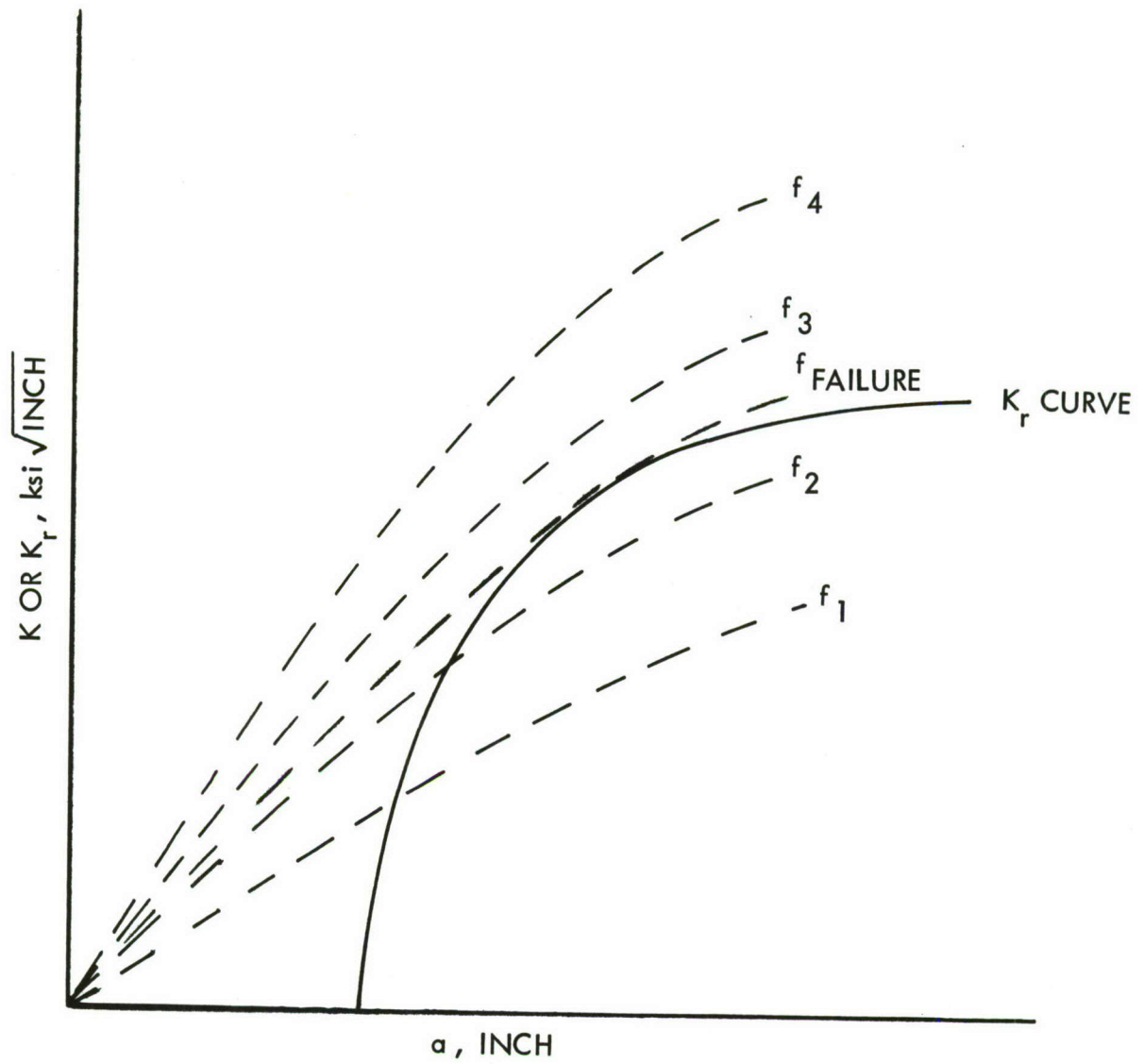


FIGURE F-1 RESISTANCE CURVE FAILURE PREDICTION

### Example 1

For a center-cracked panel  $K = f_g \sqrt{\pi a} \phi_1$  therefore  $\alpha = \sqrt{\pi a} \phi_1$ , Equation (4-6a). This is plotted for various panel widths on a semi-log grid in Figure F-2. A resistance curve ( $K_r$ ) for 2024-T3 is plotted on a semi-log grid in Figure F-3. If an initial crack length is chosen and the  $\Delta a = 0$  line (on the  $K_r$  curve) is aligned with that crack length on the  $\alpha$  plot, a tangency point can be found by vertically moving the curves relative to one another. Since  $F_g = \frac{K}{\alpha}$  and  $\log F_g = \log K - \log \alpha$ ; the value of the stress at instability is read from the  $K_r$  curve ordinate at the line corresponding to  $\alpha = 1$  ( $\log \alpha = 0$ ).  $K'_O$  is simply the value of  $K_r$  at the tangency point and  $K_O$  is the value of the  $K_r$  curve ordinate where the curve crosses the ordinate. This is schematically shown in Figure F-4.

It can be seen that using this technique allows the rapid computation of a prediction that is normally tedious to make. For example: using Figure F-2 and a transparency of Figure F-3 the failure stress for panels with an initial half-crack length of 2 inches and various panel widths can be quickly evaluated by simply moving the transparency vertically to give:

W Inches	$f_{\text{Failure}}$ ksi	$K'_O$ ksi $\sqrt{\text{in.}}$	$K_O$ ksi $\sqrt{\text{in.}}$
$\infty$	33.5	104	84
20	32	103	81
16	30.4	102	79
12	28.7	100	76
10	26.8	96	73
8	22.5	91	66

### Example 2

Using this technique, a reasonably complex structure can be analyzed rather easily. In Figure F-5 an  $\alpha$  curve is presented for a reinforced panel. This curve was developed by the method discussed in Section 4.3.6. A schematic of the failure prediction is shown in Figure F-6 for this structure.

The solution for this example problem gives the following results:

$$K_O = 123 \text{ ksi}\sqrt{\text{in.}}$$

$$K_m = 99 \text{ ksi}\sqrt{\text{in.}}$$

$$K'_O = 100 \text{ ksi}\sqrt{\text{in.}}$$

$$F_g = 48 \text{ ksi}$$



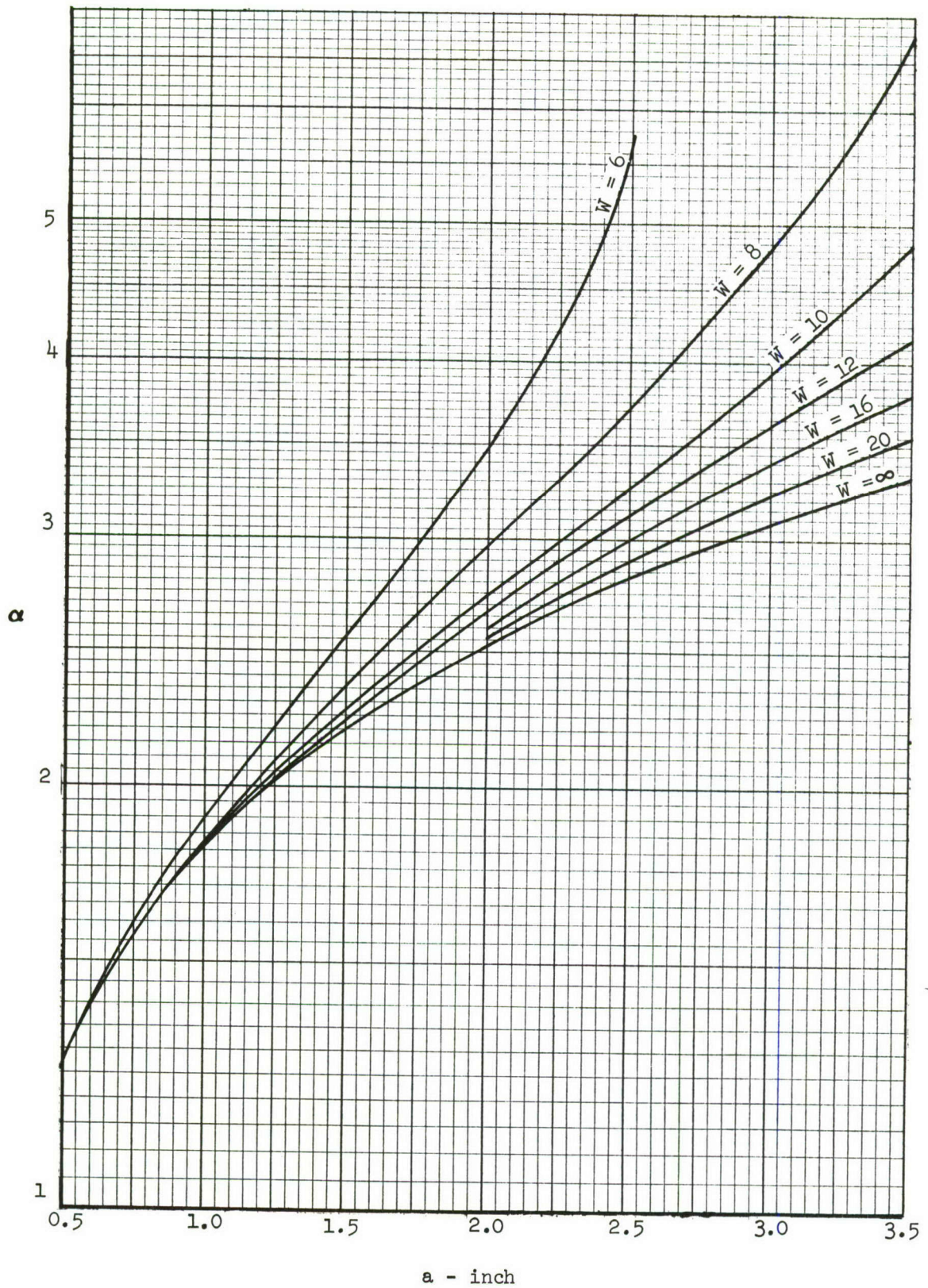


FIGURE F-2 STRESS INTENSITY STRUCTURAL COEFFICIENT FOR A CENTER-CRACKED PANEL

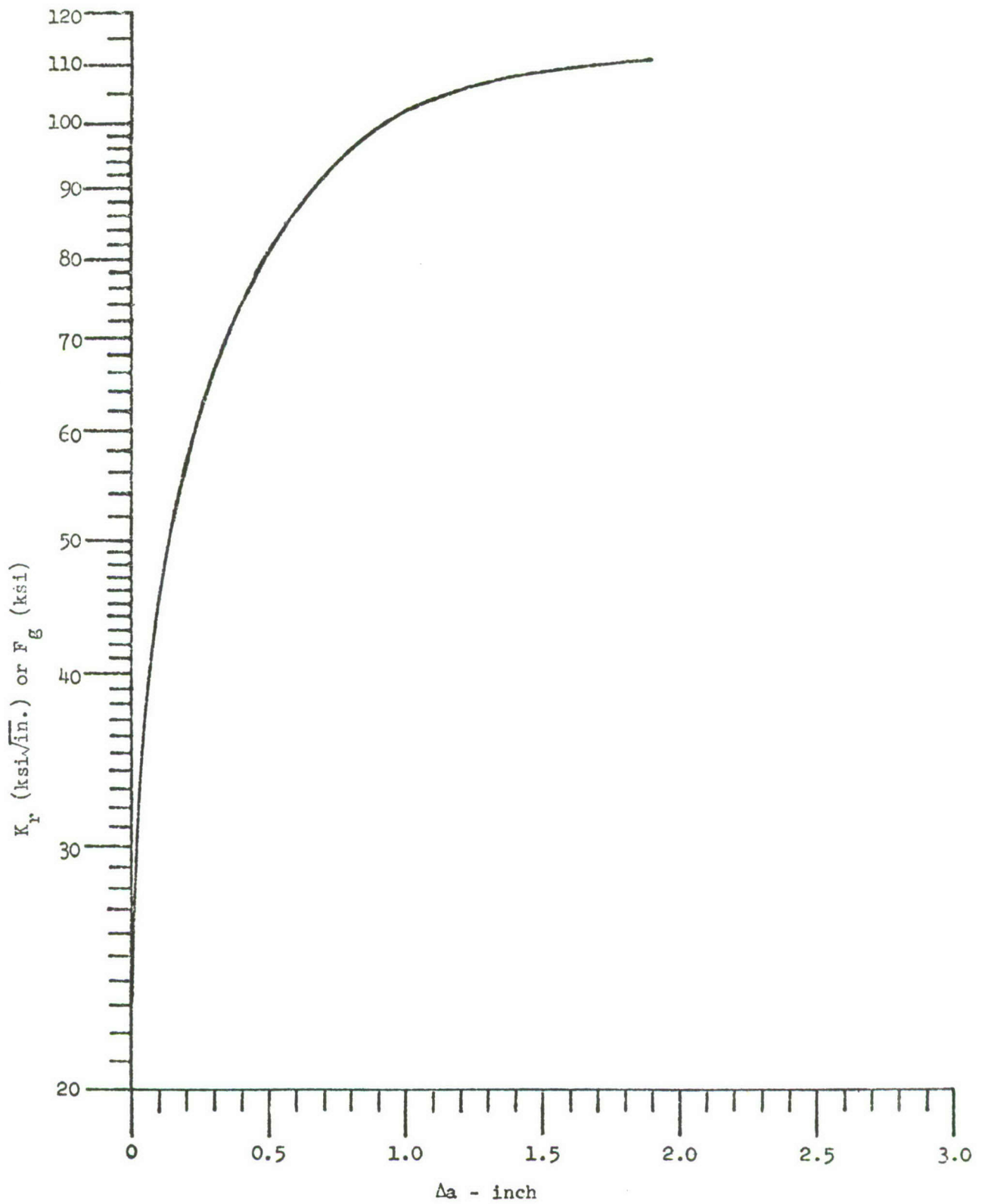


FIGURE F-3  $K_I$  CURVE FOR 2024-T3 CLAD ALUMINUM ( $t = 0.08$  INCH)

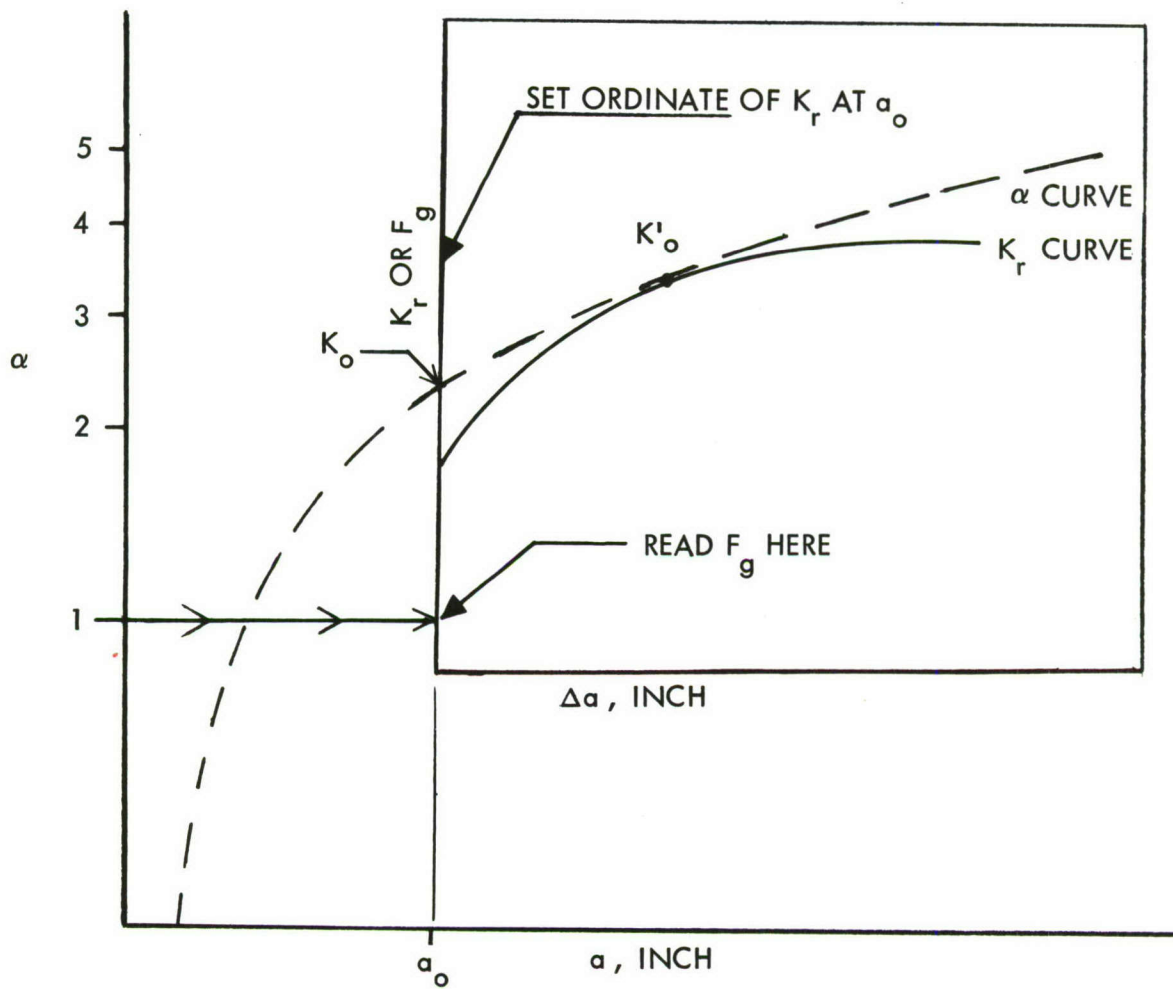


FIGURE F-4 SCHEMATIC SOLUTION TO EXAMPLE 1



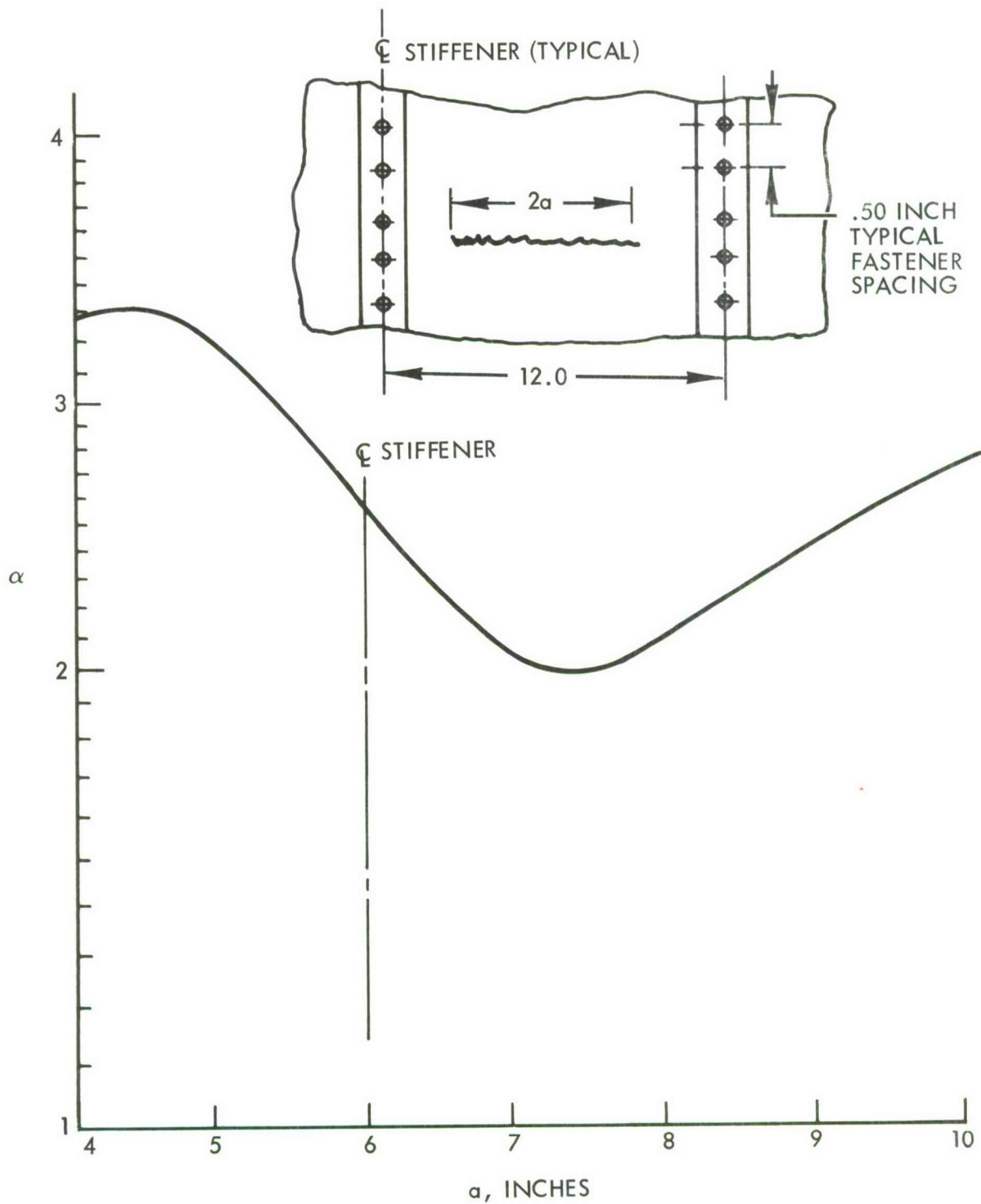


FIGURE F-5 STRESS INTENSITY STRUCTURAL COEFFICIENT FOR EXAMPLE 2  
REINFORCED PANEL (DATA FROM REFERENCE 4-16)

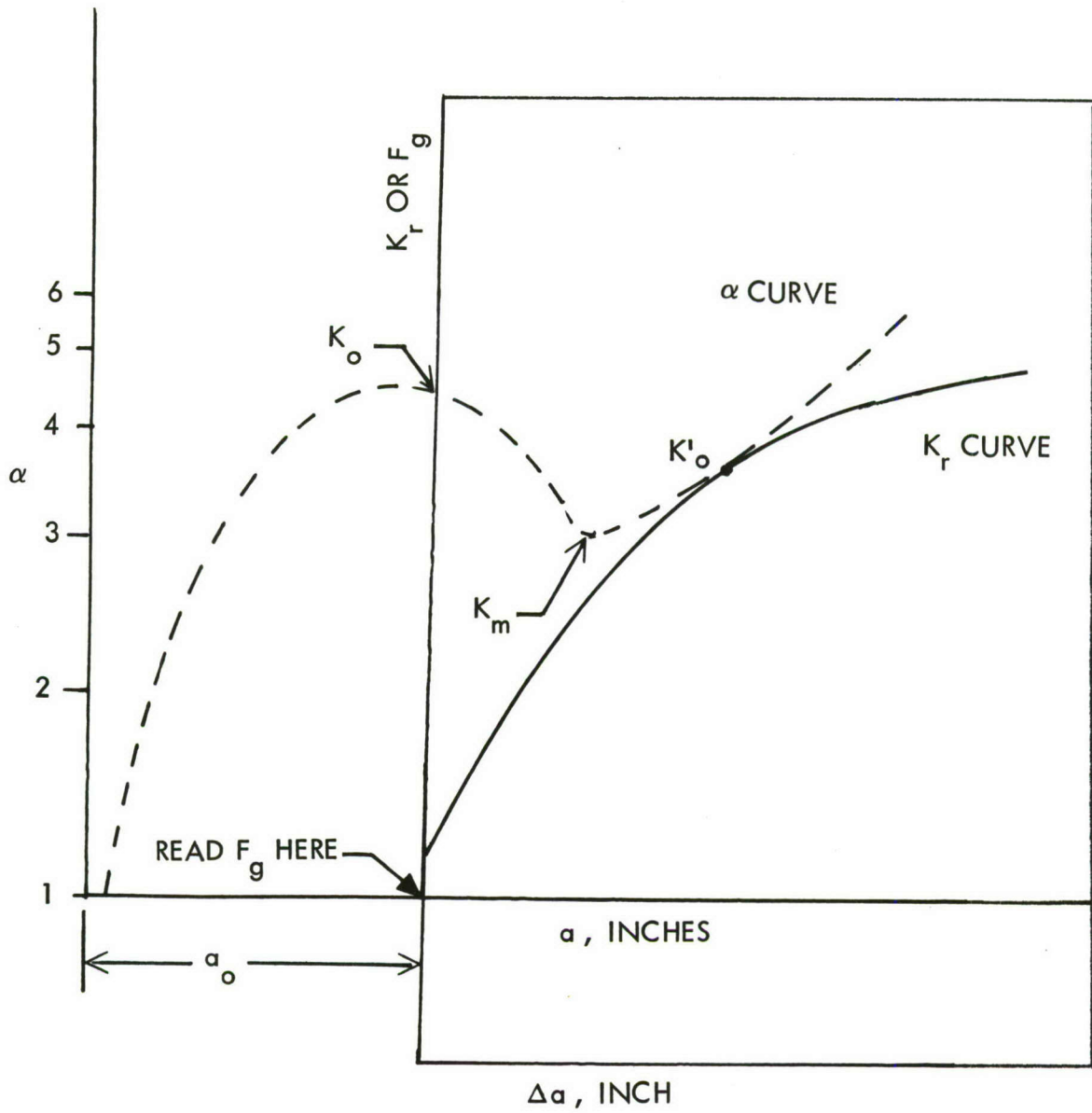


FIGURE F-6 SCHEMATIC SOLUTION FOR EXAMPLE PROBLEM 2

Note that  $K_0$  is a rather meaningless number for this structure. A more meaningful number in this case is the minimum  $K$  at the instability load. This is designated by  $K_m$  in Figure F-6. It has been observed that  $K_m$  may be considered to correspond to  $K_0$  for a center-cracked panel test ( $K_c$ ).

It should be noted that the above described procedure can still be used when local crack tip yielding affects the effective crack length. Since the stress intensity structural coefficient curves are essentially stress intensity factor versus effective crack length, all that is necessary is that the abscissa of the resistance curve be effective change in crack length. Initial alignment offers no problem; since at  $\Delta a = 0$ , effective length equals actual crack length.



## APPENDIX G

### LIST OF SYMBOLS

A	Cross sectional area, inches <sup>2</sup>  Constant relating the peak load factor for a maneuver to the cyclic frequency of a sinusoidal wave used to model the maneuver: $A = f/N_{z_{max}}$
A <sub>s</sub>	Cross sectional area of the skin of a reinforced member or panel, in. <sup>2</sup>
$\bar{A}_e$	Effective area of a stringer, that portion of the stringer cross section contributing to the residual strength of cracked reinforced structure, in. <sup>2</sup>
$\Sigma \bar{A}_e$	Sum of effective areas of the intact stiffeners (usually two in number) which stiffen the cracked area in a reinforced cracked structure, in. <sup>2</sup>
a	Crack size; the dimension associated with one tip of a crack. For example, the depth of a surface flaw or the half-length of a thru-the-thickness crack in a center-cracked panel, in.
a <sub>cr</sub>	Critical crack length for catastrophic failure under a designated load, in.
a <sub>et</sub>	The depth of a surface flaw at which the crack begins to behave as a thru-the-thickness crack, in.
a <sub>i</sub>	Maximum undetected crack size at time of fabrication, in. Crack length when $\mathcal{H}$ first equals $\mathcal{H}_c$ , in.
a <sub>o</sub>	Initial crack size at the beginning of the crack growth period, in.
a <sub>v</sub>	Maximum undetected crack size after NDI inspection, in.
a <sub>w</sub>	Maximum undetected crack size after walk-around inspection, in.
$\Delta a$	Increment of crack growth under monotonic tensile loading, in.
B	Stringer spacing, in.
C	Factor on stress which permits crack growth calculations based on the severe fatigue loading spectrum to be applied to the typical loading spectrum.  Semi-axis of an elliptic hole, measured in the line of a crack emanating from the hole, in.
C'	Factor on stress which permits crack growth calculations based on the severe fatigue loading spectrum to be applied to the "mix" spectrum used in fatigue analysis.

$c$	Stress wave velocity, ft/sec.
	Half length of a part-thru crack, measured along the specimen surface, in.
	A constant (load factor times time required for a maneuver), sec.
$da/dN$	Fatigue crack propagation rate; rate of growth of one end of a crack, in./cycle
$da/dt$	Crack propagation rate, due to sustained loads, in. per unit time
$da/dF$	Crack propagation rate due to spectrum fatigue loads, in. per flight-hour
$E$	Young's modulus, ksi
$E_f$	Young's modulus of a stringer, ksi
$E_s$	Young's modulus of skin, ksi
$F'$	Residual strength of reinforced structure, ksi
$F(L/r)$	Geometric coefficient for a crack emanating from a circular hole
$F(L/C)$	Geometric coefficient for a crack emanating from an elliptic hole
$F_{fatigue}$	Constant amplitude stress level which will result in a fatigue life of 30,000 cycles at a $K_t$ of 4 for aluminum or 5 for titanium, ksi
$F_g$	Residual strength, the stress leading to unstable crack propagation, ksi
$F_{tu}$	Ultimate tensile strength of the material, ksi
$F_{ty}$	Material tensile yield stress, ksi
$F_{tyf}, F_{tys}$	Tensile yield strength of reinforcement and skin materials, respectively, ksi
$f$	Sinusoidal cyclic frequency, cpm
$f_g$	Gross area tensile stress, directed normal to the crack unless indicated otherwise, ksi
$f_{max}$	Gross area stress resulting from application of the ultimate design load, ksi
$f_s$	Applied uniform shear stress, ksi
$f_{we}$	Added stress increment picked up by a panel due to failure of an adjacent panel, ksi

G Shear modulus, ksi

$\mathcal{E}$  Strain energy release rate based on a static analysis, in-lb. per in.

$\mathcal{G}_c$  Critical value of strain energy release rate, at which rapid crack propagation begins, in-lb. per in.

I Inspection interval, flights or flight-hours

Moment of inertia of the cross-section of a stiffener, in.<sup>4</sup>

(When used as a subscript): Indicates a plane strain condition

K Stress intensity factor, ksi $\sqrt{\text{in.}}$ .

K' Component of stress intensity of reinforced structure due only to applied load and crack length, and independent of reinforcement, ksi $\sqrt{\text{in.}}$ .

K<sub>1</sub>, K<sub>2</sub>, K<sub>3</sub> Applied stress intensities for mode 1, 2, or 3, respectively, ksi $\sqrt{\text{in.}}$ .

K<sub>1c</sub>, K<sub>2c</sub>, K<sub>3c</sub> Critical stress intensities for failure of a cracked plate under pure mode 1, 2, or 3, respectively; ksi $\sqrt{\text{in.}}$ .

K<sub>E</sub> Stress intensity factor for a through-the-thickness edge crack, ksi $\sqrt{\text{in.}}$ .

$\Delta K$  Stress intensity based on stress range in a fatigue cycle;  
 $\Delta K = (\text{max. stress} - \text{min. stress}) \cdot \alpha$ , ksi $\sqrt{\text{in.}}$ .

K 10<sup>-N</sup> Value of  $\Delta K$  (R = 0) for which the constant amplitude crack growth rate of the material (in room temperature dry air) is 10<sup>-N</sup> inches per cycle.

K<sub>c</sub> Plane stress or mixed mode fracture toughness, ksi $\sqrt{\text{in.}}$ .

K<sub>Ic</sub>, K<sub>IC</sub> Plane strain fracture toughness, ksi $\sqrt{\text{in.}}$ .

K<sub>Isc</sub> Threshold value of stress intensity for stress corrosion cracking. If the applied stress intensity is below K<sub>Isc</sub>, stress corrosion cracking will not occur.

K<sub>max</sub> Stress intensity based on the maximum stress in a fatigue cycle, ksi $\sqrt{\text{in.}}$ .  
Maximum value of local stress intensity for all points around the periphery of a surface flaw, ksi $\sqrt{\text{in.}}$ .

K<sub>i</sub> Initial stress intensity, based on initial crack length, in a sustained-load environmental crack growth test, ksi $\sqrt{\text{in.}}$ .

K<sub>o</sub>, "Engineering" stress intensity defining when unstable crack propagation commences at constant load. Based on initial crack length (at zero load prior to monotonic loading) and final load. ksi $\sqrt{\text{in.}}$ .  
K<sub>Ii</sub>



$K'_o$	True stress intensity at the point when unstable crack propagation commences at constant load. Based on final crack length and final load. ksi $\sqrt{\text{in.}}$ .
$K_r$	Material resistance to crack growth under monotonically increasing load, ksi $\sqrt{\text{in.}}$ .
$K_t$	Stress concentration factor, the peak stress at a notch divided by the net area stress
$K_\alpha, (K_{\alpha'})$	One-sided tolerance limit factor corresponding to a proportion $\alpha$ (or $\alpha'$ ) of a normal distribution.
$k$	Number of stress levels considered in the loading spectrum
$k_r$	Component of the stress intensity of a reinforced structure due to the presence of the reinforcing members, ksi $\sqrt{\text{in.}}$ .
$L$	Length of a tensile bar subjected to a dynamic load, ft. Dimension from the edge of a hole to the tip of a crack emanating from the hole, in. Longitudinal grain direction Length of a center-cracked panel, in.
$L_T$	Length required for attachments to transfer the load from a broken member to adjacent unbroken members, in.
$M$	$\left(\frac{a}{c}\right)^2 \sin^2 \theta + \cos^2 \theta^{\frac{1}{4}}$ , a factor used in the expression for an elliptical crack or surface flaw.
$M_1$	$M \cdot \alpha_p$ , a factor used in defining local stress intensity at any point $\theta$ on the periphery of a surface flaw.
$M'_1$	Maximum value of $M_1$ over all values of the angular position $\theta$
$M_p$	A factor applied to the stress intensity expression to account for the effect of local material plasticity in front of the crack.
$m$	A material constant; the exponent in the crack growth rate expression $da/dN = [K_{\max} (1 - R)^m]$ or $da/dN = CK^m$
$N_i$	Number of loading cycles to failure for the $i^{\text{th}}$ stress level, based on constant amplitude fatigue data for the applicable material and $K_t$ value Length of $i^{\text{th}}$ crack growth period, hours or flights.
$N_Z$	Vertical load factor
$n_i$	Number of loading cycles at the $i^{\text{th}}$ stress level in a spectrum
$N_Z(t)$	Vertical load factor as a function of time

$N_{Z_{max}}$	Maximum vertical load factor during a particular maneuver or fatigue cycle
$n$	Sample size Number of planks in a wing of width $W$
$P$	Load, lbs.
$P_1, P_2$	Loads corresponding to upper and lower bounds for crack arrest, lbs. If the load exceeds $P_1$ the crack will not arrest. If $P_2$ exceeds the load, the crack will arrest.
$P_A$	Allowable attachment strength, lbs.
$P_{cut}$	The "cut load" due to failure of a wing plank, kips
$P_{max}$	Limiting value of the maximum load in a stringer as the length of a skin crack increases, kips
$Q$	$\phi^2 - .212 (f_g/F_{ty})^2$ , parameter for a surface flaw
$R$	Range ratio, minimum stress in a fatigue cycle divided by maximum stress in the cycle
$R_c$	Material "cut-off" stress range ratio for fatigue crack growth under tension-compression cycling. If $R < R_c$ , $R_c$ is used in place of $R$ in the equation for crack growth rate.
$r$	Radius of a fastener hole, in. Cylindrical coordinate distance from the origin, where the origin is the crack tip, in.
$r_p$	Plastic zone size at the tip of a crack, in.
$S$	Sample standard deviation Ratio of stress to the load factor which would induce that stress for the specified structural location, ksi/g Attachment spacing, inches
$S_d$	Life reduction factor for durability
$S_i$	Number of service lifetimes that an initial damage $a_i$ must sustain according to the recommended criteria
$S_v$	Number of inspection intervals that a NDI in-service inspectable damage size $a_v$ must sustain according to the recommended criteria

T	Transverse grain direction Accumulated time above some load factor $N_Z^*$ during a maneuver, sec.
t	Time, minutes Thickness of sheet, plate or wing skin, in.
$t_m$	Thickness of broken middle wing plank, in.
$t_o$	Full time required for application of a dynamic load, sec.
$t_s$	Thickness of wing panel adjacent to a broken panel, in.
$t_{\alpha, n-1}$	T statistic for $\alpha$ confidence level and n-1 degrees of freedom
$\Delta t$	Time to grow a flaw from initial size $a_i$ to critical size, hrs.
$t^*$	Time to grow a flaw from initial size $a_i$ to a size above which the growth rate is excessive (although the growth may still be stable), flights or flight-hours
u	Empirical exponent
v	Empirical exponent
$V_D$	Design dive speed, fps
W	Width of an aircraft component, inches or ft. Width of a center-cracked plate, in.
$W'$	Distance between unbroken stringers, in.
w	Weight density of the material, lbs/in. <sup>3</sup>
$w_e$	Effective width, an experimentally determined parameter. Half the cut load after failure of a middle plank is sustained by the effective width of each of the adjacent planks; in.
$w_m$	Width of broken middle panel, in.
X	A random variable, assumed to be normally or log-normally distributed.
$X_{min}$	Value of X that will be equalled or exceeded with probability $\alpha'$ at a confidence level $\alpha$
$\bar{X}$	A sample mean
$\bar{X}_{\alpha/s}$	Tolerance for the mean (lower limit of confidence band containing the true population mean)



y	Distance from inner surface of skin to centroid of stiffener, in.
Z	A symbol representing applied load (force, load factor, etc.)
$\alpha$	Geometric factor in the stress intensity expression $K = f_g \alpha$ , for example, a center cracked panel of infinite width has $\alpha = \sqrt{\pi a}$ , $\sqrt{in.}$ Confidence coefficient on the estimate of population mean; probability that the population mean will be enclosed within the bounds estimated from the sample.
$\alpha'$	Tolerance limit. The probability that a material property measurement will equal or exceed some specified value.
$\alpha_b$	Geometric coefficient (in stress intensity expression for a part-thru crack in a plate) which accounts for the influence of the back free surface
$\alpha_f$	Geometric coefficient (in stress intensity expression for a part-thru crack) which accounts for the influence of the front free surface
$\alpha_s$	Product of the geometric factor on stress intensity, $\alpha$ , and the load-stress conversion factor, S, ksi/g
$\beta$	$\frac{2w_e}{W}$
$\gamma$	Efficiency of reinforcements in cracked reinforced structure. Ratio of residual strength of the reinforced structure to that of the unreinforced structure; $\gamma = F'/F_g$
$\theta$	A constant Angular position of a point on the periphery of a surface flaw, measured from the depth direction, degrees
$\lambda$	Geometric coefficient in the stress intensity expression $K = f_g \alpha = f_g \lambda \sqrt{\pi a}$
$\rho$	Mass density, slugs/in. <sup>3</sup> Radius of gyration of a stiffener, in. Local radius of an elliptic hole at the origin point of a crack, in.
$\sigma$	Population standard deviation
$\phi$	A complete elliptic integral used in the stress intensity expression for an elliptical crack or surface flaw
$\phi_1$	Geometric coefficient for a symmetric finite width center cracked plate loaded in tension normal to the crack
$\phi_2$	Geometric coefficient for a finite-width plate loaded in shear, Mode II.

**Security Classification**

## DOCUMENT CONTROL DATA - R&amp;D

(Security classification of title, body of abstract and indexing annotation must be entered when the overall report is classified)

1. ORIGINATING ACTIVITY (Corporate author)		2a. REPORT SECURITY CLASSIFICATION	
LOCKHEED-CALIFORNIA COMPANY Burbank, California		Unclassified	
		2b. GROUP	
3. REPORT TITLE			
ENGINEERING CRITERIA AND ANALYSIS METHODOLOGY FOR THE APPRAISAL OF POTENTIAL FRACTURE RESISTANT PRIMARY AIRCRAFT STRUCTURE			
4. DESCRIPTIVE NOTES (Type of report and inclusive dates)			
Final Report February 1971 - August 1972			
5. AUTHOR(S) (Last name, first name, initial)			
Ekvall, John C. Brussat, Thomas R.		Liu, Alan F. Creager, Matthew	
6. REPORT DATE		7a. TOTAL NO. OF PAGES	7b. NO. OF REFS
August, 1972		325	134
8a. CONTRACT OR GRANT NO.		9a. ORIGINATOR'S REPORT NUMBER(S)	
F33615-71-C-1324		LR 25388	
b. PROJECT NO.		9b. OTHER REPORT NO(S) (Any other numbers that may be assigned this report)	
1467		AFFDL-TR-72-80	
10. AVAILABILITY/LIMITATION NOTICES			
Approved for public release, distribution unlimited.			
11. SUPPLEMENTARY NOTES		12. SPONSORING MILITARY ACTIVITY	
		Air Force Flight Dynamics Laboratory Wright-Patterson AFB, Ohio 45433	
13. ABSTRACT Design criteria and analysis procedures are presented such that a design system can be implemented to minimize the occurrence of major structural failures due to the presence of undetected damage. The design criteria define a flaw growth durability requirement and crack growth structural integrity requirements for three classes of inspectability of the structure; noninspectable, NDI in-service inspectable, and walk-aroundinspectable. Currently available crack growth and residual strength methods of analysis are presented which can be used to predict the remaining life and strength of damaged structure. To illustrate the use of the criteria and methods of analysis, a design study was conducted of the lower wing surface of a fighter/attack aircraft. The results of this study indicate that the structure could meet the design criteria with little or no weight penalty using 7075-T76 aluminum and annealed Ti-6Al-4V, and provided adequate inspection techniques and inspection frequencies are applied throughout the life of the aircraft.			



# Security Classification

14. KEY WORDS	LINK A		LINK B		LINK C	
	ROLE	WT	ROLE	WT	ROLE	WT
design criteria						
damage tolerance						
crack growth analysis						
residual strength analysis						
fracture mechanics analysis						
fatigue analysis						
structural integrity						
sustained load crack growth analysis						
dynamic load effects						

## INSTRUCTIONS

1. **ORIGINATING ACTIVITY:** Enter the name and address of the contractor, subcontractor, grantee, Department of Defense activity or other organization (*corporate author*) issuing the report.

2a. **REPORT SECURITY CLASSIFICATION:** Enter the overall security classification of the report. Indicate whether "Restricted Data" is included. Marking is to be in accordance with appropriate security regulations.

2b. **GROUP:** Automatic downgrading is specified in DoD Directive 5200.10 and Armed Forces Industrial Manual. Enter the group number. Also, when applicable, show that optional markings have been used for Group 3 and Group 4 as authorized.

3. **REPORT TITLE:** Enter the complete report title in all capital letters. Titles in all cases should be unclassified. If a meaningful title cannot be selected without classification, show title classification in all capitals in parenthesis immediately following the title.

4. **DESCRIPTIVE NOTES:** If appropriate, enter the type of report, e.g., interim, progress, summary, annual, or final. Give the inclusive dates when a specific reporting period is covered.

5. **AUTHOR(S):** Enter the name(s) of author(s) as shown on or in the report. Enter last name, first name, middle initial. If military, show rank and branch of service. The name of the principal author is an absolute minimum requirement.

6. **REPORT DATE:** Enter the date of the report as day, month, year, or month, year. If more than one date appears on the report, use date of publication.

7a. **TOTAL NUMBER OF PAGES:** The total page count should follow normal pagination procedures, i.e., enter the number of pages containing information.

7b. **NUMBER OF REFERENCES:** Enter the total number of references cited in the report.

8a. **CONTRACT OR GRANT NUMBER:** If appropriate, enter the applicable number of the contract or grant under which the report was written.

8b, 8c, & 8d. **PROJECT NUMBER:** Enter the appropriate military department identification, such as project number, subproject number, system numbers, task number, etc.

9a. **ORIGINATOR'S REPORT NUMBER(S):** Enter the official report number by which the document will be identified and controlled by the originating activity. This number must be unique to this report.

9b. **OTHER REPORT NUMBER(S):** If the report has been assigned any other report numbers (*either by the originator or by the sponsor*), also enter this number(s).

10. **AVAILABILITY/LIMITATION NOTICES:** Enter any limitations on further dissemination of the report, other than those

imposed by security classification, using standard statements such as:

- (1) "Qualified requesters may obtain copies of this report from DDC."
- (2) "Foreign announcement and dissemination of this report by DDC is not authorized."
- (3) "U. S. Government agencies may obtain copies of this report directly from DDC. Other qualified DDC users shall request through \_\_\_\_\_."
- (4) "U. S. military agencies may obtain copies of this report directly from DDC. Other qualified users shall request through \_\_\_\_\_."
- (5) "All distribution of this report is controlled. Qualified DDC users shall request through \_\_\_\_\_."

If the report has been furnished to the Office of Technical Services, Department of Commerce, for sale to the public, indicate this fact and enter the price, if known.

11. **SUPPLEMENTARY NOTES:** Use for additional explanatory notes.

12. **SPONSORING MILITARY ACTIVITY:** Enter the name of the departmental project office or laboratory sponsoring (*paying for*) the research and development. Include address.

13. **ABSTRACT:** Enter an abstract giving a brief and factual summary of the document indicative of the report, even though it may also appear elsewhere in the body of the technical report. If additional space is required, a continuation sheet shall be attached.

It is highly desirable that the abstract of classified reports be unclassified. Each paragraph of the abstract shall end with an indication of the military security classification of the information in the paragraph, represented as (TS), (S), (C), or (U).

There is no limitation on the length of the abstract. However, the suggested length is from 150 to 225 words.

14. **KEY WORDS:** Key words are technically meaningful terms or short phrases that characterize a report and may be used as index entries for cataloging the report. Key words must be selected so that no security classification is required. Identifiers, such as equipment model designation, trade name, military project code name, geographic location, may be used as key words but will be followed by an indication of technical context. The assignment of links, rules, and weights is optional.